FUNCTIONAL ASPECTS OF A MUTATION IN THE $\alpha_2\delta$-2 CALCIUM CHANNEL SUBUNIT OF THE *DUCKY* MOUSE, A MODEL FOR ABSENCE EPILEPSY AND CEREBELLAR ATAXIA

JENS BRODBECK

A THESIS SUBMITTED IN FULFILLMENT OF THE
REQUIREMENTS FOR THE DEGREE OF
DOCTOR OF PHILOSOPHY
AT THE UNIVERSITY OF LONDON

DEPARTMENT OF PHARMACOLOGY
MEDAWAR BUILDING
UNIVERSITY COLLEGE LONDON
LONDON, UK

NOVEMBER 2001

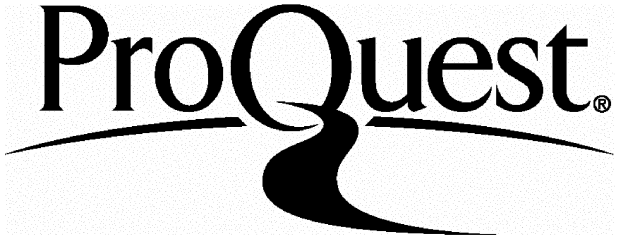

ABSTRACT

Positional cloning identified the genomic rearrangement disrupting the *Cacna2d2* gene to underlie the *ducky* mutation, a model for human absence epilepsy and cerebellar ataxia. The mutation results in the loss of full-length *Cacna2d2* transcript, encoding the $\alpha_2\delta$-2 auxiliary calcium channel subunit, and the presence of two mutant transcripts. *In situ* hybridization found $\alpha_2\delta$-2 highly expressed in +/+ cerebellar Purkinje cells, where in *du/du* mice mutant transcript 1 could be detected. This transcript consists of the first three exons of *Cacna2d2,* lacking most of the α_2-2 and all of the δ-2 subunit and is therefore not normally functional. Phenotypically this leads in homozygotes to the severe neurological defects of absence seizures, cerebellar ataxia and demyelination, as well as a failure to breed or survive beyond 35 days.

The aim of this study was to monitor functional consequences of this mutation on structure, protein expression as well as calcium homeostasis in neurones of the cerebellum. Cresyl violet-stained brain sections of P24 mice revealed normal foliation and laminar structure, although each layer was found to be reduced in size compared to age-matched wild-type animals. Lucifer yellow/neurobiotin injection, as well as Golgi impregnation, showed severe morphological alterations in cerebellar Purkinje neurones, implying a functional disruption of these cells.

Two antibodies directed against the N-terminus of $\alpha_2\delta$-2 could detect the truncated protein in Purkinje neurones of *du/du* mice. The entirely intracellular localization of this protein as well as its size has been confirmed in COS-7 cell expression.

The expression levels of the calcium-binding protein Calbindin D-28K and the astroglial marker protein GFAP quantified by western blot analysis were unchanged. Caspase 3 expression level, a protein involved in the apoptosis pathway, appeared to be elevated in Purkinje neurones of *du/du* cerebellar sections. Western blot analysis of caspase 3 and 12 however did not show a changed expression level in *du/du* compared to +/+ littermates.

Changes in free $[Ca^{2+}]_i$ in Fura-2-loaded cultured cerebellar granule cells and acutely isolated Purkinje neurones were measured by digital imaging during depolarizing K^+ stimulation. No difference in the resting $[Ca^{2+}]_i$ was observed. Peak cytoplasmic $[Ca^{2+}]_i$ transients were significantly reduced (24%) in Purkinje cells from *du/du* mice compared to +/+ mice.

Whether the loss of full-length $\alpha_2\delta$-2 and the presence of a truncated form of the protein, with subsequent reduction in calcium currents, is responsible for cerebellar degeneration and ataxia remains to be determined.

ACKNOWLEDGEMENTS

First I am sincerely grateful to my supervisor Professor Annette Dolphin for her guidance and attention throughout my PhD. I am also indebted to our collaborators Drs. Jane Barclay and Michele Rees for making this project possible.

Many people assisted me in my work and I would like to thank them all for their help and support. I thank Jo-Maree Courntey for providing excellent technical assistance in the genotyping of *ducky* mice and Mick Keegan for looking after them. Special thanks also to Professor Steven Hunt for sharing his facilities and expertise in immunohistochemistry as well as Anne Sheasby for valuable technical advice. Everyone in the confocal imaging unit deserves a mention, with particular thanks to Dr. David Becker, Darran Clements and Daniel Ciantar for their superb facilities and generous technical support and advice. Of particular help was Dr. Kevin Bittman who introduced me to the art of Purkinje cell injection. Many thanks go to Drs. Alistair Mathie and David Boyd for their help and expertise in the use of the calcium imaging system and David Osborne for his cunning design of the recording chamber.

Furthermore and above all, many thanks to the entire group of Annette Dolphin for all the little and at times not so little pieces of help and advice. Especially Dr. Nick Berrow for many helpful discussions and sound technical advice. This also includes Dr. Tony Davies and Adrian Butcher for sharing their knowledge in protein biochemistry as well as the finer nuances of English spelling. Nuria Balaguero and Dr. Carles Canti who were excellent fun to work with and definitely kept my spirits up. This is also true for Ayesha Raghib and her immunocytochemical insights, Dr. Federica Bertaso for her humour and relentless proofreading capabilities and Dr. Patricia Viard who has been a marvellous presentation coach.

Ganz besonders herzlich möchte ich mich bei meiner Mutter bedanken, ohne ihre dauerhafte Unterstützung wäre es nicht zu dieser Doktorarbeit gekommen.

This study was funded by a Prize studentship of the Wellcome Trust.

CONTENTS

LIST OF FIGURES

CHAPTER I. INTRODUCTION

CHAPTER II. MATERIALS AND METHODS

CHAPTER III. PURKINJE CELL MORPHOLOGY

CHAPTER IV. IMMUNOCYTOCHEMISTRY

CHAPTER V. CALCIUM IMAGING

CHAPTER VI. GENERAL DISCUSSION

LIST OF TABLES

CHAPTER I. INTRODUCTION

CHAPTER II. MATERIALS AND METHODS

CHAPTER III. PURKINJE CELL MORPHOLOGY

CHAPTER IV. GENERAL DISCUSSION

LIST OF ABBREVIATIONS

AA	amino acid
AD	autosomal dominant
AID	α interaction domain
AM	acetoxy-methylester
AMPA	α-amino-3-hydroxy-5-methyl-4-isoxazole proprionate
ω-Aga IVA	ω-agatoxin IVA
ω-CTX GVIA	ω-conotoxin GVIA
ω-CTX MVIIA	ω-conotoxin MVIIA
APS	ammonium persulphate
AR	autosomal recessive
BAPTA	K3-1,2-bis (aminophenoxy) ethane-N,N,N9,N9-tetra-acetic acid
BDNF	brain derived nerve growth factor
BID	β interaction domain
bp	base pairs
BSA	bovine serum albumin
Ca^{2+}	ionized calcium
$[Ca^{2+}]_i$	intracellular calcium concentration
CAM	calmodulin
CCD	charged coupled device
CICR	calcium-induced calcium release
CNS	central nervous system
DAPI	4, 6- diamidino-2-phenylindole dihydrochloride
DCN	deep cerebellar nuclei
DEPC	diethyl-pyrocarbonate
dH_2O	distilled water
DHP	dihydropyridine
DIV	day in vitro
DMEM	Dulbecco's modified Eagle's medium
dNTP	deoxynucleotide triphosphate
DNA	deoxyribonucleic acid
DOPE	dioleolyl-phosphatidyl-ethanolamine
DTT	dithiothreitol

EA2	episodic ataxia type 2
ECL	enhanced chemiluminescence
EDTA	ethylene-diamine-tetra-acetic acid
EEG	electro encephalogram
EGTA	ethylene glycol-bis(beta-aminoethyl ether)-N,N,N',N'-tetraacetic acid
EPSC	excitatory postsynaptic currents
ER	endoplasmic reticulum
FCS	foetal calf serum
FHM	familial hemiplegic migraine
FUDR	fluorodeoxyuridine
GABA	γ-amino butyric acid
GCL	granule cell layer
GFP	green fluorescent protein
GFAP	glial acidic fibrillary protein
GS	goat serum
HEK	human embryonic kidney
HEPES	N-[2-Hydroxyethyl]piperazine-N'[2-ethanesulphonic acid]
HRP	horseradish peroxidase
HS	horse serum
HVA	high voltage activated
IGE	idiopathic generalised epilepsies
$InsP_3$	inositol 1,4,5-triphosphate
$InsP_3R$	inositol 1,4,5-triphosphate receptor
kb	kilo base
kDa	kilo Dalton
LTD	long-term depression
LTP	long-term potentiation
LTS	low threshold spike
LVA	low voltage activated
MEM	minimal essential medium
MOC	mechanically operated channel
MOL	molecular layer
mRNA	messenger ribonucleic acid
NBCS	new born calf serum

NMDA	N-methyl-D-aspartate
nRT	nucleus reticularis thalami
OD	optic density
P	postnatal
PBS	phosphate buffered saline
PCL	Purkinje cell layer
PCR	polymerase chain reaction
PMCA	plasma membrane Ca^{2+} ATPase
PVDF	polyvinylidene difluoride
RMP	resting membrane potential
RN	relay neuron
RNA	ribonucleic acid
ROC	receptor operated channel
RPM	rounds per minute
RT	room temperature (21-23 C°)
RT-PCR	reverse transcription-polymerase chain reaction
RyR	ryanodine receptor
SERCA	sarcoplasmic/endoplasmic reticulum ATPase
SBTI	soybean trypsin inhibitor
SCA6	spinocerebellar ataxia type 6
S.D.	standard deviation
SDS	sodium dodecyl sulphate
S.E.M.	standard error of the mean
SNAP25	synaptosomal-associated protein of 25 kDa
SOC	store operated channel
SWD	spike wave discharge
TBS	Tris buffered saline
TEMED	N, N, N, N -tetramethylenediamine
TH	tyrosine hydroxylase
TrKB	tyrosine kinase B
UV	ultra violet
VDCC	voltage-dependent calcium channel
VN	vestibular nuclei
VOCC	voltage operated calcium channel

CHAPTER I.

INTRODUCTION

1.1 THE CONCEPT OF Ca^{2+} AS A MESSENGER

1.1.1 BEGINNINGS

Calcium was probably one of the first chemical insults with which life had to cope. When life on earth was just beginning, about three billion years ago, CO_2 tension in the oceans was low, resulting in a high pH (8 to 9). At this pH, calcium salts are relatively insoluble, and thus the concentration of ionized calcium in the sea was low, perhaps around 0.1μM. This was probably a necessary circumstance for early evolution since high concentrations of calcium would have been incompatible with the phosphate economy on which early life forms depended. However, as life expanded throughout the planet, CO_2 production gradually acidified the seas, and Ca^{2+} salts began to dissolve. Thus, by about two billion years ago the ionized Ca^{2+} concentration could have reached 10μM, on its way to the 10mM concentration in seawater today. Kazmierczak and Degens (1986) suggest that it may have been at this time that successful species began to develop mechanisms to exclude Ca^{2+} from the cytoplasm of their cells. All life forms today have retained this remarkable capacity to maintain low concentrations of cytoplasmic Ca^{2+}; in eukaryotic cells the gradient of Ca^{2+} concentration across the plasma membrane is some 10,000-fold. Disruption of the ability of the cell to preserve this gradient is generally stressful, often fatal. However, at some point in the course of evolution, certain cells also developed a means to exploit this huge [Ca^{2+}] gradient for purposes of information transfer across the membrane; i.e. the regulated introduction into the cell of small quantities of Ca^{2+} serves as an intracellular messenger.

1.1.2 INTRACELLULAR CALCIUM HOMEOSTASIS

The calcium ion is an ubiquitous intracellular messenger that controls diverse cellular processes from fertilization and cellular differentiation to muscle contraction and synaptic transmission (Clapham, 1995; Berridge *et al.*, 1998). The finely regulated spatial and temporal encoding of calcium signals ensures that these various calcium-dependent processes are activated appropriately within the cell (Bito *et al.*, 1997; Berridge, 1998). This cell type-specific simultaneous interplay of several counteracting processes of Ca^{2+} influx, transport and binding is summarized in Figure 1.1. Channels located in the plasma membrane connect the cytoplasm to the 'inexhaustible' supply of Ca^{2+} from the extracellular space. According to the stimulus triggering their opening they can be divided into voltage-dependent calcium channels (VDCCs), receptor operated Ca^{2+} channels (ROCs), store operated Ca^{2+} channels (SOCs) and mechanically operated Ca^{2+} channels (MOCs). VDCCs will be discussed in more detail in Section 1.2; ROCs (e.g. nicotinic acetylcholine receptors, N-methyl-D-aspartate (NMDA) receptors) are activated by agonist binding to the extracellular domain of the channel (e.g. ATP, serotonin, glutamate, acetylcholine); MOCs convey information into the cell relating to the stress/shape changes that a cell is experiencing (e.g. tracheal cilia beating) and SOCs are activated in response to depletion of intracellular Ca^{2+} stores, the mechanism by which the SOCs sense this is yet unknown. The channels in the plasma membrane work in combination with channels on the endoplasmic and sarcoplasmic reticulum (ER and SR respectively), which release the finite intracellular Ca^{2+} pool. They consist mainly of the ubiquitously expressed inositol 1,4,5-trisphosphate (IP_3) receptor and ryanodine receptor of excitable cells.

Upon stimulation by depolarization, mechanical deformation, or transmitter molecules, the intracellular calcium concentration can rise from around 10-100nM to over 1μM. Whereas the influx of calcium through VDCCs triggers rapid secretion at synapses (Dunlap *et al.*, 1995; Neher, 1998), the release of calcium from stores in response to IP_3 can generate sustained $[Ca^{2+}]_i$ oscillations in both excitable and non-excitable cells (Berridge, 1993). These Ca^{2+} oscillations can be decoded in the cytosol by frequency–sensitive effector proteins such as

calmodulin-dependent kinase II (De Koninck and Schulman, 1998) and have been found to increase both secretion (Tse *et al.*, 1993) and gene transcription (Dolmetsch *et al.*, 1998; Li *et al.*, 1998). Calcium oscillations can also be decoded by mitochondria (Hajnoczky *et al.*, 1995), several dehydrogenases being activated as the free $[Ca^{2+}]$ increases within the mitochondrial matrix, thereby increasing the level of NAD(P)H and the production of ATP to meet the cell energy demand. $[Ca^{2+}]_i$ mediates multiple signalling cascades that are critical for cell survival, including Ca^{2+}/calmodulin-dependent-kinase kinase, protein kinase B and the phosphorylation of BCL-2 family member BAD (Yano *et al.*, 1998).

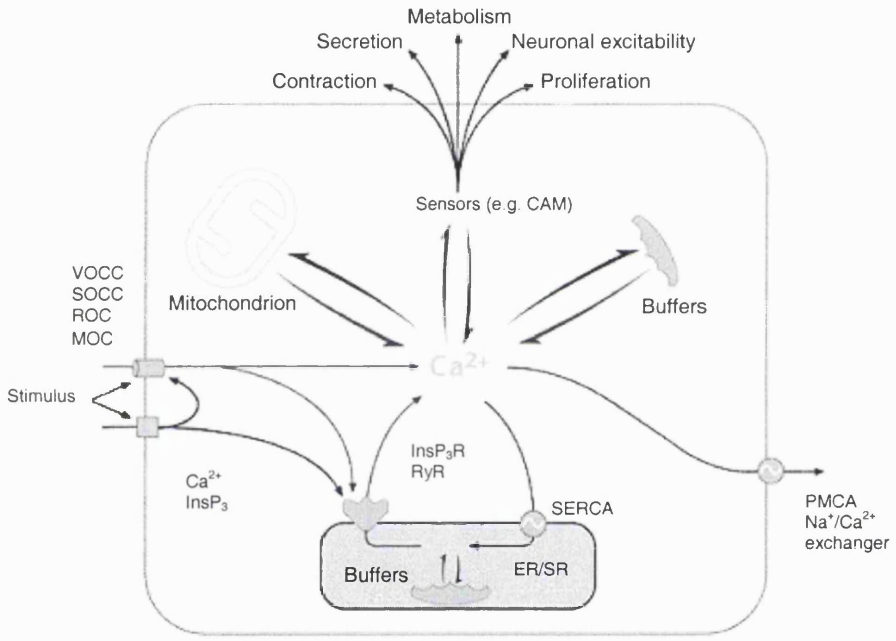

Figure 1.1 Intracellular calcium homeostasis. PMCA plasma membrane Ca^{2+} ATPase; SERCA sarcoplasmic/endoplasmic reticulum Ca^{2+} ATPase; CAM calmodulin. VOCC voltage-, ROC receptor-, SOCC store- operated calcium channel. $InsP_3R$ Inositol 1,4,5 triphosphate receptor, RyR ryanodine receptor. Different cell types express various combinations of these channels, ATPases and exchangers according to their physiologic specialization.

Routes to remove Ca^{2+} from the cytoplasm include Ca^{2+} ATPases on the plasma membrane and ER/SR, in addition to exchangers that utilize gradients of other ions to provide the energy to transport Ca^{2+}, e.g. Ca^{2+}/Na^+ exchange. In combination with these active extrusion mechanisms, the cell contains several Ca^{2+}-binding proteins (e.g. calbindin, parvalbumin). Dependent on their dissociation constant they bind and release Ca^{2+} in response to changing levels of $[Ca^{2+}]_i$ (Baimbridge *et al.*, 1992). Both increased (Choi, 1988) and decreased (Koike *et al.*, 1989; McCaslin and Smith, 1990; Koh and Cotman, 1992) intracellular Ca^{2+} have been reported to be cytotoxic in neurones.

1.2 VOLTAGE GATED CALCIUM CHANNELS

Voltage-dependent calcium channels are multimeric protein complexes of up to five components encoded by four different genes (Figure 1.2). The principal pore-forming α_1 subunit of 190 to 250 kDa is associated with a mostly extracellular $\alpha_2\delta$ subunit of 166 to 200 kDa, an entirely intracellular β subunit of 55 to 72 kDa, and in skeletal muscle and probably some brain calcium channels a membrane bound γ subunit of 25 to 38 kDa. Multiple isoforms of all subunits have been identified, a finding further diversified by the existence of splice variants. All but the two exclusively skeletal isoforms $Ca_V1.1$ and $Ca_V\gamma_1$ are expressed in the brain.

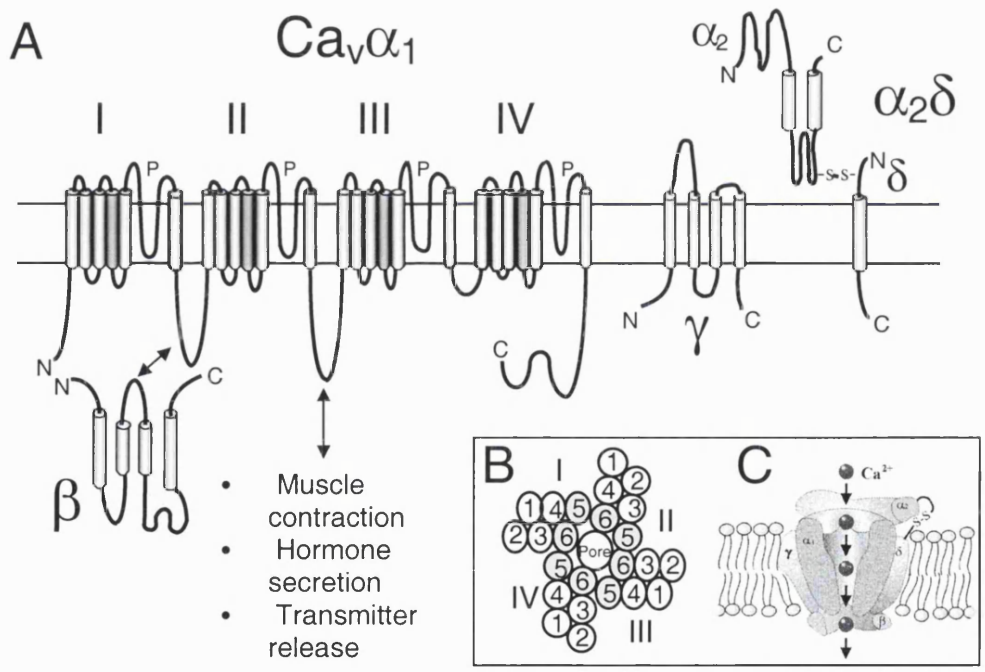

Figure 1.2 **A** Topology of VDCCs. The pore-forming α_1 subunit comprises four domains (I-IV), each consists of six transmembrane-spanning helices (S1-S6). The fourth helix (S4 dark grey) of each domain is highly charged and acts as a voltage sensor. The extracellular loop between the fifth (S5) and sixth (S6) helices dip into the membrane, and contribute to the channel pore (P). The cytoplasmic loop between domain II and III is important for excitation-contraction coupling in skeletal muscle and for excitation-secretion coupling in neurones. The whole structure is envisaged to fold around, with the amino and the carboxy termini meeting, to form a barrel like structure (see insets **B** and **C**). The β-subunit lacks α-helices capable of spanning the membrane, suggesting that it is entirely intracellular. It interacts with the α_1 subunit via the cytoplasmic loop between domains I and II. The α_2 and δ subunits are encoded by a single gene and postranslationaly processed to form two disulphide-linked polypeptides. The δ-subunit traverses the plasma membrane whilst the α_2 component is entirely extracellular. The γ-subunit has four transmembrane domains. Adapted from Walker and de Waard, 1998.

1.2.1 NOMENCLATURE OF VDCC SUBUNITS

Calcium channels have originally been divided according to their electrophysiological and pharmacological properties into $L_{ong\text{-}lasting}$–type, $P_{urkinje}$-type, Q-type, $N_{either\ L\ nor\ T}$, $R_{emaining}$–type and $T_{ransient}$-type. Molecular cloning revealed many genes encoding each type. The first consensus nomenclature resulted in the α_1X names. To bring more structure to this still-growing family of channel proteins a new nomenclature has recently been adopted (Ertel *et al.*, 2000). Based on sequence homology, it designates the permeant ion (Ca^{2+}), the mechanism of channel gating (voltage, v), followed by the gene family number and the subfamily member (Table1.1).

	Type	α_1X name	Ca_v name	Gene name	Chromosomal Location	Primary tissue	Accession No.
$Ca_v\alpha_1$ subunits	L	α_{1S}	$Ca_v1.1$	*CACNA1S*	1q31-q32	Skeletal muscle	Q13698
	L	α_{1C}	$Ca_v1.2$	*CACNA1C*	12p13.3	Heart	Q13936
	L	α_{1D}	$Ca_v1.3$	*CACNA1D*	3p14.3	Brain, Kidney, Cochlea	Q01668
	L (?)	α_{1F}	$Ca_v1.4$	*CACNA1F*	Xp11.23	Retina	AJ224874
	P/Q	α_{1A}	$Ca_v2.1$	*CACNA1A*	19p13.1-.2	Brain, Cochlea Pituitary	O00555
	N	α_{1B}	$Ca_v2.2$	*CACNA1B*	9q34	Brain, nervous system	Q00975
	R	α_{1E}	$Ca_v2.3$	*CACNA1E*	1q25-q31	Brain, cochlea, retina, heart, pituitary	Q15878
	T	α_{1G}	$Ca_v3.1$	*CACNA1G*	17q22	Brain, Nervous system	AF190860
	T	α_{1H}	$Ca_v3.2$	*CACNA1H*	16p13.3	Brain, Heart, Kidney, Liver	AF051946
	T	α_{1I}	$Ca_v3.3$	*CACNA1I*	22q12.3-q13.2	Brain	AAF25722

Table 1.1 Classification of voltage-dependent calcium channel α_1 subunits. The chromosomal location refers to the human sequence and the accession number for one representative full-length coding sequence.

The nomenclature of the auxiliary subunits remains unchanged (Table1.2).

	Subunit	Gene name	Chromosomal location	Accession No.
Ca_v auxiliary subunits	$\alpha_2\delta$-1	*CACNA2D1*	7q21-q22	P54289
	$\alpha_2\delta$-2	*CACNA2D2*	3p21.3	AF040709
	$\alpha_2\delta$-3	*CACNA2D3*	3p21.1	CAB75962
	β_1	*CACNB1*	17q11.2-q22	Q02639
	β_2	*CACNB2*	10p12	NM_000724
	β_3	*CACNB3*	12q13	P54284
	β_4	*CACNB4*	2q22-q23	O00305
	γ_1	*CACNG1*	17q24	Q06432
	γ_2	*CACNG2*	22q12-q13	AF096322
	γ_3	*CACNG3*	16p12-p13.1	AF100346
	γ_4	*CACNG4*	17q24	AF142625
	γ_5	*CACNG5*	17q24	AF142621
	γ_6	*CACNG6*	19q13.4	AF288386
	γ_7	*CACNG7*	19q13.4	AF288387
	γ_8	*CACNG8*	19q13.4	AF288388

Table 1.2 Classification of auxiliary voltage-dependent calcium channel subunits is based on proteins identified to co-purify with the skeletal muscle dihydropyridine receptor. Subsequent cloning revealed additional family members of each subunit. These are named in chronological order of discovery. Also shown are the location of the genes on human chromosomes and the accession number of a representative full-length coding sequence.

1.2.2 THE $Ca_V\alpha_1$ SUBUNIT

Voltage-dependent calcium channels consist minimally of a pore-forming, selectively calcium permeant α_1 protein (Mori *et al.*, 1991). This subunit contains the voltage sensor, interaction sites for the β, and $\alpha_2\delta$ calcium channel subunits, βγ subunits of G proteins, and is target for several agonist and antagonist drugs. According to their biophysical properties, calcium channels have been divided into high- and low- voltage-activated (HVA and LVA respectively) (Figure 1.3). Seven individual genes have been identified that code for the HVA channels and three for LVA channels. Although the co-operative modulatory effect of auxiliary subunits on HVA channels is well established, it remains to be seen as to what extent LVA channels are associated with other proteins.

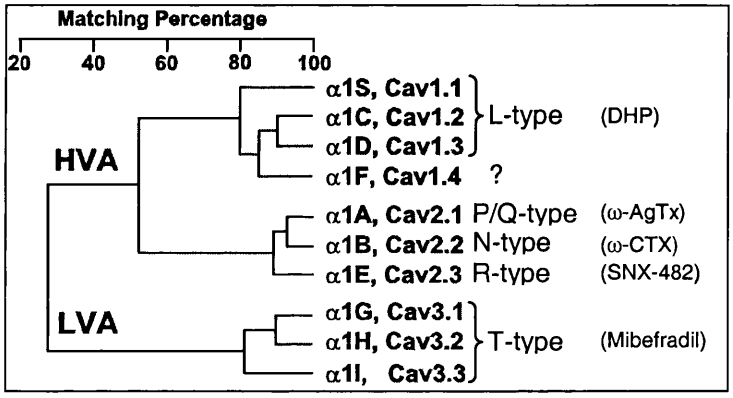

Figure 1.3 Phylogeny of VDCC α_1 subunits. Toxin sensitivity in brackets: DHP dihydropyridine, ω-AgTX ω-agatoxinIVA, ω-CTX ω-conotoxinGIVA. Adapted from Ertel *et al.*, (2000).

1.2.2.1 $Ca_V1.X$, L-type, (α_{1C}, α_{1D}, α_{1S}, α_{1F})

This calcium channel family is sensitive to dihydropyridines, phenylalkylamines and benzothiazepines. Found in skeletal, cardiac and smooth muscles, in fibroblasts, kidney and also in neuronal and endocrine tissue, their functional role is rather diverse. In skeletal muscle $Ca_V1.1$ is crucial for excitation-contraction coupling, which does not require influx of Ca^{2+} through the channel (Rios *et al.*, 1992). Mutations in the $Ca_V1.1$ produce a range of muscle-related pathologies in rodents and man, including hyperkalaemic periodic paralysis and muscular dysgenesis (Knudson *et al.*, 1989; Chaudhari, 1992; Jurkat-Rott *et al.*, 1994; Ptacek *et al.*, 1994). $Ca_V1.2$ is involved in the cardiac action potential, but also found in CNS (Mikami *et al.*, 1989). $Ca_V1.3$ is the major neuronal L-type

channel involved in Ca^{2+}-dependent gene expression (Bito *et al.*, 1997) and dendritic release of peptides (Simmons *et al.*, 1995).

$Ca_V1.3$ is also found in many endocrine cells (Seino *et al.*, 1992), where it is involved in stimulus secretion coupling (Chin *et al.*, 1992; Ashcroft *et al.*, 1994; Yang *et al.*, 1999). In neurones they activate calcium-activated potassium channels not participating in neurotransmitter secretion (Marrion and Tavalin, 1998). Recently a mutation in the retina-specific $Ca_V1.4$ (α_{1F}) subunit has been found to cause X-linked congenital stationary night blindness (Strom *et al.*, 1998; Bech-Hansen *et al.*, 1998), possibly by interfering with synaptic transmission in the retina (Schmitz and Witkovsky, 1997).

1.2.2.2 $Ca_V2.X$, P/Q-type, (α_{1A}), N-type (α_{1B}), R-type (α_{1E})

The $Ca_V2.X$ channel family is mainly neuronal and their first two members are involved in rapid release of neurotransmitters and secretion of hormones. A further characteristic is their modulation by G-proteins, whereby the $G\beta\gamma$ subunit binds to a conserved sequence (QXXER) in the I-II cytoplasmic loop of the α_1 subunit which is not present in L-type channels (Herlitze *et al.*, 1997; De Waard *et al.*, 1997; Zamponi *et al.*, 1997) close to the β subunit interaction domain (BID) and involving an interaction with β (Campbell *et al.*, 1995; Meir *et al.*, 2000).

$Ca_V2.1$ (P/Q-type, α_{1A}) is present in high levels in mammalian brain and peripheral nervous system (Mori *et al.*, 1991). High expression is found in cell bodies, dendrites and presynaptic terminals. $Ca_V2.1$ channels were first related to P/Q-type currents in an antisense study (Gillard *et al.*, 1997). P/Q-type channels are crucially involved in rapid neurotransmitter release at many excitatory and inhibitory synapses (Takahashi and Momiyama, 1993; Luebke *et al.*, 1993; Wheeler *et al.*, 1996). A direct interaction with the synaptic membrane proteins syntaxin1A and SNAP25 and their intracellular II-III loop could be shown (Walker and De Waard, 1998; Sutton *et al.*, 1999). The highest expression is found in cerebellar neurones (Westenbroek *et al.*, 1995) where α_{1A} (Stea *et al.*, 1994) produces a ω-agatoxin-IVA-sensitive current (Bourinet *et al.*, 1999). Kinetically and pharmacologically two current component can be distinguished (P- and Q-type), which arise by alternate splicing of the same gene (Starr *et al.*, 1991; Bourinet *et al.*, 1999). A preferential, but not exclusive interaction with β_4 could

further be demonstrated (Walker *et al.*, 1998). Mutations in $Ca_V2.1$ result in the human autosomal-dominant neurological disorders of familial hemiplegic migraine (Ophoff *et al.*, 1996), episodic ataxia type 2 (Ophoff *et al.*, 1996; Jodice *et al.*, 1997), spinocerebellar ataxia-6 (Zhuchenko *et al.*, 1997) and episodic-and-progressive ataxia (Yue *et al.*, 1997). In mice they cause the recessive inherited ataxic phenotypes of *tottering* (*tg*), *leaner* (tg^{la}) (Fletcher *et al.*, 1996), *rolling Nagoya* (tg^{rol}) (Oda, 1973) and *rocker* (tg^{rk}) (Zwingman *et al.*, 2001). At the neuromuscular junction the $Ca_V2.1$ subunit is believed to be important for acetylcholine release. Auto-antibodies against P/Q-type channels cause impaired neurotransmission and weakness in patients with paraneoplastic Lambert-Eaton myasthenic syndrome (Kim and Neher, 1988; Pinto *et al.*, 1998). Furthermore, a 95 kDa truncated $Ca_V2.1$ protein co-precipitates with the P/Q-type channels although its function is still unclear (Scott *et al.*, 1998).

$Ca_V2.2$ (N-type, α_{1B}) has been cloned exclusively from brain and peripheral nervous system (Lin *et al.*, 1996). N-type current can be blocked by low concentrations of ω-conotoxin GVIA (Dubel *et al.*, 1992). $Ca_V2.2$ is primarily expressed in dendrites and nerve terminals (Westenbroek *et al.*, 1992) and involved in neurotransmitter release (Dunlap *et al.*, 1995).

Initially $Ca_V2.3$ (R-type, α_{1E}) was characterized as an LVA T-type channel (Soong *et al.*, 1993). Later studies showed that the expressed channel has the activation and inactivation kinetics of an HVA calcium channel (Schneider *et al.*, 1994; Williams *et al.*, 1994) and some properties in common with the R-type current in cerebellar granule cells (Randall and Tsien, 1997).

1.2.2.3 $Ca_V3.X$, T-type, (α_{1G}, α_{1H}, α_{1I})

Three members of the T-type calcium channel family have recently been cloned (Cribbs *et al.*, 1998; Perez-Reyes *et al.*, 1998; Lee *et al.*, 1999a). They are low voltage activated and might be important for cardiac pacemaker activity and the oscillatory activity of several thalamic neurones. A role in neurotransmitter release in retinal bipolar cells has also been proposed (Pan, 2001). $Ca_V3.1$ and $Ca_V3.3$ are predominantly expressed in the central nervous system with low levels found in testis and lung (Talley *et al.*, 1999; Klugbauer *et al.*, 1999a; Kase *et al.*, 1999). In contrast, $Ca_V3.2$ is more ubiquitously expressed in many peripheral tissues, including heart, kidney and pituitary as well as the

central nervous system (Cribbs *et al.*, 1998; Williams *et al.*, 1999). When expressed in *Xenopus* oocytes, all three T-type α_1 subunits produce robust low voltage-activated currents (Cribbs *et al.*, 1998; Perez-Reyes *et al.*, 1998; Lee *et al.*, 1999; Klugbauer *et al.*, 1999; Williams *et al.*, 1999), thus implying functional expression without auxiliary subunits unless endogenous β subunits play a role (Tareilus *et al.*, 1997).

1.2.3 THE $Ca_V\beta$ SUBUNIT

Four types of β (β_{1-4}) subunits are encoded by four genes (Ruth *et al.*, 1989; Hullin *et al.*, 1992; Perez-Reyes *et al.*, 1992; Castellano *et al.*, 1993). These genes give rise to at least 13 splice variants that form entirely cytoplasmic, hydrophilic, non-glycosylated proteins between 55 and 72 kDa in size. They are expressed in a tissue-specific manner. Their general structure comprises two conserved segments around a central core region and divergence in the carboxy- and amino-terminal regions (Hanlon *et al.*, 1999). All of the isoforms have consensus sequences for phosphorylation implying common mechanisms of modulation. Coexpression with α_1 subunits increases the current amplitude and results in the modulation of both kinetics and voltage dependence of activation and inactivation (Singer *et al.*, 1991). The different β subunits produce specific inactivation behaviours. β_3 produces fast and β_2 slow, channel inactivation, whereas β_1 and β_4 induce more intermediate inactivation behaviour (Walker and De Waard, 1998). Furthermore, an apparent increase in recognition sites for channel-specific toxins has been reported, in line with their proposed role in the membrane targeting of the α_1 subunit (Brice *et al.*, 1997). Structurally this has been explained by a highly conserved α_1 subunit interaction domain (AID) found to bind (1:1) with high affinity to a highly conserved BID (β subunit interaction domain) region in the cytoplasmic loop between domain I and II of the α_1 subunit (Pragnell *et al.*, 1994) which functions as an ER retention signal (Walker *et al.*, 1998) antagonized by the β_3 subunit.

Disruption of this AID and BID interaction through point mutations also totally abolishes β subunit regulation (De Waard and Campbell, 1995). In the *lethargic* (*lh*) mutation however, the complete disruption of β_4 subunit function (Burgess *et al.*, 1997) has been shown to be compensated to some extent by other

β subunits (Burgess *et al.*, 1999a) resulting nevertheless in a severe phenotype. The knocking-out of the β_1 subunit on the other hand is lethal at birth (Gregg *et al.*, 1996), because of its role in muscle contraction.

1.2.4 THE $Ca_V\gamma$ SUBUNIT

For a long time the γ subunit was thought to be unique to the skeletal muscle $Ca_V1.1$ subunit with which it was originally co-purified (Flockerzi *et al.*, 1986) Recently a homologous gene was found to be disrupted in the *stargazer* mutation coding for the brain-specific $Ca_V\gamma_2$ subunit (Letts *et al.*, 1998). Since then, seven additional subunits have been identified in mouse and human (Black and Lennon, 1999; Burgess *et al.*, 1999b; Klugbauer *et al.*, 2000; Burgess *et al.*, 2001). Coded by eight genes, structurally the γ subunits are 35-38 kDa proteins with four putative transmembrane spanning segments according to hydrophobicity plots. The γ_1 subunit has been shown to modulate current density as well as the activation and inactivation kinetics of $Ca_V1.1$ (Singer *et al.*, 1991; Eberst *et al.*, 1997). In accordance with this, the Ca^{2+} influx was found to be increased in γ_1 subunit knock-out mice, combined with a depolarizing shift in the steady-state inactivation (Freise *et al.*, 2000). However the observed effects in the *stargazer* mutation have been only modest and γ_2 produced only a slight depolarizing shift in the steady state inactivation of $Ca_V2.1$ and not the predicted increase in current density of cerebellar granule cells. Therefore the role of neuronal gamma subunit might not entirely be connected to calcium channel function or in this case malfunction. This notion was recently further substantiated by a study which found the γ_2 subunit involved in the membrane targeting of the AMPA receptor (Chen *et al.*, 2000).

1.2.5 THE $Ca_V\alpha_2\delta$ SUBUNIT

Three genes have been identified which code for the $\alpha_2\delta$ subunit isoforms numbered $\alpha_2\delta$-1, $\alpha_2\delta$-2 and $\alpha_2\delta$-3 (Klugbauer *et al.*, 1999b). The $\alpha_2\delta$-1 subunit was initially co-purified with $Ca_V1.1$ from rabbit skeletal muscle (Nakayama *et al.*, 1987; Catterall *et al.*, 1988) and its cDNA sequence was determined by Ellis *et al.* (1988). It was also found associated with $Ca_V2.2$ (Witcher *et al.*, 1993) in brain. Expression was found to be ubiquitous, and although five tissue-specific splice variants of $\alpha_2\delta$-1 can be distinguished, their functional significance is still unclear (Angelotti and Hofmann, 1996). The second gene, *Cacna2d2* encodes a protein of approximately 190 kDa, with highest expression found in lung and testis and significant expression levels in brain, heart and pancreas (Gao *et al.*, 2000). *In situ* hybridization of mouse brain sections revealed the highest expression of the $\alpha_2\delta$-2 mRNA in the Purkinje cell layer of the cerebellum, habenula and septal nuclei, and lower expression in the cerebral cortex, olfactory bulb, thalamic and hypothalamic nuclei, as well as the inferior and superior colliculus (Barclay *et al.*, 2001). In contrast to this broad expression pattern, Northern analysis showed $\alpha_2\delta$-3 to be brain-specific.

1.2.5.1 Structure of $\alpha_2\delta$ subunits

Besides an amino acid sequence homology of 56% and 30% respectively, the $\alpha_2\delta$-2 and $\alpha_2\delta$-3 subunits share similarities in their hydrophobicity profiles and several other structural features with the $\alpha_2\delta$-1 subunit. A single transmembrane domain (AA1123 to 1139 in $\alpha_2\delta$-1) is predicted for all $\alpha_2\delta$ subunits. Encoded by a single gene the $\alpha_2\delta$ subunits are 166-200 kDa proteins that are post-translationally cleaved to yield entirely extracellular α_2 subunits which are anchored to the membrane by disulphide bonds to the membrane-spanning δ subunit, the latter having only 5 intracellular amino acids in the case of $\alpha_2\delta$-1 (Brickley *et al.*, 1995). This suggested that the interaction of this subunit with intracellular molecules such as protein kinases and G-proteins is unlikely (Gurnett *et al.*, 1996). The δ subunit has been found to be 53, 57 and 35 kDa in size for the respective subunits 1 to 3 (Marais *et al.*, 2001). Like $\alpha_2\delta$-1 (Gurnett *et al.*, 1996), $\alpha_2\delta$-2 and -3 have about 17 predicted N-glycosylation sites, their

heterogeneity might subserve tissue-specific modulation of channel function (Luo, 2000). Approximately 30-50 kDa is due to α_2 glycosylation in all isoforms (Marais *et al.*, 2001).

Structural studies have shown that the extracellular α_2 domain provides the structural elements required for channel stimulation (Gurnett *et al.* 1996) and the δ domain harbours the regions important for the shift in voltage-dependent activation, steady-state inactivation, and the modulation of the inactivation kinetics. The consensus sites on the extracellular loops of α_1 subunits to which the $\alpha_2\delta$ subunit binds have not been identified, although repeat III of $Ca_V1.1$ has been found to associate with α_2 (Gurnett *et al.*, 1997).

Two binding domains are conserved between the $\alpha_2\delta$ subunits, a von Willebrand factor type A domain and a Cache domain. Little is known about the function of the Cache domain besides its conservation in the $\alpha_2\delta$ subunits and various bacterial chemotaxis receptors (Anantharaman and Aravind, 2000). The von Willebrand factor type A domain is known to participate in cell-cell interaction, cell-matrix interaction and matrix formation in several proteins including von Willebrand factor, the α–chains of integrins and some types of collagen (Colombatti *et al.*, 1993; Lee *et al.*, 1995).

1.2.5.2 Effect of the $\alpha_2\delta$ subunit on calcium channels

Functional coexpression of the $\alpha_2\delta$-1 with various combinations of α_1 and β subunits results in an increase in the current densities. This was shown as an increase in $Ca_V1.1$ and $Ca_V1.2$ dihydropyridine binding sites, $Ca_V3.1$ immunostaining (Dolphin *et al.*, 1999) and to a lesser extent in $Ca_V2.2$ ω-conotoxin-GVIA binding sites (Singer *et al.*, 1991; Brust *et al.*, 1993; Welling *et al.*, 1993; De Waard and Campbell, 1995; Shistik *et al.*, 1995; Bangalore *et al.*, 1996; Gurnett *et al.*, 1996; Felix *et al.*, 1997; Parent *et al.*, 1997; Jones *et al.*, 1998). In agreement with these findings, $\alpha_2\delta$ increases ionic currents of $Ca_V1.1$, $Ca_V1.2$, $Ca_V2.1$ and $Ca_V3.1$ (Singer *et al.*, 1991; De Waard and Campbell, 1995; Bangalore *et al.*, 1996; Felix *et al.*, 1997; Qin *et al.*, 1998; Shirokov *et al.*, 1998; Dolphin *et al.*, 1999) and to a lesser extent also of $Ca_V2.2$. In COS-7 cells as well as oocytes, $\alpha_2\delta$ alone was ineffective in targeting $Ca_V1.2$ and $Ca_V2.1$ to the plasma membrane (Brice *et al.*, 1997; Gao *et al.*, 2000), but was sufficient in

HEK 293 cells for $Ca_V1.2$ (Felix *et al.*, 1997). For $Ca_V2.1$ the effect of $\alpha_2\delta$ is small in the absence of coexpressed β-subunits. In HEK 293 cells $\alpha_2\delta$ produced a small increase in the current densities of $Ca_V2.3$ currents, but had no effect on their biophysical properties (Jones *et al.*, 1998). Conversely in COS-7 cells as well as oocytes, the current activation of $Ca_V2.2$ was shifted to more positive potentials, whilst the effect on current density was very little (Stephens *et al.*, 1997; Qin *et al.*, 1998). A shift of the current-voltage curve in a hyperpolarizing direction could be observed for $Ca_V1.2$ (Singer *et al.*, 1991; Felix *et al.*, 1997). Taken together it appears that all HVA Ca^{2+} channel types have associated $\alpha_2\delta$ subunits, which enhance the functional expression of α_1, especially in the presence of other accessory subunits such as β. This implies a role in the spatial distribution of the Ca^{2+} channels. Less clear is the modulatory effect of $\alpha_2\delta$ subunit on calcium channel biophysical properties. One possible explanation for these discrepancies might lie in the various expression systems used in these studies. Endogenous calcium channel subunits for example, like those recently discovered in *Xenopus* oocytes, could interfere with, or occlude the observed effects (Lacerda *et al.*, 1994; Tareilus *et al.*, 1997).

1.2.5.3 Proposed mechanism of modulatory effects

Some mechanistic ideas concerning the observed modulatory effects have been developed. The increase in density of the current and DHP-binding sites can be understood by an improved targeting of the expressed α_1 subunit to the cell membrane, stability, and maturation of the channel complex (Shistik *et al.*, 1995), which leads to an increased amount of charge movement during channel activation (Bangalore *et al.*, 1996; Qin *et al.*, 1998). Deglycosylation and amino-terminal truncations involving the extracellular region of $\alpha_2\delta$ result in a reduction of the current amplitude (Gurnett *et al.*, 1996). Coexpression of the δ alone could mimic the observed shift in voltage dependence and kinetic effects of the current (Felix *et al.*, 1997). On the other hand, the sequence similarity between the three cloned subunits which are less well conserved in the δ proteins, suggests that α_2 may harbour the relevant residues responsible for the observed effects on α_1 and that the δ domain functions largely as a membrane anchor for α_2.

1.2.5.4 Gabapentin binding

Interestingly the $\alpha_2\delta$ protein has been implicated as the *in vivo* target of the antiepileptic drug gabapentin (Gee *et al.*, 1996), a structural analog of the inhibitory neurotransmitter γ-aminobutyric acid (GABA). It has been proposed that gabapentin binds preferentially to the $\alpha_2\delta$-1 subunit, based on the evidence that the partial N-terminal amino acid sequence of the binding-protein obtained from porcine brain membranes is identical with an amino-terminal peptide of $\alpha_2\delta$-1 not present in orthologs 2 and 3. *In situ* analysis of $\alpha_2\delta$-1 mRNA in brain showed the same distribution as that of gabapentin binding sites (Taylor *et al.*, 1998).

However, another study using a different purification procedure showed that there might be an additional binding protein in brain, which was detected with a polyclonal α_2 antibody (Brown and Gee, 1998). Recently it has been shown that $\alpha_2\delta$-2 also binds gabapentin, but $\alpha_2\delta$-3 does not (Marais *et al.*, 2001). For gabapentin binding, the α_2 and δ subunits are both essential although do not have to be necessarily disulphide linked (Wang *et al.*, 1999), yet the functional significance of this interaction is controversial. Reports show on the one hand no effect at therapeutic concentrations (10μM) on calcium channels (Rock *et al.*, 1993; Schumacher *et al.,* 1998), but on the other hand an inhibition of calcium currents in isolated rat neurones and synaptosomes has been reported (Stefani *et al.*, 1998; Fink *et al.*, 2000; Stefani *et al.*, 2001). A possible explanation could be a subtle action only apparent on a certain sub-population of channels or dependent on the experimental protocol used (Alden and Garcia, 2001; Maneuf and McKnight, 2001). It remains to be established whether other possible mechanisms play a role. Of particular interest is the recent report of a subtype-selective agonist action of gabapentin at the $GABA_B$ receptor (Ng *et al.*, 2001). The complexity of the gabapentin pharmacology, in that it functions as analgesic in neuropathic pain (Field *et al.*, 1997), anxiolytic (Singh *et al.*, 1996) and neuroprotective agent (Gurney *et al.*, 1996), in addition to its reported anti-convulsant properties, implies that there might be multiple biochemical events triggered by this drug (Taylor *et al.*, 1998).

1.2.6 INTERACTION OF THE $Ca_V\alpha_1$ SUBUNIT WITH INTRACELLULAR PROTEINS

In addition to the auxiliary calcium channel subunits, the α_1 subunits have been shown to interact with a wide range of intracellular proteins (Figure 1.4).

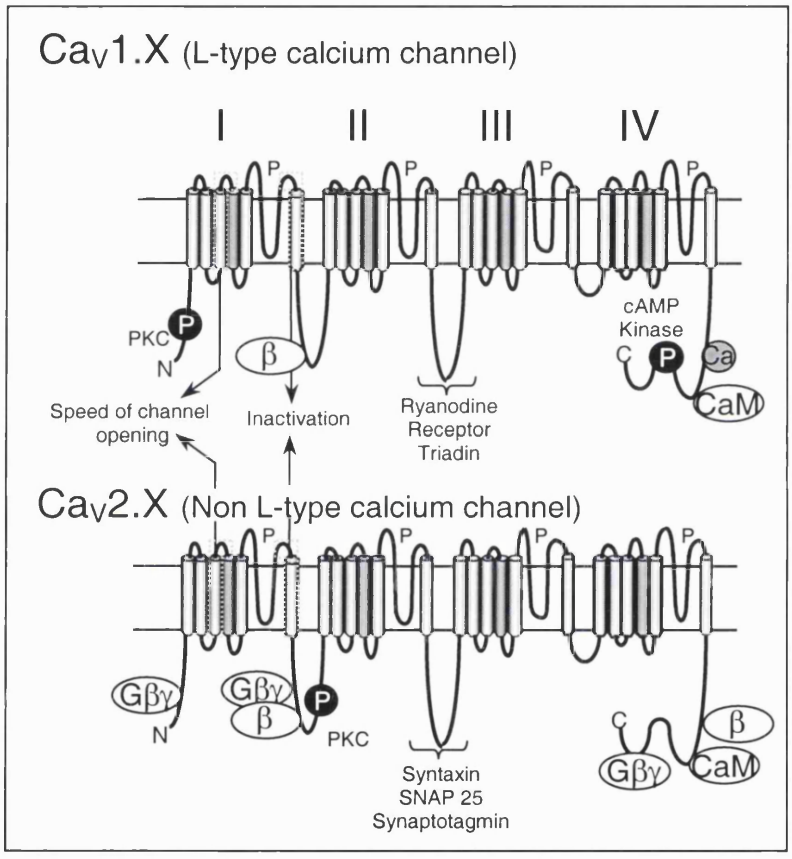

Figure 1.4 Interaction of the $Ca_V\alpha_1$ subunit with intracellular proteins. Differences between L- and non L-type HVA channels are indicated. Dotted lines show regions important for activation and inactivation kinetics. P sites for phosphorylation by protein kinase C and cAMP Kinase Ca Calcium-dependent inactivation. Binding sites for β subunits, G-protein Gβγ subunit, excitation-contraction coupling, synaptic membrane proteins SNAP25 and syntaxin are also shown.

In contrast to the rather promiscuous nature of the interaction with β–subunits, a distinction is evident between the interaction capacities of L-type and non L-type high voltage activated calcium channels, reflecting their functional separation.

1.3 ABSENCE EPILEPSY AND ATAXIA

Absence epilepsy is an idiopathic generalized, non-convulsive seizure disorder that is most common among children, with an onset between 2 and 16 years of age. Typical seizures are brief (<30s) and characterized by the spontaneous occurrence of bilaterally synchronous, symmetrical 2.5-4Hz cortical spike-wave discharges (SWD) recorded by electro encephalogram (EEG) (Noebels and Sidman, 1979), concomitant with behavioural arrest as well as impaired awareness. Until recently investigators had to rely on phenotypic criteria such as abnormal EEG discharges, associated behavioural abnormalities and profiles of pharmacological sensitivity to classify the underlying defect. Six well-defined spontaneously arising mouse models of inherited absence epilepsy have been described on this basis in the past few decades and accordingly named: *tottering* (*tg*), *lethargic* (*lh*), *stargazer* (*stg*), *mocha* (*mh*), *slow-wave epilepsy* (*swe*) and *ducky* (*du*). With the exception of *swe* (3-4Hz) they were all found to have 5-7Hz SWD bursts associated with behavioural arrest which, importantly, respond to anti-absence drugs that are efficacious in human (Noebels, 1986; Figure 1.5).

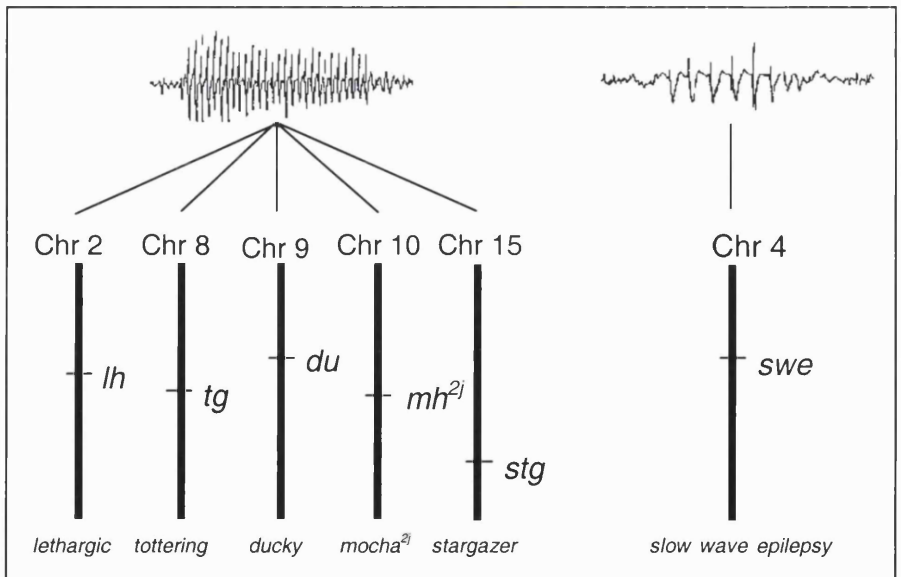

Figure 1.5 Murine mutations causing spike and wave discharges (SWD). The mutation in the calcium channel gene *Cacna2d2* is the fifth class of mutation in a calcium channel subunit to be associated with SWD in mice. Example traces of typical SWD are shown (7Hz on the left and 3 Hz on the right). The localization of the different mutation on mouse chromosomes is pictured.

Utilization of genetic mouse models, in particular, where functional properties of native channels can be readily studied, has led to significant insights into the pathological mechanisms underlying these disorders. Furthermore, the rare monogenic Mendelian nature of the epilepsies in these models has led to the identification of the underlying mutations by means of positional cloning. Thus recent analyses have revealed that four of the six mutated genes resulting in generalized SWD encode for calcium channel subunits. The *tottering* (*tg*) locus encodes the calcium channel $Ca_V2.1$ subunit gene *Cacna2.1* (Fletcher *et al.*, 1996), *lethargic* (*lh*) encodes the $Ca_V\beta_4$ subunit gene *Cacnb4* (Burgess *et al.*, 1997; McEnery *et al.*, 1998), *stargazer* (*stg*) encodes the $Ca_V\gamma_2$ subunit gene *Cacng2* (Letts *et al.*, 1998) and *ducky* encodes the $Ca_V\alpha_2\delta$-2 subunit gene *Cacna2d2* (Barclay *et al.*, 2001). The *swe* locus was identified as the ubiquitous Na^+/H^+ exchanger gene Slc9a1 (Cox *et al.*, 1997), and *mh* as the adaptor-related protein δ subunit gene Ap3d (Kantheti *et al.*, 1998) (Figure 1.6).

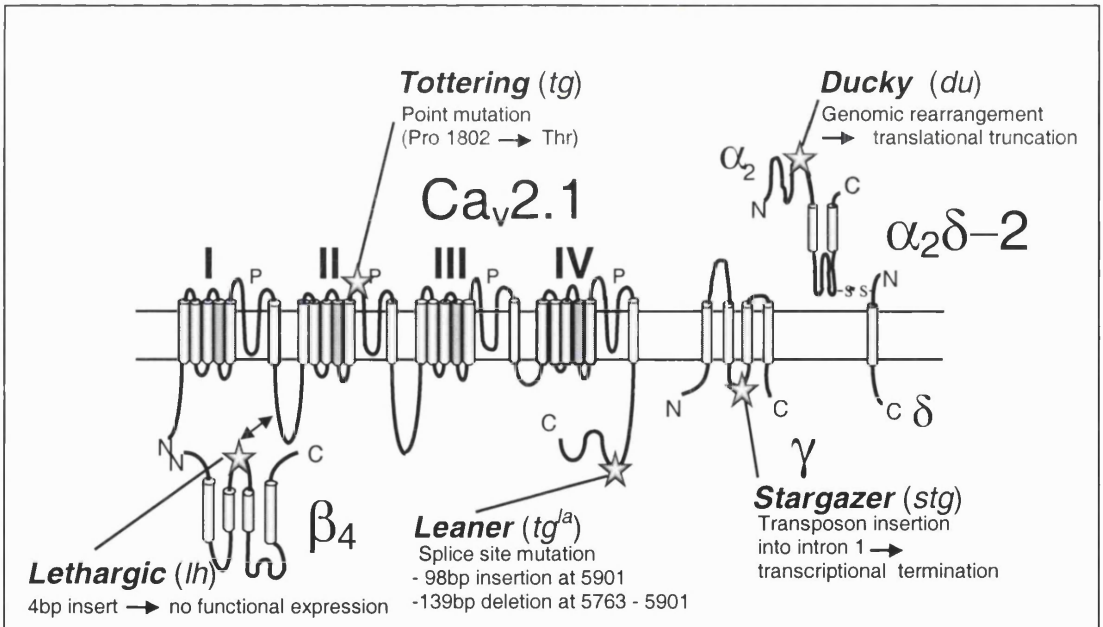

Figure 1.6 Location of five single gene mutations in VDCC subunits causing SWD. In *lethargic* loss of the β_4 subunit leads to a reduction in thalamic EPSCs, Purkinje cell calcium currents are unaffected. *Tottering* causes a reduction in Purkinje cell calcium currents and a reduction in thalamic EPSCs. *Stargazer* causes a small depolarizing shift in the $Ca_V2.1$, but no change in calcium current in cerebellar granule cells (not determined in Purkinje cells). *Ducky* leads to a reduction in calcium current in Purkinje cells.

Since the discovery of *tottering* and *leaner* in the $Ca_v2.1$ subunit additional alleles have been found: *rolling Nagoya* (*Cacna1a*$^{tg\text{-}rol}$), *rocker* (*Cacna1a*$^{tg\text{-}rk}$) and *tg*^{3J} (*Cacna1a*$^{tg\text{-}3J}$). The same is true for *stargazer* with *waggler* (*Cacng2*$^{stg\text{-}wag}$) and *stg*^{3J} (*Cacng*$^{stg\text{-}3J}$). Also for the *ducky* mutation a new allele, *du*^{2J} (*Cacna2d2*$^{du\text{-}2J}$) has recently been found (Barclay *et al.*, 2001). All these mutations are distinguishable according to the severity and onset of their phenotypic features (summarized in Table 1.3) and have in common a recessively inherited phenotype of ataxia in combination with SWD. Furthermore, in the *tottering* (*tg*) mutation and its alleles, several lines of evidence point towards an abnormal Purkinje cell function. One is a reduction in P/Q-type calcium current and changes in the voltage-dependence of channel kinetics as found in *tottering (tg)*, *rolling Nagoya* (*tg*^{rol}) and *leaner* (*tg*^{la}). Resulting in an up to 65% reduction of peak current density in the severest case of *leaner* (*tg*^{la}). Additionally in some cases (*tg*, *tg*^{la}, *tg*^{rk}), an aberrant increase in tyrosine hydroxylase (TH) expression was observed, which was found to colocalize with regions of zebrin II expression (Abbott *et al.*, 1996), indicating developmental malfunction. A malformation of Purkinje cells was found in *rocker* (*tg*^{rk}), characterized by a 'weeping willow' appearance of their dendrites. In the extreme case of the *leaner* (*tg*^{la}) mutation, Golgi and Purkinje cells are lost after the end of the first postnatal month. Furthermore, a reduced excitatory postsynaptic potential in the thalamus has been noted in *tottering* (*tg*) and *lethargic* (*lh*) as well as impaired synapse maturation in the *waggler* (*stg*^{wag}) mutation.

The study of this series of independent mutations might give insight into the molecular mechanism of SWD and might possibly reveal an underlying common pathological mechanism. Several genetic syndromes in humans and mice result from single gene mutations altering the function of neuronal ion channels (Gardiner and Lehesjoki, 2000). *Ducky* and other mice showing a phenotype of SWD are valid models for human absence epilepsy as sequence changes in *CACNAB4* and *CACNA1A* have been described in families with idiopathic generalized epilepsy (IGE) or ataxia (Yue *et al.*, 1997; Zhuchenko *et al.*, 1997; Ophoff *et al.*, 1998; Escayg *et al.*, 2000; Jouvenceau *et al.*, 2001). The *Cacna2d2* gene is therefore a candidate for human IGEs and ataxia. Elucidation of the affected pathways may allow design of novel anti-absence drug treatment aimed at a specific physiological target.

Table 1.3 Murine calcium channel mutations causing SWDs

Mutation		Phenotype: Ataxia	Seizures	Cerebellar cell death	SWD 5-7Hz	Mode of Inheritance	Gene	Gene Product	Nature of Mutation	Predicted effect	Physiological consequences	References
Tottering		√	√	√	√	← Autosomal recessive →	*Cacna1a*^{tg}	$Ca_V2.1$ (α_{1A})	Missense C1802T	P601L (IIS5-S6) Pore lining region	↓ P-type current density in Purkinje cells (-40%) changes in voltage dependence of inact. ↓EPSC ↑ $Ca_V1.2$ ↑TH $GABA_A$ receptor expression altered	1-5
Alleles	*Leaner*	√	√	√	√		*Cacna1a*$^{tg\text{-}ln}$		Splicing error 5901 98bp insertion 5763-5901 139bp deletion	Novel C-terminus from exon skip or intron inclusion Calmodulin binding domain	↓↓ P-type current in dissociated Purkinje cells (-65%) depolarizing shift in Purkinje cell current - slow cerebellar degeneration	1,2, 6-8
Alleles	*Rolling Nagoya*	√	√	-	√		*Cacna1a*$^{tg\text{-}rol}$		Missense C3784T	R1262G (IIiS5-S6)	↓ P-type current in dissociated Purkinje cells	9,10,11
Alleles	*Rocker*	√	√	-	√		*Cacna1a*$^{tg\text{-}rk}$		Missense C3929A	T1310K (IIiS5-S6) Pore lining region	↑TH, 'weeping willow' appearance of Purkinje cell dendrites	12
Alleles	*tg*^{3J}	√	√	-	√		*Cacna1a*$^{tg\text{-}3J}$		Unpublished AA substitution	(IIS5-S6) Pore lining region not far from *tg*		13
Lethargic		√	√	-	√		*Cacnb4*^{lh}	β_4	Splicing error	truncation with loss of α_1-binding site	↓EPSC ↑TH thickness of molecular layer; regional increase in $GABA_B$ receptor binding	3, 5 14-17
Stargazer		√	√	-	√		*Cacng2*^{stg}	γ_2	transposon insertion	early stop or splicing error reduced wild-type RNA	?↑ calcium entry; steady state inactivation of $Ca_V2.1$ more depolarized in absence of γ_2 ↓BDNF(-70%) TrKB pathway - immature $GABA_A$ receptor	18-21
Alleles	*Waggler*	√	√	-	√		*Cacng2*$^{stg\text{-}wag}$			reduced wild-type RNA	Impaired synapse maturation	18,19
Alleles	*stg*^{3J}	√	√	-	√		*Cacng2*$^{stg\text{-}3J}$			reduced wild-type RNA		23
Ducky		√	√	-	√		*Cacna2d2*^{du}	$\alpha_2\delta$–2	genomic rearrangement	transcriptional termination after exon 3		24
Allele	*du*^{2J}	√	√	-	√		*Cacna2d2*^{du2J}		2bp deletion	translational termination after exon 9		24

(1) Fletcher *et al.*, 1996, (2) Wakamori *et al.*, 1998; (3) Caddick *et al.*, 1999; (4) Campbell *et al.*, 1999; (5) Hess *et al.*, 1991; (6) Lorenzon *et al.*, 1998; (7) Dove *et al.*, 1998; (8) Lee *et al.*, 1999; (9) Nishimura *et al.*, 1976; (10) Mukoyama *et al.*, 1976; (11) Mori *et al.*, 2000; (12) Zwingmann *et al.*, 2001; (13) Frankel unpublished data; (14) Burgess et al., 1997; (15) Burgess *et al.*, 1999; (16) McEnery *et al.*, 1998; (17) Lin *et al.*, 1993; (18) Letts *et al.*, 1998; (19) Chen *et al.*, 1999; (20) Qiao *et al.*, 1996; (21) Qiao *et al.*, 1998; (22) Thompson *et al.*, 1998; (23) Letts unpublished data; (24) Barclay *et al.*, 2001. BNDF: Brain derived neurotrophic factor ; EPSP: Excitatory postsynaptic potential; GABA: γ–aminobutyric acid; TH: Tyrosine hydroxylase; TrkB: Tyrosine kinase B.

1.3.1 THE *DUCKY* MUTATION

The focus of this study will be on the autosomal recessive *ducky* mutation (Figure1.7), which arose spontaneously in the Jackson Lab (Snell, 1955). The *ducky* locus was mapped to mouse chromosome 9 by linkage to the markers *dilute* and *short ear* (Snell 1955). Positional cloning identified (*Cacna2d2*) the $\alpha_2\delta$-2 calcium channel subunit gene to underlie the *ducky* phenotype (Barclay *et al.*, 2001), which is apparent around day 14. Homozygote *du/du* mice show a wide based waddling gait and a tendency to fall to one side. They are smaller than normal and may occasionally have seizures. Viability is less than normal and there is usually a failure to survive beyond 35 days. Males living to maturity may be fertile, but are poor breeders. Females rarely breed (Snell 1955). Histologically, homozygotes show severe dysgenesis of the cerebellum, hindbrain and spinal chord, myelin deficiency that is more marked in the caudate CNS region, and demyelination and axonal dystrophy in selective fibre systems, including the spinocerebellar and vestibulospinal tracts (Meier, 1968).

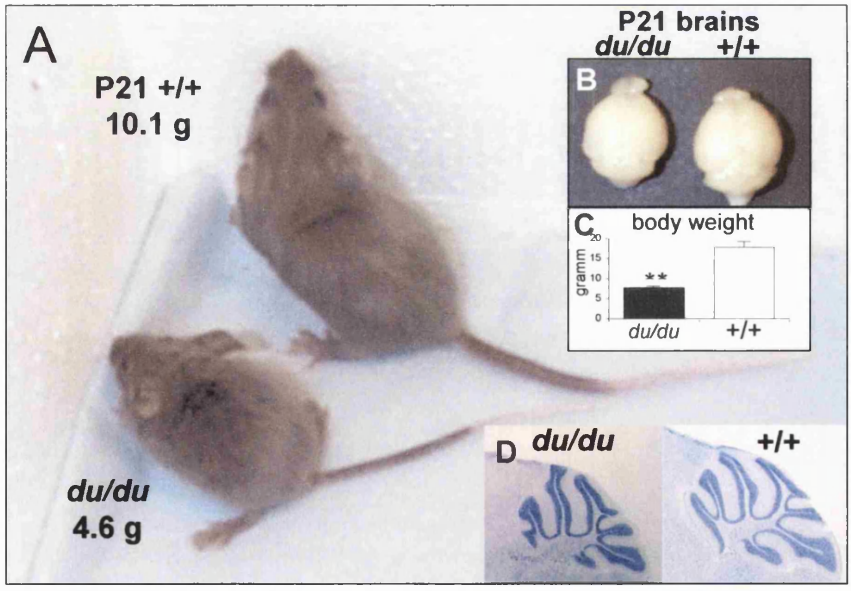

Figure 1.7 The *ducky* mouse. **A** Two littermates are shown at the weaning age of 21 days. The homozygous *du/du* is reduced in size and weight. The splayed stance results in a waddling gait. **B** shows a small size reduction in *du/du* brains compared to wild-type. A body weight comparison between +/+ (n=6) and *du/du* (n=6) mice showed a significant size reduction in *du/du* mice compared to +/+ (student's *t*-test $p<0.01$) **C**. The overall structure of the cerebellum is preserved as shown by cresyl violet staining in **D**.

1.3.1.1 PROPOSED MECHANISM OF THE DUCKY MUTATION

The *du* mutation is a genomic rearrangement involving the *Cacna2d2* gene. The proposed mechanism implies a head-to-tail duplication, a deletion and an inversion of genomic DNA (Figure 1.8). No full-length transcript (5.5kb) can be detected in *du/du* mice, but low levels of two distinct mutant transcripts (~1.5kb and 5kb respectively) have been detected by Northern blot analysis (Barclay *et al.*, 2001). Mutant transcript 1 (*du*-mut1 α_2) encodes the first 414 nucleotides of *Cacna2d2* followed by 24 novel nucleotides and a stop codon. Both mutant transcript 2 (*du*-mut2 α_2, exons 2-39) and *du*-mut1 α_2 could be amplified through RT-PCR.

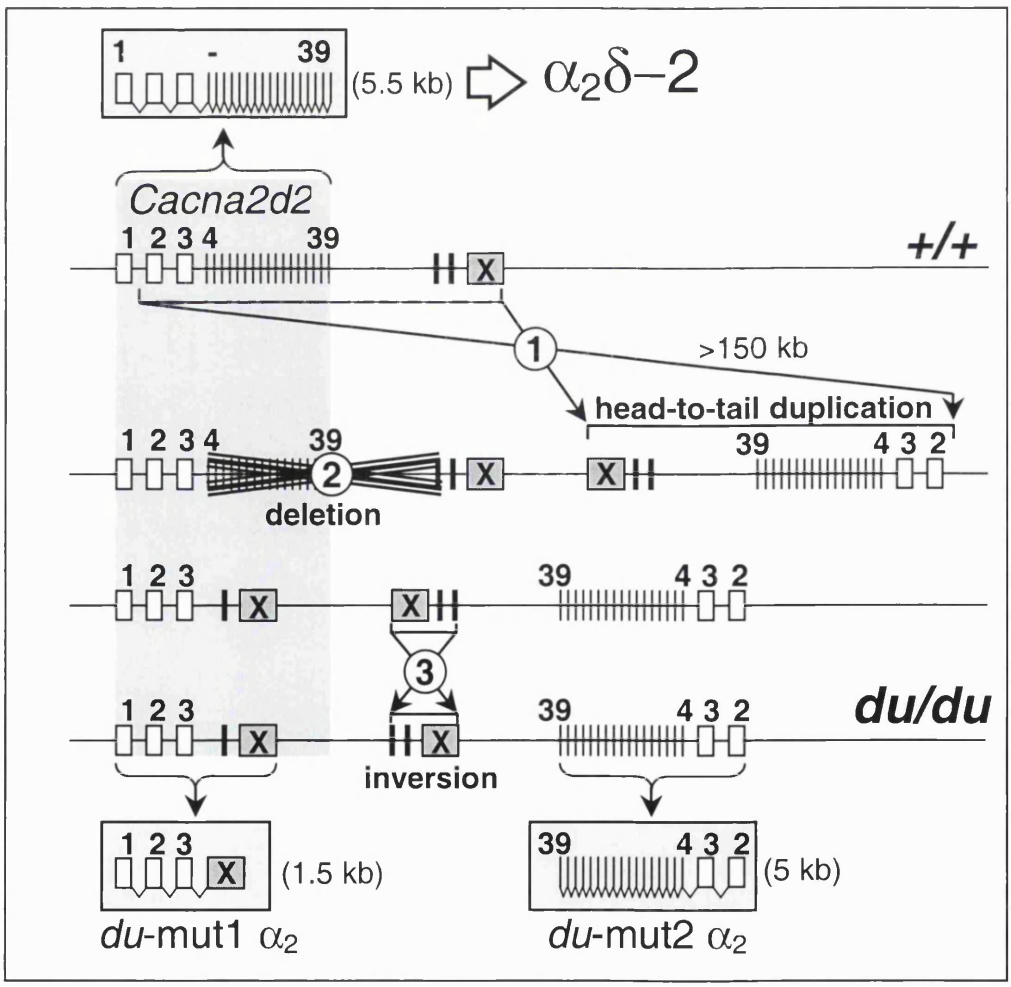

Figure 1.8 The genomic structure of the *Cacna2d2* gene (grey underlaid). The *Cacna2d2* gene consists of 39 exons spanning over a region of 85kb genomic DNA. The genomic rearrangement of the *ducky* involves a head-to-tail duplication①, a deletion②and an inversion③. The mutation is thought to results in the disruption of the *Cacna2d2* gene after exon 3, causing translational truncation (Barclay *et al.*, 2001)

The genomic rearragement in the *ducky* mutation affects over 150 kb of genomic DNA which are head-to-tail duplicated. It is therefore reasonable to consider the disruption of other genes within this region. However several lines of evidence suggest that the disruption of the *Cacna2d2* gene alone is the origin of the *ducky* phenotype resulting in a non-functional $\alpha_2\delta$–2 subunit. One of them is a recently discovered spontaneous, autosomal recessive mouse mutant with a phenotype similar to *du/du* that could be confirmed as a novel *ducky* allele; du^{2J}. Mutational analysis revealed a 2bp deletion within exon 9, predicted to cause premature truncation of the protein (GenBank accession number AF247142, Barclay *et al.,* 2001).

Interestingly all mouse mutants showing SWD, with the exception of *mocha*, have also an ataxic phenotype in common implying an involvement of the cerebellum.

Figure 1.9 Pictures were taken from the following sites

A http://www.public.iastate.edu/~cmdis470/ cerebellum

C Barclay et.al. 2001

B http://oto.wustl.edu/cerebellarconference

D www.hms.harvard.edu/research/brain/atlas.html

1.4 THE CEREBELLAR CORTEX

1.4.1 ANATOMICAL STRUCTURE OF THE CEREBELLUM

The cerebellum overlies the brainstem, behind the occipital lobes of the cerebral hemispheres. The cerebellum (little brain) represents only 10% of the total brain volume but contains more than half of the neurones in the central nervous system. This is due to the granule cells which are the most abundant neurone type in the central nervous system. Its most prominent cell type, the Purkinje cell is the biggest neurone in the cortex, comprising with up to 200,000 synaptic connections to parallel fibres also the highest number of connections for an individual neurone. The climbing fibre-Purkinje cell contact is one of the strongest synaptic connections in the whole brain. Although the cerebellum is one of the first structures of the brain to differentiate, it achieves its mature configuration in the mouse only one month after birth.

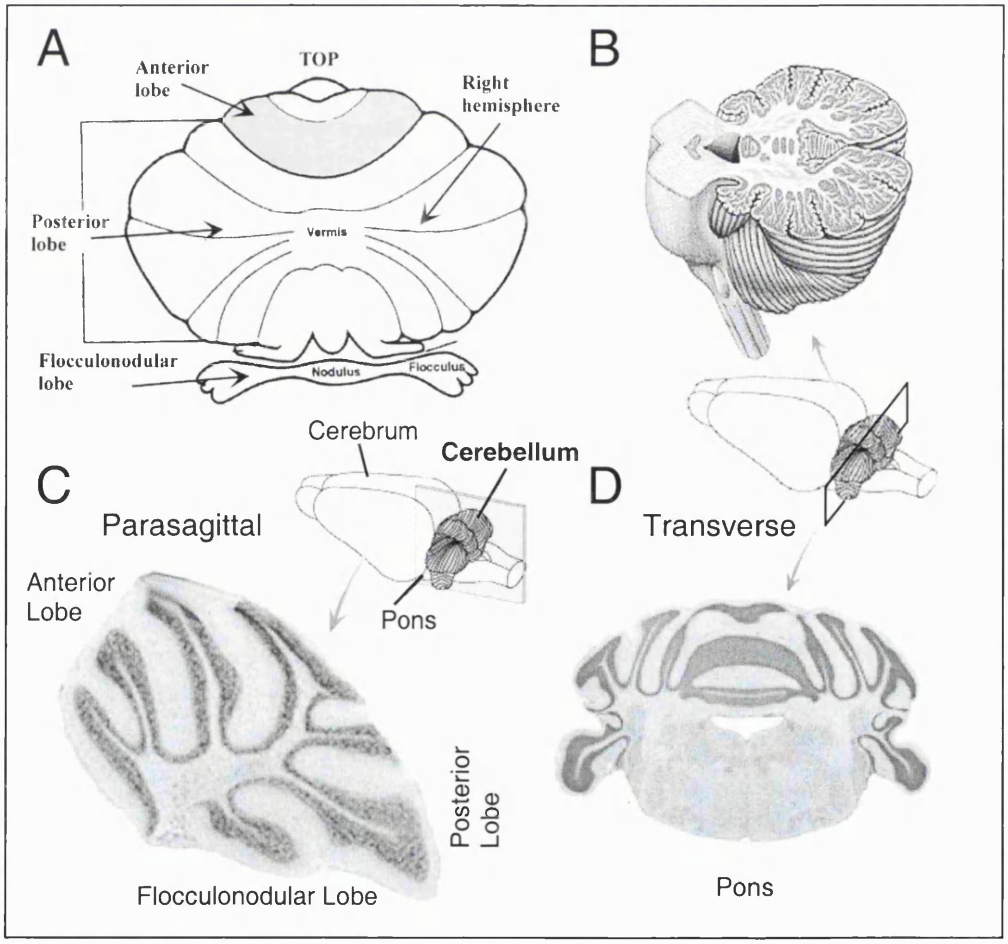

Figure 1.9 Gross anatomy of the cerebellar cortex **A** Dorsal view. Cerebellum can be divided longitudinally into a medial vermis, more lateral hemispheres and most lateral flocculi. **B** Transverse section shows its connection to the pons (ventral left anterior to the top). The cerebellar lobulation is seen in sagittal sections **C** (dorsal is upwards and anterior to the left). **D** same orientation as **B**.

1.4.2 CELL TYPES OF THE CEREBELLUM

Unlike the cerebrum, the composition of the cerebellum is remarkably simple, consisting of three layers comprising five different neuronal populations, which are structured in strict order. Purkinje cells and granule cells create the lamination of the cerebellum; the granule cells form the granule cell layer, the Purkinje cell somata form the Purkinje cell layer and the Purkinje cell dendrites and granule cell axons together form the molecular layer. The remaining classes of the cerebellar neurone populations are inhibitory interneurones including Golgi cells, which contain the neurotransmitters GABA and Glycine. They extend their axons deep into the molecular layer, receive synaptic input from parallel fibres and provide feedback inhibition to granule cell dendrites. The GABA-releasing stellate and basket cells are confined to the molecular layer. Basket cells receive their excitatory input from parallel fibres and their axons envelop Purkinje cell somata. Like basket cells, stellate cells are also excited by parallel fibres, they terminate on the shafts of the Purkinje cell dendrites, which they inhibit using GABA and possibly taurine as a neurotransmitter. Modern molecular techniques have revealed a bewildering array of subtypes of these cell types. This is most evident for the Purkinje cell, where at least six distinct molecular subtypes are known, each with a characteristic and highly stereotyped distribution, such as those that express zebrin II or aldolase C (Touri *et al.*, 1996). The functional significance of this heterogeneity remains unclear.

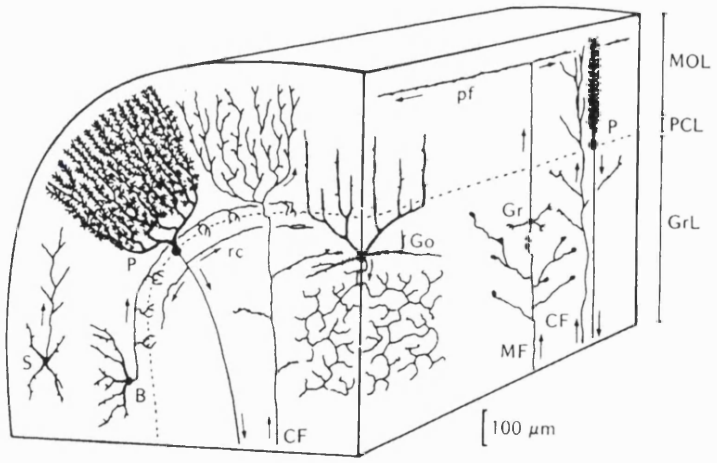

Figure 1.10 The cytoarchitecture of the cerebellar cortex. The major cell populations are shown. (MOL) molecular Layer, (PCL) Purkinje cell layer, (GrL) Granule cell layer. (pf) parallel fibre, (P) Purkinje cell, (Gr) granule cell, (CF) climbing fibre, (MF) mossy fibre (B) Basket cell (S) Stellate cell. The arrows indicate the direction of transmission. From Shephard, Neurobiology 1988.

1.4.3 CEREBELLAR CIRCUITRY

The two excitatory afferent pathways, the climbing fibres and the mossy fibres, converge onto the Purkinje cells. An individual climbing fibre synapses several hundred times on its target Purkinje cell. The identity of its neurotransmitter is still under debate, one candidate being aspartate. Climbing fibre activation leads to a large excitatory postsynaptic potential in the Purkinje cell dendrite that propagates as a calcium-dependent spike to the soma, where it triggers an all-or-nothing sodium-dependent action potential. The mossy fibre excitation passes through the granule cell relay and excites the Purkinje cells. In contrast to the climbing fibre input, mossy fibre excitation results in a graded response at the Purkinje cell that involves only the simple sodium-dependent spikes. The parallel fibre input to the Purkinje cells is highly convergent with perhaps 200,000 different parallel fibres synapsing with each Purkinje cell. Determined by its structure, the cerebellar cortex transmits the inhibitory result of cerebellar integration exclusively via Purkinje cells in a precise temporal succession directly onto target neurones of the deep cerebellar and vestibular nuclei. Thus the cerebellar cortex seems to produce a temporal pattern of inhibitory influence on these target neurones that modifies their excitatory action in such a way that an activation of muscle fibres occurs which progressively integrates the intended motion into the actual condition of the motoric repertoire. In consequence, disturbances that affect this cerebellar inhibition will cause uncoordinated and ataxic movements, commonly referred to as cerebellar ataxia.

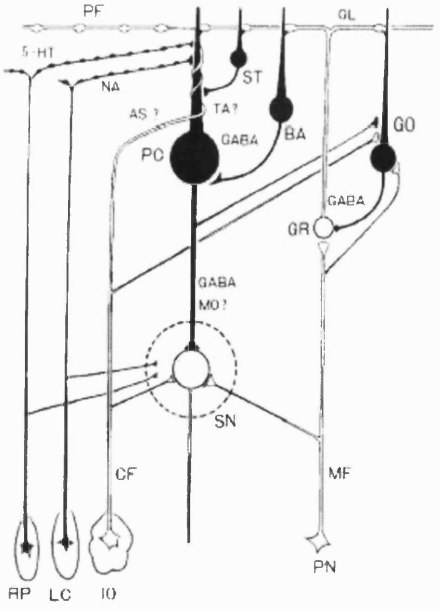

Figure 1.11 Cerebellar circuits and neurotransmitters. Cells: PC Purkinje cell, GO Golgi cell, BA basket cell, ST stellate cell, GR granule cell, SN neuron of the deep cerebellar nuclei. Fibres: PF parallel fibre, MF mossy fibre, CF climbing fibre. Inhibitory neurones and synapses black, excitatory in white. Neurotransmitter: GL Glutamate, AS Aspartate, TA Taurin, MO Motilin, NA Noradrenalin, 5-HT Serotonin. The origin of the cerebellar afferents: RP Raphe nuclei, LC Locus coreoleus, IO inferior olive. PN 'precerebellar' neurones projecting into the cerebellum. From Ito, 1984.

Cerebellar ataxia originates from a variety of hereditary as well as non-hereditary diseases (Klockgether and Evert, 1998). Recent progress in the identification of the responsible genes has allowed the classification of these diseases. Currently, the different types of spinocerebellar ataxia (SCA 1-7), the dentatorubral-pallidolysian atrophy and the group of episodic ataxias (EA) constitute the autosomal dominant ataxias, for which all the genes have been mapped. The recessively inherited ataxias include Friedreich's ataxia – the most frequent of all ataxias – the group of early onset ataxias, ataxia teleangiectasia, ataxia with isolated vitamin E deficiency, cerebrotendinious xanthomatose, abetalipo-proteinemia, Refsum's disease and granule cell layer hypoplasia.

Common to all these disorders is a combination of cerebellar motor symptoms like instability of posture and gait, incoordination, tremor and muscular hypotonia. The individual combination of symptoms, however, allows no precise prediction of the location or severity of a cerebellar lesion. Apart from secondary degenerative or compensatory mechanisms in the cerebellar cortex, the reason for this may be the neuronal reactions in the deep cerebellar (DCN) and vestibular nuclei (VN). Cerebellar pathology will lead to alterations in the inhibitory action of the cerebellar cortex on the DCN and VN, which they receive exclusively from Purkinje cells whose function or number have changed. A portion of the target neurones in the DCN and VN are extrinsic and give rise to cerebello-thalamic, cerebello-rubral, cerebello-reticular and vestibula-spinal connections thereby influencing motor performance on every level of planning and execution (Grusser-Cornehls and Baurle, 2001).

1.5 AIMS OF THIS STUDY

The aims of this study are to reveal how the mutation in the $\alpha_2\delta$–2 subunit affects cellular function, focussing mainly on the cerebellum. Mutations affect cells at different levels. In the *ducky* mutation, the first level might be an altered calcium entry, as the mutation is likely to affect the channel kinetics and activity or channel expression and turnover. The second level are consequences which an altered calcium entry might have on protein expression. These could then lead to changes in cellular functions important on the third level for neuronal interactions, which could result in a changed cell morphology. In order to address the possible alterations at these different levels, methods were chosen to examine the gross morphology of cerebellar Purkinje neurones, the expression level of selected proteins and the depolarization-induced Ca^{2+} influx (Table 1.4).

Structural Consequences	
→ Morphology	Lucifer yellow imaging
– Purkinje neurones	Golgi impregnation
→ Protein Expression	
– $\alpha_2\delta$–2 subunit	Immunocytochemistry
– Calbindin D-28K	Western Blotting
– GFAP	
– Caspases 3 and 12	
Functional Consequences	
→ Calcium Homeostasis	
– isolated Purkinje neurones	Calcium imaging
– cultured granule cells	

Table 1.4 The aims of this study in summary

CHAPTER II.

MATERIALS AND METHODS

2.1 SUPPLIERS

Unless otherwise stated, all materials were supplied by Sigma Aldrich Chemicals Ltd. (UK) at the highest available purity.

2.2 WATER QUALITY

The water used was purified through an Elga water purifier (Elga, High Wickham, UK) by reverse osmosis followed by deionisation and UV treatment to > 10MΩ. For cell culture and genotyping experiments the water was further purified to > 18MΩ (Elga, UHQ), and all solutions were additionally filter sterilized using 0.2μm membrane filters (Nalgene, Rochester, NY, USA).

2.3 CELL CULTURE AND TRANSFECTION

2.3.1 CULTURE OF tsA201 CELLS

tsA201 cells are a transformed HEK293 cell line, stably expressing a simian virus 40 (SV40) encoded large T antigen, the only viral product required to activate the SV40 origin of DNA replication. Transfection with recombinant plasmid DNA containing an SV40 origin and a functional transcription unit, leads to enhanced expression levels, as the introduced DNA is not only transcribed and translated but also multiplied through replication. Cells were kept in minimal essential medium (MEM, with Earle's salts and Glutamine; GibcoBRL, Life technologies, Paisley, UK) supplemented with 10% foetal calf serum (FCS; GibcoBRL), 1% MEM non-essential amino acids (GibcoBRL Cat.No.11140-035) and 100units/ml Penicillin-Streptomycin (GibcoBRL). Cells were fed and passaged twice weekly.

2.3.2 CULTURE OF COS-7 CELLS

This cell line is also SV40-transformed and originates from kidney cells of the african green monkey (Cercopithecus Aethiops). They have a fibroblast-like morphology and are grown in monolayers. Cells were kept in MEM (GibcoBRL), supplemented with 10% newborn calf serum (NBCS; GibcoBRL), 100units/ml Penicillin-Streptomycin. The medium was changed twice weekly when the cells were also passaged.

2.3.3 PASSAGING AND REPLATING OF CELL LINES

COS-7 and tsA201 cells were grown as adherent monolayers in T75 culture flasks. When cell monolayers reached confluency they were passaged. To passage cells, the growth medium was removed and the flask rinsed with prewarmed sterile PBS. 2ml of prewarmed Trypsin (500u/ml) was added and the flask tilted in all directions to ensure cells are in contact with the solution. This was followed by a 5 to 10 minute incubation at 37°C until cells detach from the surface, when 7ml of growth medium was added. The cells were washed off the surface and triturated by pipetting in order to break up cell clusters. The cell suspension was centrifuged at 300 x *g* for 2 minutes, the supernatant decanted and the cells resuspended in growth medium at an appropriate dilution before they were added to fresh T75 culture flasks.

For the replating of cells 24-48 hours prior to an experiment, a non-enzymatic detachment method was used to prevent the digestion of extracellular proteins. 1ml of cell dissociation solution (CDS) was added to a 35 mm diameter dish, and after a 5-10 minute incubation at 37°C, 1ml of growth medium was added. The cells were then gently washed off, triturated and the cell suspension was directly applied to poly-L-lysine coated coverslips.

2.3.4 PREPARATION OF COVERSLIPS

Sterile round 13mm diameter or square 22mm^2 glass microscope coverslips (Chance Propper Ltd, West Midlands, UK) were incubated in 15μg/ml poly-L-lysine hydrobromide (MW 150-300Da) for 30 minutes at 37°C, washed twice in sterile water and left to dry. For acutely dissociated Purkinje neurones, sufficient cell attachment for imaging experiments proved to be problematic. Therefore different coating methods have been used. Sterile coverslips were either dipped in a 1% alcian blue sterile dH_2O solution then washed thoroughly in sterile water and left to dry, or coated with Vectabond™ (Vector Laboratories, Inc. USA) according to the manufacturer's instructions. However best results were achieved by incubating the coverslips in 2 mg/ml Concanavalin A for 30 minutes at 37°C, before washing them twice in sterile water.

2.3.5 EXPRESSION VECTOR AND cDNA CONSTRUCTS

The following cDNAs were used in this study: rabbit $Ca_V2.1$ (X57689) carrying a mutation (E1740R), for enhanced channel expression (Hans *et al.*, 1999), rat β_4 *Cacnb*4 (LO2315), rat $\alpha_2\delta$–1 *Cacna2d1* (M86621), mouse $\alpha_2\delta$–2 *Cacna2d2* (AF 247139), *du* mutant transcript 1 (*du*-mut1 α_2; AF247140) and mut-3 green fluorescent protein (GFP; M2653) which has been mutated (S65G and S72A) for enhanced fluorescence (Cormack *et al.*, 1996). All recombinant constructs have previously been subcloned in the transient expression vector pMT2 (Swick *et al.*, 1992). The SV40 origin and enhancer are present in this vector. For expression of heterologous calcium channel subunits, a master mix was made with a 15:10:5 ratio of α_{1A}, β_4 and $\alpha_2\delta$ subunits respectively. GFP expression vector was added separately to the transfection at a 20 times lower DNA concentration as the master mix and used as a positive transfection control.

2.3.6 PREPARATION OF PLASMID DNA USED IN TRANSFECTION EXPERIMENTS

Plasmid DNA was prepared from *E.coli* glycerol stocks of the expression vectors using a Qiagen Maxi Kit (Qiagen, Dorking, UK), based on a modified alkaline lysis procedure followed by binding of plasmid DNA to an anion-exchange resin, according to the manufacturer's instructions.

2.3.7 TRANSFECTION OF COS-7 AND tsA201 CELLS

The GenePorter transfection reagent (Gene Therapy Systems, San Diego, CA, USA) was used to transfect COS-7 and tsA201 cells according to the manufacturer's instructions. This transfection method is also called lipofection as the reagent consists of a mixture of the neutral lipid dioleolylphosphatidyl-ethanolamine (DOPE) and a cationic lipid, which coats the DNA. It is based on the absorption of liposomes containing the DNA by the cell. In the morning of the day of transfection, cells were replated to 70-90% confluency and left for 3 hours to adhere. For a 35 mm dish, 400µl of serum-free MEM medium was used to dilute 5µl (1µg/µl) of the DNA mix. The same volume was used to dilute 20µl of the GenePorter reagent. Both dilutions were vortexed, mixed, vortexed again and incubated at room temperature (20-23°C) for 45 minutes. After aspirating the

culture medium from the cells, the DNA-GenePorter mixture was added and incubated at 37°C for 5 hours. 800µl of MEM containing 20% NBCS was then added and the cells were incubated overnight. At 24 hours post transfection the growth medium was changed and 72 hours post transfection the cells were harvested for biochemical experiments or replated for immunocytochemistry. A transfection efficiency of 50-75% was routinely reached.

2.3.8 ANIMAL HUSBANDRY

Mice of the TKDU-*du* strain carrying the *ducky* mutation were obtained from the Jackson Laboratory (Bar Harbour, ME, USA). This is an inbred strain into which *du* was transferred from the Ruby Silver strain from which it first arose (Snell, 1955). Homozygous *ducky* mice die before they reach maturity and were therefore kept as heterozygous breeding pairs. The mice were housed in a colony room with an ambient temperature of 22°C and a 12-hour alternating light/dark cycle, with food and water *ad libitum*. The experiments were conducted in agreement with the Animals (scientific procedures) Act 1986.

2.3.9 PREPARATION AND CULTURE OF NEONATAL MOUSE CEREBELLAR GRANULE NEURONES

Cerebellar granule cells were prepared according to a method described by White *et al.*, (1979), but with several modifications. Seven-day-old mice (P7, P for postnatal) of either sex and genotype were killed by decapitation. The skin was cut with fine scissors from the back of the head over the top of the skull to expose the skull. A cut was then made from the foramen magnum around the side of the head to above the eye sockets, making sure the scissors did not damage the underlying brain tissue. Forceps were used to lift the skull from the back of the head, thereby revealing the brain. The cerebellum was separated from the brainstem by pinching underneath it using curved forceps. The cerebellum was immediately rinsed in ice-cold, enriched phosphate buffered saline (PBS) solution, containing 0.3% bovine serum albumin (BSA), 14mM glucose and 1.6mM magnesium sulphate heptahydrate ($MgSO_4$-$7H_2O$). Meningeal layers and blood vessels were removed and the tissue was chopped into 0.2mm^3 cubes with a tissue chopper (McIlwain, O'Fallon, MO, USA). The chopped tissue pieces were enzymatically dissociated by a 20 minute incubation at 37°C in enriched PBS solution containing 0.25% Trypsin (type III, from bovine

pancreas). The trypsin was inactivated using soybean trypsin inhibitor (SBTI, 8 µg/ml in enriched PBS). The cells were then treated with 10kUnitz/ml Deoxyribonuclease I (DNaseI, type IV from bovine pancreas). The DNase was added to prevent cell clumping, caused by the DNA released from ruptured cells. After the suspension was mixed by gentle agitation, it was centrifuged at 300 x *g* for 1 minute to pellet cells and the supernatant was decanted. Tissue pieces were resuspended in 3ml enriched PBS solution complemented with 50µg/ml SBTI, 64kunitz/ml DNaseI, 3mM $MgSO_4$-$7H_2O$ and then dissociated by trituration with a fire-polished Pasteur pipette (Volac, John Poulten, Barking, UK). The cell suspension was underlaid with 2ml of 4%BSA in Earle's Salts (EBSS, see Table 2.1) and centrifuged at 300 x *g* for 5 minutes at RT. The supernatant was removed and the pelleted cells were resuspended in MEM 10%FCS, 20mM KCl, 30mM glucose and 2mM glutamine.

After estimating the cell density (using an Improved Neubauer Counting Chamber), the cells were plated on 13mm round coverslips at a density of 500.000 cells per coverslip in 24well plates (Techno plastic products, Trasadingen, Switzerland). The following day the medium was supplemented by addition of 500µl MEM containing 10% FCS. On the second day *in vitro* (DIV) 500µl MEM 10%HS and 80µM fluorodeoxyuridine (FUDR) was added to reduce non-neuronal cell proliferation. The medium was replaced on the fourth day after the preparation and then cells were fed twice weekly. All media was supplemented with 2.5% chick embryo extract, 33mM D-glucose, 2mM glutamine, 23mM KCl and 100u/ml Penicillin-Streptomycin.

Description	Compound	Concentration
	BSA	4%
	$MgSO_4$-$7H_2O$	1.24 mM
Earle's balanced salt solution	NaCl	116 mM
	KCl	5.36 mM
	D-glucose	5.5 mM
	$NaHCO_3$ ·$2H_2O$	1 mM
	NaH_2PO_4	2.6 mM
	Phenol red	0.026 mM

Table 2.1 Composition of Earle's salt solution supplemented with BSA and $MgSO_4$-$7H_2O$.

2.3.10 ACUTE DISSOCIATION OF PURKINJE NEURONES

This method was modified from Mintz *et al.* (1992b). Neurones were obtained from cerebella of P5 to P8 mice of either sex and genotype. All solutions (Table 2.2) were bubbled for 30 minutes with O_2 containing 5%CO_2 and the pH was readjusted before use. The cerebella were chopped into 0.5-1mm^3 pieces with a tissue chopper. The tissue pieces were incubated in the enzymatic solution for 20 minutes, then transferred to the 37°C prewarmed dissociation solution and allowed to cool to room temperature for 5 minutes. The tissue pieces were then triturated twice by aspiration through a 10ml syringe with three 200µl pipette tips attached to it.

Dissociated cells were plated on 13mm round coverslips coated with 2mg/ml Concanavalin A. Cells were subsequently allowed to attach for 1 hour under an O_2 atmosphere containing 5%CO_2 at room temperature.

Description	Compound	Concentration
Solution 1 pH 7.4,	Na_2SO_4	82 mM
	K_2SO_4	30 mM
	$MgCl_2$	5 mM
	Hepes	10 mM
	D-glucose	10 mM
	$CaCl_2$	50 µM
Enzymatic solution (in Solution 1)	protease XXIII	0.5 mg/ml
Dissociation solution (in DMEM) pH 7.4	BSA	1 mg/ml
	SBTI	1 mg/ml
	D-glucose	10 mM
	Hepes	15 mM

Table 2.2 Composition of the solutions used for the acute isolation of Purkinje neurones.

2.4 THE GENOTYPING OF MICE FOR THE *DUCKY* MUTATION

2.4.1 RNA PREPARATION

Special care was taken in the following reactions to reduce contamination with ribonucleases (RNases). The water for the following solutions was diethyl-pyrocarbonate (DEPC) treated to inactivate RNases and additionally reactions were performed on ice to slow down degenerative processes. Total RNA was isolated either from mouse brain or liver biopsies (25-50mg tissue) using the RNeasy Mini Kit (Qiagen) following the manufacturer's protocol. Paraformaldehyde-fixed liver biopsies were treated with 500µg proteinase K (Boehringer Mannheim, Mannheim, Germany) in 600µl digestion buffer (in mM: 50 Tris-HCl, 100 NaCl, 10 EDTA, 1% SDS, pH 8.0) for 1 hour at 45°C. The RNA was extracted from the tissue lysate with 600µl Phenol/Chloroform/Isoamylalcohol (25:24:1). After a 5-minute incubation on ice the mixture was centrifuged at 13,000 x *g* for 20 minutes at 4°C. The upper aqueous phase was transferred to a fresh tube and 600µl of chloroform was added. To the collected aqueous phase an equal amount of isopropanol was added, and the RNA was precipitated in the presence of 300mM sodium acetate for 1 hour at -20°C. The precipitate was dissolved in 100µl RNase-free water.

2.4.2 DETERMINATION OF RNA CONCENTRATION

5µl of the isolated RNA solution was diluted in 595µl dH_2O and the absorbance measured at 260 and 280nm. 5µl 1% SDS in 595µl DEPC dH_2O was used as a blank. The absorbance ratio A260/280nm is an indication of the purity of the isolated nucleic acid. An $OD_{260/280}$ ratio under 1.8 indicates protein contamination and over 2.0 indicates RNA degradation. The concentration was then calculated using the formula:

$$OD_{260} \text{ x dilution factor x average extinction coefficient} = \mu g/ml$$

For single stranded nucleic acid solutions the average extinction coefficient is 40 $(\mu g/ml)^{-1}$. An OD_{260} value of one, therefore equals 40µg/ml single stranded DNA or RNA.

2.4.3 DNASE TREATMENT AND FIRST STRAND SYNTHESIS

The whole yield of the RNA preparation was DNase treated (see Table 2.3), to remove genomic DNA contamination. The materials for DNase treatment and reverse transcription (RT) were supplied by Promega (Madison, WI, USA). Dithiothreitol (DTT) in the reaction buffer is essential for the activity of the ribonuclease inhibitor (RNasin). RQ1 is a RNase-free desoxyribonuclease (DNase 1) that degrades single and double-stranded DNA.

Compound	Concentration
RNA	20-100 µg
RNasin	1u/µl
RQ1 DNase	0.01 u/µl
Tris-HCl	50 mM
KCl	75 mM
$MgCl_2$	3 mM
DTT	10 mM

Table 2.3 Composition of the DNase reaction.

After a reaction time of 15 minutes at 37°C the enzyme was denatured for 5 minutes at 90°C. The reaction mixture was then purified from nucleotides and enzymes through an RNeasy column and eluted twice with 30µl elution buffer. This was followed by the First strand synthesis of the complementary DNA (cDNA) from RNA using reverse transcriptase (RT) derived from the moloney-murine leukaemia virus (M-MLV) and random Hexamer primers, see Table 2.4.

Compound	Concentration
RNA	30 µl
M-MLV RT	5u/µl
RNasin (40u/µl)	1u/µl
Random Hexamer primers	10 pmol/µl
DNTP	25 mM
Tris-HCl	50 mM
KCl	75 mM
$MgCl_2$	3 mM
DTT	10 mM

Table 2.4 Composition of the first strand synthesis reaction.

The reaction mixture was incubated for 2 hours at 37°C and then diluted 1:2 in dH_2O.

2.4.4 TWO GENOTYPING STRATEGIES

2.4.4.1 METHOD 1: FROM REVERSE TRANSCRIBED RNA PREPARATIONS

Polymerase chain reaction (PCR) was used to amplify a sequence of interest on a cDNA template using a pair of oligonucleotide primers each complementary to the target sequence on the cDNA template. One primer binding upstream (5') and the other downstream (3'), thereby encompassing the region to be amplified. A thermostable DNA polymerase extends the primers towards each other in a reaction cycle of three steps: denaturation, primer annealing and extension. The region of DNA encompassed by the primer pair is greatly amplified (2^n after n cycles per target sequence if the PCR is 100% efficient) by repetition of these cycles. 30 cycles were routinely used. The presence of a 156bp-sized PCR product, amplified through the primer pair 49F and 11R in PCR1 indicates that the RNA preparation, the reverse transcription, as well as the PCR have worked successfully and gives a standard level of expression. It amplifies from wild-type and *ducky* mice. An additional 387bp product in PCR1 indicates the presence of a wild-type copy of $\alpha_2\delta$-2, therefore the animal is either homozygous (+/+) or heterozygous (+/*du*). The distinction between these two genotypes is possible through PCR2 with the primer pair 20F and 87R amplifying a 456bp fragment specific for the mutation, which is therefore only present in (*du/du*) or (+/*du*) (Figure 2.1).

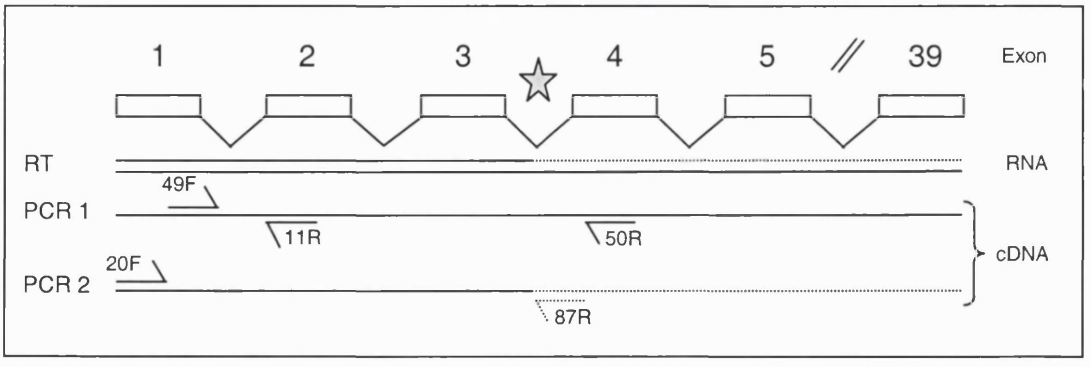

Figure 2.1 Genotyping PCR (Method 1). Numbers in the top row indicate exons drawn as boxes below. The star shows the position of the *ducky* mutation. For genotyping RNA is prepared, reverse transcribed (RT) and used for PCR1 and PCR2. Two RNA populations are shown, as they are present in a heterozygous (+/*du*) animal; a dashed line indicates mutated sequence or primers specific for this sequence. The location of the different primer pairs pictured are not to scale. Primer pair 49F/11R amplifies a 156bp fragment from (+/+) as well as (*du/du*); 49F/50R a 387bp fragment from (+/+) or (+/*du*) and primer pair 20F/87R a (*du/du*) specific 456bp fragment (see Table 2.9 for primer sequences).

2.4.4.1.1 GENOTYPING PCR (METHOD 1)

For each cDNA sample two polymerase chain reactions with different primer sets were performed (Table 2.5). A master mix was used to reduce tube variations. The PCR was then performed for 30 and 35 cycles respectively. Control reactions of known wild-type (+/+) and *ducky* (*du/du*) as well as a dH_2O control were always included.

Description	Compound	PCR 1	PCR 2
		Concentration	
Buffer	Tris-HCl	10 mM	
	KCl	50 mM	
	$MgCl_2$	1.5 mM	
	dimethylsulfoxide (DMSO)	8%	
Taq Polymerase		1u/25µl	
Primer (pmol)	49F	0.8	
	11R	0.5	
	50R	0.5	
	20F		0.5
	87R		0.5
cDNA		5µl	

Table 2.5 Composition of the genotyping PCR (Method1).

Before use the cDNA was denatured at 90°C for 5 minutes and cooled on ice. 5µl cDNA was added to 20µl mastermix and the PCR was performed on a Hybaid Touch Down Thermocycler (Thermo-Hybaid, Ashford, UK) (Table 2.6).

Cycles	Step Description	PCR1	PCR2	Time
		Temperature in °C		
x1	Initial Melting	95°C		120 s
PCR1 x30 PCR2 x35	Annealing	60°C	52°C	45 s
	Extension	72°C		30 s
	Melting	95°C		30 s
x1	Final Extension	72°C		300 s

Table 2.6 Cycle conditions of the genotyping PCR reactions (Method 1).

The PCR products were separated by electrophoresis on a 2.5% agarose gel. Agarose at the appropriate concentration was dissolved in Tris acetate (TAE) buffer (0.04 M Tris acetate, 1mM EDTA, pH7.4). Gels were cast in a gel apparatus from Flowgen (Novara Group Ltd., Ashby de la Zouche, UK) and submerged in TAE buffer before loading. Loading buffer (final concentration: 5% glycerol, 0.05% bromophenol blue) was always mixed with sample before loading and a 100bp marker ladder (GibcoBRL) was separated in adjacent lanes. Gels were routinely run at 110V/80mA. At the end of the run DNA bands were visualized by staining the gel in a $1\mu g.ml^{-1}$ solution of ethidium bromide in TAE for 10-15 minutes and subsequent placement on a ultraviolet light box. Agarose gels were photographed using a Polaroid camera (Kodak) and black-and-white film (type 667) as shown in the example in Figure 2.2.

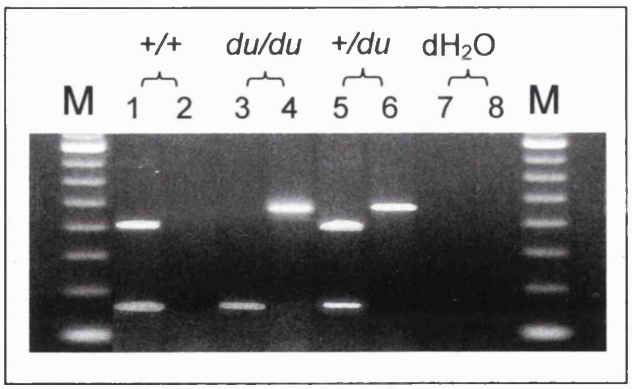

Figure 2.2 Typical PCR products in a genotyping PCR (Method1). Shown are the three genotypes and a water control alongside two 100bp marker lanes (M). In lanes 1, 3, 5 and 7 products of PCR1 are separated, 150bp lower and 400bp upper band. In lanes 2, 4, 6 and 8 accordingly the 450bp product for PCR2.

2.4.4.2 METHOD 2: FROM DNA USING TAIL-SNIP BIOPSIES

As an alternative to the above method DNA was extracted by incubating 2mm tail-snip tissue in 75µl 25mM NaOH, 0.2mM Na_2EDTA at 95°C for 30 minutes. After cooling to 4°C, 75µl 40mM Tris/HCl was added and 5µl of the resultant solution was used as template for PCR amplification. Primer pair 98F and 120R are specific to a region duplicated in the *du* allele (Figure 2.3). Following a *Bsp*HI digest the amplification products were separated by agarose gel electrophoresis. The wild-type genotype can be identified by the presence of a single band of 541bp. Heterozygous and *du/du* mice each show two bands, 268bp and 273bp in size, and can be distinguished on the basis of the relative intensities of the bands.

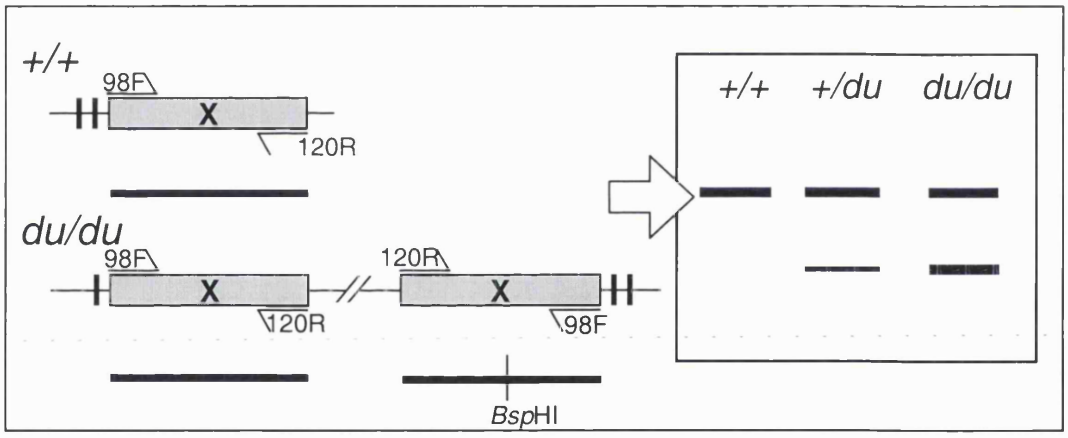

Figure 2.3 Genotyping PCR (Method 2). Primer pair 98F and 120R produce a fragment of 541bp from a region, which is duplicated in the *du* allele. In the *du* allele this region contains a *Bsp*HI restriction site. Restriction results in two fragments of 286bp and 273bp in *du* whilst the wild-type allele remains uncut.

2.4.4.2.1 GENOTYPING PCR (METHOD 2)

The genotyping PCR (Method 2) was conducted according to the following composition and cycle conditions (Table 2.7 and 2.8), very similar to those described for Method 1 (Section 2.4.4.1.1)

Description	Compound	PCR3 Concentration
Buffer	Tris-HCl	10 mM
	KCl	50 mM
	$MgCl_2$	1.5 mM
	dimethylsulfoxide (DMSO)	8%
Taq Polymerase		1u/25µl
Primer (pmol)	20F	0.5
	87R	0.5
DNA		5µl

Table 2.7 Composition of the genotyping PCR (Method2).

Cycles	Step Description	PCR3 Temperature in °C	Time
x1	Initial Melting	95°C	180 s
PCR3 x33	Annealing	53°C	45 s
	Extension	72°C	30 s
	Melting	95°C	30 s
x1	Final Extension	72°C	120 s

Table 2.8 Cycle conditions for the genotyping PCR reaction (Method 2).

After completion of PCR 3, 10µl cDNA was digested with *Bsp*HI for one hour at 37°C and separated on a 1.5% agarose gel as described in Section 2.4.4.1.1. A typical result is shown in Figure 2.4

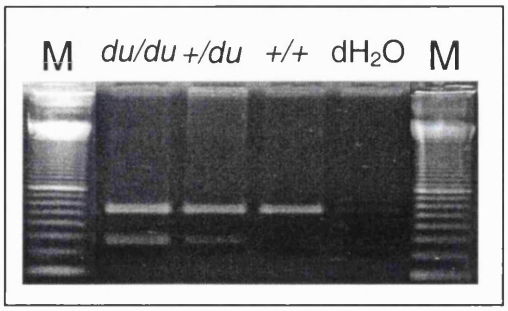

Figure 2.4 Typical PCR products in a genotyping PCR (Method 2). Shown are the three genotypes and a water control alongside two 100bp marker lanes (M). For all three genotypes a 541bp is visible, amplified through the primer pair 98F/120R (see Table 2.9 for sequence). The merged product of the restriction digest of 273bp and 286bp is only visible for *du/du* and *du/+*. The *du/+* genotype can be distinguished when compared to *du/du* as the band is about half its intensity.

2.4.5 PRIMER SEQUENCES

Name	5'-Sequence-3'	Length	Position
20F	GCCGCATCTTGAATGGAAAC	20mer	nt 424-443
49F	ACGCCCGCTCTTGCTCTTGCT	21mer	nt 566-586
98F	ACCTATCAGGCAAAAGGACG	20mer	intronic
11R	CCTCCAAAAATCCGCATCAC	20mer	nt 702-721
50R	TCAGCCTTGGCATCGTAGTA	20mer	nt 933-952
87R	CAGAGACCAATGAGACTGGA	20mer	nt 859-879
120R	AGGGATGGTGATTGGTTGGA	20mer	intronic

Table 2.9 List of primers used for genotyping. The primers were designed and provided by Jane Barclay (Novartis, London, UK). The nucleotide numbers refer to accession number AF247139, with the exception of 87R. This primer is specific for the *ducky* mutation and refers to accession number AF247140.

2.5 IMMUNOCYTOCHEMISTRY

For immunocytochemical studies results were obtained from at least three or more independent transfections. Cerebellar sections for each experiment were derived from three or more littermate pairs of wild-type and *du/du* mice respectively.

2.5.1 STAINING OF COS-7 CELLS

COS-7 cells were replated on 22mm^2 coverslips the day after the transfection and immunocytochemistry was performed on day four post-transfection. After two 5-minute washes with Tris-buffered saline (TBS, see Table 2.10) cells were fixed with 4% paraformaldehyde in TBS for 15 minutes at room temperature. For permeabilization, cells were incubated twice for 7 minutes in 0.02% Triton X-100 in TBS, otherwise cells were washed twice with TBS for the same time period. After 15 minutes incubation in blocking solution (Table 2.10), to block non-specific binding sites, 200µl of primary antibody, diluted to the appropriate concentration with a 1:2 dilution of the blocking solution in TBS (Table 2.11), was incubated overnight at 4°C. The next day, coverslips were washed 4 times for 5 minutes with blocking solution. Secondary antibody (a biotinylated goat anti-rabbit or anti-mouse IgG), was then incubated for 2 hours at 4°C. To visualize and amplify the signal, a streptavidin conjugate coupled to the fluorescent dye Texas-red (Molecular Probes, Eugene, OR, USA), was incubated for one hour at room temperature in the dark following four 5-minute washes with blocking solution. The coverslips were then washed twice with TBS and incubated for 2 minutes with the nuclear marker 4', 6-diamidino-2 phenylindole (DAPI, Molecular Probes) for nuclear staining at a concentration of 1mM in TBS. After five 5-minute TBS washes, excess fluid was dried off, before mounting the samples on glass slides with the antifading solution VECTASHIELD (Vector Laboratories, Burlingame CA), which were then sealed with nail polish. Slides were stored in the dark at 4°C until use.

Description	Compound	Concentration
TBS pH 7.4	NaCl	150 mM
	Tris Sigma 7-9	20 mM
Blocking solution (in TBS)	BSA	4%
	Goat serum (GibcoBRL)	5%
	D-L-lysine	0.1%

Table 2.10 Composition of TBS and blocking solutions.

2.5.2 PARAFORMALDEHYDE PERFUSION AND CRYO-SECTIONING

P21-24 mice were either anaesthetized by pentobarbitone injection (200 mg/kg i.p.) or asphyxiated with CO_2 and perfused transcardially via the ascending aorta, initially with 10ml of a 100mM sodium phosphate buffer (PBS, pH 7.2) and then with 10ml 4% paraformaldehyde (Agar Aids, Stansted, UK) in PBS. The brains were immediately removed from the cranium and postfixed for 2 hours at 4°C with fresh 4% paraformaldehyde in PBS and then incubated over-night in PBS with 30% sucrose and 0.02% sodium azide at 4°C for cryoprotection. The brains were then frozen in isopentane, previously precooled with liquid nitrogen and 15µm parasagittal sections were cut with a cryostat (CM 1900, Leica). The sections were transferred to poly-L-lysine-coated microscope slides (BDH, Merck Ltd, Lutterworth, UK), left to dry and stored at –70 °C until the day of use.

2.5.3 STAINING OF BRAIN SECTIONS

The primary antibody was appropriately diluted (Table 2.11) in PBS containing 0.3% Triton X-100 and 0.02% sodium azide. 200µl of this dilution was applied per slide, where the sections were circled with a Pap Pen (Daido Sangyo Co Ltd., Japan), and incubated overnight at 4°C. The following day sections were washed twice with 200µl PBS for 15 minutes before incubation with biotinylated goat anti-rabbit or anti-mouse IgG (1:200 dilution) as the secondary antibody. Following a second washing step with two changes of PBS, the sections were incubated with a Texas-red-coupled streptavidin conjugate (1:400

dilution), for one hour at room temperature and in the dark. After an additional washing step with PBS, the sections were incubated for 1 minute with 1mM DAPI in PBS. They were successively washed four times with PBS, left to dry before mounting 22x50mm coverslips (BDH, Merck Ltd., Lutterworth, UK) with VECTASHIELD and sealing the microscope slides with nail polish. Slides were kept in the dark at 4°C until use.

2.5.4 PEPTIDE CONTROLS

For peptide controls, the appropriately diluted antibody was incubated for 1 hour at 37°C with a 10x higher concentration (w/v) of the immunizing peptide, before application onto slices. This was not always possible as in the cases of anti-Calbindin D28-K, anti-GFAP, and anti-caspase 3 and 12, the immunizing antigen was not available.

2.5.5 ANTIBODIES

The antibodies used in this study are listed in Table 2.11 below.

Name	Antigen	Source	Format	Supplier	Dilution
Ab16-29	$\alpha_2\delta$–2, AA 16-29 VRTARPWPGRGPRP	rabbit	affinity purified 1mg/ml	Eurogentec, Angers, France for M.Rees	1:1000 (Blot) 1:400
Ab102-117	$\alpha_2\delta$–2, AA 102-117 KDNRNLFEVQENEPQK	rabbit	affinity purified 0.5 mg/ml	Eurogentec, Angers, France for M.Rees	1:1000 (Blot) 1:400
Caspase 12	AA 16-29 VRTARPWPGRGPRPC	rat	ascites monoclonal	(Nakagawa *et al.* 2000)	1:100 (Blot) 1:20
CPP32	AA 29-175 Hamster Caspase P32	rabbit	affinity purified	(Wang *et al.*, 1996)	1:1000 (Blot) 1:400
CD28K Cat. AB1778	Calbindin D-28K	rabbit	affinity purified	Chemicon, Temeluca, CA, USA	1:10000 (Blot) 1:1000
GFAP	GFAP	mouse	affinity purified monoclonal 20µg/ml	Boehringer Mannheim, Germany	1:300 (Blot) 1:3
GFP	GFP	mouse	affinity purified monoclonal 1mg/ml	Clontech, Palo Alto, CA, USA	1:100
$Ca_V2.1$	PSSPERAPGREGPYGRE AA865-881	rabbit	affinity purified 1mg/ml	Alomone Labs, Jerusalem, Israel	1:200
biotinylated anti-rabbit IgG	rabbit IgGs	goat	whole molecule	Sigma Cat.No.;B-8895	1:200
biotinylated anti-mouse IgG	mouse IgGs	goat	whole molecule	Sigma Cat.No.;B-0529	1:200

2.5.6 THE FLUORESCENCE PROCESS

A Photon of the energy $h\nu_{EX}$ is supplied by an external light source (e.g. a laser) and absorbed by the fluorophore, creating an excited electronic singlet state (S_1'). Some of this originally absorbed energy is lost during a specific time span (1-10x10^{-9}sec.), were the fluorophore reaches a relaxed singlet state (S_1) from which fluorescence originates. In the last step a photon of the energy $h\nu_{EM}$ is emitted returning the fluorophore to its ground state (S_0). Due to the energy dissipation in step 2, the wavelength becomes greater with the reduced energy of this photon. This allows emission photons to be detected against a low background.

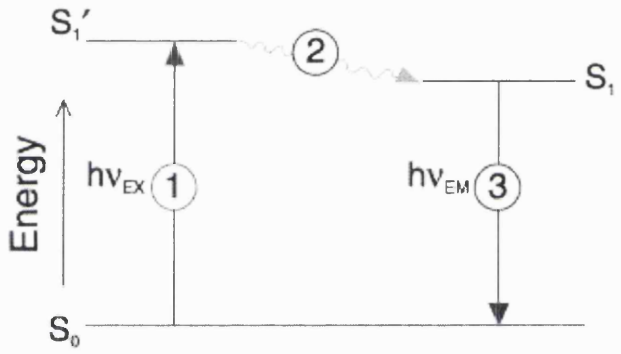

Figure 2.5 The Jablonski diagram. The three processes in fluorescence are illustrated. (1) Excitation (2) Excited state energy loss (3) Emission at a different wavelength. From Molecular Probes literature.

2.5.7 EXCITATION EMISSION SPECTRA OF DAPI, GFP, TEXAS-RED AND LUCIFER YELLOW

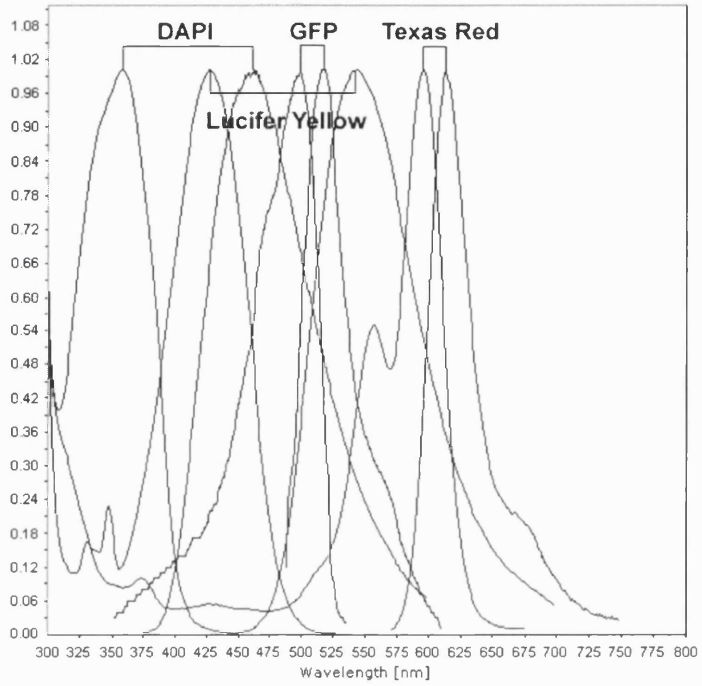

Figure 2.6 Excitation (Ex) and emission (Em) spectra of the fluorescent dyes used in confocal microscopy. The more energetic excitation peak is always on the left. The peak values in nm are: DAPI Ex359–Em461, Lucifer Yellow Ex428-Em536, GFP Ex498-Em516 and Ex595-Em615 for the Texas-red-conjugate (modified Bio-Rad fluorochrome database at http://microscopy.bio-rad.com).

2.5.8 LASER SCANNING CONFOCAL MICROSCOPY

For the visualization of fluorescence-labelled antibodies as well as nuclear DAPI staining a Leica DMRE upright microscope equiped with a Leica TCS SP1 scanhead (Leica, Heidelberg, Germany) was used. An air-cooled Krypton laser (Omnichrome, Melles Griot, Irvine, CA, USA) tuned to 568 nm served as a light source for Texas-red staining with an excitation wavelength of 595nm and emission at 615 nm. DAPI staining, with a excitation wavelength of 359 nm and emission at 461 nm was illuminated by a water-cooled UV laser (Coherent Inc., Santa Clara, CA, USA) tuned to 450nm. Pictures were collected on a 400MHz Intel Pentium II-based system running Leica TCS NT confocal control software with a 3D module enabled. A confocal system with its simplified components is shown diagramatically in Figure 2.7.

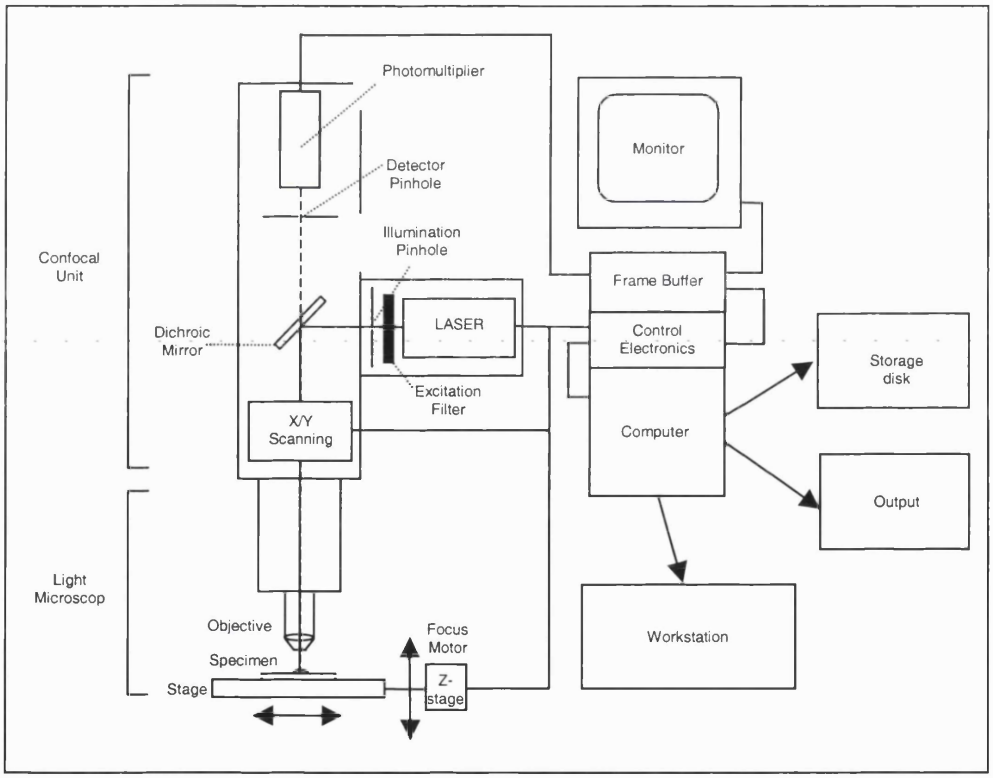

Figure 2.7 Setup of a laser scanning confocal microscope. Laser light is guided through a small pinhole and reflected by a dichroic mirror through the objective lens onto the specimen. Fluorescence emitted by the specimen is collected by the same objective. The dichroic mirror separates the longer wavelength fluorescent light from any unabsorbed exciting light and is guided through the detector pinhole into the photomultiplier.

2.5.9 THE CONFOCAL PRINCIPLE

The confocal principle (Minsky, 1961) overcomes limitations of the standard light microscope, which occur through the detection of scattered light as well as the detection of light from above and below the focal plane. Light scattering occurs when randomly deflected light enters the detector. The advantage of epifluorescence microscopy used in this study is that a single lens acts as both the objective and condenser. Illuminating and imaging light paths are necessarily perfectly aligned, hence the name confocal (Figure 2.8).

The confocal principle further depends on the presence of two pinhole apertures in the light path. The first aperture (illumination pinhole) produces a sharp, intense point of illumination, the intensity of which is low either side of a chosen focal plane within the specimen. The second aperture (detector pinhole) serves to process the emitted fluorescent light and allows only light information from that illuminated point to reach the detectors. The restricted depth of field intrinsic to the confocal principle effectively produces 'optical sections' of the specimen, making it the technique of choice for the study of thick biological sections. Emission light passing through the detector pinhole is dispersed by a prism and guided to different photodetectors. A computer is used to control the sequential scanning of the sample and to assemble the image for display onto a video monitor.

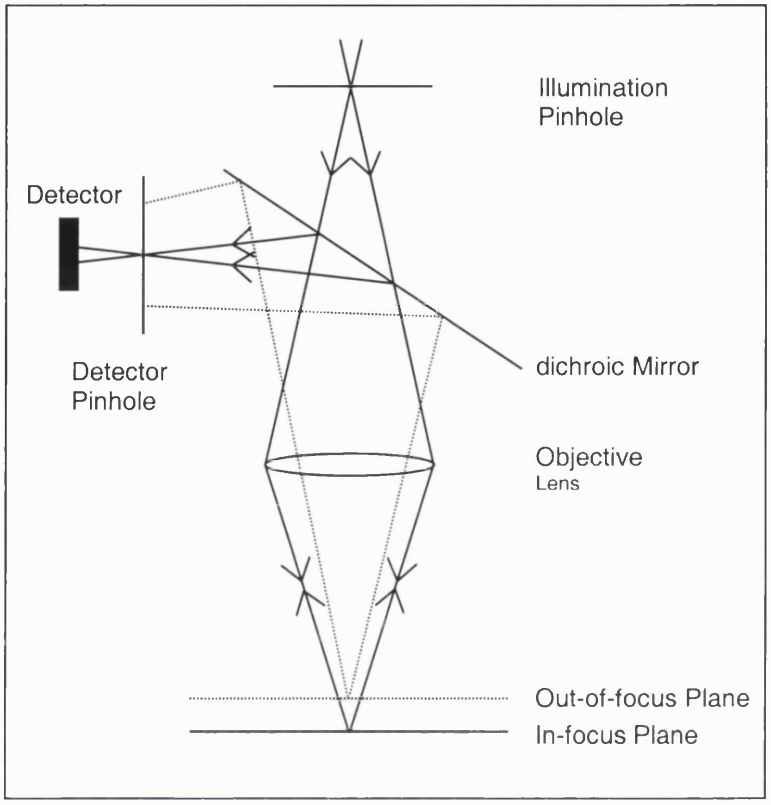

Figure 2.8 The principles of confocal optics. For simplicity only out of focus light from above the focal plane (dotted line) is shown in this diagram. Laser light passes through the illumination pinhole, the objective lens focuses the light on the specimen, at the focal plane of the objective lens, so that its intensity is low above and below the focal plane. The same lens collects light emitted by the specimen upon excitation and the dichroic mirror then functions to separate the longer wavelength fluorescent light from any unabsorbed excitation light. The detector pinhole is what gives the system its confocal property, by rejecting light that did not originate from the focal plane.

2.5.10 DATA ANALYSIS

To allow comparison between different specimens, experiments with a particular antibody were always performed in groups. The acquisition parameters as well as the iris aperture were adjusted at the start of each experiment to the sample with the brightest staining and then kept constant. However the correlation of fluorescence intensity of the staining to the absolute protein concentration is impaired by a variety of factors and should therefore be seen qualitatively rather than quantitatively. Variations can arise through:

(a) differences in exposure time of the nonphotostable fluorophores to the laser

(b) the non-linear binding of antibody to antigen and streptavidin to biotin

(c) steric hindrance of antibody binding in areas of high antigen concentration

(d) storage of slides

(e) the power cycle of the laser, which causes short term fluctuation

2.5.11 PROCESSING OF CONFOCAL IMAGES

Confocal images were post-processed using Adobe Photoshop 5.5 software (Adobe Systems, London, UK) for presentation purposes

2.6 LUCIFER YELLOW/NEUROBIOTIN INJECTION

2.6.1 SLICE PREPARATION, VISUALIZATION AND INJECTION

The preparation of cerebellar slices was similar to the method described by Stuart and Hauser (1994). Brains from P24-27 mice killed through cervical dislocation and decapitation were removed and cerebella embedded in 3% agarose before 400μm parasagittal slices were cut using a vibrating slicer (Campden Instruments, London, UK) in cold (4°C) artificial cerebrospinal fluid (ACSF, see Table 2.12). The ACS fluid was bubbled continuously with 95%O_2 containing 5% CO_2 starting 30 minutes prior to the experiment to allow equilibration. Slices were kept at room temperature (21-23°C). Upon usage, slices were floated onto a glass coverslip, sealed to a hole in a Petridish, and held in place with a mesh weight. During injections the slices were perfused with O_2-enriched ACS fluid in order to prolong cell survival. Experiments were performed under visual control using an upright microscope (Axioskop FS; Zeiss, Göttingen, Germany) with a ×40 Achroplan water-immersion objective.

Dendrites and somata of Purkinje cells were visualized using infrared differential interference contrast (IR-DIC) video-microscopy (Stuart *et al.*, 1993). An infrared filter (RG-9; Schott, Mainz, Germany) was placed between the light source and the condensor and the tissue was observed using a Newvicon camera (C2400-07-C; Hamamatsu, Joko-cho, Japan). Glass microelectrodes (GC 200-F, Clark Electromedical Instruments, Reading, UK) were pulled with a Sutter Instrument (Model P-87, Novato, CA) to an outer tip diameter of 0.3 µm with a resistance of 20-30 mΩ as measured in the solutions used. Lucifer yellow/neurobiotin solutions were filtered at 0.2µm membrane filter (Nalgene) and centrifuged for 5 minutes at 12,000 x *g*. Pipettes were then placed with their blunt end in an eppendorf tube containing a 10% aqueous solution of Lucifer yellow (lithium salt) and a 10% aqueous solution of neurobiotin (Vector Laboratories). After the dye became visible at the tip, the pipettes were backfilled with 1M LiCl. Dye was injected iontophoretically into Purkinje cell somata by alternating the current repeatedly from –40nA to +40nA, over a period of 5 minutes. Routinely up to 10 cells were injected per slice.

After the dye injection was completed, the tissue slices were fixed for 1hour in 4% paraformaldehyde in PBS, and immunostained for neurobiotin with Texas-red-coupled streptavidin overnight.

Description	Compound	Concentration
ACSF pH 7.4	NaCl	125 mM
	$CaCl_2$	2 mM
	KCl	2.5 mM
	$MgCl_2$	1 mM
	D-glucose	25 mM
	$NaHCO_3$	25 mM
	NaH_2PO_4	1.25 mM

Table 2.12 Composition of the artificial cerebrospinal fluid (ACSF).

2.6.2 TECHNIQUE FOR QUANTIFICATION OF THE PURKINJE CELL MORPHOLOGY

For each of the two genotypes (+/+ and *du/du*) four randomly selected previously injected cells were scanned under identical parameters of imaging, pinholes, objective, filter and laser power. Selected fields were optically sectioned using 1 µm steps. Levels were set according to standardized procedures to ensure that the image collected displayed a full range of grey level values from black (0 pixel intensity) to peak white (255 pixel intensity level). The entire z-series was finally projected as a single composite image by superimposition. The final image was thresholded to form a binary image for analysis by ImageJ software 1.62 (National Institute of Health, USA). Dendrites were counted crossing a horizontal and diagonal line, respectively. Branchpoints were determined through counts going from the soma to the longest dendritic extension closest to the pial surface of the molecular layer, through averaging three different routes.

2.6.3 STATISTICAL ANALYSIS

All data are expressed as the mean ± standard error of mean (S.E.M.) of 4 cells of each group. Analysis was carried out using a student's *t*-test. $p < 0.05$ was considered as significant.

2.7 GOLGI-COX STAINING

First devised by Camillo Golgi in 1873, the Golgi impregnation techniques are still used today as a tool to visualize neuronal cell bodies, dendrites, dendritic spines and axons. The Golgi-Cox method is a mercury-based membrane staining that shows the full extent of all the processes of a cell, but stains only about 1% of the cells in a section. The specific reaction mechanism of this precipitation reaction still remains unclear, but the method has shaped our thinking about the interaction of neuronal elements and how they might contribute in the overall brain structure. Perhaps ironically, Golgi was devoted to the 'reticular theory' and his method had a major role in the eventual rejection of this theory.

Two P24 mice, *du/du* and +/+ respectively, were asphyxiated with CO_2, their brains removed from the cranium and immersed immediately in fixative (Table 2.13). The brains were then left undisturbed for 12 weeks in the dark at 4°C in polypropylene tubes (Falcon, Becton Dickinson Labware, Franklin Lakes, NJ, USA) wrapped with tin foil. 100 µm parasagittal vibratome sections were developed for 20 minutes in a 5% sodium sulphite (Na_2SO_3) solution, before they were mounted on microscope slides and coverslipped with VECTASHIELD. Pictures were taken on a Leica microscope (DMR) using x64 magnification. Image sections were grabbed through an attached cooled charged coupled device (CCD) camera (KY-F50, JVC, London, UK), connected to a Power G3 Macintosh computer using 'Vision Explorer' software (Alliance Vision, Mirmande, France), enabling the deconvolution and projection of different optical planes. Digital information was then imported into Photoshop 5.5 for Macintosh (Adobe, London, UK) to adjust brightness and contrast.

Compound	Concentration
Potassium Dichromate ($K_2Cr_2O_7$)	34 mM
Potassium Chromate (K_2CrO_4)	23 mM
Mercuric chloride ($HgCl_2$)	37 mM

Table 2.13 Composition of Fixative for Golgi-Cox staining.

2.8 ESTIMATION OF $[Ca^{2+}]_i$ IN INTACT CELLS USING THE RATIOMETRIC DYE FURA-2AM

A structural analogue of the $[Ca^{2+}]_i$ chelators EGTA and BAPTA, Fura-2 (Molecular Probes) binds $[Ca^{2+}]_i$ in a 1:1 stoichiometry (K_d = 224nM at pH 7.2 and 22°C). Fura-2 is capable of multiple photon absorption/emission cycles thus providing a stronger signal than luminescent indicators. The excitation spectrum of Fura-2 changes on binding calcium, so that the fluorescence emitted during excitation at 380nm (I_{380}) falls, while the fluorescence emitted during excitation at 340nm (I_{340}) increases (Grynkiewicz *et al.*, 1985). When the fluorescence emitted during excitation at 340nm is divided by the fluorescence emitted during excitation at 380nm, the resulting ratio value F_{340nm}/F_{380nm} depends only on the concentration of calcium ions and not on the path length through the cytoplasm or the intracellular dye concentration.

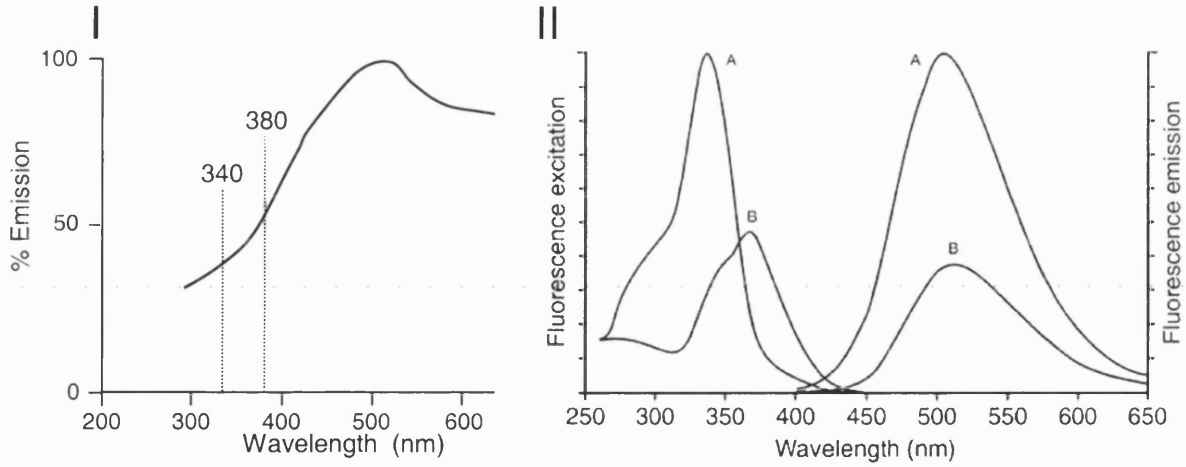

Figure 2.9 (**I**) Emission spectrum of a Xenon arc lamp used for the excitation of the fluorophore Fura-2. (**II**) Fluorescence excitation emission spectra of Fura-2 in solutions containing zero (B) to high (A) free $[Ca^{2+}]_i$. The absorption shift at 380 towards 340nm upon calcium binding becomes apparent, while the emission remains stable. Spectra taken from the Molecular Probes literature.

The acetoxy-methylester of Fura-2 can passively diffuse across cell membranes. Inside the cell, the ester is cleaved by intracellular esterases to yield a cell-impermeant fluorescent indicator. It has been shown that loading cells with Fura-2 at 5μM does not interfere with $[Ca^{2+}]_i$ transients by chelating a significant proportion of the free $[Ca^{2+}]_i$ (Fierro *et al.*, 1998; Dove *et al.*, 2000).

2.8.1 EXPERIMENTAL SETUP FOR CALCIUM IMAGING

The fluorescence measurements on individual cells were performed on an inverted microscope (Nikon Diaphot) with a x40 objective using a quantitative real-time imaging system comprising a cooled CCD camera (C4880-80, Hamamatsu Photonics, Hamamatu, Japan) and software (Kinetic Imaging, Liverpool, UK). Cells were excited alternately at 340 and 380nm by means of a rotating block switched by a filter changer (Cairn, Faversham, UK). Excitation light was reflected by a 400nm dichroic mirror and focused onto the cells with a x 40 objective. A cooled CCD camera captured the emission at 510nm. Output from the CCD camera was digitised and stored on a computer for subsequent analysis.

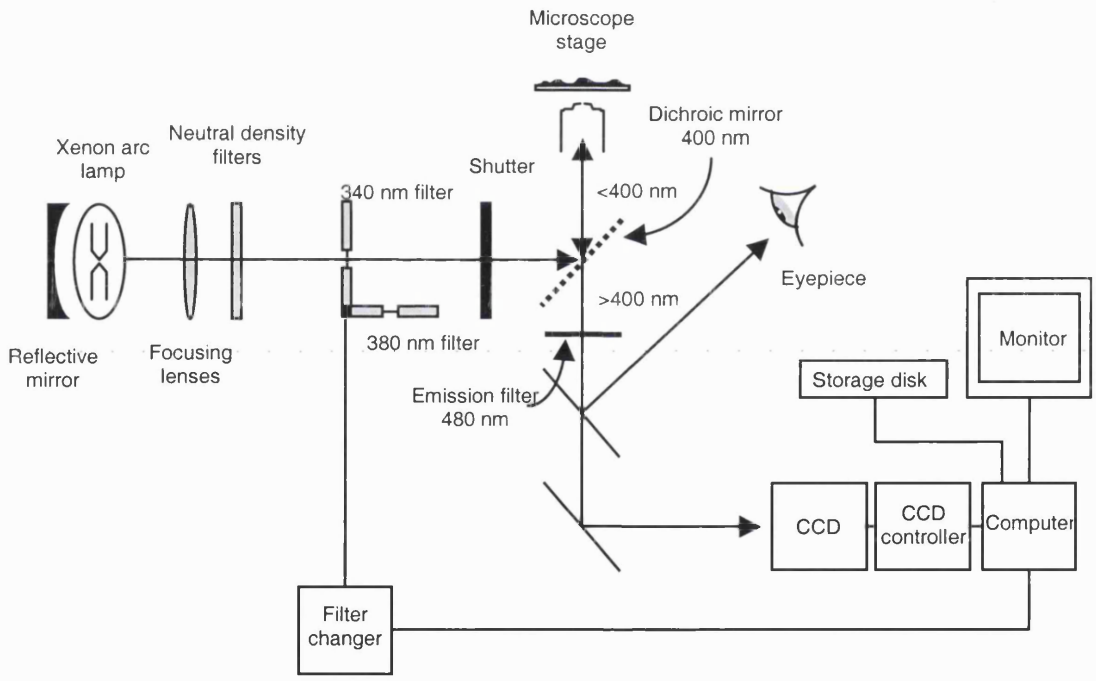

Figure 2.10 The lightpath and components of the imaging equipment used to measure $[Ca^{2+}]_i$. Light from a xenon arc lamp (Nikon) was focused onto a filter changer, which could alternate between 340 and 380nm filters and was controlled by the image acquisition software. A shutter could also be placed in the light path when images were not being acquired. The optics employed a dichroic mirror that reflected light of <400nm and passed light of >400nm which then passed through the emission filter (480nm). The light was then collected by a cooled CCD camera and individual images captured and stored by the computer for later analysis.

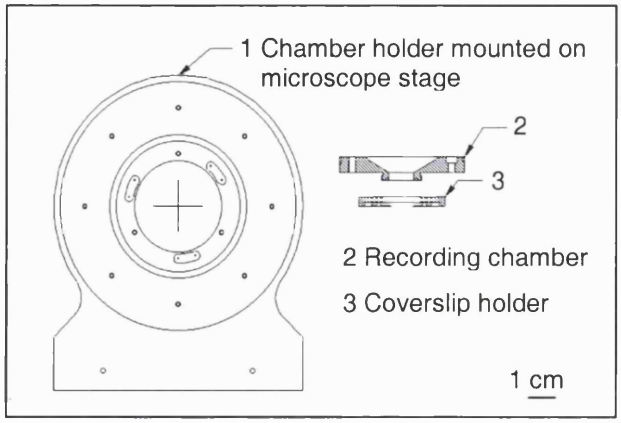

Figure 2.11 Diagram of the recording chamber used in calcium imaging experiments. The small inner diameter (9mm) of the chamber enabled the rapid exchange of small volumes. Drawing modified with permission of David Osborne.

2.8.2 CALCIUM IMAGING EXPERIMENTS

2.8.2.1 K^+ DEPOLARIZATION-EVOKED Ca^{2+} RESPONSES

In current clamp experiments, the steady-state voltages obtained during K^+ depolarization were measured for cerebellar granule cells in culture (Marchetti *et al.*, 1995). In this study 15mM KCl caused a depolarization of 20mV to a membrane potential of –45mV and 70-75mM KCl caused a depolarization to 0 mV. These values are close to the threshold and peak value of the calcium current. For depolarising K^+stimulations, the [K^+] of the extracellular solution was elevated as indicated. The [NaCl] was proportionately reduced to maintain isotonicity.

2.8.2.2 CEREBELLAR GRANULE CELLS

Cerebellar granule cells cultured for 7 days on Ø13mm round coverslips in 24 well plates were thoroughly rinsed with extracellular solution (see Table 2.14) to remove serum and culture medium. This solution contained tetrodotoxin (TTX) and kynurenic acid to block sodium channels and NMDA, Ampa/Kainate receptors respectively (Narahashi *et al.*, 1967; Stone, 2000). This was done as opening of sodium channels might change the resting membrane potential of the cells and NMDA, Ampa/Kainate receptors might cause non-specific calcium influx. The Fura-2 AM was prepared as a 1mM stock solution in anhydrous DMSO and stored at –20°C. Imaging experiments were carried out at room temperature (20-23°C). Extracellular solution containing 5μM Fura-2 AM and supplemented with 0.5% (w/v) BSA to aid the dye loading process was mixed vigorously to thoroughly disperse the dye. The cells were then incubated with this

loading solution at 37°C for 40 minutes. Cells were subsequently washed with 200µl extracellular solution to remove excess dye and left for a further 20 minutes at 37°C to allow completion of cleavage of the acetoxy-methylester by non-specific esterases within the cell, ensuring stable fluorescence. Cells were then washed with 200µl extracellular solution and the coverslip was fixed as the bottom of the recording chamber (Figure 2.11). The recording chamber contained 100µl extracellular solution at the start of each experiment. The collection times were adjusted, as the fluorescence intensity at 340nm is much less than at 380nm (Figure 2.9). Thus the collection period for 340nm excitation was three times that for 380nm excitation, generally 600ms compared to 200ms respectively once every second resulting in two images per episode. Before recording signal from the cells, an area containing no cells or processes was measured for 10 episodes to subtract background fluorescence. A suitable field of cells was then selected, ensuring cell somata were well attached, evenly spaced and not touching each other. After 10 episodes to establish the resting $[Ca^{2+}]_i$ or baseline value for the cells, 100µl of a solution with elevated $[K^+]$ was directly pipetted into the stimulation chamber. After either 10 or 20 further episodes cells were washed by adding 1ml of extracellular solution to the recording chamber, thereby diluting the $[K^+]$ of the extracellular solution to control values. For determination of the local $[Ca^{2+}]_i$ from the ratio images, a square of approximately 5µm^2 in the soma of the cells of interest was chosen. The background subtracted average fluorescence ratio value for the designated area was then calculated and plotted as a function of time.

2.8.2.3 ACUTELY ISOLATED PURKINJE NEURONES

For cerebellar Purkinje cells the conditions were identical to those described in section 2.8.2.2, with the two exceptions that the dye loading time could be reduced to 20 minutes at 27°C to reach similar levels of fluorescence-intensity and the somatic field from which signal was recorded could be enlarged to approximately 10µm^2.

Description	Compound	Concentration
Extracellular solution pH 7.4	NaCl	140 mM
	KCl	2.5 mM
	$MgSO_4$	1.18 mM
	$CaCl_2$	1.3 mM
	D-glucose	10 mM
	Hepes	5 mM
	TTX	1 μM
	kynurenic acid	1 mM

Table 2.14 Composition of extracellular solution.

2.8.3 CALIBRATION OF $F_{\Delta(340/380nm)}$ RATIO IN CEREBELLAR GRANULE CELLS

Intracellular calcium values were estimated by an *in vivo* calibration method performed on cerebellar granule cells in three independent experiments using the ionophore ionomycin in the presence of thapsigargin. Ionomycin is a lipid-soluble divalent cation-specific ionophore that transports divalent cations across membranes by a carrier-type mechanism. The generalized reaction catalysed by ionomycin is: C^{2+} (outside) <=> C^{2+} (inside) (C^{2+} = divalent cation)
Thapsigargin blocks the sarcoplasmic/endoplasmic Ca^{2+} ATPase (SERCA), an enzyme that uses ATP to transport Ca^{2+} from the cytosol into intracellular compartments. In the presence of thapsigargin, the equilibrium of intracellular and extracellular $[Ca^{2+}]_i$ generated by ionomycin is reached more rapidly.

2.8.4 STATISTICAL ANALYSIS

Unless otherwise stated values throughout the text are given as mean ± S.E.M. with *n* as the number of cells examined. Statistical analysis was performed using a student's *t*-test with paired comparisons if relevant. Probabilities are given for two-tailed tests. Results were considered significantly different when $p<0.05$.

2.9 PROTEIN BIOCHEMISTRY

2.9.1 PREPARATION OF COS-7 CELL LYSATES

COS-7 cells were transfected with either $\alpha_2\delta$–1, $\alpha_2\delta$–2 or *du*-mut1 α_2 as described in Section 2.3.7. On day 4 post-transfection, the cells were resuspended in detergent-free buffer A (in mM: 10 Hepes, 150 NaCl, 5 EDTA and protease inhibitors (Complete EDTA free, Roche, Welwyn Garden City, UK 1 tablet/50ml), pH 7.4). Cells were spun at 300 x *g* for 2 minutes and resuspended in buffer A before solubilization in an equal amount of SDS-PAGE loading buffer (see Table 2.15) and denaturing the samples by boiling for 3 minutes.

2.9.2 PREPARATION OF CEREBELLAR PROTEIN

This method is modified from Westenbroek *et al.* (1995). To prevent proteolysis, the whole procedure was performed on ice, and all buffers and rotors were precooled. For the inhibition of serine and cysteine proteases during the extraction, one tablet of a protease inhibitor cocktail (Complete, EDTA free, Roche) was dissolved in 25ml homogenisation buffer A supplemented with 350 mM sucrose. The cerebellum was homogenized in a polytron-like homogenizer. For the preparation of cerebellar membranes the homogenate was subsequently centrifuged at 2000 x *g* for 10 minutes at 4° C to pellet larger cell fragments and debris. The supernatant was then centrifuged at 50,000 x *g* for 45 minutes at 4° C to collect the membrane proteins. The pellet was resuspended in the same buffer and aliquots of total or membrane protein stored immediately at –80°C.

2.9.3 FILTER PAPER DYE-BINDING PROTEIN ASSAY

This method is modified from Macart and Gerbaut (1988). A 24cm diameter Whatman No.1 filter paper was divided into 96 1.5 x 1.5cm squares with a pencil. 0.2, 0.4, 0.6, 0.8, 1, 2 and 4µg of BSA standard solution and the samples were spotted on squares in triplicate together with 2 triplicate samples buffer alone to serve as blank and left to dry. After a one minute rinse in methanol, the air-dried filter paper was incubated for half an hour in 0.5% Coomassie Brilliant Blue G in a 7% acetic acid solution. The staining solution was then decanted and any excess rinsed off with UHQ dH_2O, before a 7% acetic acid destaining solution

was added for 1–3 hours until the blue background colouration is minimal. This step was repeated as necessary. The air-dried filter paper was cut into squares and placed into glass tubes. One ml of extraction buffer (66% methanol 33%H_2O and 1%NH_4OH) is then added to each tube. The vortexed tubes were left for 15 minutes, vortexed again and 150µl of each sample was read in duplicate using a multi-well plate reader at 620nm. The standard curve was extrapolated to give the protein concentration of the samples.

2.9.4 SDS POLYACRYLAMIDE GEL ELECTROPHORESIS

In this technique, protein samples to be separated are denatured and coated with detergent by heating in the presence of SDS and including 2-mercaptoethanol as a thiol-reducing agent (see Loading Buffer in Table 2.15). The SDS coating gives proteins a high net negative charge that is proportional to the length of the polypeptide chain, allowing separation solely on the basis of their molecular mass.

A discontinuous buffer system was subsequently used to separate the denatured protein samples (Laemmli, 1970). The upper gel layer is known as the stacking gel (Table 2.16). This is a large-pore gel, which is non-restrictive to the migration of the protein sample. The buffer in which the stacking gel is made contains Cl^- as an anion, whose electrophoretic motility is greater than that of the protein, while the tank buffer, or electrode buffer, contains glycine whose motility is less than that of the protein (see Table 2.15). As electrophoresis begins, the leading Cl^- ions in the stacking gel move faster than the protein and leaves behind a zone of lower conductivity. The higher voltage gradient of this zone causes the protein to move faster and to 'stack' at the boundary between the leading and trailing ions. Below the stacking gel is a deeper layer of gel with smaller pore size, known as the resolving or separating gel (Table 2.16). This gel is prepared in a buffer of higher ionic concentration and pH. The motility of the trailing ion increases so that its boundary moves ahead of the protein. The protein is resolved into individual bands according to size. The molecular mass of the protein was estimated by comparison to gel motilities of a lane with protein standard. Gradient or single percentage Hoefer minigels (Hoefer Scientific Instruments CA, USA) of 1.5mm thickness with a resolving gel size of 8.5 x 5.5cm were routinely used. In one occasion precast 10-20% Tricine gels

(Invitrogen, CA, USA) were used according to the manufacturers instructions to give higher resolution of low molecular weight proteins (Figure 4.9).

Description	Compound	Concentration
2x Loading Buffer pH 6.8	Tris/HCl	125 mM
	SDS	4 %
	Glycerol	20 %
	2-Mercaptoethanol	10 %
Reservoir Buffer pH 8.3	Tris/HCl	25 mM
	Glycine	192 mM
	SDS	0.1 %
Solution1 (Monomer solution)	Acrylamide	40 %
	Bisacrylamide	0.5 %
Solution2 (Resolving Gel Buffer)	Tris/HCl pH 8.8	1.5 M
	SDS	0.2 %
Solution3 (Stacking Gel Buffer)	Tris/HCl ph6.8	0.5 M
	SDS	0.2 %
Initiator	Ammonium persulphate (APS)	10 %

Table 2.15 Composition of buffers and solutions used to cast and run polyacrylamide gels of 1.5mm thickness with a resolving gel size of 8 x 5.5cm.

Description	Compound	Concentration
Stacking Gel	Acrylamide (Solution 1)	3.4%
	Tris/HCl (Solution 3)	125 mM
	SDS	0.05%
	Sucrose	20%
	APS	0.15%
	Tetraethylenediamine (TEMED)	0.15%
Resolving Gel	Acrylamide (Solution 1)	X %
	Tris/HCl (Solution 2)	375 mM
	SDS	0.05 %
	APS	0.05 %
	TEMED	0.7 %

Table 2.16 Final composition of polyacrylamide gels. The X% acrylamide indicates variable percentages according to the desired resolution of the gel.

2.9.5 WESTERN BLOTTING

To increase transfer efficiency of proteins from gel to the Polyvinyldenefluoride (PVDF) membrane (Bio-Rad, Hemel Hempstead, UK) a discontinuous buffer system was used in combination with a semi-dry electrophoretic transfer cell (Trans-Blot SD, Bio-Rad). The opposing effects of methanol and SDS in blotting can be exploited in semi-dry transfer, because the buffer reservoirs and the filter paper on each side of the gel are independent. Methanol increases the affinity of a protein for the PVDF membrane by removing the SDS from the protein. This increases the available hydrophobic sites on the protein for binding to the membrane support. It is for this reason methanol is often used in transfer buffers. While advantageous for binding of the protein to the membrane, methanol causes the pores in the gel to constrict. This makes it mechanically more difficult for the protein to exit the gel. SDS is used in Western blotting transfer buffer to aid in the elution of proteins from the gel matrix. While it inhibits the binding of the protein to the membrane, it is often necessary to facilitate complete transfer of proteins from the gel. In a discontinuous system, methanol is included in the buffer on the membrane side (anode) of the blot assembly and SDS is used on the gel side (cathode), taking advantage of the positive effect of each component (Table 2.17).

Anode buffer:	Cathode buffer
60mM Tris base, 40 mM CAPS, pH 9.6	
15% Methanol	0.1% SDS

Table 2.17 Composition of Anode and Cathode Buffer
(Tris[hydroxymethyl]aminomethane)/(3-[Cyclohexylamino]-1-propanesulfonic acid)

The PVDF membrane was pre-wetted in 100% methanol before equilibration in anode buffer for at least 30 minutes. Three sheets of Whatman filter paper (Grade 3) were also wetted in anode buffer. The acrylamide gel was equilibrated in cathode buffer in which three sheets of Whatman paper were also soaked. For the composition of the gel sandwich see Table 2.18.

Top	stainless steel cathode
Three sheets of Whatman filter paper wetted in top/cathode buffer	
Protein Gel equilibrated in cathode buffer	
PVDF Membrane equilibrated in anode buffer	
Three sheets of Whatman filter paper wetted in bottom/anode buffer	
Bottom	platinum anode

Table 2.18 Assembly of the gel sandwich used in the semidry electrophoretic transfer cell.

The stainless steel cathode top was secured, the cover closed and the apparatus run at a constant current of 5mA/h per square centimeter of gel (for example, 250mA for a small 5.5 x 8.5 cm gel) for 2 hours. Non-specific binding sites on the PVDF membrane were blocked by incubating the membrane in TBS buffer containing 5% non-fat milk powder and 1% Tween 20 (BDH, Poole, UK) for one hour at 65°C. The primary antibody, diluted in a TBS solution containing 5% non-fat milk powder, 10% goat serum and 0.5% of the nonionic detergent IGEPAL™ was subsequently added and incubated at room temperature overnight in a polypropylene tube on a mechanical roller. The next morning, after discarding the antibody solution, the membrane was washed three times for 20 minutes with 20ml of TBS/0.5% IGEPAL™ on a mechanical roller. The secondary antibody, HRP-coupled to either goat anti-rabbit- or anti-mouse- IgG, was then incubated for one hour at room temperature using the same antibody diluent, followed by three washing steps with 20 ml TBS/0.5% IGEPAL™ for 20 minutes. Bound antibodies were then detected using the Enhanced Chemo-Luminescence Kit (ECL, Amersham Pharmacia Biotech UK Limited, Little Chalfont, UK) according to the manufacturer's instructions described in Section 2.9.6.

2.9.6 THE ECL-SYSTEM

The PVDF membrane is incubated for 1 minute with the detection reagent. This elicits a peroxidase-catalysed oxidation of luminol and subsequently enhanced chemi-luminescence, where the HRP-labelled protein is bound to the antigen on the membrane (Figure 2.12). The resulting light is detected subsequently on Hyperfilm ECL (Amersham) in seconds.

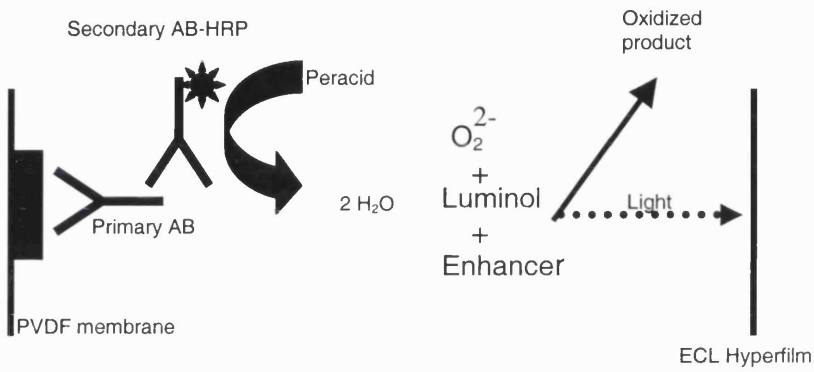

Figure 2.12 Schematic diagram of the ECL reaction. On the left a protein (black square) has been resolved on a SDS-PAGE gel and is now bound to the PVDF membrane, transferred through Western Blotting. On this protein an epitope is recognized by a specific primary antibody. A species-specific secondary antibody coupled to horse radish peroxidase can then bind to the primary antibody and catalyse the luminescence reaction (modified from the Amersham ECL catalogue).

2.9.7 QUANTIFICATION OF ECL HYPERFILMS

To compare the expression level of different proteins between the two genotypes the Imagequant software version 3.3 (Molecular Dynamics, Sunnyvale, CA, USA) was used to quantify ECL Hyperfilms by means of volume integration.

CHAPTER III.

PURKINJE CELL MORPHOLOGY

3.1 AIMS

The ataxic phenotype of homozygous *ducky* mutant mice in conjunction with the high level of $\alpha_2\delta$–2 transcript in cerebellar Purkinje cells (Barclay *et al.*, 2001) prompted the close examination of this prominent cerebellar cell type. The dendritic tree of a murine Purkinje neurone develops dramatically between postnatal days nine and twenty, coinciding with the first phenotypic manifestation of the *ducky* mutation at about P14. The purpose of the present study was to question if, and to what extent, the truncation of the $\alpha_2\delta$–2 subunit affects the morphology of developed Purkinje cells in *du/du* mice. As *du/du* animals do not survive beyond 35 days, P24-27 animals were examined. At this age the development of dendritic branch length as well as dendritic spine formation have peaked (P20), and the Purkinje cell dendritic field has reached its adult dimensions Sadler and Berry (1983). Two independent methods were chosen for this investigation: The non-invasive traditional Golgi-Cox impregnation method and as a complementary approach Purkinje neurones were directly microinjected with Lucifer yellow/neurobiotin in unfixed cerebellar slices.

3.2 RESULTS

3.2.1 GOLGI IMPREGNATION

The Golgi-Cox method is based on heavy metal precipitation (Hg^{2+}), which randomly impregnates approximately 1% of the neuronal population. Following Golgi-Cox impregnation as described in Section 2.7, two brains of P24 wild-type and *du/du* littermates respectively, were sectioned at 100μm thickness and analysed by light microscopy. By focusing through the section, it was ascertained that the individual cells observed were undamaged and below the cutting plane of the section. No gross histological abnormalities in *du/du* mutant mice were noted previously (Barclay *et al.*, 2001). The *du/du* cerebellum, though reduced in size, exhibits normal foliation, with the tri-laminar structure of the cerebellar cortex, i.e. the molecular layer, the granule cell layer and the Purkinje cell monolayer aligned between them. The cerebellar granule cells migrate completely into the internal granule cell layer and survive normally (Barclay *et al.*, 2001). Six Purkinje cells from *du/du* mice were examined in detail and one +/+ Purkinje cell, as they were very similar. Golgi-impregnated Purkinje cells of *du/du* mice show a dramatically reduced and malformed dendritic arborization compared to age-matched wild-type animals (compare +/+ in Figure 3.1A to *du/du* Figure 3.1B-F). A number of abnormal features could be discerned. Firstly, the dendritic field of *du/du* Purkinje cells was reduced in size and complexity (e.g. Figure 3.1B). Secondly, whereas the primary dendrites in +/+ animals extended almost perpendicular to the Purkinje cell layer, with their tertiary branchlets reaching the pial surface (Figure 3.1A), the primary dendrites in *du/du* animals extended often initially lateral before bending apical towards the pia, frequently not reaching its surface (Figure 3.1B, C, F). A thickening of primary and secondary dendrites in *du/du* was also observed (Figure 3.1B-E). Furthermore, thickened secondary and tertiary branchlets bent backwards towards the granule cell layer in a 'weeping willow'-like manner (Figure 3.1D). Additionally, multipolar Purkinje cell somata were observed, extending up to three primary dendrites (Figure 3.1D-F) terminating in dendritic branchlets.

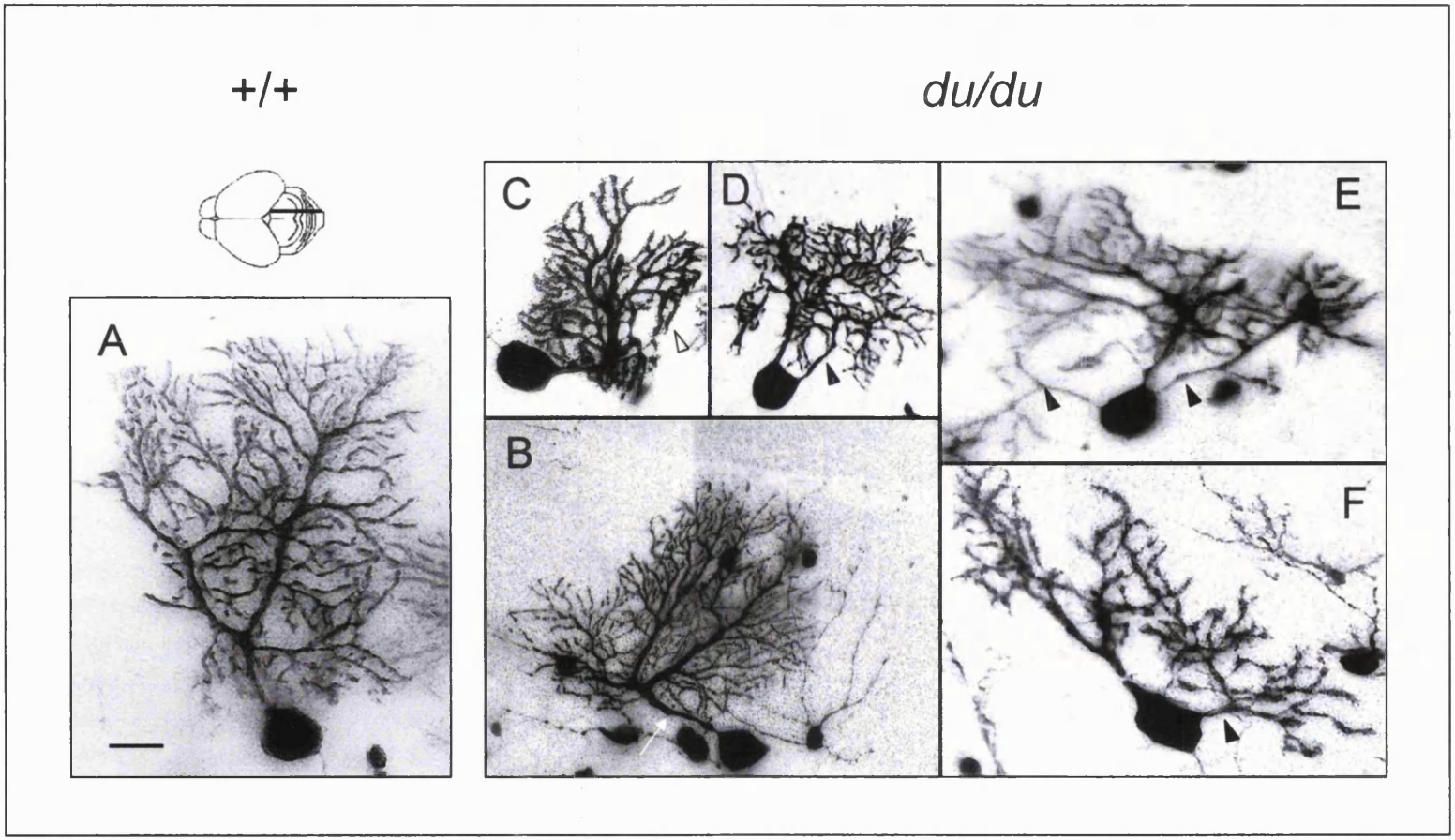

Figure 3.1 Reconstructed light micrographs (see Section 2.7) showing individual Golgi impregnated cerebellar Purkinje neurones. (**A**) +/+, (**B-F**) *du/du*. The diagram (top left) shows the parasagittal sectioned vermal region of the cerebellum. *du/du* Purkinje neurones are characterised by a reduced and malformed dendritic arborization (**B-F** compared to **A**), the absence of an apically orientated primary dendrite (arrow in **B**), a 'weeping willow'-like backbending of thickened tertiary branchlets towards the granule cell layer (**C**, open arrow), and multipolar nonapical primary dendrites extending laterally not targeting the pial surface (arrowheads in **D-F**). Scale bar 20 μm.

In contrast, second and third layer Pyramidal cells of the cerebral cortex of *du/du* mice did not show any obvious morphological alterations that could be distinguished with a light microscope (Figure 3.2).

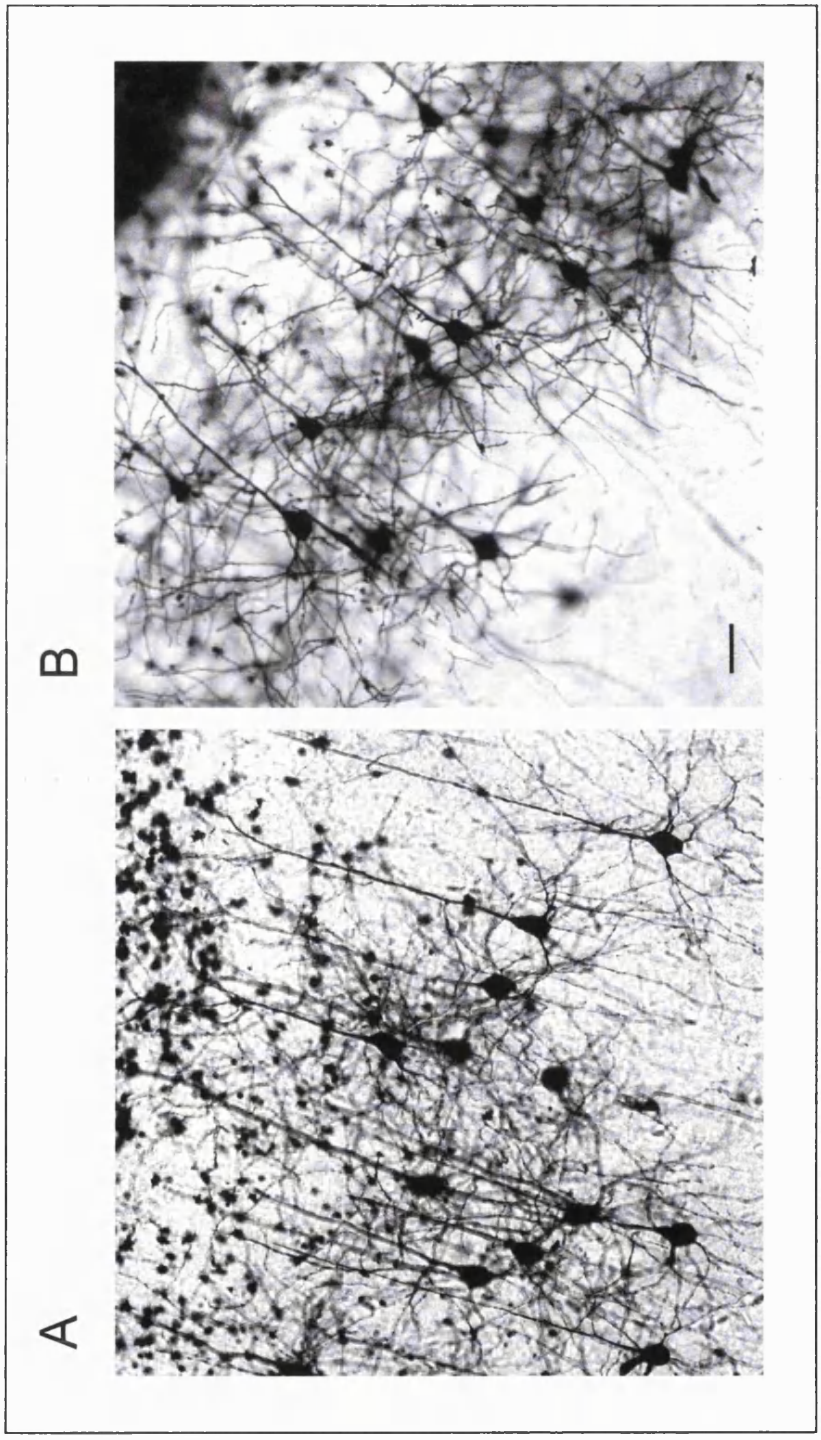

Figure 3.2 Golgi impregnated +/+ (**A**) and (**B**) *du/du* first and second layer Pyramidal cells of the cerebral cortex with their apical dendrites. No structural differences between the two genotypes were apparent. Scale bar 20μm.

3.2.2 LUCIFER YELLOW/NEUROBIOTIN IONTOPHORESIS

As complementary approach the polar tracers Lucifer yellow and neurobiotin (MW 457.24 and 367.3 Da respectively) were introduced iontophoretically into cell somata according to the method described in Section 2.6. Once inside the cell they penetrate the finest neuronal processes by diffusion. Reactive groups in their structure allow the subsequent aldehyde-fixation to biomolecules. Visualization was possible directly (Lucifer yellow, Figure 3.3A-C) or through detection with a Texas-red streptavidin conjugate (neurobiotin; Figure 3.3D). Experiments were performed on brain sections from 24-27 day old mice. An aqueous mixture of 10% neurobiotin and 10% Lucifer yellow was iontophoresed into the somata of Purkinje neurones in 400µm thick slices of unfixed cerebellar tissue. Direct observation of fluorescence at the time of injection established that dye diffusion was very rapid and confined to an intracellular distribution, so that the detailed shapes of neuronal cell bodies and dendrites, as well as some axonal features, were visualized. By filling several Purkinje cells spaced along a given folium, variations in cell shape could be correlated with their position along the changing curvature of the folium. The size and localization of their perikarya was normal, whereas the thickness of the molecular layer and granule cell layer appeared to be smaller in *du/du* compared to control animals (for comparison see Figure 3.4A and B). More importantly, the dendritic tree pattern appeared to be deranged (Figure 3.3, 3.4), with deformations similar to those seen in Golgi impregnated *du/du* Purkinje cells. *du/du* Purkinje cells displayed a dendritic arbor that was significantly reduced in size and dendritic mass, either reaching the border of the molecular layer only partially or not at all (Figure 3.4B). In extreme cases the dendrites completely bent back towards the granule cell layer in a 'weeping willow'-like manner (see open arrow, Figure 3.4B). Additionally, the shafts of the main Purkinje dendrites, as well as secondary dendritic branchlets, were often thickened in the upper molecular layer (Figure 3.3B *du/du*, Figure 3.4B), and focal axonal swellings were found in the granule cell layer (Figure 3.3C).

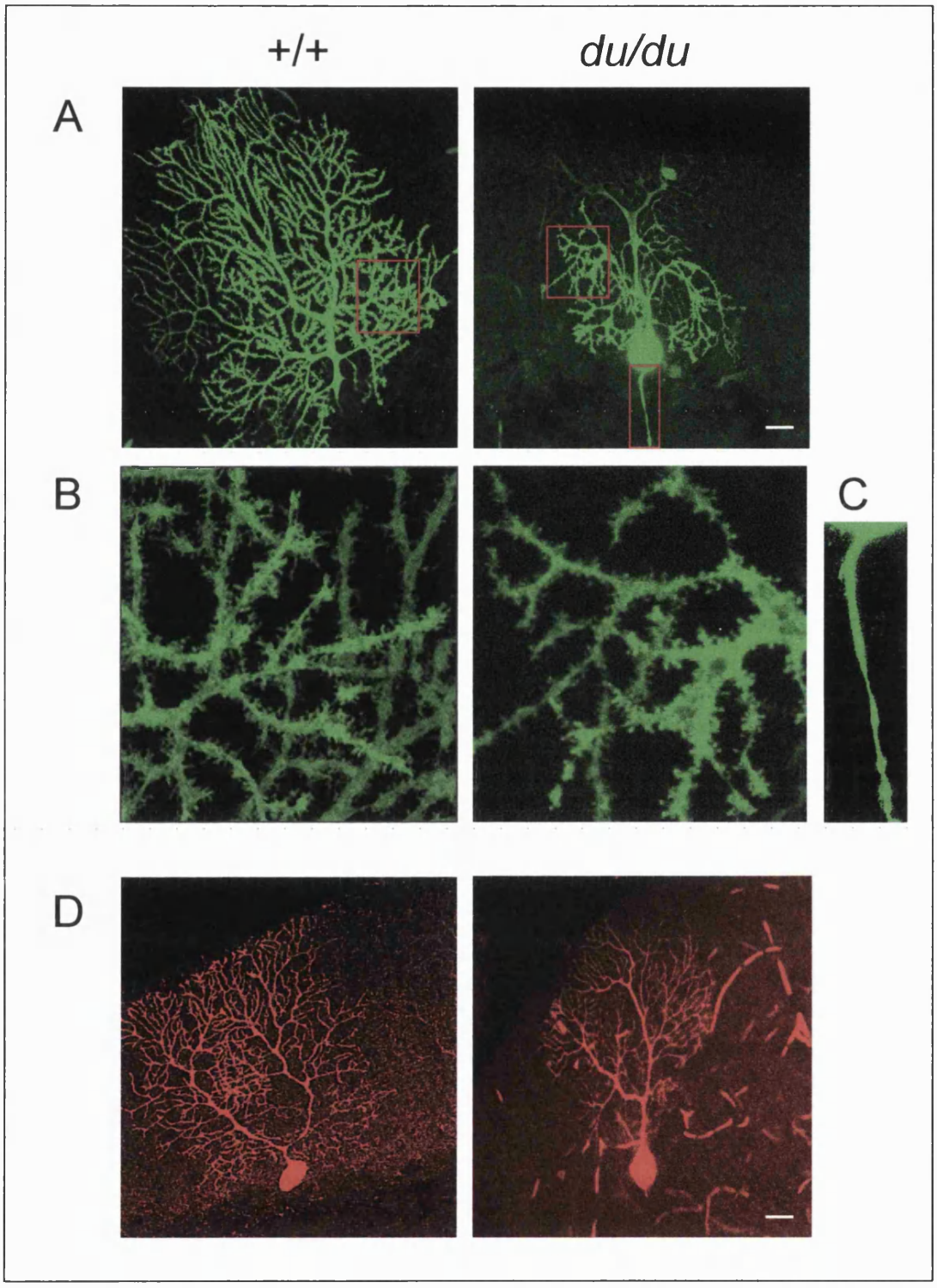

Figure 3.3 Examples of Lucifer yellow/neurobiotin microinjected cerebellar Purkinje cells. Lucifer yellow fluorescence in +/+ and *du/du* Purkinje cells is shown in **A**. Areas marked by a red square are magnified in **B**, showing dendritic spines in *du/du*, but also thickened tertiary branchlets. (**C**) the axon of the *du/du* Purkinje cell in **A** enlarged, showing focal swellings. In **D** the neurobiotin visualization with Texas-red-streptavidin shows the partial attainment of the pial surface by *du/du* Purkinje cell dendrites. Scale bar 10μm. Note that A and D are different cells for the respective genotype.

An attempt has been made to quantify the observed differences as described in Section 2.6.2 (Figure 3.4). Following skeletonization of the dendritic trees (Figure 3.4C), the number of dendrites were found to be significantly reduced as well as the extension of the dendritic tree in *du/du* Purkinje cells compared to +/+ (Figure 3.4D a, c). However the number of branchpoints on the longest dendrites was unchanged (Figure 3.4D b).

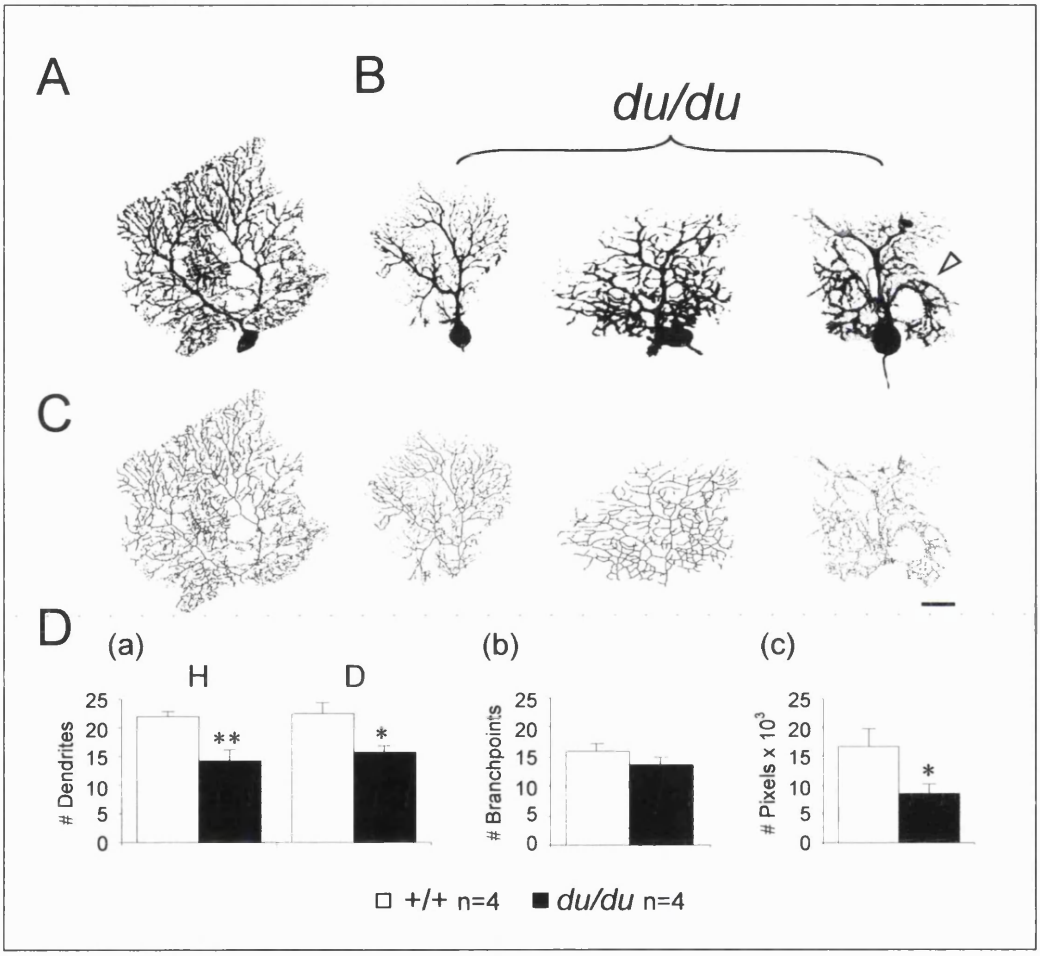

Figure 3.4 Evaluation of Lucifer yellow/neurobiotin injected cerebellar Purkinje neurones. (**A**) +/+ (neurobiotin staining for one cell shown as morphology was very similar) and (**B**) *du/du* (3 cells shown to illustrate variation in morphologies, the first imaged with neurobiotin staining, the other two with lucifer yellow). The open arrow in (**B**) points to dendritic branches bent back towards the granule cells layer in a 'weeping willow' like manner. (**C**) skeletonized dendritic tree for the cells shown in A and B for evaluation of arborization complexity independent of dendritic width. This is quantified in (**D**) according to three criteria:
(a) Dendrites crossing a horizontal (H) or diagonal (D) line.
(b) Number of branchpoints.
(c) Black pixels as indication of the dendritic field extension.
n=4 for both +/+ and *du/du* Purkinje cells. Asteriks indicate a statistically significant difference: *p<0.05, **p<0.01, student's *t* test. Scale bar 10μm.

3.2.3 SUMMARY OF MORPHOLOGIC ALTERATIONS IN PURKINJE CELLS

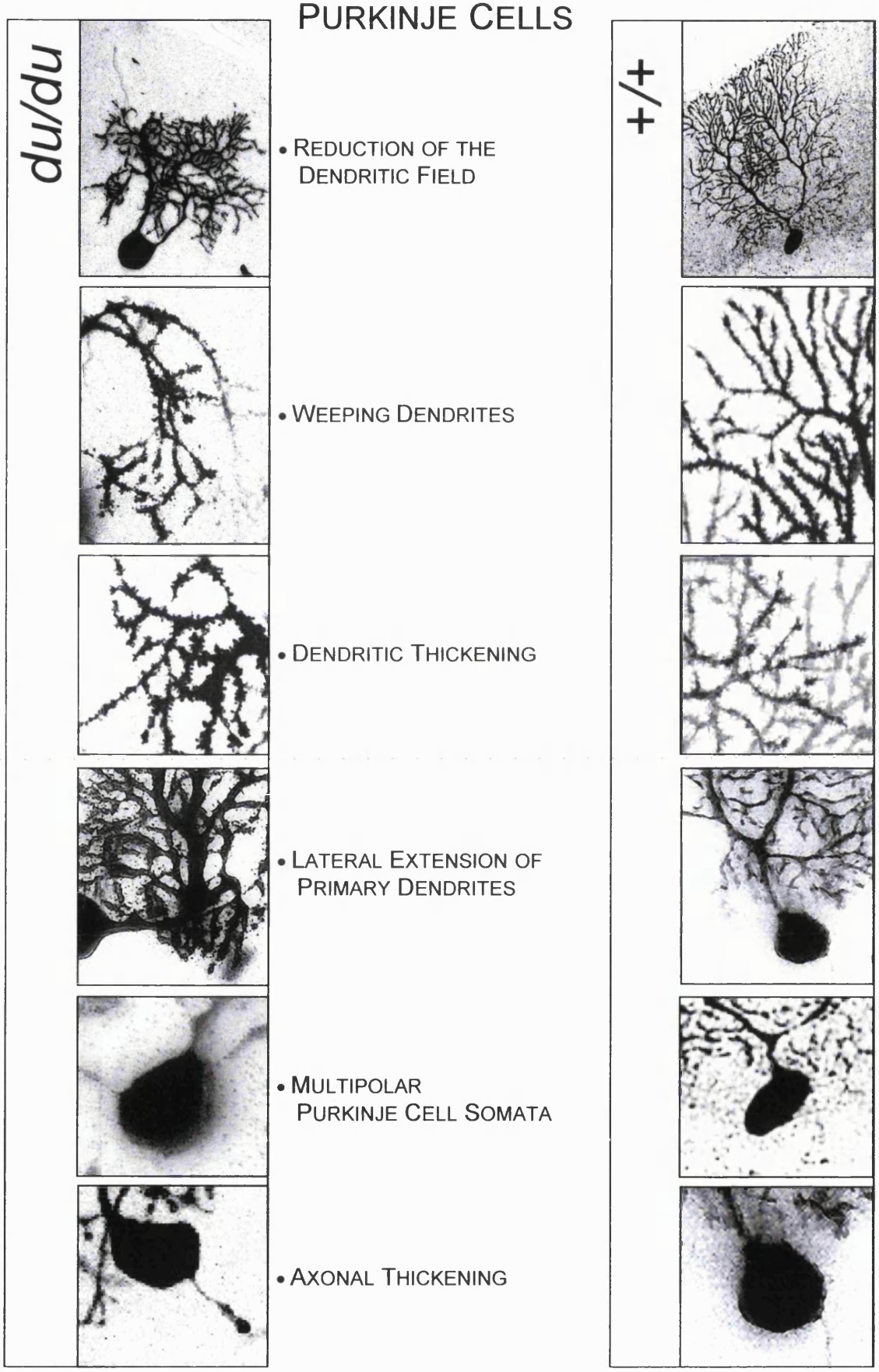

Figure 3.5 Summary of morphologic alterations seen in *du/du* Purkinje cells.

3.3 DISCUSSION

The appropriate development of dendritic form is a crucial element in ensuring the ability of a neurone to fulfill its physiological role. Two independent techniques point to a severe alteration in the morphologic structure of *du/du* Purkinje neurones in P24-27 animals. The protracted and sometimes capricious Golgi technique has the advantage of noninvasively impregnating 1% of the neuronal population at random, whereas instant microinjection involves manipulation of the tissue. Complete cell filling proved at times to be problematic, as frequently the cell soma became attached to the sharp electrode after the extended period necessary to fill the whole neurone (e.g. Figure 3.3A +/+). However both techniques presented the most dramatic abnormalities in the overall configuration and branching pattern of the cerebellar Purkinje cell dendritic tree, with a drastically reduced dendritic field and malformed dendritic arborization in *du/du* mice. Additionally, multipolar primary dendrites could be observed, which often appeared thickened and misorientated, in extreme cases resulting in their complete bending backwards towards the granule cell layer. This weeping appearance was also noticed in secondary and tertiary dendritic branchlets. Furthermore proximal Purkinje cell axons showed focal swellings, indicating a severe disturbance in their output, as seen in other cerebellar disorders that result in ataxia (Sotelo, 1990; Rhyu *et al.*, 1999a; Rhyu *et al.*, 1999b; Jeong *et al.*, 2000; Yang *et al.*, 2000; Zwingman *et al.*, 2001).

In order to consider the possible causes for these morphological alterations, it is necessary to briefly summarize the major time points of normal cerebellar development in the mouse (Figure 3.6), before relating the observed structural alterations to mouse models where cerebellar afferents have been differentially abolished or retarded and to examples of spontaneous mouse mutants like *ducky*.

Coordinated motor behaviour in the mouse, evident at the end of the second postnatal week, results from a condensed period of cerebellar synaptic development. The most superficial external granule cell layer is thickest at P7 (Miale and Sidman, 1961). At this time granule cells start migrating inwards through the arising molecular layer to form the granule cell layer, leaving their T-shaped axons (parallel fibres) behind thereby generating the molecular layer. They pass through the Purkinje cell layer, which at P7 forms a monolayer

between the molecular and granule layer, with their dendritic processes orientated towards the pial surface (Altman, 1969).

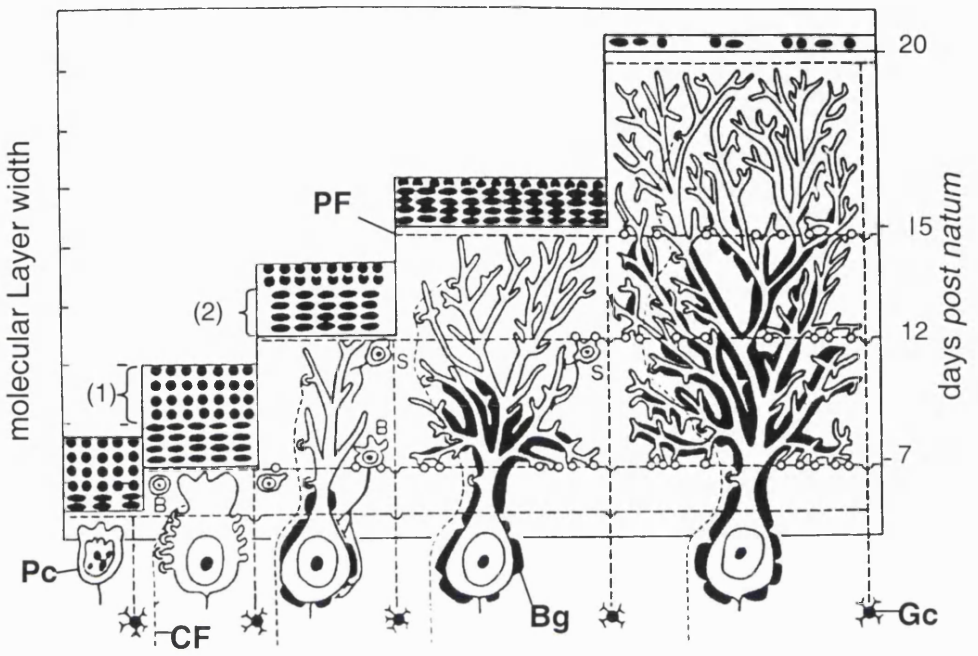

Figure 3.6 Illustration of the major time points in murine cerebellar Purkinje cell development. (1) Cells of the proliferative and (2) premigratory zone. Pc, Purkinje cell; Gc Granule cell; PF parallel fibres; CF, Climbing fibre, S, stellate cell; B, basket cell, Bg Bergmann glia. Adapted from Altman 1972.

Between P12 and P15 the lateral boundaries of the growing tree are reached, and dendrites constrained by the proximity of neighbouring trees start advancing towards the pial surface. Immature Purkinje cells receive innervations from multiple climbing fibres, whereas by P15 the adult one-to-one relationship is attained. The arborization of climbing fibres and the Purkinje cell development proceed simultaneously, whereby climbing fibres and parallel fibres induce the formation of somatic processes in Purkinje cells. In the mouse granule cell migration with parallel fibre production is complete at P20, when Purkinje cell dendrites reach the pial surface (Fujita, 1967). From P20 onwards further dendrite growth does not expand the outside boundaries of the dendritic field of the Purkinje cell arbor (Weiss and Pysh, 1978). Drug- or virus-induced abolition of granule cell growth as well as climbing fibre, stellate, or basket cell deafferentation greatly influences the Purkinje cell morphology, as reflected in decreased dendrite length, segment number, orientation of the dendritic tree,

multipolar somata as well as position and alignment of Purkinje cell somata in the cerebellar cortex (Ito, 1984). Dendrites probably advance through the neuropil at a constant rate and the frequency at which they encounter afferent input (i.e. through parallel fibres) in the proximity of their terminals may determine the number of branches formed by adhesive interaction with dendritic growth cone filopodia. The earlier insults are imposed during development, the more severe are the resulting morphologic alterations. Even altered timing through the drug-induced slowing of granule and molecular layer expansion greatly influences the Purkinje cell morphology, resulting in ectopic somata and multiple somatic often s-shaped dendrites (Ito, 1984). In contrast, the destruction of granule cells in adult rodents has little or no effect on Purkinje cell dendritic morphology (Ito, 1984). This accentuates how crucial afferent input is for the formation rather than the maintenance of the dendritic tree.

These findings are complemented through studies on a large number of phenotypically ataxic mouse mutants, spontaneous in origin, with different impairments in the cerebellar circuitry at different developmental stages. Although their histological and behavioural phenotypes are very diverse, they can be grouped into mutations where postnatally the majority of Purkinje cells degenerate (i.e. purkinje cell degeneration (*pcd*) and *lurcher* (*lc*)), mutations leading to the degeneration of Purkinje cells only in reciprocal alternate parasagittal zones (*leaner* (tg^{ln}) and *nervous* (*nv*)) and mutations where granule cells are lost (i.e. *weaver* (*wv*), *staggerer* (*sg*), *rolling Nagoya* (tg^{rol})). Interestingly, the severity of degeneration does not necessarily correlate with the gravity of the ataxic phenotype, as *pcd/pcd* or *lc/lc* show milder motor signs than *wv/wv*, despite the lack of virtually all Purkinje cells. This might be partly due to compensatory secondary processes.

Leaner (tg^{ln}) and *rolling Nagoya* (tg^{rol}) are both allelic to the *tottering* (*tg*) mutation, disrupting the gene coding for the calcium channel $Ca_V2.1$ subunit. Together with the recently discovered allele *rocker* (tg^{rkr}), the *tottering* (tg) mutation illustrates the broad phenotypic spectrum that the disruption of a single gene product can cause. These range from the nonviable *leaner* (tg^{ln}) showing Purkinje cell degeneration, through to the intermediate *tottering* (*tg*) and *rolling Nagoya* (tg^{rol}) with ectopic spines and axonal torpedoes and to the much milder

rocker (*tg*^{rkr}) where a decrease in branching and weeping dendrites is only manifest in older animals (Table 3.1).

Phenotypes of *tg/tg* alleles	*leaner*	*rolling Nagoya*	*tottering*	*rocker*
Viability	reduced	normal	normal	normal
Age of onset	P8-10	P10-14	P21-28	P21-28
Ataxia	+++ (1)	++ (2)	+ (1)	+ (3)
Cerebellar cell death	+ (4)	- (5)	- (6)	- (3)
Purkinje cell axonal torpedoes	+ (7)	+ (8)	+ (7)	- (3)
Purkinje cell current density	40% of control (9, 11)	60% of control (5)	60% of control (9)	?

Table 3.1 Comparison of phenotypical severity between alleles of the *tottering* mutation. (1) Meier and MacPike, (1971); (2) Oda, (1973); (3) Zwingman *et al.*, (2001); (4) Herrup and Wilczynski (1982); (5) Mori *et al.*, (2000); (6) Isaacs and Abbott, (1995); (7) Rhyu *et al.*, (1999a); (8) Rhyu *et al.*, (1999b) (9) Wakamori *et al.*, (1998); (10) Dove *et al.*, (1998).

I stressed in the introduction the importance of tightly regulated and balanced intracellular calcium signals for cell survival and gene transcription (Section 1.1.2). This is especially important in complex processes like development. Although a calcium imbalance seems the likely cause for changes in the morphology observed in *du/du* Purkinje cells, it also raises several questions: do the observed morphological alterations result from a failure of dendritogenesis or the atrophy of previously normal cells? Considering the early developmental stage in which they occur in *du/du* mutant mice, it is most probable that during the critical period of the first postnatal days Purkinje cells fail to make productive afferent contacts. This 'deafferentation' is the very likely cause of a retarded and malformed dendritic growth and ultimately dendritic retractions leading to thickening and atrophy. Sotelo (1975) considered the appearance of multipolar Purkinje cells in *weaver* and *staggerer* mutant mice as a remnant of their immature state, in which the normal resorption of all somatic filopodia fails to occur, with some of these processes continuing to develop into real dendrites. This leads to the question, can *du/du* Purkinje cells form functional post-synaptic entities? The presence of dendritic postsynaptic spines alone (Figure 3.3 B) is no clear indication of functional synapse formation, as

there is no correlation between spine shape and the capability of presynaptic input reception. Electron-microscopy studies showed that the Purkinje cell dendritic spines in the agranular *weaver* cerebellum, which are morphologically similar to those normally arising from spiny branchlets, are either postsynaptic to mossy fibres and Golgi cell dendrites, something which never occurs under normal conditions, or do not appose to any presynaptic element (Abbott and Sotelo, 2000)

Furthermore, the question needs to be addressed as to whether the observed morphologic alterations are limited to a certain Purkinje cell subpopulation as in *leaner* mutants (Heckroth and Abbott, 1994), or if they are uniform effects as seen in the s*taggerer* mutation?

Whether these morphologic alterations are a direct effect of the loss of the $\alpha_2\delta$-2 subunit in Purkinje cells or their afferent granule cells, a secondary effect altering synaptic function, or even a toxic effect of the truncated form of α_2-subunit, remains to be determined.

CHAPTER IV.

IMMUNOCYTOCHEMISTRY

4.1 AIMS

In order to extend the morphological analysis of cerebellar alterations in *du/du* mice, *du/du* cerebellar cryosections were immuno-labelled with antibodies against several neuronal antigens. In the *du/du* cerebellum regional loss of Purkinje cells at an unspecified age has been reported (Meier and McPike, 1970), hence the Purkinje cell-specific marker Calbindin D-28k was used to examine the potential loss of Purkinje cell bodies at P24. Additionally, as it has been suggested that Calbindin D-28k acts as endogenous calcium buffer in neuronal cells (Fierro and Llano, 1996), the expression level of this protein was analysed by Western blot experiments.

In situ hybridization with a *Cacna2d2* anti-sense RNA probe detected no full-length transcript in *du/du* Purkinje cells (Barclay *et al.*, 2001). However, *in situ* hybridization with a 5'*Cacna2d2* anti-sense RNA probe showed low levels of *du* mutant transcript 1 (*du*-mut1 α_2) in *du/du* Purkinje cells (Brodbeck *et al.*, submitted for publication). Anti peptide antibodies generated against the N-terminal region of the $\alpha_2\delta$–2 subunit were therefore used in order to determine whether a mutant protein is expressed within the *du/du* cerebellum.

In parallel, the expression of the glial fibrillary acidic protein (GFAP) in cerebellar sections was studied, which is a hallmark of reactive gliosis (Eng *et al.*, 2000). GFAP is expressed by the Bergmann glia surrounding Purkinje cells and an upregulation in its expression has been found in rats with genetic absence epilepsy (Dutuit *et al.*, 2000), a possible sign of neurodegeneration.

Additionally the activation of an apoptotic pathway was considered by using antibodies to caspases, the effector proteins of programmed cell death (Yuan and Yankner, 1999), whose expression levels were also compared between the different genotypes in Western blot experiments.

4.2 RESULTS

For the following immunohistochemistry performed on cerebellar cryosections, animals were perfused transcardially as described in Section 2.5.2. The cryoprotected brains were sectioned parasagittally at a thickness of 25μm and immunostained as described in Section 2.5.3.

4.2.1 CALBINDIN D-28K IN CEREBELLAR CRYOSECTIONS

Considering the cerebellar phenotype of ataxia in *du/du* mice, the strong expression of the $\alpha_2\delta$–2 transcript in +/+ cerebellar Purkinje cells as well as the observed alterations in Purkinje cell morphology (Chapter 3) Calbindin D-28k was used as a marker in order to determine the possible loss of Purkinje neurones, as previously reported by Meier and McPike (1970). The largely cytosolic calcium-binding protein Calbindin D-28k, a member of the EF-hand family (Baimbridge *et al.*, 1992), is known to act as a high-affinity buffer for intracellular calcium ($[Ca^{2+}]_i$; Lledo *et al.,* 1992). $[Ca^{2+}]_i$ is thought to reflect the firing frequency in neurones and it has been proposed that the concentration of intracellular Calbindin D-28k is likely to reflect the activity level of the respective neurones (Boukhaddaoui *et al.*, 2000). Furthermore Calbindin D-28k expression can be used as a specific marker for neuronal subpopulations such as Purkinje neurones of the cerebellum (Abe *et al.*, 1992).

Anti-Calbindin D-28K immunohistochemistry in *du/du* cerebella revealed no cell-loss at P24 (Figure 4.1). Purkinje cells appeared normal in respect to their general shape and arrangement, forming a continuous monolayer between the granule cell and molecular layers in all cerebellar sections examined. Staining intensity, as indicative of the level of protein expression was comparable between *du/du* and age-matched wild-type animals. Other than the reduction in the extent of the molecular layer reported earlier (Meier, 1968), no gross alteration in the cytoarchitecture could be distinguished between the genotypes.

As the use of confocal microscopy for quantitation has limitations as outlined in Section 2.5.10, Western blot analysis was carried out to examine the expression levels of Calbindin D-28k quantitatively (Figure 4.2).

At least 20 sections of each genotype derived from 5 or more different litters have been closely examined.

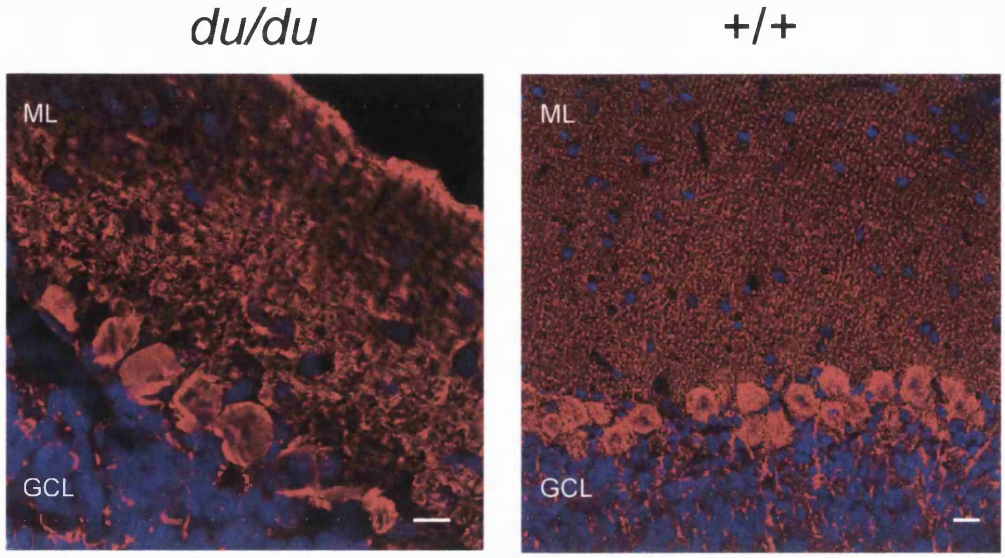

Figure 4.1 Calbindin D-28K in cerebellar sections of *du/du* and +/+ P24 mice. The pial surface is visible on the left. Aligned somata of Purkinje cells mark the border between molecular (ML) and granule cell layer (GCL). The cell dense granule cell layer is visible through blue nuclear DAPI staining.
Scale bars 15μm.

Equal amounts of total protein were compared between littermates of *du/du* and control animals (a representative sample is shown in Figure 4.2). To assess the ECL signals obtained quantitatively, the Imagequant 3.3 software (Molecular Dynamics) was used for densitometric measurements by means of volume integration. No significant differences could be detected in pairs from three different litters.

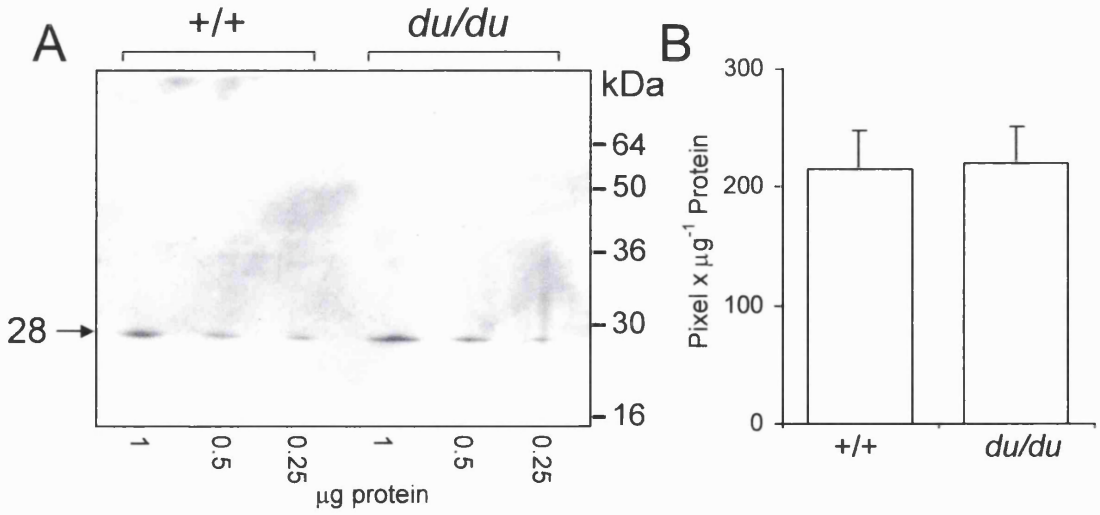

Figure 4.2 (**A**) Cerebellar membranes (of the indicated concentration) were prepared from P27 mice (see Section 2.9.2) and separated through SDS/12.5% PAGE, transferred to a PVDF membrane, incubated with anti-Calbindin D-28K antibodies and visualized using the ECL system. A calbindin D-28K-specific band of 28 kDa is visible. (**B**) Quantification of **A** using Imagequant 3.3 software.

4.2.2 GLIAL FIBRILLARY ACIDIC PROTEIN (GFAP) IN CEREBELLAR SECTIONS

Neuronal activity depends on brain homeostasis, controlled mainly by astrocytes (see Iino *et al.* (2001) and Oliet *et al.* (2001) for examples). Disturbances triggered by injury of the central nervous system result in reactive gliosis (Eddleston and Mucke, 1993; Ridet *et al.*, 1997). The major cellular hallmark for astroglial hypertrophy or reactive gliosis is an increased immunoreactivity to GFAP by resident astrocytes (Eng *et al.*, 2000). In the cerebellum GFAP is strongly expressed by the Bergmann glia surrounding the Purkinje cells (Eddleston and Mucke, 1993). This cell type has its cell body in the Purkinje cell layer and extends long processes through the molecular layer to the pia.

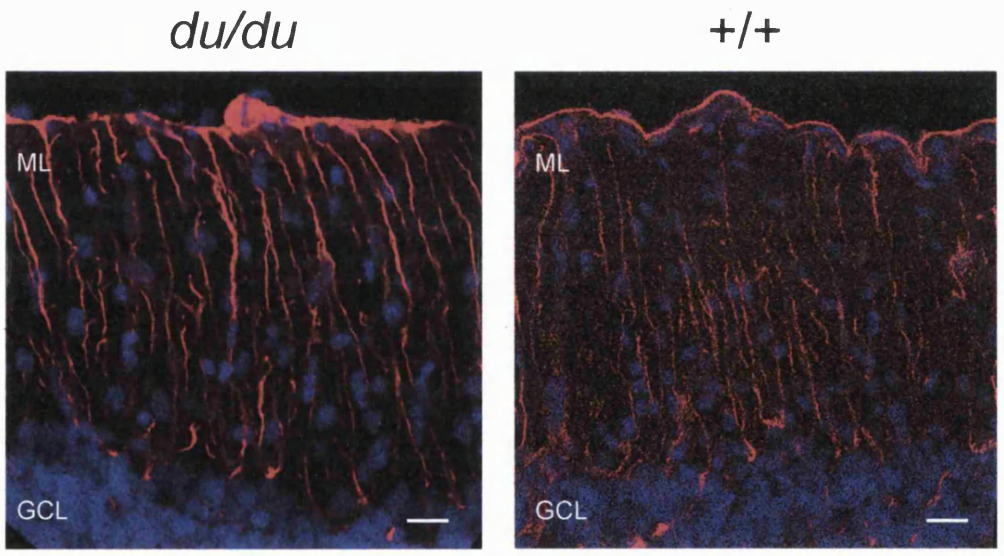

Figure 4.3 Red shows GFAP-specific staining in parasagittal cerebellar sections of *du/du* and +/+ P24 mice, traversing the molecular layer (ML). Blue nuclear DAPI staining marks the cell dense granule cell layer (GCL). Scale bars 15μm.

Immunohistochemical labelling of GFAP showed no differences in the intensity of Texas-red fluorescence as an indication of the expression level and distribution of the protein between the two genotypes (Figure 4.3). Cerebellar sections were taken from three different littermates. Bergmann glia cells of *du/du* and control animals show a comparable striped cytoarchitecture of Bergmann fibres.

At least 20 cerebellar sections taken from three different littermates were closely examined.

4.2.3 THE $\alpha_2\delta$-2 SUBUNIT

In situ hybridization with a 5'*Cacan2d2* anti-sense RNA probe showed the *du* mutant transcript 1 is present in *du/du* cerebellar Purkinje neurones at a low level. If we compare the modular architecture of the different $\alpha_2\delta$ subunits using the SMART database (http://smart.embl-heidelberg.de; Schultz *et al.*, 2000) it becomes apparent that two binding domains, a domain similar to von Willebrand factor type A (VWF, Ponting *et al.*, 2000) and a Cache domain (Anantharaman and Aravind, 2000) are highly conserved between $\alpha_2\delta$ subunits (Figure 4.4). Interestingly, the signal sequence for the $\alpha_2\delta$-2 subunit is obscured by a sequence of N-terminal hydrophilic amino acids and was therefore not recognized by the search engine.

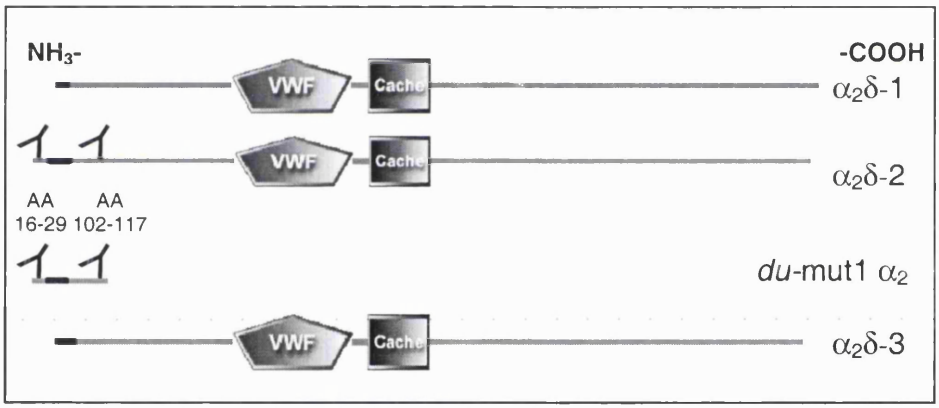

Figure 4.4 Modular architecture of the $\alpha_2\delta$ subunits. Differences in the signal sequence of $\alpha_2\delta$-2 are indicated (darkened line). The binding sites for the $\alpha_2\delta$-2 anti-peptide antibodies are shown. Each would recognize both the full-length $\alpha_2\delta$-2 as well as the truncated du-mut1 α_2 form arising from the ducky mutation.

To determine if this is functionally significant and to trace the distribution and processing of the full-length and possibly the truncated *du*-mut1 α_2 form of the $\alpha_2\delta$-2 subunit, we designed two anti-peptide antibodies directed against N-terminal amino acids unique to $\alpha_2\delta$-2. One recognizes amino acids 16-29 (referred to as Ab16-29) located before the putative signal sequence of $\alpha_2\delta$-2 and the other further downstream recognizes amino acids 102-117 (referred to as Ab102-117) near the N-terminus of the fully processed $\alpha_2\delta$-2 subunit.

4.2.3.1 SPECIFICITY OF THE $\alpha_2\delta$-2 ANTIBODIES

In order to characterize the specificity of the $\alpha_2\delta$-2 anti-peptide antibodies, proteins from the lysates of COS-7 cells transfected with a pMT2 vector expressing either $\alpha_2\delta$-1 or $\alpha_2\delta$-2 were separated (SDS/7.5% PAGE), transferred to PVDF membranes and then incubated with Ab16-29 or Ab102-117. Gel electrophoresis was routinely performed under thiol-reducing conditions, where α_2 is separated from the δ moiety to which it is coupled via a disulphide bond under native conditions. Distinct bands could only be visualized in cell membranes expressing $\alpha_2\delta$-2 but not in cell membranes expressing $\alpha_2\delta$-1 indicating the specificity of both antibodies (Figure 4.5). The observed size differences are likely to represent different maturation states of the α_2 protein. The band with the apparent molecular weight of 120 kDa recognized by Ab16-29 corresponds to the predicted size for the unglycosylated immature form of the α_2-2 protein with its signal sequence still attached. The band with the apparent molecular weight of 150 kDa recognized by Ab102-117 represents the mature glycosylated form of the protein from which the signal sequence has been cleaved (Marais *et al.*, 2001).

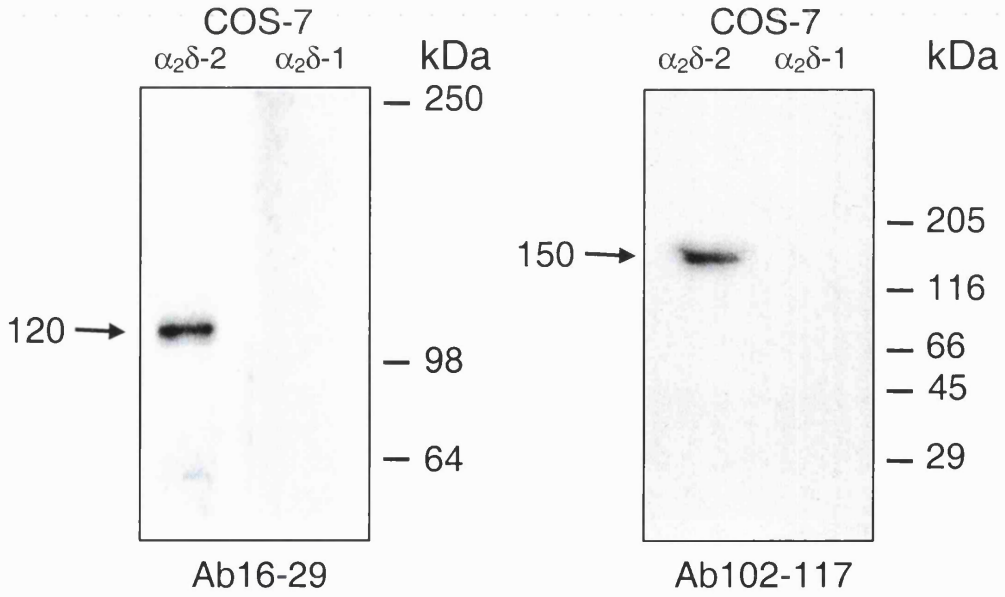

Figure 4.5 COS-7 cell lysates (40µg total protein) overexpressing either $\alpha_2\delta$-1 or $\alpha_2\delta$-2 were separated by SDS/7.5% PAGE under denaturing conditions and transferred to PVDF membranes, probed with the two anti peptide antibodies against $\alpha_2\delta$-2 (Ab16-29 or Ab102-117) and visualized using the ECL system.

As an additional control COS-7 cell lysates expressing either $\alpha_2\delta$-1, $\alpha_2\delta$-2 or *du*-mut1 α_2 were incubated with preimmune serum isolated before the immunization of the rabbits with peptide 16-29 or peptide 102-117 (Figure 4.6).

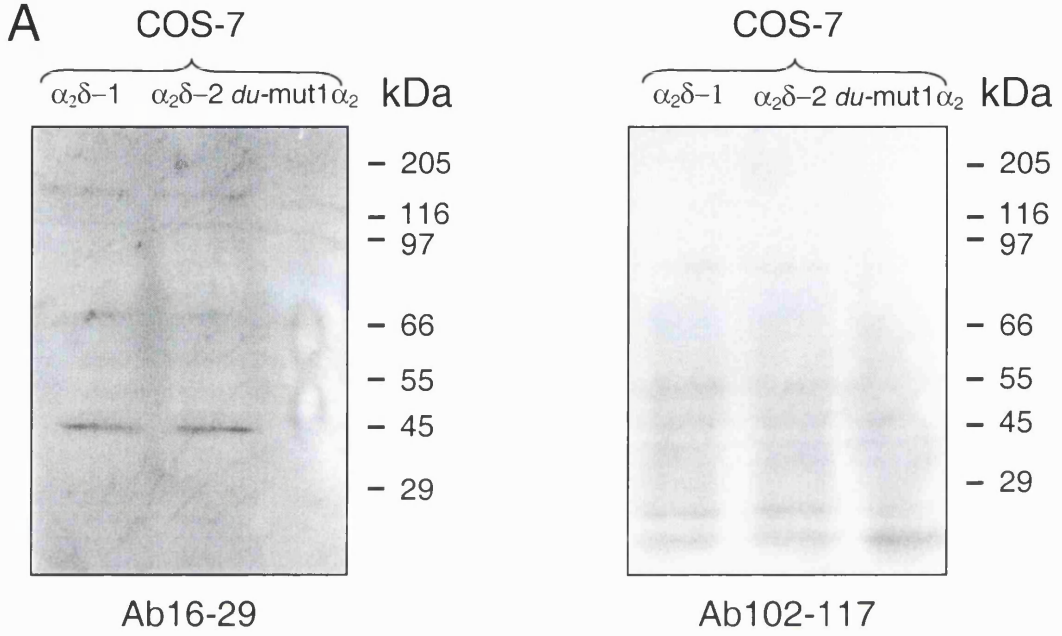

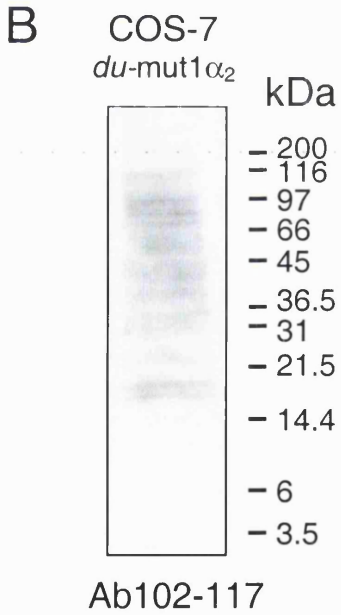

Figure 4.6 Pre-immune serum control. SDS/4-20% (**A**) or SDS/10-20% (**B**) PAGE of COS-7 cell lysates (80µg/lane) expressing the indicated protein was separated and after the transfer onto PVDF membranes incubated with protein A-purified rabbit preimmune serum IgG collected before the immunization with the peptides 16-29 or 102-117 respectively.

Although some staining is visible, it does not correspond with the predicted size of any of the transfected proteins and was furthermore also observed in untransfected COS-7 cell lysate and must therefore be unspecific. This is a further indication for the $\alpha_2\delta$-2 specificity of the antibodies Ab16-29 and Ab102-117.

4.2.3.2 TRANSIENT EXPRESSION OF *du*-MUT1 TRANSCRIPT IN COS-7 CELLS

In situ hybridization of *du/du* cerebellar sections with a 3'*Cacna2d2* antisense RNA probe showed the absence of the full-length message in *du/du* Purkinje neurones (Barclay *et al.*, 2001). However using a 5'*Cacna2d2* antisense RNA probe a faint signal was detected indicating the presence of a truncated form of the *Cacna2d2* message. To answer the question as to whether the truncated nonsensical transcript is also translated we expressed a pMT2 vector coding for *du*-mut1 α_2 in COS-7 cells. Lysates of these cells were electrophoretically separated together with COS-7 cell lysate expressing the full-length $\alpha_2\delta$-2 protein for size comparison and then probed with the respective anti $\alpha_2\delta$-2 antibodies after transfer to PVDF membranes.

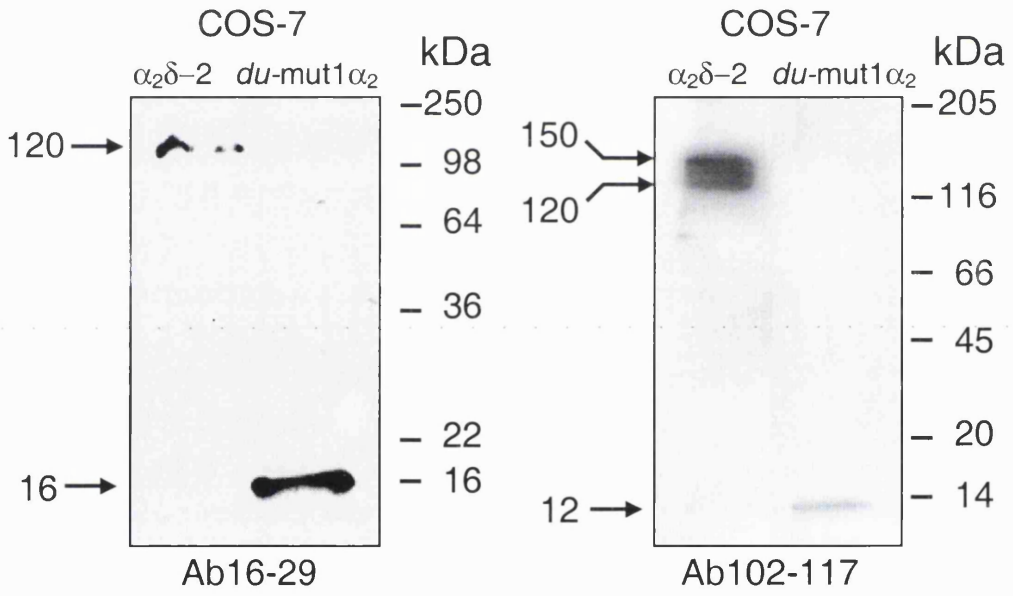

Figure 4.7 SDS/4-20% gradient PAGE of COS-7 cell lysates. The indicated COS-7 cell lysates (40µg total protein/lane) were separated and after transfer onto PVDF membranes incubated with the respective anti $\alpha_2\delta$-2 antibodies. The 'broad band' seen with Ab102-117 stretching from 150 kDa to 120 kDa could result from different glycosylation states of the protein. The reduction in the apparent molecular weight for the *du*-mut1 α_2 protein compared with that seen for Ab16-29 may result from the cleavage of the signal peptide.

The *du*-mut1 α_2 transcript as found in *du/du* cerebellar Purkinje neurones is translated when overexpressed in COS-7 cells and recognized by both antibodies (Figure 4.7). Ab16-29 recognizes a band of approximately 16 kDa corresponding to the predicted size of the translated product derived from the *du*-mut1 α_2 transcript with its signal sequence still attached (Figure 4.7). Once the signal sequence is cleaved, the apparent molecular weight decreases to approximately 10 kDa. Ab102-117 recognizes a band with the approximate molecular weight of 10 kDa; this corresponds very likely to the N-terminus of *du*-mut1 α_2, after cleavage of the signal sequence. In Figure 4.8 the predicted molecular sizes of the *du*-mut1 α_2 transcript and fragments derived from it are illustrated (see also 4.10).

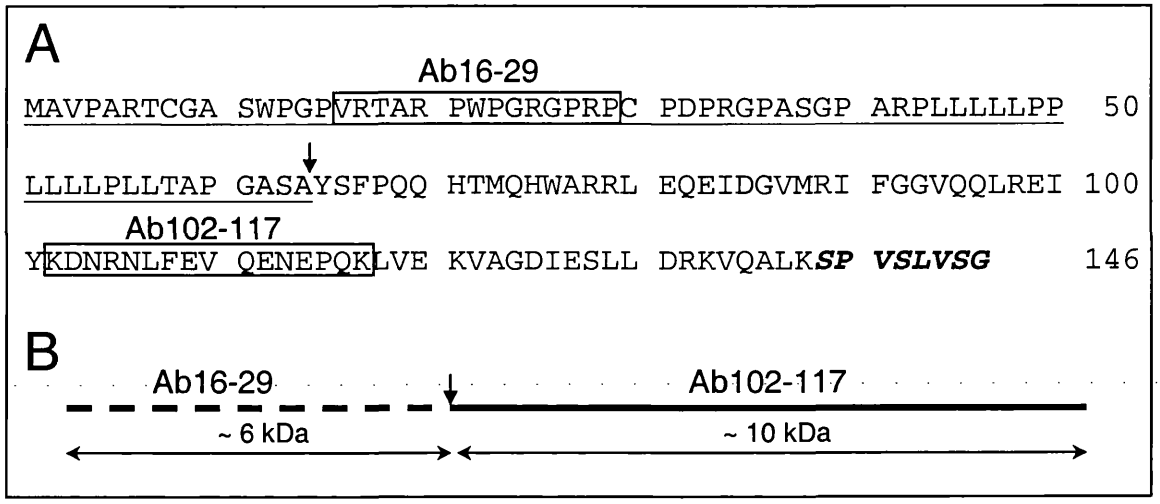

Figure 4.8 (**A**) Amino acid sequence of *du*-mut1 α_2. The respective binding sites for Ab16-29 and Ab102-117 are shown in boxes. The signal sequence is underlined with its predicted cleavage site (Nielsen et. al., 1997) marked by an arrow. *du/du*-specific amino acids are in italics. **B** shows the estimated molecular weights for the different fragments of *du*-mut1 α_2. The absolute molecular weight for the *du*-mut1 α_2 subunit, the signal sequence and the *du*-mut1 α_2 subunit without the signal sequence were calculated using the Omiga program (Version1.1, Accelrys Cambridge, UK). The molecular weights were determined as 16 kDa, 6 kDa and 10 kDa respectively.

In order to get a better estimation of the apparent molecular weight for the *du*-mut1 α_2 subunit, and derived fragments, COS-7 cell lysates expressing *du*-mut1 α_2 were separated on a 10-20% Tricine gel for better resolution of low molecular weight species (Figure 4.9).

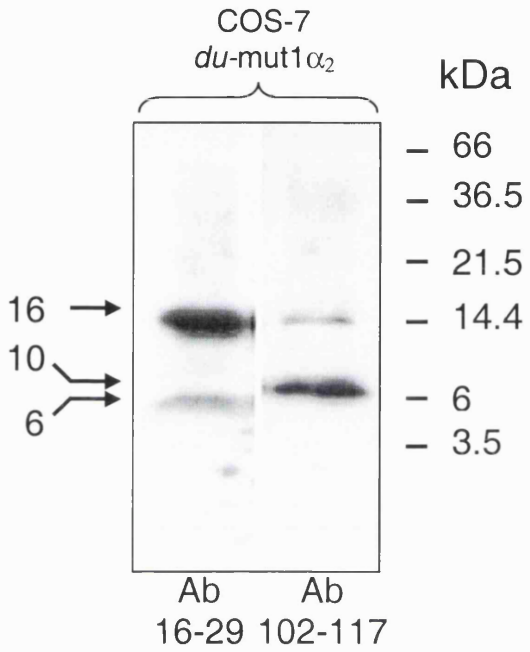

Figure 4.9 SDS/10-20% PAGE of COS-7 cell lysates (80 μg protein/lane) expressing *du*-mut1 α_2 were separated and after the transfer onto PVDF membranes incubated with the respective antibodies for $\alpha_2\delta$-2.

Both antibodies recognize a band of 16 kDa, which is the predicted size for *du*-mut α_2 with its signal sequence still attached. The difference in staining intensity might arise through affinity differences to their respective epitopes. In addition Ab16-29 recognizes a band of 6 kDa and Ab102-117 a band of approximately 10 kDa molecular weight, these are the predicted sizes for the signal sequence and *du*-mut α_2 with cleaved signal sequence respectively.

Figure 4.10 The amino acid sequence of the $\alpha_2\delta$–2 subunit. The putative signal sequence underlined. The dotted line surrounds *du*-mut1 α_2 (16 kDa) containing 8 novel amino acids (*SPVSLVSG*) in *italics*. The epitopes for the antibodies Ab16-29 and Ab102-117 in bold. The bold **A** at position 1000 is conserved in all three $\alpha_2\delta$ subunits and has been identified as cleavage site between α_2 and δ–1, the putative δ–2 subunit in grey. The predicted transmembrane region is indicated in dark grey. ( ) marks putative N-glycosylation sites. The respective sizes for the alternate subunits are shown on the left.

4.2.3.3 IMMUNO-LOCALIZATION OF $\alpha_2\delta$-2 AND *du*-mut1 α_2 IN TRANSIENTLY TRANSFECTED COS-7 CELLS

To determine the localization of the full-length $\alpha_2\delta$-2 subunit in COS-7 cells at different stages of protein maturation and to address the question as to where the truncated form of the $\alpha_2\delta$-2 subunit *du*-mut1 α_2 is targeted, COS-7 cells were used as a heterologous expression system for overexpression and subsequent visualization of the $\alpha_2\delta$-2 subunit in immunocytochemical experiments utilizing confocal microscopy.

It was first necessary to establish if COS-7 cell membranes remain intact throughout the different immunocytochemical processing steps. For this purpose, COS-7 cells were transiently transfected with a pMT2 vector expressing GFP, an entirely intracellular protein (Tsien, 1998). Transfected cells expressing GFP were identified by its characteristic green fluorescence (see spectrum in Section 2.5.7). In addition cells were incubated with an antibody directed against GFP either under permeabilizing (+0.02% Triton X-100) or non-permeabilizing conditions and then visualized with a Texas-red streptavidin conjugate following incubation with a biotinylated goat anti-mouse antibody (Figure 4.11 B). The results indicate the integrity of the cell membrane, as under non-permeabilizing conditions the antibody did not penetrate the cell. This heterologous expression system can therefore be used to investigate the localization of the $\alpha_2\delta$-2 subunit during different stages of maturation, but similar results were also obtained with tsA cells.

If the full-length form of the $\alpha_2\delta$-2 subunit is transiently expressed in COS-7 cells, Ab16-29 shows no Texas-red staining in non-permeabilized cells (Figure 4.11 C top left). GFP was used in this experiment as a positive transfection control and has been co-transfected with $\alpha_2\delta$-2 at a 20 times lower DNA concentration. Under the same non-permeabilizing conditions, the N-terminal $\alpha_2\delta$-2 epitope is accessible to Ab102-117 exofacially, thereby distinctly outlining the membraneous border of the cell (Figure 4.11 C top right). If the cells are permeabilized prior to antibody incubation, Ab16-29 shows a diffuse overall staining of the entire cytoplasm (Figure 4.11 C bottom left). However, Ab102-117 presents a more restricted staining, possibly confined to specific intracellular

compartments. The perinuclear staining might resemble the endoplasmic reticulum (ER), with adjacent Golgi and trans-Golgi network exporting the protein to the plasma membrane.

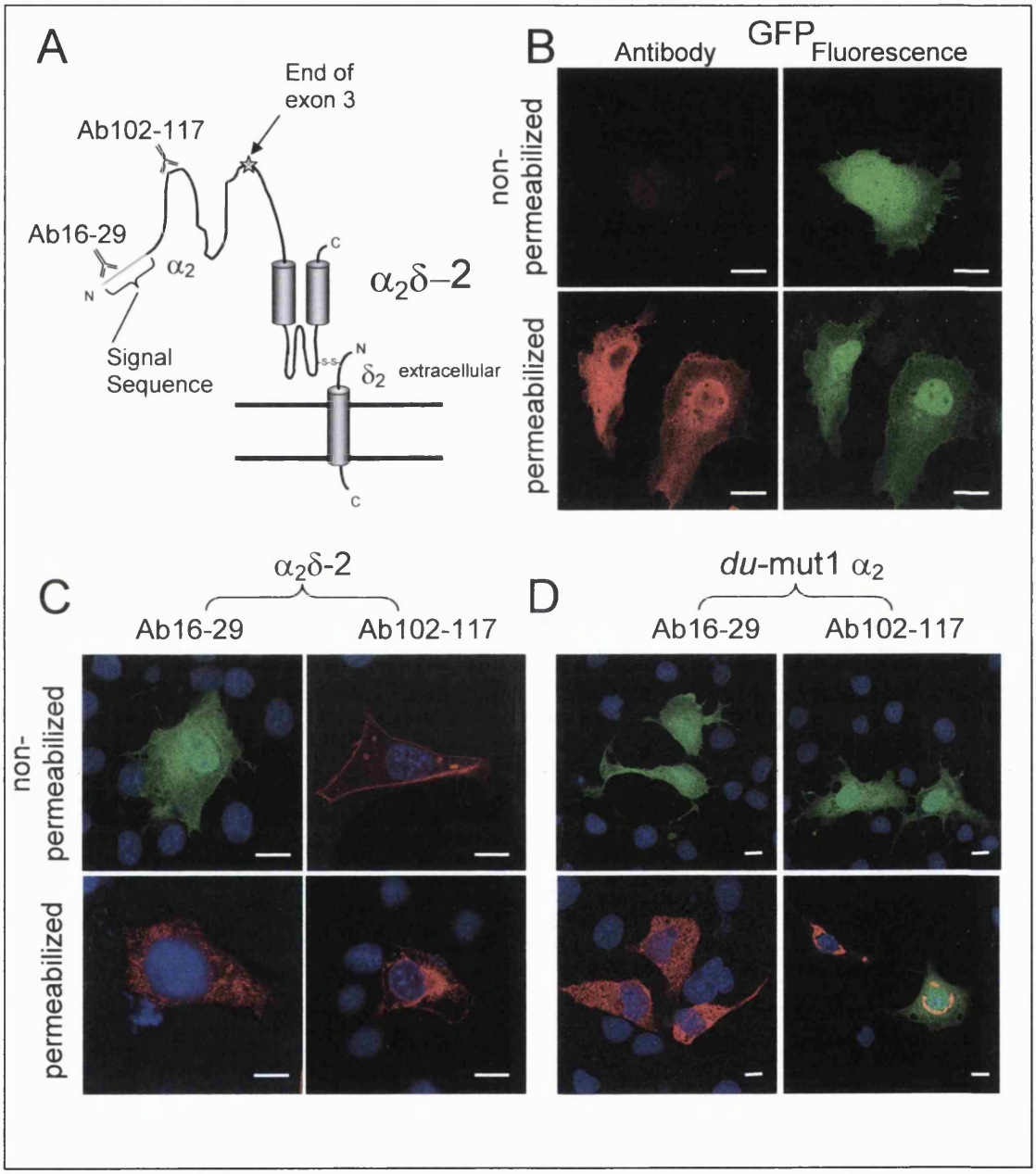

Figure 4.11 Localization of the full-length and truncated $\alpha_2\delta$-2 subunits expressed in transiently transfected COS-7 cells. The epitopes of Ab16-29 and Ab102-117 are illustrated in **A**. To ascertain that the cell membrane remains unscathed during immunocytochemical procedures, the conditions were tested using a GFP antibody (**B**). Full-length $\alpha_2\delta$-2 is detected exofacially in non-permeabilized cells by Ab102-117, which also shows a more confined intracellular localization in permeabilized cells compared to Ab16-29 (**C**). Neither Ab16-29 nor Ab102-117 recognizes the truncated $\alpha_2\delta$-2 subunit *du*-mut1 α_2 in non-permeabilized cells. The intracellular distribution of *du*-mut1 α_2 is more ubiquitous for Ab16-29 and confined to specific intracellular compartments for Ab102-117 in permeabilized cells (**D**). Scale bars 10μm

In non-permeabilized cells expressing *du*-mut1 α_2, neither $\alpha_2\delta$-2-specific antibody recognized the epitope exofacially (Figure 4.11D top panel). Under permeabilized conditions Ab16-29 gives a diffuse overall cytoplasmic staining (Figure 4.11 D bottom left), similar to that seen in cells transfected with the full-length $\alpha_2\delta$-2 subunit. Ab102-117 shows a very distinct staining, localizing this truncated form of the protein in very restricted compartments of the cell where it appears to accumulate (Figure 4.11D bottom right).

4.2.3.4 ANTI-PEPTIDE CONTROL FOR ANTIBODIES Ab16-29 AND Ab102-117

As a control to question the specificity of the observed fluorescent signal the immunizing peptide for either Ab16-29 or Ab102-117 was pre-incubated with the respective diluted antibody, before their application onto slides (Figure 4.12).

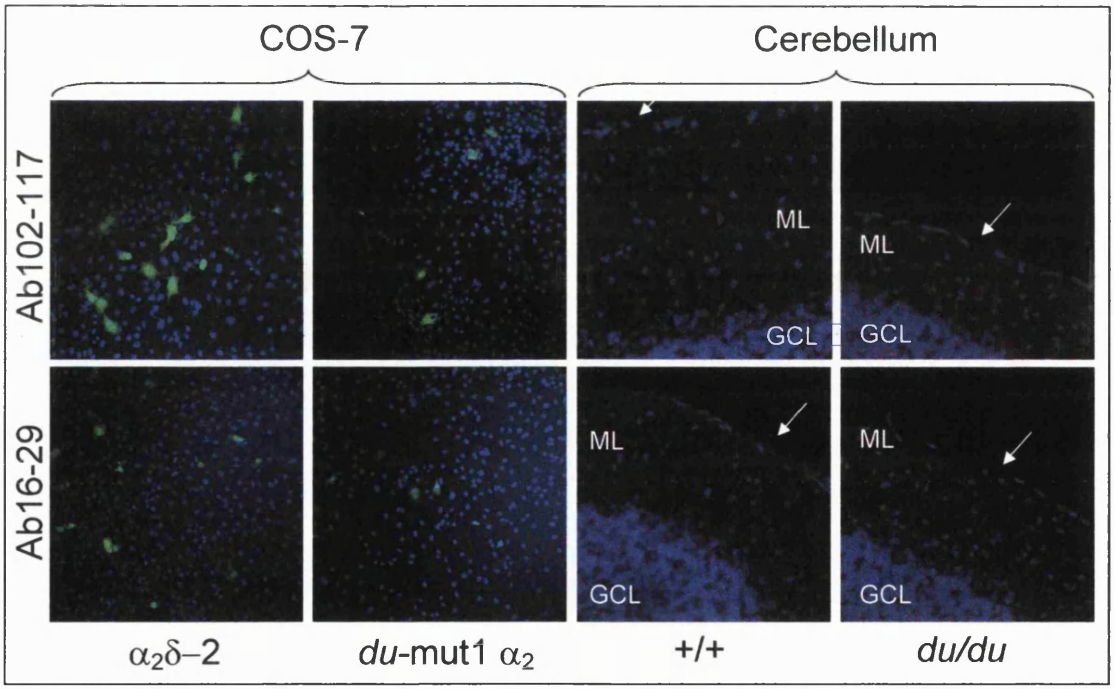

Figure 4.12 Anti peptide control for Ab16-29 and Ab102-117. Blue, nuclear DAPI staining. On the left, panels showing COS-7 cells, transfected with either $\alpha_2\delta$-2 or *du*-mut1 α_2. GFP (green fluorescence) was co-transfected and used as a positive transfection marker. The panels on the right show cerebellar sections of P26 animals of the indicated genotype. GCL markes the granule cell layer and the arrow indicates the border of the molecular layer (ML).

With both antibodies non-specific background staining was absent, both in COS-7 cells expressing $\alpha_2\delta$-2 or *du*-mut1 α_2 as well as in cerebellar sections. This is a further indication for the specificity of both antibodies.

4.2.3.5 IMMUNO-LOCALIZATION OF THE $\alpha_2\delta$-2 SUBUNIT IN CEREBELLAR TISSUE

To compare the expression levels of the $\alpha_2\delta$-2 subunit in +/+ and *du/du* cerebellum, Western blot experiments were performed. A 150 kDa band was only obtained with Ab102-117, but no bands were observed with Ab16-29 (Figure 4.13). This is either an indication that the immature, unglycosylated form of the protein is not present in a high enough concentration to be detected, which might also be true for the truncated form of the protein, or that the affinity of Ab16-29 is lower.

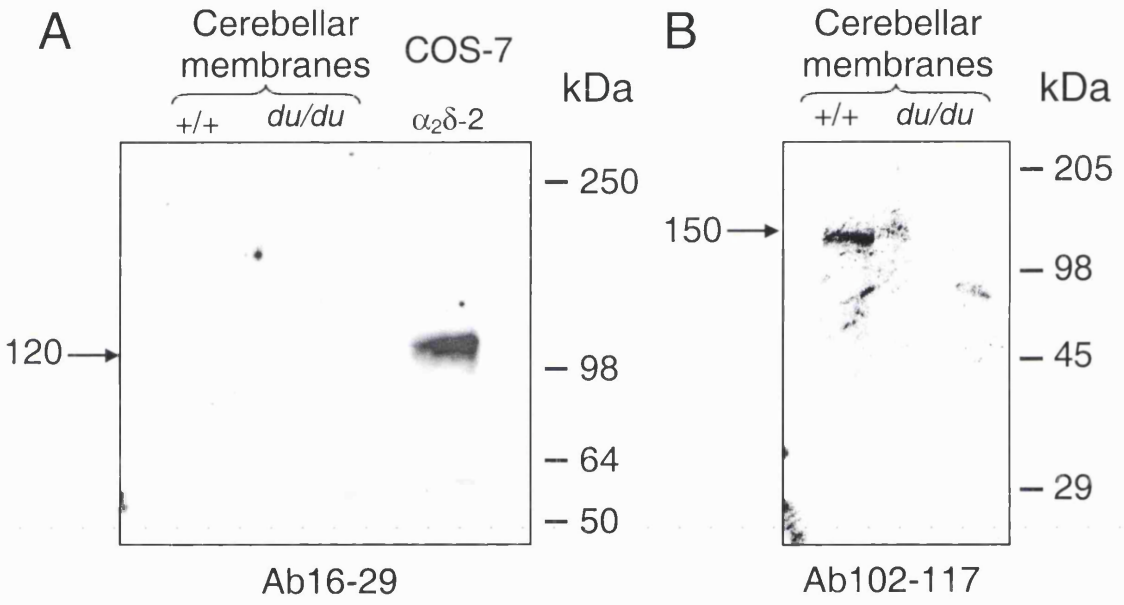

Figure 4.13 Expression of the $\alpha_2\delta$-2 subunit in the cerebellum. SDS/4-12% gradient PAGE of 200µg total cerebellar membrane protein from P27 animals of the indicated genotype. Immunolabelled with Ab16-29 (**A**) and Ab102-117 (**B**).

However both forms of the protein could be detected in cerebellar protein using both antibodies following immunoaffinity concentration (Dr. Tony Davies personal communication).

In order to localize the $\alpha_2\delta$-2 subunit in the cerebellum and compare its expression between the different genotypes, parasagittal sections of P24 *du/du* and control cerebella were incubated with the $\alpha_2\delta$-2-specific antibodies. Ab16-29 shows strong immunoreactivity in somata of cerebellar *du/du* Purkinje cells (Figure 4.14 top left), where the *du*-mut1 α_2 protein appears to accumulate,

compared to a more uniform staining observed in control animals (Figure 4.14 top right). At least 30 sections from 6 different littermates were closely examined.

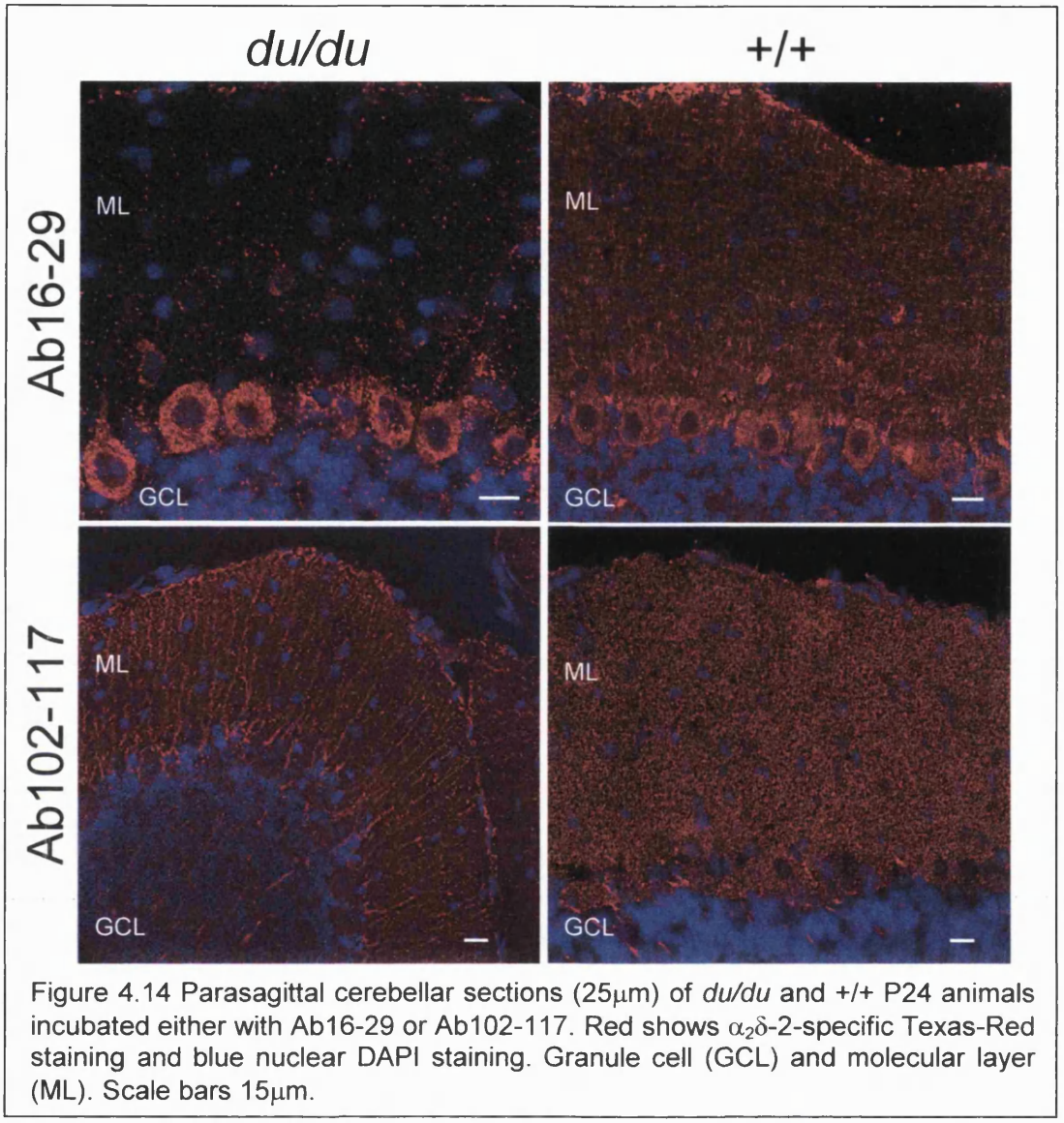

Figure 4.14 Parasagittal cerebellar sections (25μm) of *du/du* and +/+ P24 animals incubated either with Ab16-29 or Ab102-117. Red shows $\alpha_2\delta$-2-specific Texas-Red staining and blue nuclear DAPI staining. Granule cell (GCL) and molecular layer (ML). Scale bars 15μm.

The observation that the translated *du*-mut1 α_2 protein appears to be in part retained in a perinuclear compartment, very likely the ER, when overexpressed in COS-7 cells (Figure 4.11 D), or as seen in *du/du* Purkinje cell somata with probable subsequent proteosomal degradation, might suggest the activation of stress-induced signalling pathways. These have been found to be triggered following the accumulation of misfolded proteins in the ER (Kaufman, 1999) and/or disturbed calcium homeostasis (Mattson *et al.*, 2000), both of which are likely consequences of the *ducky* mutation. Prolonged ER stress in turn can contribute to cell death and is linked to the pathogenesis of several neurodegenerative disorders (Sherman and Goldberg, 2001).

4.2.4 IMMUNO-LOCALIZATION OF CASPASE 3 AND 12 IN CEREBELLAR TISSUE

Apoptosis, or programmed cell death occurs under either physiological or pathological conditions and can be initiated by a multitude of environmental factors (Sastry and Rao, 2000; Nijhawan *et al.*, 2000). Specific receptors, direct activation, permeabilization of the mitochondrial outer membrane, as well as disturbances in protein folding and calcium homeostasis lead ultimately to the activation of cysteinyl aspartate-specific proteinases as the point of irreversibility (Earnshaw *et al.*, 1999).

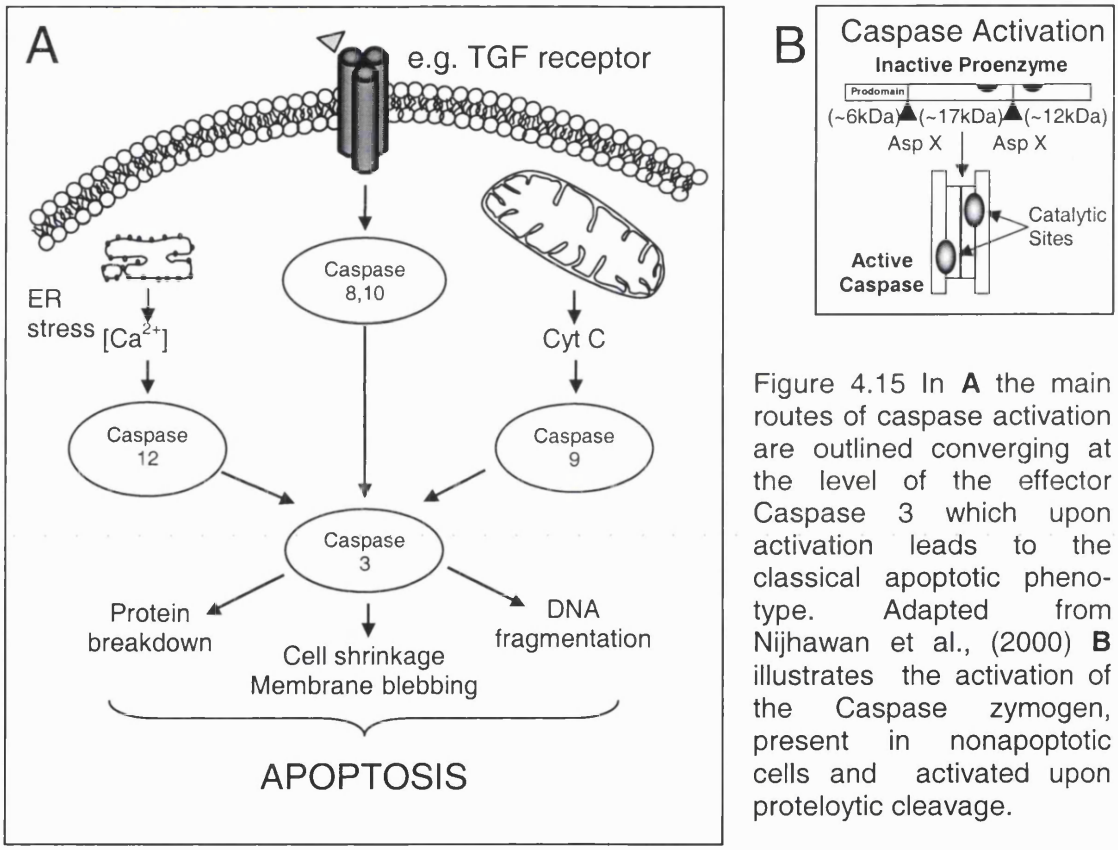

Figure 4.15 In **A** the main routes of caspase activation are outlined converging at the level of the effector Caspase 3 which upon activation leads to the classical apoptotic phenotype. Adapted from Nijhawan et al., (2000) **B** illustrates the activation of the Caspase zymogen, present in nonapoptotic cells and activated upon proteloytic cleavage.

Caspases are present in the cytoplasm as inactive proenzymes, which upon activation are cleaved to yield the active tetrameric protease (Hengartner *et al.,* 2000; Figure 4.15). Activated caspases cleave specific key cellular proteins, thereby disabling and disassembling the dying cell. There appears to be a hierarchy of caspases, with some acting as initiators of proteolysis and others acting downstream as executioners (Thornberry and Lazebnik, 1998).

To examine the possible activation of apoptotic proteases in the pathogenesis of the *du/du* mutation, two prominent caspases involved in

neuronal apoptosis were targeted immunocytochemically. Caspase 12 has recently been related to ER stress-induced apoptosis (Nakagawa *et al.*, 2000). The zymogen of caspase 12 is localized to the ER and upon activation functions as initiator for downstream caspase activation. Caspase 3 activation has been demonstrated in several models for neurodegeneration *in vitro* (Du *et al.*, 1997; Marks *et al.*, 1998), plays a key role in developmental neuronal apoptosis (Kuida *et al.*, 1996) and was found to be involved in apoptotic cell death following experimental ischemia (Namura *et al.*, 1998) and epileptic seizures (Henshall *et al.*, 2000). To compare the cerebellar expression level of these caspases in *du/du* and control mice at P24 specific antibodies against caspase 3 (Wang *et al.*, 1996) and caspase 12 (Nakagawa *et al.*, 2000) have been employed.

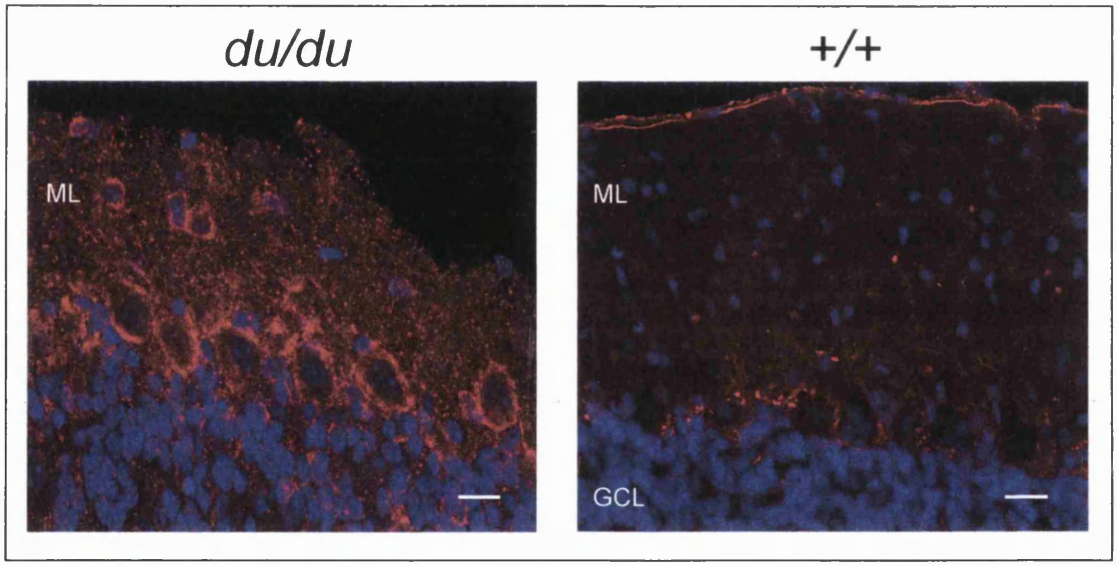

Figure 4.16 Immuno-localization of caspase 3 (red) in cerebellar tissue. Blue nuclear DAPI staining. Parasagittal sections (25μm) of paraformaldehyde perfused and cryoprotected brains of P24 mice of the indicated genotype. Granule cell layer (GCL) and molecular Layer (ML). Scale bars 10μm.

In *du/du* Purkinje cells a stronger pro-caspase 3 staining was observed in their somata when compared to wild-type littermates, indicating an upregulation of caspase 3 expression (Figure 4.16). At least 15 slices from three different littermates were closely examined.

This apparent upregulation in the expression of the caspase 3 proenzyme could be seen in preparations taken from three separate litters. However Western blot experiments, carried out with cerebellar protein homogenates of the different genotypes did not corroborate the immunocytochemical findings (a representative sample is shown in Figure 4.17), as the differences were not significant.

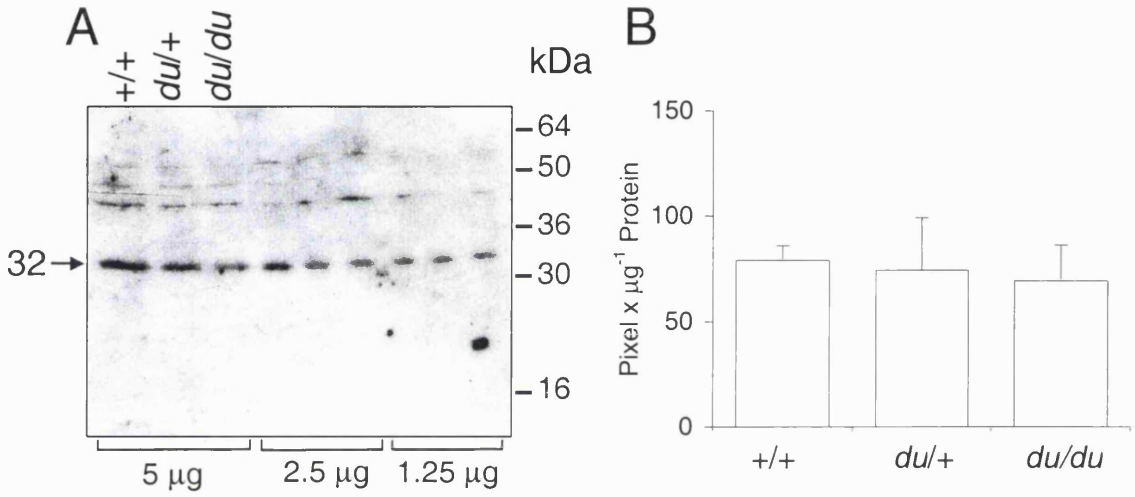

Figure 4.17 **A** The indicated amount of protein homogenate from P27 cerebella was separated by SDS/7.5% PAGE. Transfer onto a PVDF membrane was followed by the incubation with the caspase 3 antibody recognizing the ~32 kDa propeptide of the enzyme. A band of the predicted size is marked by an arrow. **B** Quantification of protein bands in blot **A** using Imagequant 3.3 software.

Similarly Western blots of cerebellar protein labelled with an anti-caspase 12 antibody showed no difference in staining intensity as an indication for its expression level in the two genotypes (Figure 4.18).

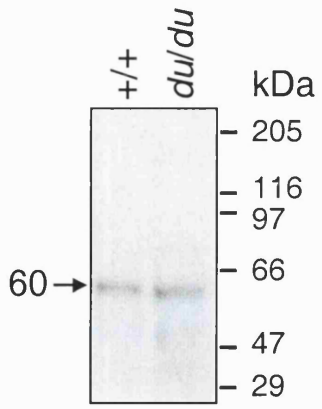

Figure 4.18 SDS/7.5% PAGE of 25µg total protein from P27 cerebella was separated. Transfer onto PVDF membrane was followed by the incubation with the caspase 12 antibody recognizing the ~60 kDa propeptide.

4.3 DISCUSSION

4.3.1 CALBINDIN

In mature Purkinje cells (4 weeks postnatally in mice, Kurobe *et al.*, 1992) Calbindin D-28k contributes about 15% of total cellular protein (Baimbridge and Miller, 1982). Its high affinity for calcium (K_d is submicromolar, Nagerl *et al.*, 2000a) influences important neuronal characteristics by (a) altering the temporal and spatial spreading of an action potential thereby modifying calcium-dependent intracellular signalling; (b) by inhibiting the Ca^{2+}-dependent K^+ current neuronal 'bursting activity' is promoted; (c) by inhibiting Ca^{2+}-dependent inactivation of VDCCs the contribution of Ca^{2+} entry to the overall membrane depolarization is increased (Nagerl *et al.*, 2000b) and finally a role in protecting the cells against the damaging effect of excessive calcium influx during prolonged periods of high activity is assumed (D'Orlando *et al.*, 2001). No gaps in the Purkinje cell monolayer as assessed by Purkinje cell-specific Calbindin D-28k immunocytochemistry were observed at P24. Also no loss of granule cells was observed in a previous study using calretinin as a marker (Barclay *et al.*, 2001). Furthermore, the level of Calbindin D-28k protein expression was found to be similar between *du/du* and +/+ mice. This result is somewhat surprising given the phenotypical severity of the *du/du* mutation, which might originate in a disturbed calcium homeostasis and considering that Calbindin D-28k expression has been found to be Ca^{2+} dependent (Arnold and Heintz, 1997).

In situ hybridization showed a reduction of Calbindin D-28K mRNA in the *leaner* mutant (tg^{la}) and is seen as a compensation for reduced P-type calcium channel function (Dove *et al.*, 2000).

4.3.2 GFAP

In the microscopic analysis of GFAP through immunohistochemical labelling, no obvious abnormalities in the cytoarchitecture were observed in the cerebellum of *du/du* mutant mice. GFAP is strongly expressed by Bergmann glia, which is the main astrocytic subpopulation in this area of the brain.

Immunohistochemical labelling of GFAP in *du/du* cerebellum revealed Bergmann fibres spanning upward through the molecular layer similar to the wild-type processes. This result suggests that the architecture of Bergmann glia is complete in *du/du* mutant mice and not affected by the mutation. During development, Bergmann fibres display a tight association with migrating granule cells. This observation gave rise to the concept of glia-guided neuronal migration (Rakic, 1971). Their role in Purkinje cell development is less well understood, but considering that the formation of radial Bergmann fibres in the cerebellar cortex precedes dendritogenesis, it is conceivable that they provide both trophic substances and adhesive structural scaffolds for growing Purkinje cell dendrites (Yamada *et al.*, 2000). Their adult cytologic and molecular features certainly suggest their active interdependent participation in the cerebellar cortex (Muller and Kettenmann, 1995). Beside the efficient uptake of neurotransmitter (e.g. glutamate, Clark and Barbour, 1997) and a more general role in the support of neuronal metabolism, recent findings point increasingly towards their direct role in chemical and electrical signalling (Haydon, 2001; Oliet *et al.*, 2001). The formation of separate glia microdomains capable of autonomous interactions with particular synapses between axon terminals of parallel fibres and the dendritic spines of Purkinje cells they ensheath (Grosche *et al.*, 1999), as well as the findings that astrocytes profoundly increase neuronal synapse number *in vitro* and are required for their maintenance (Ullian *et al.*, 2001) support this idea. On the other hand, intense neuronal activity influences astroglial gene expression (Steward *et al.*, 1997) and GFAP expression among other proteins has been found to be upregulated in thalamocortical structures of a rat model for absence epilepsy even before the onset of spike and wave discharges (Dutuit *et al.*, 2000). However at present it is unclear if these adaptive astrocytic changes minimize or contribute to the process of epileptogenesis.

4.3.3 THE $\alpha_2\delta$-2 SUBUNIT

4.3.3.1 Mutant protein *du*-mut1 α_2 is expressed in *du/du* mice

In situ hybridization has shown that a full-length $\alpha_2\delta$-2 transcript is absent from the *du/du* mouse brain due to the genomic rearrangement that disrupts the *Cacna2d2* gene (Barclay *et al.*, 2001). However *in situ* hybridization showed that

a 5' mutant transcript (*du* mutant transcript1) is present in *du/du* Purkinje cells at a low level (Brodbeck *et al.,* submitted for publication). This transcript is predicted to encode a protein (*du*-mut1 α_2) that lacks most of the α_2 subunit (~90%) and the whole of the δ subunit, including the transmembrane domain. mRNA encoding mutant transcripts, where a frame-shift or point mutation introduces one or more premature stop or nonsense codons is unstable and subject to nonsense-mediated mRNA decay (Culbertson, 1999). This might be true for *du* mutant transcript 2, which has been found on Northern blots of *du/du* brains and could subsequently be identified by RT-PCR as exon 2-39 of *Cacna2d2.* However only the 5' mutant transcript 1 appears to be present at a low level in *du/du* brain.

Studies using site-directed anti peptide antibodies were used to establish the topology of the $\alpha_2\delta$-1 subunit. The α_2 subunit has been found to be entirely extracellular (Brickley *et al.*, 1995; Gurnett *et al.*, 1996; Gurnett *et al.*, 1997) and disulphide-linked to the δ subunit which anchors the protein to the membrane. Both subunits have been found to be involved in the interaction with the $Ca_V1.2$ subunit (Felix *et al.*, 1997; Gurnett *et al.*, 1997). Now that two other $\alpha_2\delta$ subunits have been cloned it is assumed that they have a similar topology as their hydrophobicity profiles are very similar (Klugbauer *et al.*, 1999b). High homology is present between N-termini of $\alpha_2\delta$–1 and $\alpha_2\delta$–3 with the clear prediction of a cleavage site in their signal sequence in both cases. In contrast, although a putative signal peptide is found in $\alpha_2\delta$–2, it is much longer. Using prediction analysis, it is found to have a potential cleavage site after position 64, whereas only 2% of eukaryotic signal peptides are longer than 35 residues (Nielsen *et al.*, 1997). In particular it has a longer sequence N-terminal to the putative hydrophobic signal sequence (approximately 42 amino acids) than $\alpha_2\delta$–1 and $\alpha_2\delta$–3 (with approximately 3 and 11 amino acids respectively). Such 'n regions' are found to be less than 25 amino acids in 80% of secreted or transmembrane proteins in which they occur (Martoglio and Dobberstein, 1998). Therefore it remains unclear whether this signal sequence is cleaved efficiently, as cleavage is often delayed when the signal sequence is long (Li *et al.*, 1994). This results in extended transit times through the endoplasmic reticulum-Golgi apparatus, which might be required for highly glycosylated proteins (Li *et al.*, 1994). Such an

explanation is likely to be the reason for the detection of a 120 kDa immunolabelled protein using Ab16-29 when $\alpha_2\delta$–2 is expressed in COS-7 cells. Under the thiol-reducing conditions used this is likely to represent the immature unglycosylated α_2 moiety, as the predicted molecular weight with no added carbohydrate is 113 kDa.

For the *du*-mut1 α_2 expressed in COS-7 cells the signal sequence remains at least in part uncleaved since both Ab16-29 and Ab102-117 recognized a band of ~16 kDa, the predicted size for the truncated protein with signal sequence. Additionally Ab16-29 also recognized a fainter band of about 6 kDa, which is the size of the cleaved signal sequence. A likely explanation for the intensity differences observed with the two antibodies lies in affinity differences for the two epitopes. The predominant band recognized by Ab102-117 was a ~10 kDa protein, which is likely to represent *du*-mut1 α_2 with its signal sequence cleaved. This result corresponds exactly with the molecular weight of the native *du*-mut1 α_2 immunocaptured from *du/du* cerebellum by the same antibody. This indicates that it is a stable *in vivo* species in these mice. A ~16 kDa protein was also immunocaptured by Ab16-29 from *du/du* cerebellum which shows that the signal sequence remains at least in part uncleaved from *du*-mut1 α_2 (Brodbeck *et al.*, submitted for publication).

4.3.3.2 Immuno-localization of $\alpha_2\delta$–2 and *du*-mut1 α_2

When *du*-mut1 α_2 was expressed in COS-7 cells both Ab16-29 and Ab102-117 recognized an epitope that was only expressed intracellularly, indicating that *du*-mut1 α_2 is unlikely to be secreted or inserted into the plasma membrane as a functional transmembrane protein. Furthermore, with Ab102-117 an accumulation was visible in intracellular organelles, which might indicate aggregation or delayed degradation of the overexpressed peptide. Misfolded proteins detected by the ER quality control machinery are retro-translocated into the cytoplasm where they are ubiquinated and degraded by the proteasome (Ellgaard *et al.*, 1999).

Using Ab102-117 in cerebellar sections $\alpha_2\delta$–2 expression could be detected in wild-type Purkinje cell somata and also in the molecular layer. With the same antibody a low level of immunostaining was observed in *du/du* Purkinje cells.

Immunoreactivity in *du/du* cerebellar sections was also observed using Ab16-29 where staining presumably representing the uncleaved *du*-mut1 α_2 peptide, was found to be concentrated in Purkinje cell somata. These results support the findings that *du*-mut1 α_2 is expressed in *du/du* cerebellum.

Interestingly analysis with PSORT II, a knowledge-based, multicategory subcellular localization prediction program (Nakai and Horton, 1999) could foretell the localization of the full-length $\alpha_2\delta$-2 AA sequence correctly: 33.3% ER 33.3% Golgi 33.3% plasma membrane, which are the anticipated processing steps for this protein. For the *du*-mut1 α_2 AA sequence the same program however predicted a rather aberrant localization (52.2% nucleus, 26.1% mitochondrial, 8.7% cytoplasmic, 4.3% vesicles of secretory system, 4.3% extracellular, 4.3% endoplasmic reticulum). Although the current methods for prediction of subcellular localization of proteins are not yet completely reliable, it is a indication of the deficient targeting of this truncated protein, which complements the presented immunocytochemical results. The cellular consequences are however not yet fully understood.

4.3.4 CASPASE 3 AND 12

Immunocytochemical experiments performed on cerebellar sections prepared from three different litters (P24-27) revealed an upregulation of caspase 3 detectable by immunolabelling in *du/du* animals. However, if the expression level of caspase 3 was compared by Western blot analysis, the same upregulation was not seen. This result is not entirely surprising, considering that Purkinje cells constitute only 1% of the total neurone number in the cerebellum, such that a localized upregulation, which is visible through confocal microscopy might not be discernible biochemically. Furthermore, it is feasible that a certain subset of the Purkinje cell population is more severely affected by the *du/du* upregulation, which could ultimately result in regional differences of Purkinje cell degeneration, as seen in the leaner mutation (Herrup and Wilczynski, 1982). An alternative explanation might be that it is too early in the development of these mice for neurodegeneration to occur.

Similarly immunolabelling with a caspase 12 antibody also showed no significant upregulation in *du/du* cerebellum.

CHAPTER V.

CALCIUM IMAGING

5.1 AIMS

The tightly controlled spatio-temporal fluctuations of cytoplasmic free calcium ion concentration ($[Ca^{2+}]_i$) plays a pivotal role in the regulation of neuronal functions as diverse as transmitter release, spiking behaviour and gene transcription. The role of $\alpha_2\delta$ subunits in calcium channel function has been ascertained in several *in vitro* studies to increase the current density of different $Ca_V\alpha_1$ subunit combinations. In order to evaluate possible alterations in $[Ca^{2+}]_i$ homeostasis caused by the disruption of the $\alpha_2\delta$–2 calcium channel subunit in the *du/du* mutation, K^+ depolarization-induced $[Ca^{2+}]_i$ transients were monitored in the somata of cerebellar neurones using digital imaging of the ratiometric calcium indicator Fura-2. The $[Ca^{2+}]_i$ responses of granule cells maintained for 7 days in culture, as well as acutely isolated Purkinje neurones, were recorded and compared between the different genotypes.

5.2 RESULTS

5.2.1 CALCIUM IMAGING EXPERIMENTS OF CEREBELLAR GRANULE CELLS

At birth, mouse cerebellar granule cell precursors are found in the germinal zones on the exterior surface of the cerebellum. During the first postnatal weeks, they divide, become postmitotic, and migrate through the molecular layer, finally settling in the internal granule cell layer (Hatten *et al.*, 1997). It has been shown that granule cells possess functional L-, N-, P/Q- and putative R-type calcium channels even in culture (Pearson *et al.*, 1995; Randall and Tsien, 1995). The neonatal granule cells were prepared from seven-day-old mice and cultured for up to two weeks. Their long term survival is dependent on the partial depolarization of their plasma membrane by high $[K^+]$(25mM), which is thought to mimic the *in vivo* effect of glutamatergic innervation by mossy fibres (Hack *et al.*, 1993) and was therefore present in their growth medium. The phenotype of the granule cells changes during culture from small spherical isolated cells to a complex neurite network organization at 7 days in culture. This was the point in time when calcium-imaging experiments were performed for the following five days. During this time cells did not show a consistent increase in peak $[Ca^{2+}]_i$ elevations. Furthermore, the kinetics of the $[Ca^{2+}]_i$ rise were also indistinguishable. Therefore recordings derived from all cultured cells were pooled. In order to obtain comparable results, a small recording field (~5μm^2) in the centre of a granule cell soma situated in the focal field of the fluorescent microscope was chosen. Care was also taken that cell somata were clearly distinguishable from their neighbours and were firmly attached during stimulation. Additionally, for better comparison, cells were only stimulated once with high $[K^+]$ as the size of the transients tended to decrease even after a 5 minute washing period in extra-cellular solution.

5.2.1.1 CALIBRATION OF CALCIUM IMAGING EXPERIMENTS

Calibration of the $F_{340/380nm}$ ratio in terms of $[Ca^{2+}]_i$ was carried out on cultured granule cells *in vitro* in three independent experiments. Cells were incubated with Fura-2 AM as described in Section 2.8.2.2 and exposed to a 'zero' calcium solution for 5 minutes in the presence of 5μM ionomycin and 1μM thapsigargin containing 5mM EGTA with no added calcium to obtain the minimum $F_{340/380nm}$ ratio (R_{min}). Cells were then incubated with a 'high' calcium solution containing 5mM Ca^{2+} to obtain the maximum $F_{340/380nm}$ ratio (R_{max})(Figure 5.1).

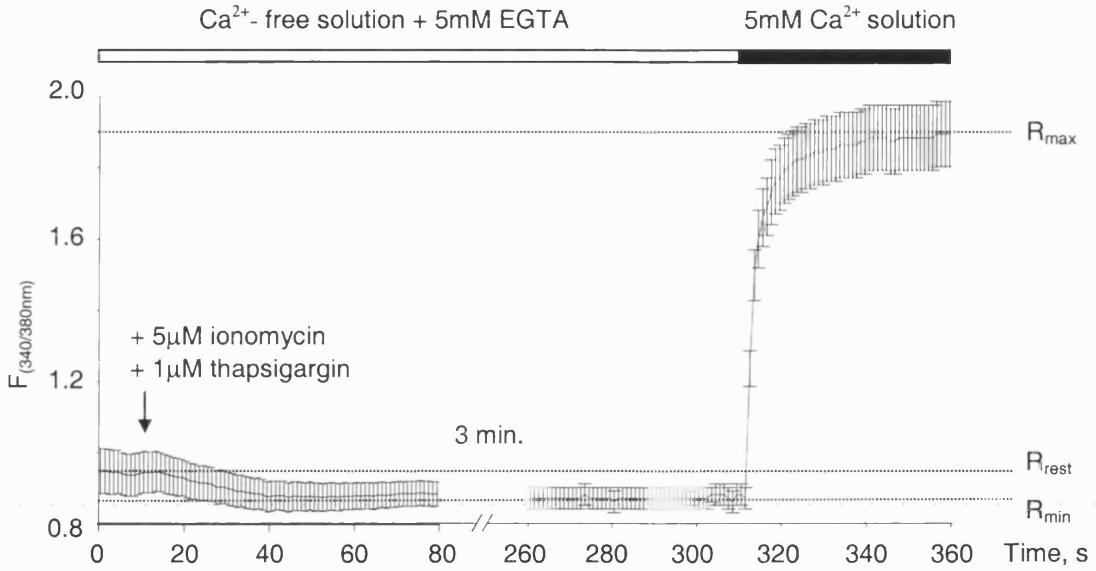

Figure 5.1 Example traces (n=9) of a calibration experiment performed in order to estimate the $[Ca^{2+}]_i$. The bar at the top of the figure denotes the $[Ca^{2+}]$ of the solution in the recording chamber. The application of 5μM ionomycin and 1μM thapsigargin is indicated by an arrow. After 5 minute incubation to ascertain cells have reached a stable R_{min} value, the solution was changed for a 5mM Ca^{2+} solution to obtain the R_{max} value.

The average values from these calibrations can be used to quantify intracellular $[Ca^{2+}]_i$ using the following equation (Grynkiewicz *et al.*, 1985):

$$[Ca^{2+}]_{free} = K_d \times \left[\frac{R - R_{min}}{R_{max} - R}\right] \times \left[\frac{F^{380}_{max}}{F^{380}_{min}}\right] \qquad (1)$$

Where R is the measured ratio, R_{min} and R_{max} are the ratios recorded with zero and high extracellular calcium, respectively. F^{380}_{max} and F^{380}_{min} are the signals at 380nm in zero and high calcium respectively and K_d is the apparent dissociation constant for Fura-2 (224nM).

For granule cells in 3 separate calibration experiments the resting calcium concentration was found to be 33nM (±19nM, n=9), 71nM (±41nM, n=14), 58nM (±30nM, n=9). The average of 54nM (±30nM) is close to the basal $[Ca^{2+}]_i$ levels found by others in cerebellar granule cells (20-40nM, Harrold *et al.,* 1997) 60nM, Kirischuk and Verkhratsky, 1996). However it is unlikely that the observed variations in the tightly controlled resting calcium concentration, reflect real differences and can rather be ascribed to experimental limitations, which will be addressed in more detail in the Discussion. To illustrate how the naturally occurring variations when recording signals from different cells translate into actual calcium concentrations, the values from Figure 5.1 were used in Figure 5.2 to plot a calibration curve using equation (1) for the indicated ratio values.

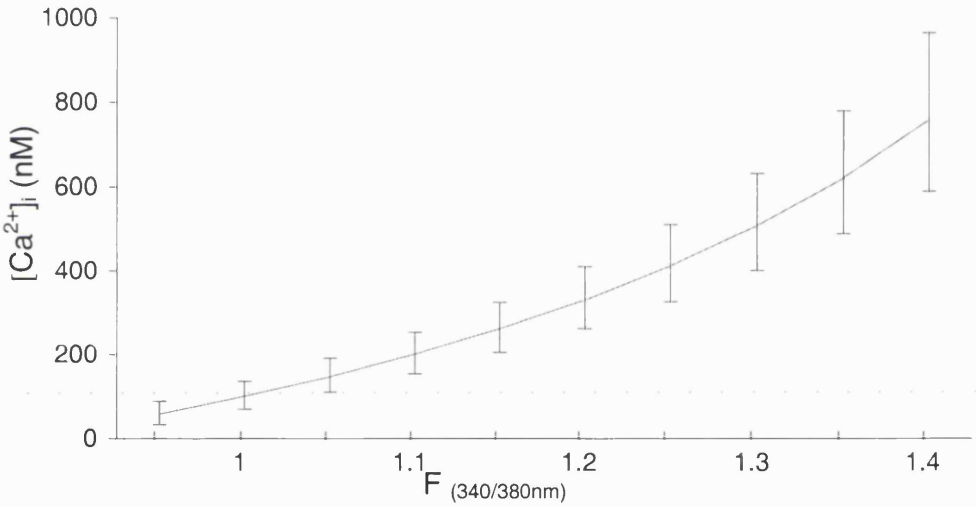

Figure 5.2 Calibration curve for Fura-2 in cerebellar granule cells

The error-bars derive from the standard error of the mean (S.E.M.) values in Figure 5.1 translated into absolute $[Ca^{2+}]_i$ using equation (1). In the example the calcium concentration at rest ($F_{(340/380nm)}$ = 0.95) of 58nM varies ±30nM and at a change of ratio resembling stimulation ($F_{(340/380nm)}$ = 1.4) the variation is 758nM±200nM, both variation are quite considerable. Therefore, in the following results the observed $F_{\Delta(340/380nm)}$ ratio has not been translated into absolute $[Ca^{2+}]$ values. However, in order to keep experimental variations at a minimum where possible experiments were paired between the different genotypes and conditions.

5.2.1.2 K^+-INDUCED $[Ca^{2+}]_i$ TRANSIENTS IN CEREBELLAR GRANULE CELLS

Cerebellar granule cells in culture for 7 days were incubated with the ratiometric dye Fura-2 AM, before stimulation with different K^+ concentrations in order to depolarize the cells. The cell shape and neurite network organisation after one week in culture were indistinguishable between the genotypes. An example group is shown at rest under the light microscope and Fura-2 fluorescence at F_{380nm} in Figure 5.3 I and II, respectively. In Figure 5.3 III, IV and V, the fluorescence ratio at $F_{\Delta(340/380nm)}$ of granule cells is shown in pseudo-colour to illustrate the K^+-evoked changes in $[Ca^{2+}]_i$ before, during and after a K^+ stimulation, respectively. A transient rise from an initial low $[Ca^{2+}]_i$ level is clearly visible, as pink to blue colours reflect low and orange to red colours high $[Ca^{2+}]_i$ see scale bar in Figure 5.3. The time points at which pictures III, IV and V were taken are shown in Figure 5.4 D to illustrate the time scale of this response.

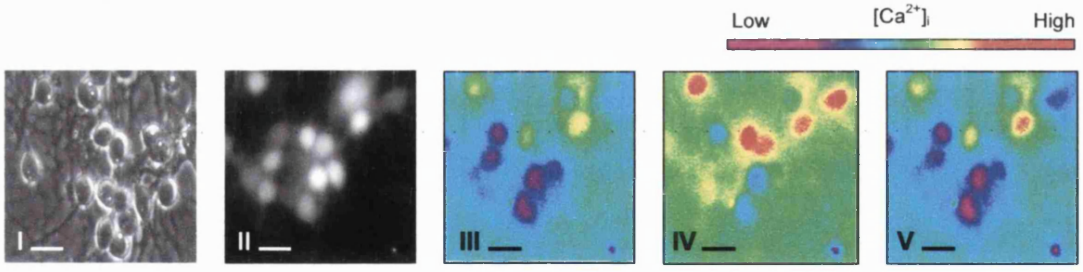

Figure 5.3 Cerebellar granule cells seven days in culture. In **I** under the light microscope and **II** Fura-2 fluorescence at F_{380nm}. In **III**, **IV** and **V** the ratio fluorescence at $F_{\Delta(340/380nm)}$ is shown in pseudo-colour to illustrate different $[Ca^{2+}]_i$. Scale bar 10μm.

Averaged example traces of depolarization-induced $[Ca^{2+}]_i$ transients in cerebellar granule cells for +/+, *du/+* and *du/du* are shown in Figure 5.4 (A-D). Cells of all genotypes reached a plateau of increased $[Ca^{2+}]_i$ approximately 6 seconds after stimulation; the stimulation time was therefore subsequently reduced to 10 seconds. The kinetics of the evoked $[Ca^{2+}]_i$ transients were very similar between the different genotypes. In Figure 5.4 D $[Ca^{2+}]_i$ transients are shown for +/+, *du/+* and *du/du* during a 40mM K^+ application, which resembles a half-maximal stimulation.

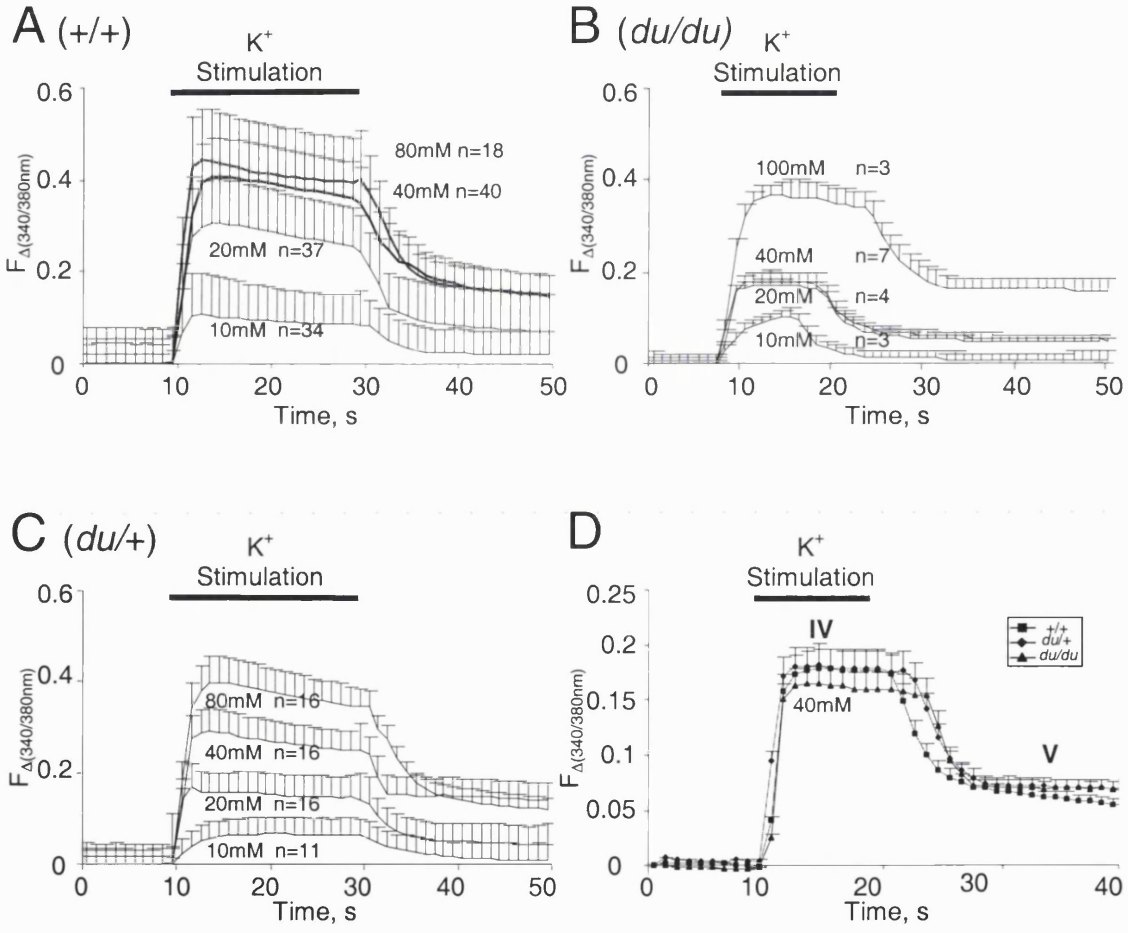

Figure 5.4 $[K^+]$-evoked $[Ca^{2+}]_i$ transients in cerebellar granule cells 7 days in culture. **A-D** averaged sample $[Ca^{2+}]_i$ transients stimulated with varying K^+ concentrations for each genotype (**A-C**) and at 40mM K^+ compared between the different genotypes (**E**). The background and baseline $F_{\Delta(340/380nm)}$ ratio has been subtracted.

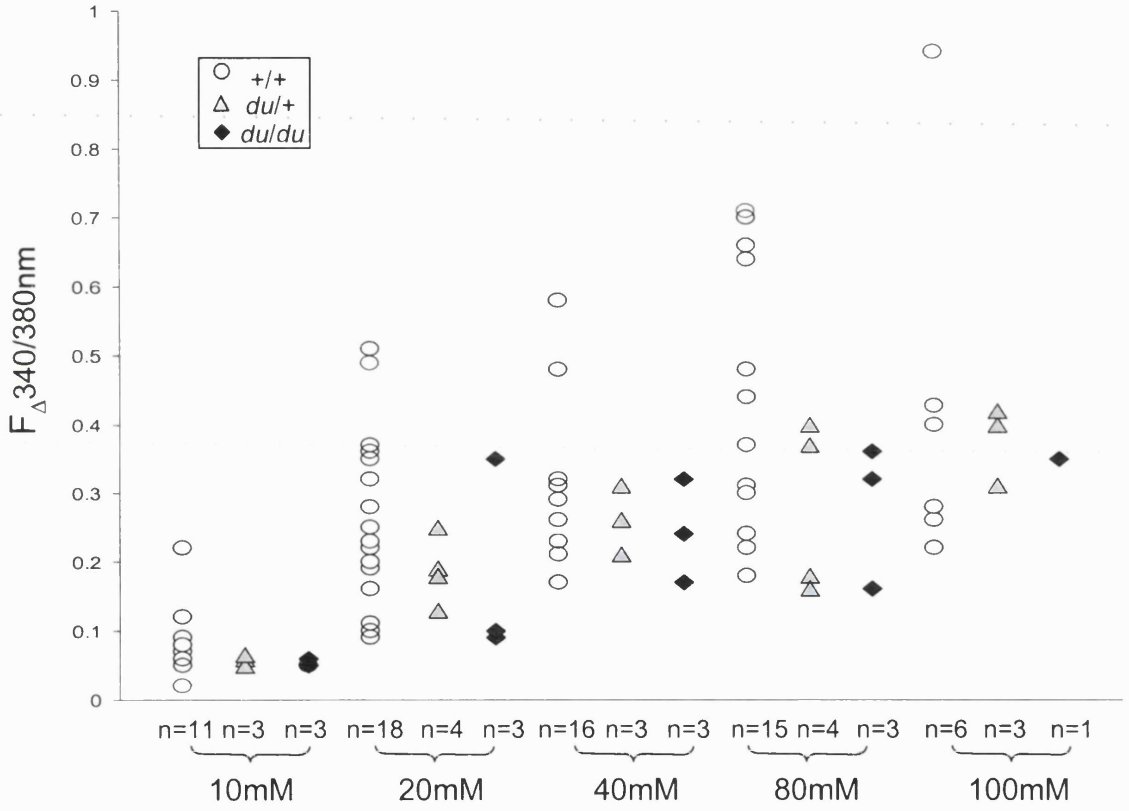

Supplementary data to Figure 5.6 illustrating variations in the mean peak values between experiments. n= number of experiments where 5-10 cells taken from 4 or more preparations were imaged.

The $F_{(340/380nm)}$ ratio at rest did not vary significantly between different genotypes or ages (Figure 5.5) and was therefore subtracted for better comparison.

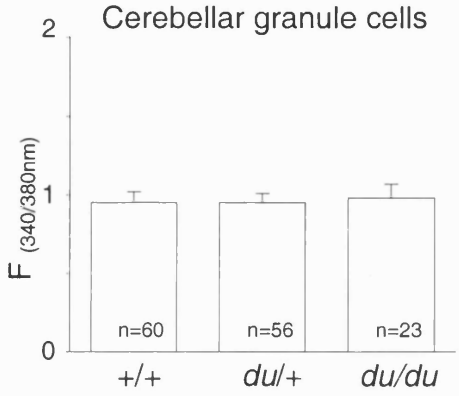

Figure 5.5 $F_{\Delta(340/380nm)}$ ratio at rest compared between the genotypes.

The K^+-induced peak $[Ca^{2+}]_i$ elevations were compared at increasing $[K^+]$ concentrations reflecting different depolarization potentials (Marchetti *et al.*, 1995). No significant difference could be observed between the different genotypes over the whole concentration range (Figure 5.4).

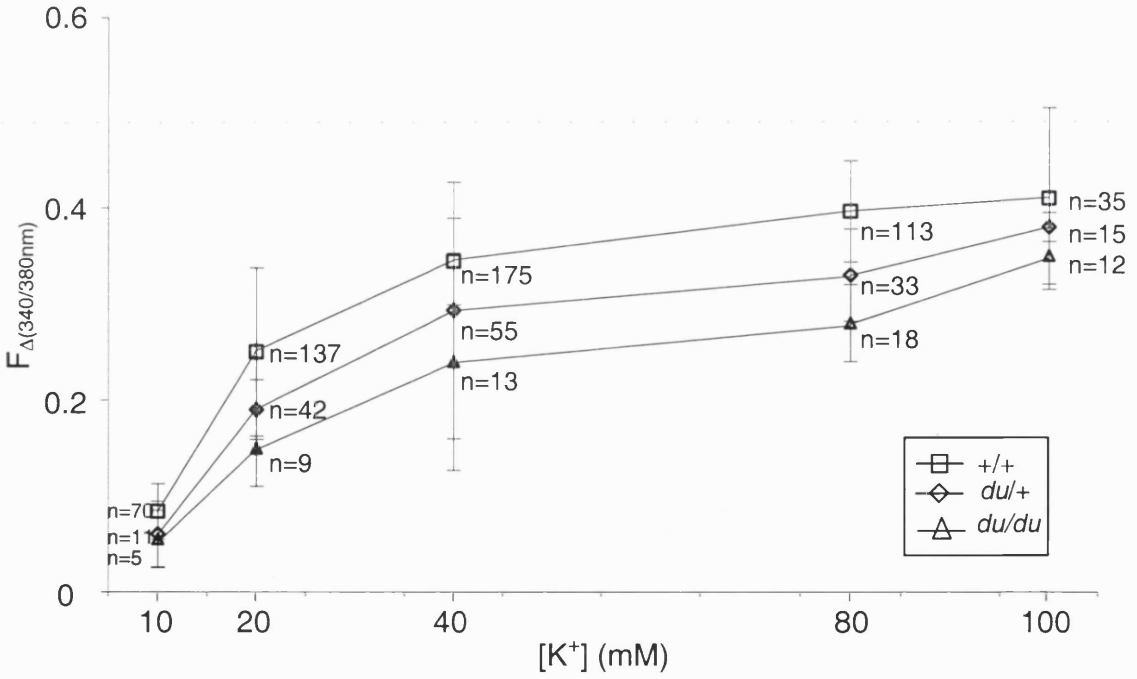

Figure 5.6 Depolarization-induced peak $[Ca^{2+}]_i$ transients (± S.D) in cerebellar granule cells. The baseline and background subtracted $F_{\Delta 340/380nm}$ ratio of episode 15-20 was averaged for the cell numbers indicated at the specified K^+ concentration.

5.2.2 CALCIUM IMAGING EXPERIMENTS IN ACUTELY ISOLATED PURKINJE NEURONES

Purkinje neurones were dissociated from P4-P8 old mice and plated onto Concanavalin A-coated coverslips. After one hour to allow for attachment, cells were incubated for 20 minutes with the ratiometric dye Fura-2 AM as described in Section 2.8.3.2. Purkinje cells were routinely identified by their characteristic size and shape. Their identity was further verified using the Purkinje cell-specific anti-Calbindin D-28k antibody (n>70) as seen in Figure 5.7 A. As indication for the basal $[Ca^{2+}]_i$ level the value of the $F_{(340/380nm)}$ ratio was compared between the different genotypes. No significant differences were observed between +/+ and *du/du* (student's *t*-test p=0.25)(Figure 5.7 B). Thus *du/du* Purkinje cells are able to maintain a normal basal or resting calcium concentration despite a major disruption in their calcium homeostasis as seen in Figure 5.8. To illustrate the $[Ca^{2+}]_i$ imaging experiments with acutely isolated Purkinje neurones an example cell is shown under the light microscope and Fura-2 fluorescence at F_{380nm}, Figure 5.7 C I and II respectively. In Figure 5.7 C III, IV and V the fluorescence ratio at $F_{\Delta(340/380nm)}$ is shown in pseudo-colour to illustrate the K^+-evoked changes in $[Ca^{2+}]_i$ before, during and after a K^+ stimulation, respectively, a transient rise from an initial low $[Ca^{2+}]_i$ level is visible.

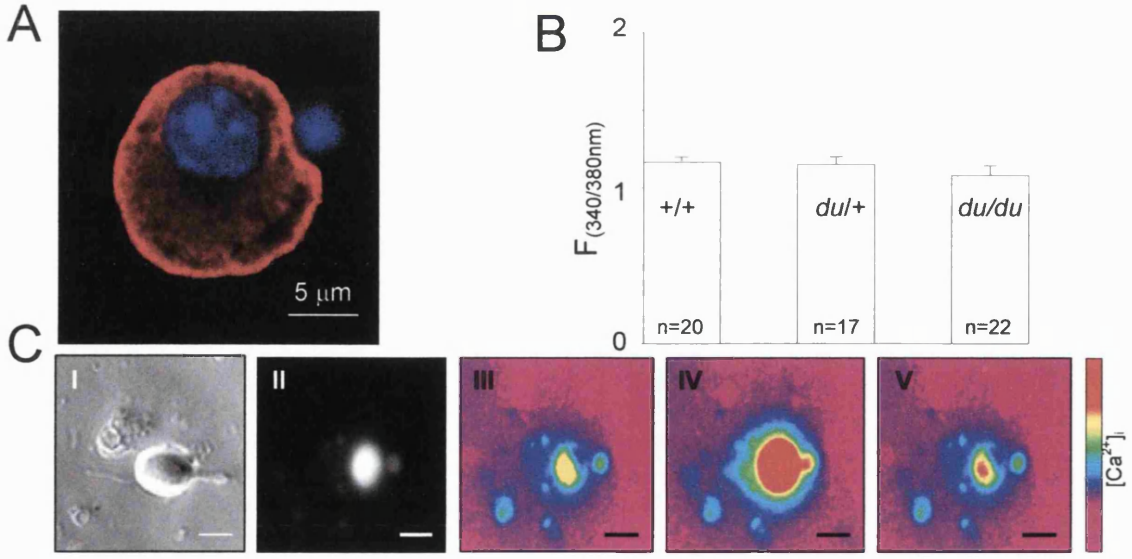

Figure 5.7 **A** Calbindin D-28k staining of an acutely isolated Purkinje cell in red. Nuclear DAPI staining in blue. The smaller nucleus of a granule cell on the right. **B** Comparison of the $F_{\Delta(340/380nm)}$ fluorescence as reflection of the basal $[Ca^{2+}]_i$ levels in isolated Purkinje neurones of the indicated genotype. **C** Example Purkinje cell seen in (**I**) under the light microscope and in (II-V) Fura-2 fluorescence ratio at F_{380nm} (III-V). The $F_{\Delta(340/380nm)}$ ratio is shown in pseudo-colour before (**III**), at the peak (**IV**) and after (**V**) the stimulation, see Figure 5.8 A. Scale bars 15µm.

5.2.2.1 K+-INDUCED $[Ca^{2+}]_i$ TRANSIENTS IN SOMATA ACUTELY ISOLATED PURKINJE NEURONES

Purkinje cell somata isolated from P7-10 *du/du* mice showed a significant reduction in their depolarization-induced $[Ca^{2+}]_i$ transients when compared to +/+ or *du/+* neurones (Figure 5.8A). The peak of the $[Ca^{2+}]_i$ rise in *du/du* Purkinje cells was reduced by 24% compared to +/+; this was statistically significant (student's *t*–test $p<0.05$, Figure 5.8B). The kinetics of the observed $[Ca^{2+}]_i$ transients were comparable between the different genotypes and reached near-resting values after the stimulation.

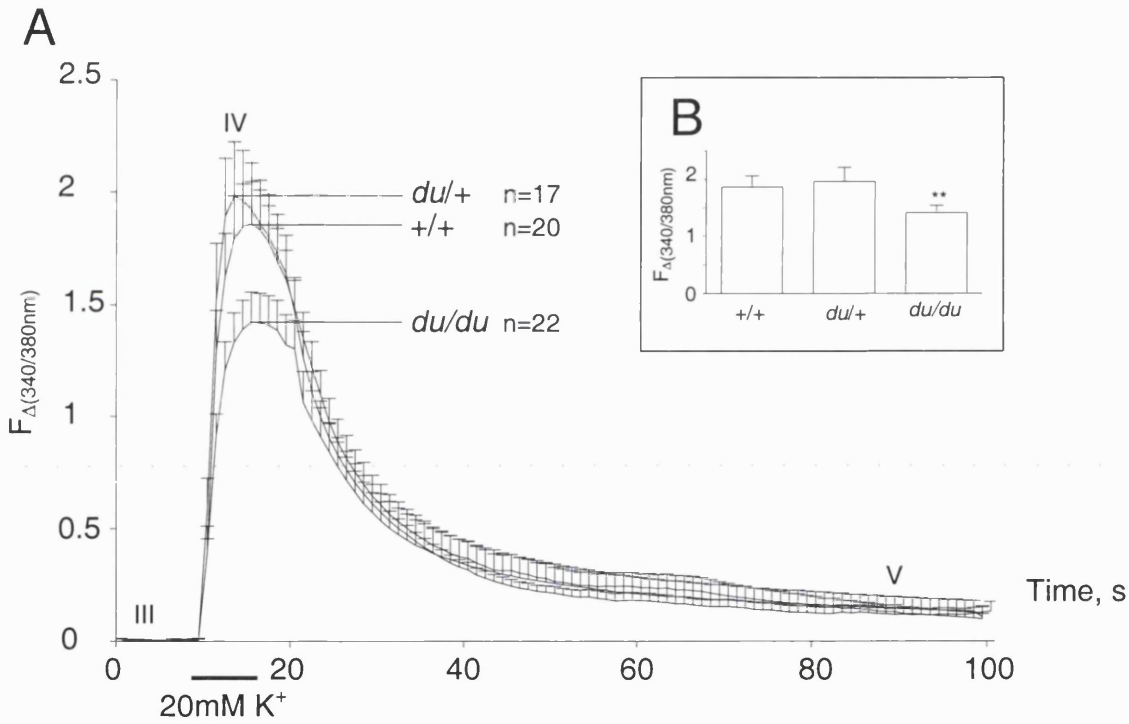

Figure 5.8 Depolarization-induced $[Ca^{2+}]_i$ transients in somata of acutely isolated Purkinje neurones. **A** Murine P7-10 Purkinje neurones were stimulated with 20mM K^+ for 10 seconds, then washed with extracellular solution (see Section 2.6.3.2). Results are expressed as means ± SEM. The background and baseline for each cell has been subtracted. **B** For comparison the peak $F_{\Delta(340/380nm)}$ ratios of episode 15-20 were averaged.

The observed depolarization-induced $[Ca^{2+}]_i$ transients can be completely blocked with the non-specific channel blocker Cd^{2+} (10μM)(Figure 5.9).

This indicates the involvement of extracellular calcium as initial trigger of the observed $[Ca^{2+}]_i$ transients.

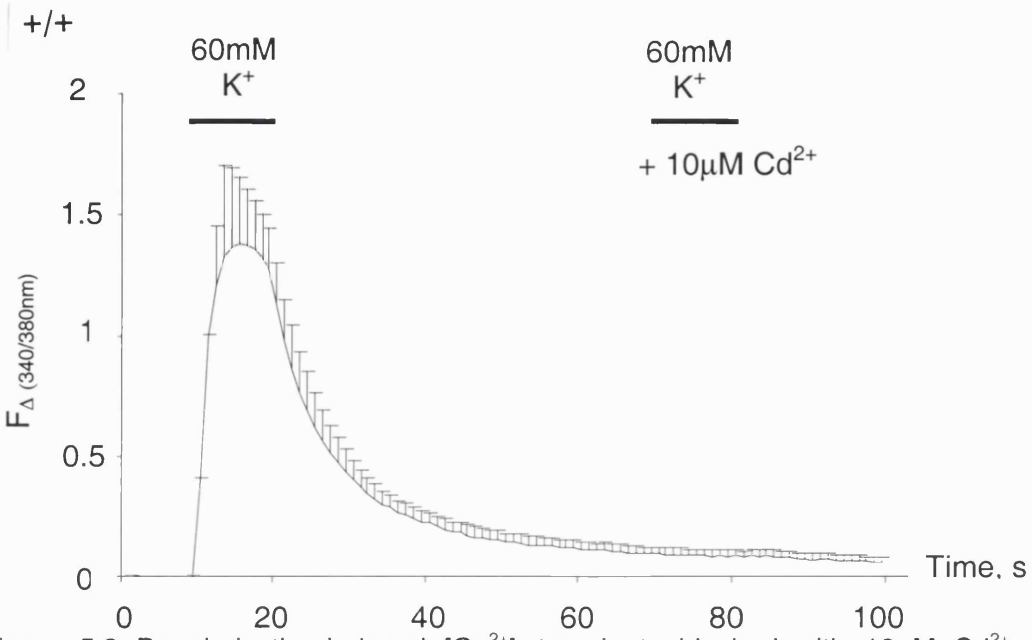

Figure 5.9 Depolarization-induced $[Ca^{2+}]_i$ transients blocked with 10μM Cd^{2+} (n=6). The bars indicate the application of high potassium solution, the second application in the presence of 10μM Cd^{2+}.

More specifically a second $[Ca^{2+}]_i$ rise can also be blocked with the P/Q-type current antagonist ω-agatoxinIVA (100nM, Figure 5.10) indicative of the involvement of $Ca_V2.1$ channels as a trigger of the observed $[Ca^{2+}]_i$ transients.

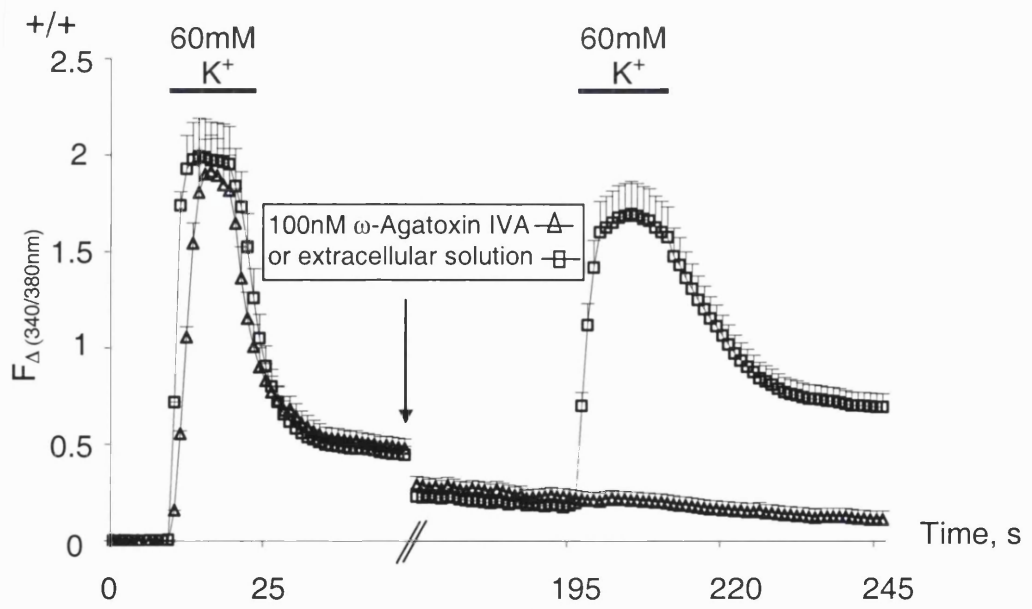

Figure 5.10 Depolarization-induced $[Ca^{2+}]_i$ transients blocked with 100nM ω-agatoxin IVA (n=3). The arrow indicates the application of either toxin Δ or control □ solution followed by a 2 minute incubation period before a second stimulation.

The $Ca_V2.1$ calcium channel is present in high concentration in these cells and contributes over 90% to their calcium current (Mintz *et al.*, 1992b). Purkinje neurones express these calcium channels at high density even at this early developmental stage as seen in the incompletely triturated cell cluster in Figure 5.11.

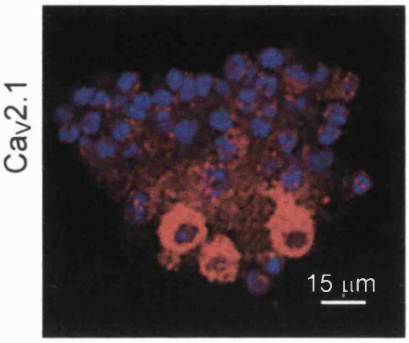

Figure 5.11 Acutely isolated Purkinje neurones immunolabelled for $Ca_V2.1$ (red) and nuclear DAPI in blue. At this developmental stage (P6) granule cells start migrating from the external granule cell layer (ECL) through the Purkinje cell layer (PCL) to form the granule cell layer leaving their axons behind which form the molecular layer.

The observed reduction in the K^+-induced $[Ca^{2+}]_i$ transients is therefore likely to involve disruption of $Ca_V2.1$ function.

5.3 DISCUSSION

5.3.1 CALIBRATION OF THE $F_{\Delta(340/380nm)}$ RATIO IN CEREBELLAR GRANULE CELLS

The evaluation of three independent calibration experiments resulted in a resting calcium concentration of 54±30nM, which is close to the concentration determined by others (Kirischuk and Verkhratsky, 1996; Harrold *et al.*, 1997). However the observed cell-to-cell variations (see Figure 5.2) were considered too large to allow the translation of the $F_{(340/380nm)}$ ratio into absolute $[Ca^{2+}]_i$ values. Additional sources of error such as variations in the light source, the use of an approximation of the K_d value of Fura-2, and the internal compartmentation or incomplete hydrolysis of Fura-2 have led to the use of ratio values in many studies (e.g. Simpson *et al.*, 1996). In particular, the exact determination of a R_{min} has to be considered critically as even in the presence of EGTA the Ca^{2+} concentration is likely to be in the low nanomolar range. This will have profound effects on calibration considering the low resting $[Ca^{2+}]_i$ in cerebellar granule cells. Therefore, the K^+-induced $[Ca^{2+}]_i$ transients have been compared as F_Δ(340/380nm) ratio values between the different genotypes. Furthermore, due to limitations in the availability of cells (especially Purkinje neurones), it proved impractical to conduct stimulations and calibrations for each genotype after each experiment.

5.3.2 CALCIUM IMAGING IN CEREBELLAR GRANULE CELLS

In agreement with the low expression level of $\alpha_2\delta$-2 in cerebellar granule cells as shown by *in situ* hybridization (Barclay *et al.*, 2001) the differences in K^+-induced $[Ca^{2+}]_i$ transients proved not to be statistically significant. This could be an indication that the role of the $\alpha_2\delta$-2 subunit in this cell type is less crucial and can be compensated by other channels. An alternative explanation might be that granule cells are undifferentiated when taken in culture and the elevated $[K^+]$ necessary for their survival obscures possible differences occurring *in vivo*. This might be an explanation for the absence of a significant reduction in $[K^+]$-induced $[Ca^{2+}]_i$ transient in *du/du* cerebellar granule cells. The response of the $[K^+]$ depolarization appeared to be monophasic, consisting of only a plateau which was quite variable between different preparations. The typical biphasic $[Ca^{2+}]_i$

transients induced by high [K^+] as reported by Ciardo and Meldolesi (1991) could not be observed.

5.3.3 CALCIUM IMAGING OF ACUTELY ISOLATED PURKINJE NEURONES

Variations in intracellular [Ca^{2+}] levels play vital roles in the information processing of cerebellar Purkinje cells, since several forms of synaptic plasticity at their excitatory (Sakurai, 1990) and inhibitory inputs (Marty and Llano, 1995) are triggered by rises in $[Ca^{2+}]_i$. These include long-term potentiation (Daniel *et al.*, 1998), long-term depression (Konnerth *et al.*, 1992) and rebound potentiation of inhibitory synapses (Kano *et al.*, 1992). The dynamic control of intracellular $[Ca^{2+}]_i$ in Purkinje cells involves influx of Ca^{2+} through voltage-dependent calcium channels. Upon depolarization, transient increases in $[Ca^{2+}]_i$ have been shown in these cells on a dendritic as well as a somatic level (Eilers *et al.*, 1995; Kano *et al.*, 1995). P-type channels contribute over 90% to the whole cell calcium current (Mintz *et al.*, 1992a; Mintz *et al.*, 1992b) and in the present study the observed $[Ca^{2+}]_i$ transients could be completely blocked by 100nM P/Q-type-specific ω-agatoxinIVA. A simple way to explain the origin and reduction of the observed $[Ca^{2+}]_i$ increase would be that they are due to opening of voltage-dependent calcium channels and reflect a reduction in VDCC function in the case of the *du/du* mutation. However, the limited temporal resolution of these recordings (1 Hz) does not allow exclusion of Ca^{2+} release from intracellular IP_3- and ryanodine-sensitive stores as well as differences in the buffering by Ca^{2+}-binding proteins and sequestration by intracellular organelles (Eilers *et al.*, 1996). Nevertheless, the dependence of these $[Ca^{2+}]_i$ signals on initial extracellular Ca^{2+} influx strongly suggests that these $[Ca^{2+}]_i$ transients were due to Ca^{2+} entry through voltage-gated Ca^{2+} channels located in the somatic membrane, as concluded by others (Kano *et al.*, 1995). Therefore it is very likely that the reduction in calcium channel function is caused by the disruption of the $\alpha_2\delta$-2 subunit even at this early developmental stage. These findings were confirmed by electrophysiological recordings in the same preparations of Purkinje cells conducted by Nuria Balaguero in our laboratory (Barclay *et al.*, 2001). Interestingly, the observed reduction in peak calcium current density between +/+ and *du/du* of acutely isolated Purkinje neurones was 35% at -10 mV, very similar to the 24% reduction observed in calcium imaging experiments.

Furthermore, studies in *Xenopus* and COS-7 expression systems where $Ca_V2.1/\beta_4$ was expressed in combination with either $\alpha_2\delta$-1 or $\alpha_2\delta$-2 showed a selective enhancement of $Ca_V2.1$ current density (Barclay *et al.*, 2001, Brodbeck *et al.,* submitted for publication). Taken together, this indicates a striking parallel to the *tottering* (*tg*) and *leaner* (*tg^{la}*) mutations, where the $Ca_V2.1$ function is disrupted. P/Q-type calcium channels play a prominent role in neurotransmitter release in many synapses (Dunlap *et al.*, 1995). Furthermore, their localization in dendrites and cell bodies suggest additional postsynaptic roles. In the *lethargic* (*lh*) mutation where the β_4 subunit expression is disrupted (Burgess *et al.*, 1997) no reduction in Ca^{2+} current in Purkinje neurones could be measured, as the loss of β_4 in this mutation appears to be partially compensated for by a reshuffling mechanism in which β_{1b} replaces β_4 (Burgess *et al.*, 1999). However, the disruption of the previously demonstrated preferential interaction of $Ca_V2.1$ with β_4 (Walker *et al.*, 1998) seems nevertheless to be causative for the severe *lethargic* (*lh*) phenotype. In addition, *Cacna1a* null mutant mice show ataxia similar to *du/du* mice in conjunction with reduction in animal size and cytoarchitectonic conservation of the cerebellum, and most do not survive past weaning (Jun *et al.*, 1999; Fletcher *et al.*, 2001).

CHAPTER VI.

GENERAL DISCUSSION

6.1 SUMMARY OF THIS STUDY

The genomic rearrangement in the *ducky* mutation causes disruption of the *Cacna2d2* gene, which encodes the $\alpha_2\delta$–2 auxiliary calcium channel subunit. The result is a loss of full-length *Cacna2d2* transcript in *du/du* mice and the presence of two mutant transcripts at low levels as seen by Northern blot analysis (Barclay *et al.*, 2001). *In situ* hybridization of mouse brain sections showed the highest expression level of $\alpha_2\delta$-2 mRNA in cerebellar Purkinje cell somata (Barclay *et al.*, 2001), where in *du/du* mice only mutant transcript 1 could be detected (Brodbeck *et al.*, submitted for publication). The predicted product of this transcript lacks most (~90%) of the α_2-2 and all of the δ-2 subunit including the transmembrane domain and is therefore not normally functional.

6.1.1 IMMUNOCYTOCHEMISTRY

Two antibodies (Ab16-29, Ab102-117) directed against N-terminal amino acids of the $\alpha_2\delta$-2 subunit recognized the truncated du-mut1 α_2 protein in cerebellar sections of *du/du* mice. Antibody Ab16-29, which binds an epitope within its signal sequence, showed the truncated protein accumulated in *du/du* Purkinje cell somata, whereas Ab102-117 showed a less pronounced, more diffuse staining. Western blot analysis of cerebellar membranes with antibody Ab102-117 identified a protein of 150 kDa in +/+ animals, which is the predicted size for the full-length α_2 moiety of $\alpha_2\delta$-2, but not in *du/du* littermates as predicted. Possibly due to its low expression level, the truncated form of the protein present in *du/du* mice could not be visualized directly by Western blotting of cerebellar protein, but has subsequently been immunocaptured in our laboratory.

In expression studies of $\alpha_2\delta$-2 in COS-7 cells Ab16-29 recognized a protein of 120 kDa, which corresponds to the predicted size of a premature α_2 moiety with no added carbohydrates. With antibody Ab102-117 a protein of 150 kDa could be visualized which was identical in size to the $\alpha_2\delta$-2 subunit identified in cerebellar membranes of +/+ mice. Both antibodies also recognized different sized products of the *du/du* mutant transcript 1 which could be correlated to the

predicted sizes of expressed *du*-mut1 α_2 protein with and without its signal sequence, respectively. The *du*-mut1 α_2 protein, detected with either antibody (Ab16-29, Ab102-117), was localized entirely intracellularly and its processed form lacking the signal sequence appeared to be accumulated by intracellular organelles. In contrast, full-length $\alpha_2\delta$-2 was recognized exofacially by antibody Ab102-107.

Structurally, although *du/du* brains were found to be reduced in size, their overall cytoarchitecture was found to be similar to that of *du/du* and +/+ animals at an age of P24-27. With an antibody directed against the Purkinje cell-specific marker Calbindin D-28k, no cell-loss was observed in P24 *du/du* cerebella. The expression level of this predominant calcium-binding protein in Purkinje neurones was found to be unaltered by Western blot analysis of cerebellar protein from +/+ compared to *du/du* animals. Furthermore no indication of structural disturbance or neurodegeneration was observed with an antibody directed against the astroglial marker protein GFAP, expressed by the Bergmann glia surrounding the Purkinje cells. However, with an antibody directed against caspase 3, a protease involved in the apoptosis pathway, increased staining intensity was observed in *du/du* cerebellar brain sections even though this difference was not apparent if the protein expression was compared by Western blot analysis. In addition, no difference in expression was observed for caspase 12, a second protease that has recently been related to ER stress-induced apoptosis.

6.1.2 PURKINJE CELL MORPHOLOGY

In contrast to the similarities described above, the morphology of cerebellar Purkinje cells was severely altered as seen by Golgi impregnation and Lucifer yellow/neurobiotin injection. The size and complexity of the dendritic tree of Purkinje neurones was significantly reduced in *du/du* mice when compared to +/+ littermates, to the extent that dendritic branches often did not reach the border of the molecular layer. Although *du/du* Purkinje cell dendrites possess dendritic spines, the dendrites were often found thickened and mis-orientated. Atypically, primary dendrites frequently extended initially lateral before targeting the pial surface. In the extreme dendrites bent back towards the granule cell

layer resulting in a 'weeping willow'-like appearance. Furthermore, Purkinje cell somata were often multipolar and their axons exhibited focal swellings (axonal torpedo structures), which are indicative of a severe disruption of Purkinje cell output.

6.1.3 CALCIUM IMAGING

The calcium homeostasis in cerebellar neurones was compared at rest and during K^+ depolarization in calcium imaging experiments using the ratiometric dye Fura-2. No significant difference in $[Ca^{2+}]_i$ of cerebellar granule cells, isolated from P7 animals cultured for a further seven days, could be observed in *du/du* compared to +/+ animals, either at rest or during depolarizing stimulations with increasing concentrations of K^+. In contrast, the peak $[Ca^{2+}]_i$ transients in cerebellar Purkinje neurones acutely isolated from P5-P8 mice were significantly reduced by 24% in *du/du* compared to +/+ animals, whereas their resting $[Ca^{2+}]_i$ remained unchanged. The K^+-induced $[Ca^{2+}]_i$ transients were completely blocked by 10 μM Cd^{2+} indicating that the rise in $[Ca^{2+}]_i$ is triggered by initial Ca^{2+} influx. More specifically, these transients were also blocked with 100nM ω–agatoxin IVA a $Ca_V2.1$-specific calcium channel blocker. This indicates that the disruption of the $\alpha_2\delta$-2 subunit in the *ducky* mutation interferes with $Ca_V2.1$ function, the predominant calcium channel in cerebellar Purkinje cells.

6.2 GENERAL DISCUSSION

The data of this study indicate that the alterations in cerebellar function seen in the *ducky* mutation are likely to be caused by a reduction of P/Q-type calcium channel function. Electrophysiological recordings in our laboratory on the same cerebellar Purkinje cell preparations, where the calcium current density was found to be similarly reduced, corroborate this finding. The predominant calcium channel in Purkinje neurones is $Ca_V2.1$, coinciding with the highest neuronal expression level of the $\alpha_2\delta$-2 subunit. In addition, there is a striking similarity of the *ducky* phenotype with other murine mutations in voltage-dependent calcium channel subunits. These involve both the pore-forming $Ca_V2.1$ subunit itself (recently summarized in Zwingman *et al.,* 2001) as well as the auxiliary subunits β_4 (Burgess *et al.*, 1997) and γ_2 (Letts *et al.*, 1998). All these mutations have an overlapping expression pattern in common. Furthermore, a preferential interaction of the β_4 subunit with $Ca_V2.1$ has been demonstrated (Walker *et al.*, 1998). Although in the *lethargic* (*lh*) mutation in β_4, some form of compensation by other β subunits seems to take place (Burgess *et al.*, 1999), which leaves P/Q-type currents unchanged, the strong phenotype nevertheless indicates a major disruption of cellular function in this mutant. A specific interaction of γ_2 with $Ca_V2.1$ has not been demonstrated. In coexpression experiments of γ_2 with $Ca_V2.1/\beta_{1A}$ and $\alpha_2\delta$, this subunit seems to mimic the effect of skeletal muscle γ subunits on L-type channels, which consists mainly of a negative shift of the steady-state inactivation, thereby significantly reducing channel availability at a neuronal resting potential of –70mV. However the predicted increase in calcium current was not observed in *stargazer* granule cells, which might emphasize additional functions of this subunit as recently reported by Chen *et al.,* 2000.

On the other hand co-expression studies of $\alpha_2\delta$-2 with $Ca_V2.1/\beta_4$ conducted in our laboratory indicate a selective interaction of this subunit combination in COS-7 cells as well as in *Xenopus* oocytes. In both expression systems the current density was strongly enhanced (3.5-fold and 2.8-fold, respectively), an effect not seen with the $\alpha_2\delta$-1 subunit. In a previous study where $Ca_V2.1/\beta_{2a}$ was coexpressed in combination with either $\alpha_2\delta$-1, -2 or –3, this selective current

enhancement was not observed (Hobom *et al.*, 2000). This might be a further indication that $Ca_V2.1/\beta_4/\alpha_2\delta$-2 combination is interacting selectively.

Furthermore if the *du* mutant transcript 1 was expressed in COS-7 cells in our laboratory a consistent reduction of the $Ca_V2.1/\beta_4$ current was observed (Brodbeck *et al.,* submitted). This might suggest that a dominant negative effect contributes to the *du/du* phenotype in addition to the loss of a functional $\alpha_2\delta$-2 subunit, possibly by interfering with the expression of the pore-forming α_1 subunit.

It has been shown previously that the effects of $\alpha_2\delta$ subunits on biophysical parameters such as kinetics and voltage-dependence of activation of several different α_1 subunits are relatively minor (Walker and De Waard, 1998; Klugbauer *et al.*, 1999). In agreement, findings of our group show that the expression of $\alpha_2\delta$-2 influences neither the voltage-dependent properties, the single channel conductance, nor other biophysical parameters of $Ca_V2.1/\beta_4$ currents. Therefore it is very likely that the $\alpha_2\delta$-2 subunit influences the lifetime of the channel complex in the plasma membrane, either by enhancing trafficking or reducing turnover, resulting in reduced functional channel expression.

The *tottering* (*tg*) mutation also gives rise to a decrease in calcium channel function (Wakamori *et al.*, 1998). However a compensatory upregulation of other types of calcium channels could still be responsible for Ca^{2+} influx-mediated neurodegeneration in *du/du* mice at a later developmental stage as seen for L-type calcium channels in mice carrying the *tottering* (*tg*) mutation at two to three months of age (Campbell and Hess, 1999). Possible mechanisms for the changed expression of non-P/Q-type channels might include competition with $Ca_V2.1$ auxiliary subunits (Dunlap *et al.*, 1995; Brice *et al.*, 1997; Catterall, 1998) or $Ca_V2.1$- dependent changes in protein trafficking or gene expression (Sutton *et al.*, 1999). A pharmacological characterization of Purkinje cell Ca^{2+} currents in *du/du* mice was not performed by Barclay *et al.,* (2000) and a distinction in the way of entry is therefore not possible. The ω–agatoxinVIA-sensitive $[Ca^{2+}]_i$ transients in cerebellar Purkinje cells however point towards the involvement of $Ca_V2.1$.

In addition to their role in the integration of postsynaptic input in cerebellar Purkinje cells, calcium channels of the P/Q-type are widely expressed in the mammalian brain in a predominantly presynaptic distribution (Westenbroek *et al.*, 1995) and have an important role in mediating neurotransmitter release. The major decrease in P/Q-type currents might therefore alter the balance of excitatory and inhibitory output of many synapses. This balance is of great importance in the thalamus, since oscillations generated here by a feedback loop are known to be sensitive to small changes in either excitation or inhibition and might lead to abnormal network synchrony (Huntsman *et al.*, 1999). This is thought to be an important factor underlying the generation of seizures as has been proposed for *tottering* mice for which a decrease in glutamate, but not γ-aminobutyric acid release, has been observed in the neocortex (Ayata *et al.*, 2000) and thalamus (Caddick *et al.*, 1999).

6.2.1 THALAMOCORTICAL CIRCUITRY PROMOTES RHYTHMICITY

The imbalance of excitation and inhibition within the thalamocortical network has been suggested to be critical for the genesis of seizures (Gloor and Fariello, 1988). SWD could be generated in the cortex of athalamic animals suggesting a determinant role of the cortex as minimal substrate for their generation (Steriade and Contreras, 1998). Nevertheless the thalamocortical circuit is a good example for the generation of hypersynchronized oscillations like those occurring during absence seizures. During normal slow-wave sleep spindle waves are generated in the thalamus as interaction between the GABAergic reticular neurones (nRT) and thalamic relay neurones (RN) (Figure 6.1). Efferent pathways from thalamic relay neurones (RNs) activate a long-loop reciprocal inhibitory feedback circuit that is mediated by neurones in the nucleus reticularis (nRt) of the thalamus (Steriade *et al.*, 1993). These neurones hyperpolarize RNs through activation of their postsynaptic $GABA_B$ receptors. A unique finding in RNs is the relatively large low-threshold transient (T-type) current enabling them to generate a low-threshold spike (LTS). The presence or absence of low threshold spikes (LTS) is directly dependent on the resting membrane potential. At the resting membrane potential (around -60 mV) these

channels are inactivated, but become ready to be activated again when the membrane potential is depolarized by only about 7-15 mV. Hyperpolarization deactivates the Ca^{2+} conductance underlying LTS and promotes burst discharge. $GABA_B$-mediated inhibition via nRt would actually tend to increase rhythmic firing through deactivation of the LTS.

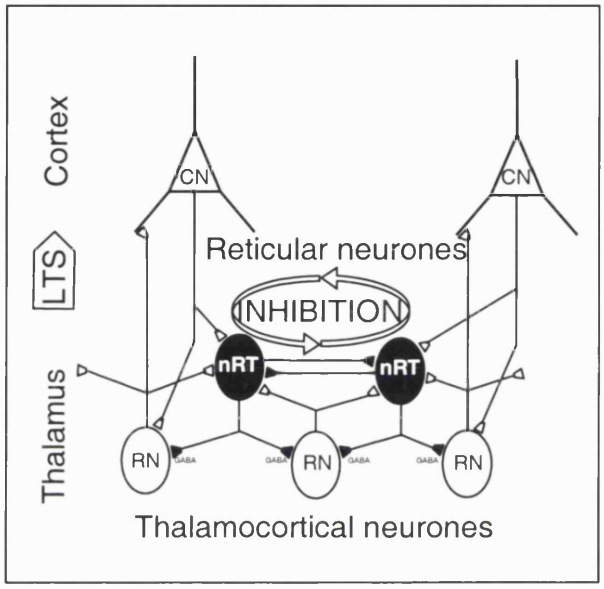

Figure 6.1 Thalamocortical circuitry promotes rhythmicity. Activation of reticular neurones (•) inhibits thalamocortical relay neurones (O) which generate Ca^{2+}-mediated action potentials that excite the reticular neurones again. CN cortical neurones. LTS low threshold spike.

Thus the following functional feedback loop may promote rhythmicity:

(1) activation of nRt cells results in inhibition of RNs.

(2) release of the hyperpolarization in RNs, because withdrawal of the inhibitory influence or direct excitatory input, would promote activation of LTS and associated multiple Na-dependent action potentials.

(3) the burst output of RNs would then evoke excitation of both nRt and cortical neurones.

(4) The activated nRt neurones might then restart the entire cycle.

The activation of GABAergic nRT neurones causes $GABA_A$- and $GABA_B$-mediated hyperpolarization of thalamocortical relay neurones so that rebound bursts are generated, leading to reexcitation of nRT neurones (Huguenard and Prince, 1994; Destexhe *et al.*, 1996). These thalamic GABAergic mechanisms are also involved in spike wave seizures as $GABA_A$ and $GABA_B$ agonists exacerbate seizures, whereas their antagonists suppress them (Hosford *et al.*, 1992; Snead, 1992). It has also been shown that suppression of $GABA_A$-mediated inhibition between nRT neurones leads to hypersynchronization of the reciprocal thalamic network (Huntsman *et al.*, 1999). Furthermore an elevated level of $GABA_B$ receptors has been proposed as a mechanism of seizure susceptibility of *lethargic* (*lh*) mutant mice (Lin *et al.*, 1993). The *tottering* (*tg*) and *lethargic* (*lh*) mouse models for human absence epilepsy show a pronounced decrease in excitatory postsynaptic currents (EPSCs) and a smaller reduction in inhibitory postsynaptic currents (IPSCs). This might result in a net increase in inhibition to RN neurones (Caddick *et al.*, 1999). Interestingly, nRT neurones predominantly express $Ca_V3.2$ and $Ca_V3.3$, whereas RN express mainly $Ca_V3.1$ (Talley *et al.*, 1999), and recently generated $Ca_V3.1$ knock-out mice do not show $GABA_B$-mediated SWD in the thalamus, the hallmark of absence epilepsy (Kim *et al.*, 2001). Finally Song *et al.* (2001) report that in double mutant mice, lacking both the $Ca_V2.1$ and the $Ca_V3.1$ encoding genes, SWD disappeared, which is an inherent feature of $Ca_V2.1$ knock-out mice (Jun *et al.*, 1999; Fletcher *et al.*, 2001).

6.2.2 RELEVANCE TO HUMAN PATHOLOGY

Several human neurological and muscular disorders are attributable to mutations in genes encoding calcium channel subunits and show some similarity to their murine counterparts (Table 6.1). These, in contrast to the mouse, mostly dominantly inheritable disorders include familial hemiplegic migraine (FHM), episodic ataxia type 2 (EA2), spinocerebellar ataxia type 6 (SCA6), epilepsy, X-linked congenital stationary night blindness and malignant hyperthermia.

Three different allelic mutations in humans are attributable to disruptions in *CACNA1A* gene function, the human ortholog to *Cacna1a* mutated in *tottering* (*tg*) mice. Truncations leading to a total loss of channel function cause EA2, characterized by abnormal eye movement (interictal nystagmus) and episodes of vertigo and truncal instability triggered by stress or fatigue. The EA2 phenotype overlaps with the allelic disorders FHM and SCA6.

Several missense mutations have been identified in patients with FHM, a particularly severe form of migraine. Electrophysiological analysis of the mutant channels in heterologous expression systems found them to be functional but their properties were altered. However the disease mechanism is complex as both gain of function (e.g. shift-of the voltage dependence to less depolarized potential, Kraus *et al.*, 1998) and loss of function (e.g. lower single-channel conductance, Hans *et al.*, 1999a) have been observed. The loss of function mutations are associated with human phenotypes showing characteristic cerebellar dysfunction.

SCA6 is caused by an expansion of CAG repeats (polyglutamines) within an intron, which is incorporated into the open reading frame in one *CACNA1A* splice variant (normal individuals, 4-20 repeats; SCA6 patients, 21-33 repeats). It has been shown that these expansions cause intracellular aggregation of the mutated protein both in cell culture and in patients, inducing apoptosis (Ishikawa *et al.*, 1999).

A mutation in the P/Q-type calcium channel subunit in a patient with human absence epilepsy has recently been reported (Jouvenceau *et al.*, 2001).

Mutations of $Ca_V2.1$ are associated with three distinct human diseases and two distinct mouse neurologic phenotypes. The human SCA6 and mouse *leaner* (tg^{la}) both disrupt the intracellular carboxy tail of the calcium channel (Fletcher *et*

al., 1996; Zuchenko *et al.,* 1997) and cause a persistent debilitating ataxia associated with severe degeneration of cerebellar neurones (Herrup and Wilczynski, 1982; Zhuchenko *et al.*, 1997). In contrast, the human disorders FHM and EA2 as well as the *tottering* mutation alter the transmembrane and/or pore regions of the channel (Fletcher *et al.,* 1996; Ophoff *et al.,* 1996) and cause episodic attacks of neurological dysfunction with little or no effect on cerebellar morphology (Isaacs and Abbott, 1995)

The phenotypic diversity of this group of allelic disorders exemplifies the complex but incompletely understood role that calcium channels play in heterogeneous cell populations making a strict genotype-phenotype correlation difficult. In addition, the dominant form of inheritance suggests some 'gain of function' in addition to altered channel properties.

Another set of mutations cause incomplete X linked congenital stationary night blindness, which is a recessive non-progressive retinal disorder characterized by night blindness, decreased visual acuity, myopia, nystagmus and strabismus. Electrophysiological data suggest a defect in retinal neurotransmission, while molecular studies have identified twenty different mutations in the *CACNA1F* gene encoding the $Ca_V1.4$ subunit with no apparent clustering (Bech-Hansen *et al.*, 1998; Boykott *et al.,* 2001). *CACNA1F* shares high homology with the dihydropyridine sensitive L-type calcium channels (α_{1S}, α_{1C}, α_{1D}).

Hyperkalaemic periodic paralysis is an autosomal dominant muscle disease manifested by episodic weakness associated with low serum K^+ and caused by missense mutations in *CACNA1S* (Jurkatt-Rott *et al.*, 1994). Functional expression of mutated $Ca_V1.1$ channels in *Xenopus* oocytes showed reduced L-type current amplitude and altered activation properties. An allelic mutation causes malignant hyperthermia, which is a skeletal muscle disorder triggered by the inhalation of volatile anaesthetics and parenteral injection of depolarizing muscle relaxants (Monnier *et al.*, 1997). It is characterized by a combination of hyperthermia, skeletal muscle rigidity, tachycardia or arrhythmia, respiratory and metabolic acidosis and rhabdomyolysis.

Two mutations in the gene encoding β_4 have been reported in patients with juvenile myoclonic epilepsy and episodic ataxia respectively (Escayg *et al.,*

2000). One is a point mutation and the other a mutation leading to the truncation of 38 C-terminal amino acids. Besides similarities in the phenotype to the murine *lethargic* mutation, there are also only subtle effects on calcium channel function in heterologous expression studies (Escayg *et al.*, 2000). These are so far the only mutations involving auxiliary calcium channel subunits in humans.

The discovery of genes involved in all these disorders has not only allowed DNA-based diagnostic tests but also increased information about the pathogenesis of the disorders and the normal functioning of ion channels. Increased understanding of the pathophysiological mechanisms that underlie neurological disorders will allow a more rational approach to their diagnosis, classification and perhaps subsequent therapy.

Phenotype	Gene (Product)	Nucleotide change	Predicted effect (location)	Physiologic consequences	References
FHM (familial hemiplegic migraine) ± progressive ataxia	*CACNA1A* ($Ca_V2.1$)	Missense G850A	R192Q (IS4)	↑Channel density ↑Open probability	1, 2,3
		Missense C2272T	T666M (IIS5-S6)	↓Channel density ↓Unitary conductance +state switching ?↓ Calcium entry	1, 4,3
		Missense T2416C	V714A (IIS6)	Negative voltage shift ↑Open probability ↑Recovery from inactivation ↓Unitary conductance+state switching	1, 2,3
± progressive ataxia		Missense C2418G	D715E (IIS6)	Unknown	4
± progressive ataxia		Missense A5706C	I1811L (IVS6)	↓Channel density ↑Recovery from inactivation ↑Open probability ?↓ Calcium entry	1, 2,3
EA2 (episodic ataxia type2) ± hemiplegia ± migraine Severe progressive ataxia ± migraine		Nonsense 4073Cdel	Stop codon (IIIS1)		1
		Splicing G 4270+1A	Splicing error (IIIS2)		
		Nonsense C4110T	R1279stop (IIIS2-S3)		5
		Nonsense C4110T	R1547stop (IVS1)		6
		Missense G1152A	G293R (IS5-S6)		7
		Missense T4747C	Phe1491Ser (IIIS6)	non-functional channel in HEK293 cells	8
Absence epilepsy, Episodic ataxia		C5733T	R1820Stop (IVS6)	non-functional channel in oocytes	9
SCA6 (spinocerebellar ataxia type 6)		CAG expansion	Poly-glutamines in C-terminus	altered channel function, rate of activation and inactivation, positive and negative shift respectively	10, 11, 12
X-linked congenital stationary night blindness	*CACNA1F* ($Ca_V1.4$)	20 known mutations no apparent clustering	70% truncations 30% amino acid substitutions		13, 14
Hypokalaemic periodic paralysis	*CACNA1S* ($Ca_V1.1$)		Arg1239His (IVS4) Arg1239Gly (IVS4) Arg528His (IIS4)	negative voltage shift of channel activation not reproduced in expression systems	15
Malignant hyper-thermia		A3333G	Arg1086His IIS3-S4		16
Juvenile myoclonic epilepsy	*CACNAB4* ($Ca_V\beta_4$)	R482X	Stop code 38AA c-term truncation		17
Episodic Ataxia		C→T	Cys104Phe		

Table 6.1 Human mutations in voltage-dependent calcium channel subunits

(1) Ophoff *et al.*, (1996); (2) Kraus *et al.*, (1998); (3) Hans *et al.*, (1999ab); (4) Ducros *et al.*, (1999); (5) Yue *et al.*, (1998); (6) Jen *et al.*, (1999); (7) Yue *et al.*, (1997); (8) Guida *et al.*, 2001; (9) Jouvenceau *et al.*, (2001); (10) Zhuchenko *et al.*, (1997); (11) Restituito et al., (2000); (12) Toru et al., (2000) ; (13) Bech-Hansen *et al.*, (1998); (14) Boycott *et al.*, (2001) ; (15) Jurkat-Rott *et al.*, (1994); (16) Monnier *et al.*, (1997); (17) Escayg *et al.*, (2000).

6.3 Future work

Despite the identification of the *du/du* mutation in the $\alpha_2\delta$-2 subunit the question of how mutations in calcium channel genes may trigger episodic neurological symptoms as well as cause persistent changes like progressive ataxia and cerebellar atrophy still remains largely open.

Direct questions arising from this study are abundant. One would be to question the role of mutant transcript 1 in the *du/du* phenotype and to identify the organelles in which the truncated *du*-mut1 protein accumulates, and why. Is the truncated α_2 subunit similarly transcribed and translated in the du^{2J} mutation described by Barclay *et al.* (2001), and is calcium homeostasis equally disrupted and are the differences in its phenotype compared to *du/du* attributable to differences in the genetic background of the different mouse strains? The alterations in the Purkinje cell morphology makes appropriate synaptic connectivity doubtful (Chen *et al.*, 1999). This could be addressed by electron-microscopic analysis but also through electrophysiological recordings in brain slices, where alterations in neuronal circuitry could be taken into account.

Recent studies have indicated that neurotransmitter release is impaired in hippocampus neuronal slices (Qin and Nobles, 2001) and in neuromuscular junctions of *tottering* mice (Plomp *et al.*, 2000). It would therefore be interesting to examine whether this also true in *du/du* mice.

Furthermore, abnormal calcium signalling especially during development could disrupt calcium-regulated gene expression (Finkbeiner and Greenberg, 1998) as seen for example in the reduced expression of the brain derived neurotrophic factor (BDNF) in the *stargazer* (*stg*) mutation (Qiao *et al.*, 1996). Because BNDF regulates neuronal differentiation, survival, and synaptogenesis, this may potentially result in aberrant synapse formation and neuronal circuitry. BDNF also induces the expression of transcription factors (Pax2, Pax3 and Pax6; Kioussi and Gruss 1994). It is therefore very likely that far-reaching perturbations within important transcriptional cascades could be initiated by a single calcium channel mutation and result in altered gene expression.

REFERENCES

Abbott, L.C., Isaacs, K.R., and Heckroth, J.A. (1996): Co-localization of tyrosine hydroxylase and zebrin II immunoreactivities in Purkinje cells of the mutant mice, tottering and tottering/leaner. *Neuroscience* **71**, 461-475.

Abbott, L.C and Sotelo, C. (2000): Ultrastructural analysis of catecholaminergic innervation in weaver and normal mouse cerebellar cortices. J.Comp.Neurol. **426**: 316-329.

Abe, H., Watanabe, M., Yamakuni, T., Kuwano, R., Takahashi, Y., and Kondo, H. (1992): Localization of gene expression of calbindin in the brain of adult rats. *Neurosci. Lett.***138**, 211-215.

Alden, K.J. and Garcia, J. (2001): Differential effect of gabapentin on neuronal and muscle calcium currents. *J. Pharmacol. Exp. Ther.* **297**, 727-735.

Altman, J. (1969): Autoradiographic and histological studies of postnatal neurogenesis. 3. Dating the time of production and onset of differentiation of cerebellar microneurons in rats. *J. Comp. Neurol.* **136**, 269-293.

Altman, J. (1972): Postnatal development of the cerebellar cortex in the rat. I. The external germinal layer and the transitional molecular layer. *J. Comp. Neurol.* **145**, 353-397.

Anantharaman, V. and Aravind, L. (2000): Cache - a signaling domain common to animal Ca2+-channel subunits and a class of prokaryotic chemotaxis receptors. *Trends in Biochem. Sci.* **25**, 535-537.

Angelotti, T. and Hofmann, F. (1996): Tissue-specific expression of splice variants of the mouse voltage-gated calcium channel $\alpha 2/\delta$ subunit. *FEBS Lett.* **397**, 331-337.

Arnold, D.B. and Heintz, N. (1997): A calcium responsive element that regulates expression of two calcium binding proteins in Purkinje cells. *Proc. Natl. Acad. Sci. U S A* **94**, 8842-8847.

Ashcroft, F.M., Proks, P., Smith, P.A., Ammala, C., Bokvist, K., and Rorsman, P. (1994): Stimulus-secretion coupling in pancreatic beta cells. *J. Cell. Biochem.* **55** Suppl., 54-65.

Ayata, C., Shimizu-Sasamata, M., Lo, E.H., Noebels, J.L., and Moskowitz, M.A. (2000): Impaired neurotransmitter release and elevated threshold for cortical spreading depression in mice with mutations in the alpha1A subunit of P/Q type calcium channels. *Neurosci.* **95**, 639-645.

Baimbridge, K.G., Celio, M.R., and Rogers, J.H. (1992): Calcium-binding proteins in the nervous system. *Trends in Neurosci.* **15**, 303-308.

Baimbridge, K.G. and Miller, J.J. (1982): Immunohistochemical localization of calcium-binding protein in the cerebellum, hippocampal formation and olfactory bulb of the rat. *Brain. Res.* **245**, 223-229.

Bangalore, R., Mehrke, G., Gingrich, K., Hofmann, F., and Kass, R. S. (1996): Influence of L-type Ca^2+ channel $\alpha 2\delta$-subunit on ionic and gating current in transiently transfected HEK 293 cells. *Am. J.Physiol.* **270**, H1521-H1528.

Barclay, J., Balaguero, N., Mione, M., Ackerman, S.L., Letts, V.A., Brodbeck, J., Canti, C., Meir, A., Page, K.M., Kusumi, K., Perez-Reyes, E., Lander, E.S., Frankel, W.N., Gardiner, R.M., Dolphin, A.C., and Rees, M. (2001): Ducky Mouse Phenotype of Epilepsy and Ataxia Is Associated with Mutations in the Cacna2d2 Gene and Decreased Calcium Channel Current in Cerebellar Purkinje Cells. *J. Neurosci.* **21**, 6095-6104.

Barclay, J. and Rees, M. (2000): Genomic organization of the mouse and human α2δ2 voltage-dependent calcium channel subunit genes. *Mamm.Genome* **11**, 1142-1144.

Bech-Hansen, N., Naylor, M.J., Maybaum, T.A., Pearce, W.G., Koop, B., Fishman, G.A., Mets, M., Musarella, M.A., and Boycott, K.M. (1998b): Loss-of-function mutations in a calcium-channel alpha1-subunit gene in Xp11.23 cause incomplete X-linked congenital stationary night blindness. *Nat. Genet.* **19**, 264-267.

Berridge, M.J. (1993): Cell signalling. A tale of two messengers. *Nature* **365**, 388-389.

Berridge, M.J. (1998): Neuronal calcium signaling. *Neuron* **21**, 13-26.

Berridge, M.J., Bootman, M.D., and Lipp, P. (1998): Calcium, a life and death signal. *Nature* **395**, 645-648.

Bito, H., Deisseroth, K., and Tsien, R.W. (1997): Ca2+-dependent regulation in neuronal gene expression. *Curr. Opin. Neurobiol.* **7**, 419-429.

Black, J.L. and Lennon, V.A. (1999): Identification and cloning of putative human neuronal voltage-gated calcium channel gamma-2 and gamma-3 subunits: Neurologic implications. *Mayo Clin.Proc.* **74**, 357-361.

Boukhaddaoui, H., Sieso, V., Scamps, F., Vigues, S., Roig, A., and Valmier, J. (2000): Q- and L-type calcium channels control the development of calbindin phenotype in hippocampal pyramidal neurons in vitro. *Eur. J. Neurosci.* **12**, 2068-2078.

Bourinet, E., Soong, T.W., Sutton, K., Slaymaker, S., Mathews, E., Monteil, A., Zamponi, G.W., Nargeot, J., and Snutch, T.P. (1999): Splicing of alpha 1A subunit gene generates phenotypic variants of P- and Q-type calcium channels. *Nat. Neurosci.* **2**, 407-415.

Boycott, K.M., Maybaum, T.A., Naylor, M.J., Weleber, R.G., Robitaille, J., Miyake, Y., Bergen, A.A., Pierpont, M.E., Pearce, W.G., and N.T. (2001): A summary of 20 CACNA1F mutations identified in 36 families with incomplete X-linked congenital stationary night blindness, and characterization of splice variants. *Hum. Genet.* **108**, 91-97.

Brice, N.L., Berrow, N.S., Campbell, V., Page, K.M., Brickley, K., Tedder, I., and Dolphin, A.C. (1997): Importance of the different β subunits in the membrane expression of the α1A and α2 calcium channel subunits: studies using a depolarisation-sensitive α1A antibody. *Eur. J. Neurosci.* **9**, 749-759.

Brickley, K., Campbell, V., Berrow, N., Leach, R., Norman, R.I., Wray, D., Dolphin, A.C., and Baldwin, S. (1995): Use of site-directed antibodies to

Brodbeck J, Davies A, Courtney JM, Meir A, Balaguero N, Canti C, Moss FJ, Page KM, Pratt WS, Hunt SP, Barclay J, Rees M, Dolphin AC. (2002): The ducky mutation in Cacna2d2 results in altered Purkinje cell morphology and is associated with the expression of a truncated $\alpha_2\delta$–2 protein with abnormal function. *J. Biol. Chem.* in press.

probe the topography of the α_2 subunit of voltage-gated Ca^{2+} channels. *FEBS Lett.* **364**, 129-133.

Brown, J.P. and Gee, N.S. (1998): Cloning and deletion mutagenesis of the $\alpha_2\delta$ calcium channel subunit from porcine cerebral cortex. *J. Biol. Chem.* **273**, 25458-25465.

Brust, P.F., Simerson, S., McCue, A.F., Deal, C.R., Schoonmaker, S., Williams, M.E., Veliçelebi, G., Johnson, E.C., Harpold, M.M., and Ellis, S.B. (1993): Human neuronal voltage-dependent calcium channels: Studies on subunit structure and role in channel assembly. *Neuropharm.* **32**, 1089-1102.

Burgess, D.L., Biddlecome, G.H., McDonough, S.I., Diaz, M.E., Zilinski, C.A., Bean, B.P., Campbell, K.P., and Noebels, J.L. (1999a): β subunit reshuffling modifies N- and P/Q-type Ca^{2+} channel subunit compositions in lethargic mouse brain. *Mol. Cell. Neurosci.* **13**, 293-311.

Burgess, D.L., Davis, C.F., Gefrides, L.A., and Noebels, J.L. (1999b): Identification of three novel Ca(2+) channel gamma subunit genes reveals molecular diversification by tandem and chromosome duplication. *Genome Res.* **9**, 1204-1213.

Burgess, D.L., Gefrides, L.A., Foreman, P.J., and Noebels, J.L. (2001): A cluster of three novel Ca2+ channel gamma subunit genes on chromosome 19q13.4: evolution and expression profile of the gamma subunit gene family. *Genomics* **71**, 339-350.

Burgess, D.L., Jones, J.M., Meisler, M.H., and Noebels, J.L. (1997): Mutation of the Ca2+ channel beta subunit gene Cchb4 is associated with ataxia and seizures in the lethargic (lh) mouse. *Cell* **88**, 385-392.

Caddick, S.J., Wang, C.S., Fletcher, C.F., Jenkins, N.A., Copeland, N.G., and Hosford, D.A. (1999): Excitatory but not inhibitory synaptic transmission is reduced in lethargic(Cacnb4(1h)) and tottering (Cacnala(tg)) mouse thalami. *J. Neurophysiol.* **81**, -2074

Campbell, D.B. and Hess, E.J. (1999): L-type calcium channels contribute to the tottering mouse dystonic episodes. *Mol. Pharmacol.* **55**, 23-31.

Campbell, V., Berrow, N.S., Fitzgerald, E.M., Brickley, K., and Dolphin, A.C. (1995): Inhibition of the interaction of G protein G(o) with calcium channels by the calcium channel beta-subunit in rat neurones. *J. Physiol.* **485** (Pt 2), 365-372.

Castellano, A., Wei, X., Birnbaumer, L., and Perez-Reyes, E. (1993): Cloning and expression of a neuronal calcium channel beta subunit. *J. Biol. Chem.* **268**, 12359-12366.

Catterall, W.A. (1998): Structure and function of neuronal Ca^{2+} channels and their role in neurotransmitter release. *Cell Calcium* **24**, 307-323.

Catterall, W.A., Seagar, M.J., and Takahashi, M. (1988): Molecular properties of dihydropyridine-sensitive calcium channels in skeletal muscle. *J. Biol. Chem.* **263**, 3535-3538.

Chaudhari, N. (1992): A single nucleotide deletion in the skeletal muscle-specific calcium channel transcript of muscular dysgenesis (mdg) mice. *J. Biol. Chem.* **267**, 25636-25639.

Chen, L., Bao, S., Qiao, X., and Thompson, R.F. (1999): Impaired cerebellar synapse maturation in waggler, a mutant mouse with a disrupted neuronal calcium channel gamma subunit. *Proc. Natl. Acad. Sci. U S A* **96**, 12132-12137.

Chen, L., Chetkovich, D.M., Petralia, R.S., Sweeney, N.T., Kawasaki, Y., Wenthold, R.J., Bredt, D.S., and Nicoll, R.A. (2000): Stargazing regulates synaptic targeting of AMPA receptors by two distinct mechanisms. *Nature* **408**, 936-943.

Chin, H., Smith, M.A., Kim, H.L., and Kim, H. (1992): Expression of dihydropyridine-sensitive brain calcium channels in the rat central nervous system. *FEBS Lett.* **299**, 69-74.

Choi, D.W. (1988): Calcium-mediated neurotoxicity: relationship to specific channel types and role in ischemic damage. *Trends in Neurosci.* **11**, 465-469.

Ciardo, A. and Meldolesi, J. (1991): Regulation of intracellular calcium in cerebellar granule neurons: effects of depolarization and of glutamatergic and cholinergic stimulation. *J. Neurochem.* **56**, 184-191.

Clapham, D.E. (1995): Calcium signaling. *Cell* **80**, 259-268.

Clark, B.A. and Barbour, B. (1997): Currents evoked in Bergmann glial cells by parallel fibre stimulation in rat cerebellar slices. *J. Physiol.* **502** (Pt 2), 335-350.

Colombatti A, Bonaldo P, Dolian R. Type A modules (1993): interacting domains found in several non-fibrillar collagens and in other extracellular matrix proteins. *Matrix* **13**(4):297–306.

Cormack, B.P., Valdivia, R.H., and Falkow, S. (1996): FACS-optimized mutants of the green fluorescent protein (GFP). *Gene* **173**, 33-38.

Cox, G.A., Lutz, C.M., Yang, C.L., Biemesderfer, D., Bronson, R.T., Fu, A., Aronson, P.S., Noebels, J.L., and Frankel, W.N. (1997): Sodium/hydrogen exchanger gene defect in slow-wave epilepsy mutant mice. *Cell* **91**, 139-148.

Cribbs, L.L., Lee, J.-H., Yang, J., Satin, J., Zhang, Y., Daud, A., Barclay, J., Williamson, M.P., Fox, M., Rees, M., and Perez-Reyes, E. (1998): Cloning and characterization of α1H from human heart, a member of the T type Ca^{2+} channel gene family. *Circ. Res.* **83**, 103-109.

Culbertson, M.R. (1999): RNA surveillance. Unforeseen consequences for gene expression, inherited genetic disorders and cancer. *Trends in Genet.* **15**, 74-80.

D'Orlando, C., Fellay, B., Schwaller, B., Salicio, V., Bloc, A., Gotzos, V., and Celio, M.R. (2001): Calretinin and calbindin D-28k delay the onset of cell death after excitotoxic stimulation in transfected P19 cells. *Brain Res.* **909**, 145-158.

Daniel, H., Levenes, C., and Crepel, F. (1998): Cellular mechanisms of cerebellar LTD. *Trends in Neurosci.* **21**, 401-407.

De Koninck, P. and Schulman, H. (1998): Sensitivity of CaM kinase II to the frequency of Ca2+ oscillations. *Science* **279**, 227-230.

De Waard, M. and Campbell, K.P. (1995): Subunit regulation of the neuronal α_{1A} Ca^{2+} channel expressed in *Xenopus* oocytes. *J. Physiol.* **485**, 619-634.

De Waard, M., Liu, H., Walker, D., Scott, V.E., Gurnett, C.A., and Campbell, K.P. (1997): Direct binding of G-protein betagamma complex to voltage-dependent calcium channels. *Nature* **385**, 446-450.

Destexhe, A., Bal, T., McCormick, D.A., and Sejnowski, T.J. (1996): Ionic mechanisms underlying synchronized oscillations and propagating waves in a model of ferret thalamic slices. *J. Neurophysiol.* **76**, 2049-2070.

Dolmetsch, R.E., Xu, K., and Lewis, R.S. (1998): Calcium oscillations increase the efficiency and specificity of gene expression. *Nature* **392**, 933-936.

Dolphin, A.C., Wyatt, C.N., Richards, J., Beattie, R.E., Craig, P., Lee, J.-H., Cribbs, L.L., Volsen, S.G., and Perez-Reyes, E. (1999): The effect of $\alpha 2$-δ and other accessory subunits on expression and properties of the calcium channel $\alpha 1$G. *J. Physiol.* **519**, 35-45.

Dove, L.S., Abbott, L.C., and Griffith, W.H. (1998): Whole-cell and single-channel analysis of P-type calcium currents in cerebellar purkinje cells of leaner mutant mice. *J. Neurosci.* **18**, 7687-7699.

Dove, L.S., Nahm, S.S., Murchison, D., Abbott, L.C., and Griffith, W.H. (2000): Altered Calcium Homeostasis in Cerebellar Purkinje Cells of Leaner Mutant Mice. *J. Neurophysiol.* **84**, 513-524.

Du, Y., Dodel, R.C., Bales, K.R., Jemmerson, R., Hamilton-Byrd, E., and Paul, S.M. (1997): Involvement of a caspase-3-like cysteine protease in 1-methyl-4-phenylpyridinium-mediated apoptosis of cultured cerebellar granule neurons. *J. Neurochem.* **69**, 1382-1388.

Dubel, S.J., Starr, T.V., Hell, J., Ahlijanian, M.K., Enyeart, J.J., Catterall, W.A., and Snutch, T.P. (1992): Molecular cloning of the alpha-1 subunit of an omega-conotoxin-sensitive calcium channel. *Proc. Natl. Acad. Sci. USA* **89**, 5058-5062.

Ducros, A., Denier, C., Joutel, A., Vahedi, K., Michel, A., Darcel, F., Madigand, M., Guerouaou, D., Tison, F., Julien, J., Hirsch, E., Chedru, F., Bisgard, C., Lucotte, G., Despres, P., Billard, C., Barthez, M.A., Ponsot, G., Bousser, M.G., and Tournier-Lasserve, E. (1999): Recurrence of the T666M calcium channel CACNA1A gene mutation in familial hemiplegic migraine with progressive cerebellar ataxia. *Am. J. Hum. Genet.* **64** , 89-98.

Dunlap, K., Luebke, J.I., and Turner, T.J. (1995): Exocytotic Ca2+ channels in mammalian central neurons. *Trends in Neurosci.* **18**, 89-98.

Dutuit, M., Didier-Bazes, M., Vergnes, M., Mutin, M., Conjard, A., Akaoka, H., Belin, M.F., and Touret, M. (2000): Specific alteration in the expression of

glial fibrillary acidic protein, glutamate dehydrogenase, and glutamine synthetase in rats with genetic absence epilepsy. *Glia* **32**, 15-24.

Earnshaw, W.C., Martins, L.M., and Kaufmann, S.H. (1999): Mammalian caspases: structure, activation, substrates, and functions during apoptosis. *Annu. Rev. Biochem.* **68**, 383-424.

Eberst, R., Dai, S.P., Klugbauer, N., and Hofmann, F. (1997): Identification and functional characterization of a calcium channel gamma subunit. *Pflügers Arch.* **433**, 633-637.

Eddleston, M. and Mucke, L. (1993): Molecular profile of reactive astrocytes--implications for their role in neurologic disease. *Neurosci.* **54**, 15-36.

Eilers, J., Augustine, G.J., and Konnerth, A. (1995): Subthreshold synaptic Ca2+ signalling in fine dendrites and spines of cerebellar Purkinje neurons. *Nature* **373**, 155-158.

Eilers, J., Plant, T., and Konnerth, A. (1996): Localized calcium signalling and neuronal integration in cerebellar Purkinje neurones. *Cell Calcium* **20**, 215-226.

Ellgaard, L., Molinari, M., and Helenius, A. (1999): Setting the standards: quality control in the secretory pathway. *Science* **286**, 1882-1888.

Ellis, S.B., Williams, M.E., Ways, N.R., Brenner, R., Sharp, A.H., Leung, A.T., Campbell, K.P., McKenna, E., Koch, W.J., Hui, A., Schwartz, A., and Harpold, M.M. (1988): Sequence and expression of mRNAs encoding the α_1 and α_2 subunits of a DHP-sensitive calcium channel. *Science* **241**, 1661-1664.

Eng, L.F., Ghirnikar, R.S., and Lee, Y.L. (2000): Glial fibrillary acidic protein: GFAP-thirty-one years (1969-2000). *Neurochem. Res.* **25**, 1439-1451.

Ertel, E.A., Campbell, K.P., Harpold, M.M., Hofmann, F., Mori, Y., Perez-Reyes, E., Schwartz, A., Snutch, T.P., Tanabe, T., Birnbaumer, L., Tsien, R.W., and Catterall, W.A. (2000): Nomenclature of voltage-gated calcium channels. *Neuron* **25**, 533-535.

Escayg, A., De Waard, M., Lee, D.D., Bichet, D., Wolf, P., Mayer, T., Johnston, J., Baloh, R., Sander, T., and Meisler, M.H. (2000): Coding and noncoding variation of the human calcium-channel β_4-subunit gene *CACNB4* in patients with idiopathic generalized epilepsy and episodic ataxia. *Am. J. Hum. Genet.* **66**, 1531-1539.

Felix, R., Gurnett, C.A., De Waard, M., and Campbell, K.P. (1997): Dissection of functional domains of the voltage-dependent Ca2+ channel alpha2delta subunit. *J. Neurosci.* **17**, 6884-6891.

Field, M.J., Oles, R.J., Lewis, A.S., McCleary, S., Hughes, J., and Singh, L. (1997): Gabapentin (neurontin) and S-(+)-3-isobutylgaba represent a novel class of selective antihyperalgesic agents. *Br. J. Pharmacol.* **121**, 1513-1522.

Fierro, L., DiPolo, R., and Llano, I. (1998): Intracellular calcium clearance in Purkinje cell somata from rat cerebellar slices. *J. Physiol.* **510** (Pt 2), 499-512.

Fierro, L. and Llano, I. (1996): High endogenous calcium buffering in Purkinje cells from rat cerebellar slices. *J. Physiol.* **496** (Pt 3), 617-625.

Fink, K., Meder, W., Dooley, D.J., and Gothert, M. (2000): Inhibition of neuronal Ca(2+) influx by gabapentin and subsequent reduction of neurotransmitter release from rat neocortical slices. *Br. J. Pharmacol.* **130**, 900-906.

Finkbeiner, S. and Greenberg, M.E. (1998): Ca2+ channel-regulated neuronal gene expression. *J. Neurobiol.* **37**, 171-189.

Fletcher, C.F., Lutz, C.M., O'Sullivan, T.N., Shaughnessy, J.D., Jr., Hawkes, R., Frankel, W.N., Copeland, N.G., and Jenkins, N.A. (1996): Absence epilepsy in tottering mutant mice is associated with calcium channel defects. *Cell* **87**, 607-617.

Fletcher, C.F., Tottene, A., Lennon, V.A., Wilson, S.M., Dubel, S.J., Paylor, R., Hosford, D.A., Tessarollo, L., McEnery, M.W., Pietrobon, D., Copeland, N.G., and Jenkins, N.A. (2001): Dystonia and cerebellar atrophy in Cacna1a null mice lacking P/Q calcium channel activity. *FASEB J.* **15**, 1288-1290.

Flockerzi, V., Oeken, H.J., Hofmann, F., Pelzer, D., Cavalie, A., and Trautwein, W. (1986): Purified dihydropyridine-binding site from skeletal muscle t-tubules is a functional calcium channel. *Nature* **323**, 66-68.

Freise, D., Held, B., Wissenbach, U., Pfeifer, A., Trost, C., Himmerkus, N., Schweig, U., Freichel, M., Biel, M., Hofmann, F., Hoth, M., and Flockerzi, V. (2000): Absence of the gamma subunit of the skeletal muscle dihydropyridine receptor increases L-type Ca2+ currents and alters channel inactivation properties. *J. Biol. Chem.* **275**, 14476-14481.

Fujita, S. (1967): Quantitative analysis of cell proliferation and differentiation in the cortex of the postnatal mouse cerebellum. *J. Cell Biol.* **32**, 277-287.

Gao, B.N., Sekido, Y., Maximov, A., Saad, M., Forgacs, E., Latif, F., Wei, M.H., Lerman, M., Lee, J.H., Perez-Reyes, E., Bezprozvanny, I., and Minna, J.D. (2000): Functional properties of a new voltage-dependent calcium channel $\alpha_2\delta$ auxiliary subunit gene (CACNA2D2). *J. Biol. Chem.* **275**, 12237-12242.

Gardiner, M. and Lehesjoki, A.E. (2000): Genetics of the epilepsies. *Curr. Opin. Neurol.* **13**, 157-164.

Gee, N.S., Brown, J.P., Dissanayake, V.U., Offord, J., Thurlow, R., and Woodruff, G.N. (1996): The novel anticonvulsant drug, gabapentin (Neurontin), binds to the alpha2delta subunit of a calcium channel. *J. Biol. Chem.* **271**, 5768-5776.

Gillard, S.E., Volsen, S.G., Smith, W., Beattie, R.E., Bleakman, D., and Lodge, D. (1997): Identification of pore-forming subunit of P-type calcium channels: an antisense study on rat cerebellar Purkinje cells in culture. *Neuropharm.* **36**, 405-409.

Gloor, P. and Fariello, R.G. (1988): Generalized epilepsy: some of its cellular mechanisms differ from those of focal epilepsy. *Trends in Neurosci.* **11**, 63-68.

Gregg, R.G., Messing, A., Strube, C., Beurg, M., Moss, R., Behan, M., Sukhareva, M., Haynes, S., Powell, J.A., Coronado, R., and Powers, P.A. (1996): Absence of the beta subunit (cchb1) of the skeletal muscle dihydropyridine receptor alters expression of the alpha 1 subunit and eliminates excitation-contraction coupling. *Proc. Natl. Acad. Sci. USA* **93**, 13961-13966.

Grosche, J., Matyash, V., Moller, T., Verkhratsky, A., Reichenbach, A., and Kettenmann, H. (1999): Microdomains for neuron-glia interaction: parallel fiber signaling to Bergmann glial cells. *Nat. Neurosci.* **2**, 139-143.

Grusser-Cornehls, U. and Baurle, J. (2001): Mutant mice as a model for cerebellar ataxia. *Prog. Neurobiol.* **63**, 489-540.

Grynkiewicz, G., Poenie, M., and Tsien, R.Y. (1985): A new generation of Ca2+ indicators with greatly improved fluorescence properties. *J. Biol. Chem.* **260**, 3440-3450.

Guida, S., Trettel, F., Pagnutti, S., Mantuano, E., Tottene, A., Veneziano, L., Fellin, T., Spadaro, M., Stauderman, K., Williams, M., Volsen, S., Ophoff, R., Frants, R., Jodice, C., Frontali, M., and Pietrobon, D. (2001): Complete loss of P/Q calcium channel activity caused by a CACNA1A missense mutation carried by patients with episodic ataxia type 2. *Am. J. Hum. Genet.* **68**, 759-764.

Gurnett, C.A., De Waard, M., and Campbell, K.P. (1996): Dual function of the voltage-dependent Ca^{2+} channel $\alpha_2\delta$ subunit in current stimulation and subunit interaction. *Neuron* **16**, 431-440.

Gurnett, C.A., Felix, R., and Campbell, K.P. (1997): Extracellular interaction of the voltage-dependent Ca^{2+} channel $\alpha_2\delta$ and α_1 subunits. *J. Biol. Chem.* **272**, 18508-18512.

Gurney, M.E., Cutting, F.B., Zhai, P., Doble, A., Taylor, C.P., Andrus, P.K., and Hall, E.D. (1996): Benefit of vitamin E, riluzole, and gabapentin in a transgenic model of familial amyotrophic lateral sclerosis. *Ann. Neurol.* **39**, 147-157.

Hack, N., Hidaka, H., Wakefield, M.J., and Balazs, R. (1993): Promotion of granule cell survival by high K+ or excitatory amino acid treatment and Ca2+/calmodulin-dependent protein kinase activity. *Neurosci.* **57**, 9-20.

Hajnoczky, G., L.D., Seitz, M.B., and Thomas, A.P. (1995): Decoding of cytosolic calcium oscillations in the mitochondria. *Cell* **82**, 415-424.

Hanlon, M.R., Berrow, N.S., Dolphin, A.C., and Wallace, B.A. (1999): Modelling of a voltage-dependent Ca2+ channel beta subunit as a basis for understanding its functional properties. *FEBS Lett.* **445**, 366-370.

Hans, M., Luvisetto, S., Williams, M.E., Spagnolo, M., Urrutia, A., Tottene, A., Brust, P.F., Johnson, E.C., Harpold, M.M., Stauderman, K.A., and Pietrobon, D. (1999a): Functional consequences of mutations in the human alpha1A calcium channel subunit linked to familial hemiplegic migraine. *J. Neurosci.* **19**, 1610-1619.

Hans, M., Urrutia, A., Deal, C., Brust, P.F., Stauderman, K., Ellis, S.B., Harpold, M.M., Johnson, E.C., and Williams, M.E. (1999b): Structural elements in domain IV that influence biophysical and pharmacological properties of human alpha1A-containing high-voltage-activated calcium channels. *Biophys. J.* **76**, 1384-1400.

Harrold, J., Ritchie, J., Nicholls, D., Smith, W., Bowman, D., and Pocock, J. (1997): The development of Ca2+ channel responses and their coupling to exocytosis in cultured cerebellar granule cells. *Neurosci.* **77**, 683-694.

Hatten, M.E., Alder, J., Zimmerman, K., and Heintz, N. (1997): Genes involved in cerebellar cell specification and differentiation. *Curr. Opin. Neurobiol.* **7**, 40-47.

Haydon, P.G. (2001): GLIA: listening and talking to the synapse. *Nat. Rev. Neurosci.* **2**, 185-193.

Heckroth, J.A. and Abbott, L.C. (1994): Purkinje cell loss from alternating sagittal zones in the cerebellum of leaner mutant mice. *Brain Res.* **658**, 93-104.

Hengartner, M.O. (2000): The biochemistry of apoptosis. *Nature* **407**, 770-776.

Henshall, D.C., Chen, J., and Simon, R.P. (2000): Involvement of caspase-3-like protease in the mechanism of cell death following focally evoked limbic seizures. *J. Neurochem.* **74**, 1215-1223.

Herlitze, S., Hockerman, G.H., Scheuer, T., and Catterall, W.A. (1997): Molecular determinants of inactivation and G protein modulation in the intracellular loop connecting domains I and II of the calcium channel alpha1A subunit. *Proc. Natl. Acad. Sci. USA* **94**, 1512-1516.

Herrup, K. and Wilczynski, S.L. (1982): Cerebellar cell degeneration in the leaner mutant mouse. *Neurosci.* **7**, 2185-2196.

Hess, E.J. and Wilson, M.C. (1991): Tottering and leaner mutations perturb transient developmental expression of tyrosine hydroxylase in embryologically distinct Purkinje cells. *Neuron* **6**, 123-132.

Hobom, M., Dai, S., Marais, E., Lacinova, L., Hofmann, F., and Klugbauer, N. (2000): Neuronal distribution and functional characterization of the calcium channel $\alpha_2\delta$-2 subunit. *Eur. J. Neurosci.* **12**, 1217-1226.

Hosford, D.A., Clark, S., Cao, Z., Wilson, W.A.J., Lin, F.H., Morrisett, R.A., and Huin, A. (1992): The role of GABAB receptor activation in absence seizures of lethargic (lh/lh) mice. *Science* **257**, 398-401.

Huguenard, J.R. and Prince, D.A. (1994): Intrathalamic rhythmicity studied in vitro: nominal T-current modulation causes robust antioscillatory effects. *J. Neurosci.* **14**, 5485-5502.

Hullin, R., Singer-Lahat, D., Freichel, M., Biel, M., Dascal, N., Hofmann, F., and Flockerzi, V. (1992): Calcium channel beta subunit heterogeneity: functional expression of cloned cDNA from heart, aorta and brain. *EMBO J.* **11**, 885-890.

Huntsman, M.M., Porcello, D.M., Homanics, G.E., DeLorey, T.M., and Huguenard, J.R. (1999): Reciprocal inhibitory connections and network synchrony in the mammalian thalamus. *Science* **283**, 541-543.

Iino, M., Goto, K., Kakegawa, W., Okado, H., Sudo, M., Ishiuchi, S., Miwa, A., Takayasu, Y., Saito, I., Tsuzuki, K., and Ozawa, S. (2001): Glia-Synapse Interaction Through Ca2+-Permeable AMPA Receptors in Bergmann Glia. *Science* **292**, 926-929.

Isaacs, K.R. and Abbott, L.C. (1995): Cerebellar volume decreases in the tottering mouse are specific to the molecular layer. *Brain. Res. Bull.* **36**, 309-314.

Ishikawa, K., Fujigasaki, H., Saegusa, H., Ohwada, K., Fujita, T., Iwamoto, H., Komatsuzaki, Y., Toru, S., Toriyama, H., Watanabe, M., Ohkoshi, N., Shoji, S., Kanazawa, I., Tanabe, T., and Mizusawa, H. (1999): Abundant expression and cytoplasmic aggregations of [alpha]1A voltage-dependent calcium channel protein associated with neurodegeneration in spinocerebellar ataxia type 6. *Hum. Mol. Genet.* **8**, 1185-1193.

Ito, M. (1984): The cerebellum and neuronal control. *Raven Press*, New York

Jen, J., Yue, Q., Nelson, S.F., Yu, H., Litt, M., Nutt, J., and Baloh, R.W. (1999): A novel nonsense mutation in CACNA1A causes episodic ataxia and hemiplegia. *Neurol.* **53**, 34-37.

Jeong, Y.G., Hyun, B.H., and Hawkes, R. (2000): Abnormalities in cerebellar Purkinje cells in the novel ataxic mutant mouse, pogo. *Brain Res. Dev. Brain Res.* **125**, 61-67.

Jodice, C., Mantuano, E., Veneziano, L., Trettel, F., Sabbadini, G., Calandriello, L., Francia, A., Spadaro, M., Pierelli, F., Salvi, F., Ophoff, R.A., Frants, R.R., and Frontali, M. (1997): Episodic ataxia type 2 (EA2) and spinocerebellar ataxia type 6 (SCA6) due to CAG repeat expansion in the CACNA1A gene on chromosome 19p. *Hum. Mol. Genet.* **6** , 1973-1978.

Jones, L.P., Wei, S.K., and Yue, D.T. (1998): Mechanism of auxiliary subunit modulation of neuronal alpha1E calcium channels. *J. Gen. Physiol.* **112**, 125-143.

Jouvenceau, A., Eunson, L.H., Spauschus, A., Ramesh, V., Zuberi, S.M., Kullmann, D.M., and Hanna, M.G. (2001): Human epilepsy associated with dysfunction of the brain P/Q-type calcium channel. *Lancet* **358**, 801-807.

Jun, K., Piedras-Renteria, E.S., Smith, S.M., Wheeler, D.B., Lee, S.B., Lee, T.G., Chin, H., Adams, M.E., Scheller, R.H., Tsien, R.W., and Shin, H.S. (1999): Ablation of P/Q-type Ca2+ channel currents, altered synaptic transmission, and progressive ataxia in mice lacking the alpha 1A-subunit. *Proc. Natl. Acad. Sci. USA* **96**, 15245-15250.

Jurkat-Rott, K., Lehmann-Horn, F., Elbaz, A., Heine, R., Gregg, R.G., Hogan, K., Powers, P.A., Lapie, P., J.E., and Weissenbach, J. (1994): A calcium channel mutation causing hypokalemic periodic paralysis. *Hum. Mol. Genet.* **3**, 1415-1419.

Kano, M., Rexhausen, U., Dreessen, J., and Konnerth, A. (1992): Synaptic excitation produces a long-lasting rebound potentiation of inhibitory synaptic signals in cerebellar Purkinje cells. *Nature* **356**, 601-604.

Kano, M., Schneggenburger, R., Verkhratsky, A., and Konnerth, A. (1995): Depolarization-induced calcium signals in the somata of cerebellar Purkinje neurons. *Neurosci. Res.* **24**, 87-95.

Kantheti, P., Qiao, X., Diaz, M.E., Peden, A.A., Meyer, G.E., Carskadon, S.L., Kapfhamer, D., Sufalko, D., Robinson, M.S., Noebels, J.L., and Burmeister, M. (1998): Mutation in AP-3 delta in the mocha mouse links endosomal transport to storage deficiency in platelets, melanosomes, and synaptic vesicles. *Neuron* **21**, 111-122.

Kase, M., Kakimoto, S., Sakuma, S., Houtani, T., Ohishi, H., Ueyama, T., and Sugimoto, T. (1999): Distribution of neurons expressing alpha 1G subunit mRNA of T-type voltage-dependent calcium channel in adult rat central nervous system. *Neurosci. Lett.* **268**, 77-80.

Kaufman, R.J. (1999): Stress signaling from the lumen of the endoplasmic reticulum: coordination of gene transcriptional and translational controls. *Genes Dev.* **13**, 1211-1233.

Kazmierczak, J., Degens, E.T. (1986): Calcium and the early eukaryotes. *Mitt. Geol.-Paleont. Inst.Univ. Hamburg* **61**, 1-20

Kim, D., Song, I., Keum, S., Lee, T., Jeong, M.J., Kim, S.S., McEnery, M.W., and Shin, H.S. (2001): Lack of the burst firing of thalamocortical relay neurons and resistance to absence seizures in mice lacking alpha(1G) T-type Ca(2+) channels. *Neuron* **31**, 35-45.

Kim, Y.I. and Neher, E. (1988): IgG from patients with Lambert-Eaton syndrome blocks voltage-dependent calcium channels. *Science* **239**, 405-408.

Kioussi, C. and Gruss, P. (1994): Differential induction of Pax genes by NGF and BDNF in cerebellar primary cultures. *J. Cell. Biol.* **125**, 417-425.

Kirischuk, S. and Verkhratsky, A. (1996): [Ca2+]i recordings from neural cells in acutely isolated cerebellar slices employing differential loading of the membrane-permeant form of the calcium indicator fura-2. *Pflugers Arch.* **431**, 977-983.

Klockgether, T. and Evert, B. (1998): Genes involved in hereditary ataxias. *Trends in Neurosci.* **21**, 413-418.

Klugbauer, N., Dai, S.P., Specht, V., Lacinová, L., Marais, E., Bohn, G., and Hofmann, F. (2000): A family of gamma-like calcium channel subunits. *FEBS Lett.* **470**, 189-197.

Klugbauer, N., Marais, E., Lacinova, L., and Hofmann, F. (1999a): A T-type calcium channel from mouse brain. *Pflugers Arch.* **437**, 710-715.

Klugbauer, N., Lacinová, L., Marais, E., Hobom, M., and Hofmann, F. (1999b): Molecular diversity of the calcium channel $\alpha_2\delta$ subunit. *J. Neurosci.* **19**, 684-691.

Knudson, C.M., Chaudhari, N., Sharp, A.H., Powell, J.A., Beam, K.G., and Campbell, K.P. (1989): Specific absence of the alpha 1 subunit of the dihydropyridine receptor in mice with muscular dysgenesis. *J. Biol. Chem.* **264**, 1345-1348.

Koh, J.Y. and Cotman, C.W. (1992): Programmed cell death: its possible contribution to neurotoxicity mediated by calcium channel antagonists. *Brain Res.* **587**, 233-240.

Koike, T., Martin, D.P., and Johnson, E.M.J. (1989): Role of Ca2+ channels in the ability of membrane depolarization to prevent neuronal death induced by trophic-factor deprivation: evidence that levels of internal Ca2+ determine nerve growth factor dependence of sympathetic ganglion cells. *Proc. Natl. Acad. Sci. USA* **86**, 6421-6425.

Konnerth, A., Dreessen, J., and Augustine, G.J. (1992): Brief dendritic calcium signals initiate long-lasting synaptic depression in cerebellar Purkinje cells. *Proc. Natl. Acad. Sci. USA* **89**, 7051-7055.

Kraus, R.L., Sinnegger, M.J., Glossmann, H., Hering, S., and Striessnig, J. (1998): Familial hemiplegic migraine mutations change alpha1A Ca2+ channel kinetics. *J. Biol. Chem.* **273**, 5586-5590.

Kuida, K., Zheng, T.S., Na, S., Kuan, C., Yang, D., Karasuyama, H., Rakic, P., and Flavell, R.A. (1996): Decreased apoptosis in the brain and premature lethality in CPP32-deficient mice. *Nature* **384**, 368-372.

Kurobe, N., Inaguma, Y., Shinohara, H., Semba, R., Inagaki, T., and Kato, K. (1992): Developmental and age-dependent changes of 28-kDa calbindin-D in the central nervous tissue determined with a sensitive immunoassay method. *J. Neurochem.* **58**, 128-134.

Lacerda, A.E., Perez-Reyes, E., Wei, X., Castellano, A., and Brown, A.M. (1994): T-type and N-type calcium channels of *Xenopus* oocytes: Evidence for specific interactions with β subunits. *Biophys. J.* **66**, 1833-1843.

Laemmli, U.K. (1970): Cleavage of structural proteins during the assembly of the head of bacteriophage T4. *Nature* **227**, 680-685.

Lee J.O., Rieu P., Arnaout M.A., Liddington R. (1995): Crystal structure of the A domain from the alpha subunit of integrin CR3 (CD11b/CD18). Cell **80**(4), 631–8.

Lee, J.-H., Daud, A.N., Cribbs, L.L., Lacerda, A.E., Pereverzev, A., Klockner, U., Schneider, T., and Perez-Reyes, E. (1999a): Cloning and expression of a novel member of the low voltage activated T type calcium channel family. *J. Neurosci.* **19**, 1912-1921.

Lee, A., Wong, S.T., Gallagher, D., Li, B., Storm, D.R., Scheuer, T., and Catterall, W.A. (1999b): Ca^{2+}/calmodulin binds to and modulates P/Q-type calcium channels. *Nature* **399**, 155-159.

Letts, V.A., Felix, R., Biddlecome, G.H., Arikkath, J., Mahaffey, C.L., Valenzuela, A., Bartlett, F.S., Mori, Y., Campbell, K.P., and Frankel, W.N. (1998): The

mouse stargazer gene encodes a neuronal Ca^{2+} channel gamma subunit. *Nature Genet.* **19**, 340-347.

Li, W., Llopis, J., Whitney, M., Zlokarnik, G., and Tsien, R.Y. (1998): Cell-permeant caged InsP3 ester shows that Ca2+ spike frequency can optimize gene expression. *Nature* **392**, 936-941.

Li, Y., Luo, L., Thomas, D.Y., and Kang, C.Y. (1994): Control of expression, glycosylation, and secretion of HIV-1 gp120 by homologous and heterologous signal sequences. *Virology* **204**, 266-278.

Lin, F.H., Cao, Z., and Hosford, D.A. (1993): Increased number of GABAB receptors in the lethargic (lh/lh) mouse model of absence epilepsy. *Brain Res.* **608**, 101-106.

Lin, Z., Harris, C., and Lipscombe, D. (1996): The molecular identity of Ca channel alpha 1-subunits expressed in rat sympathetic neurons. *J. Mol. Neurosci.* **7**, 257-267.

Lledo, P.M., Somasundaram, B., Morton, A.J., Emson, P.C., and Mason, W.T. (1992): Stable transfection of calbindin-D28k into the GH3 cell line alters calcium currents and intracellular calcium homeostasis. *Neuron* **9**, 943-954.

Lorenzon, N.M., Lutz, C.M., Frankel, W.N., and Beam, K.G. (1998): Altered calcium channel currents in Purkinje cells of the neurological mutant mouse *leaner*. *J. Neurosci.* **18**, 4482-4489.

Luebke, J.I., Dunlap, K., and Turner, T.J. (1993): Multiple calcium channel types control glutamatergic synaptic transmission in the hippocampus. *Neuron* **11**, 895-902.

Luo, Z.D. (2000): Rat dorsal root ganglia express distinctive forms of the alpha2 calcium channel subunit. *Neuroreport* **11**, 3449-3452.

Macart, M. and Gerbaut, L. (1988): Optimization of protein measurement in biological fluids by the dye-binding-SDS method. *Clin. Chem.* **34**, 998-999.

Maneuf, Y.P. and McKnight, A.T. (2001): Block by gabapentin of the facilitation of glutamate release from rat trigeminal nucleus following activation of protein kinase C or adenylyl cyclase. *Br. J. Pharmacol.* **134**, 237-240.

Marais, E., Klugbauer, N., and Hofmann, F. (2001): Calcium channel alpha(2)delta subunits-structure and Gabapentin binding. *Mol. Pharmacol.* **59**, 1243-1248.

Marchetti, C., Amico, C., and Usai, C. (1995): Functional characterization of the effect of nimodipine on the calcium current in rat cerebellar granule cells. *J. Neurophysiol.* **73**, 1169-1180.

Marks, N., Berg, M.J., Guidotti, A., and Saito, M. (1998): Activation of caspase-3 and apoptosis in cerebellar granule cells. *J. Neurosci. Res.* **52**, 334-341.

Marrion, N.V. and Tavalin, S.J. (1998): Selective activation of Ca2+-activated K+ channels by co-localized Ca2+ channels in hippocampal neurons. *Nature* **395**, 900-905.

Martoglio, B. and Dobberstein, B. (1998): Signal sequences: more than just greasy peptides. *Trends Cell. Biol.* **8**, 410-415.

Marty, A. and Llano, I. (1995): Modulation of inhibitory synapses in the mammalian brain. *Curr. Opin. Neurobiol.* **5**, 335-341.

Mattson, M.P., LaFerla, F.M., Chan, S.L., Leissring, M.A., Shepel, P.N., and Geiger, J.D. (2000): Calcium signaling in the ER: its role in neuronal plasticity and neurodegenerative disorders. *Trends in Neurosci.* **23**, 222-229.

McCaslin, P.P. and Smith, T.G. (1990): Low calcium-induced release of glutamate results in autotoxicity of cerebellar granule cells. *Brain. Res.* **513**, 280-285.

McEnery, M.W., Copeland, T.D., and Vance, C.L. (1998): Altered expression and assembly of N-type calcium channel α1B and β subunits in epileptic *lethargic (lh/lh)* mouse. *J. Biol. Chem.* **273**, 21435-21438.

Meier, H. (1968): The neuropathology of ducky, a neurological mutation of the mouse. A pathological and preliminary histochemical study. *Acta Neuropathol. Berl.* **11**, 15-28.

Meier, H. and MacPike, A.D. (1971): Three syndromes produced by two mutant genes in the mouse. Clinical, pathological, and ultrastructural bases of tottering, leaner, and heterozygous mice. *J. Hered.* **62**, 297-302.

Meier, H. and McPike, A.D. (1970): Ducky, a neurological mutation in mice characterized by deficiency of cerebrosides. *Exp. Med. Surg.* **28**, 256-269.

Meir, A., Bell, D.C., Stephens, G.J., Page, K.M., and Dolphin, A.C. (2000): Calcium channel beta subunit promotes voltage-dependent modulation of alpha 1 B by G beta gamma. *Biophys. J.* **79**, 731-746.

Miale, I. And Sidman, R.L. (1961): An autoradiographic analysis of histogenesis in mouse cerebellum. *Expl. Neurol.* **4**, 277-296

Mikami, A., Imoto, K., Tanabe, T., Niidome, T., Mori, Y., Takeshima, H., Narumiya, S., and Numa, S. (1989): Primary structure and functional expression of the cardiac dihydropyridine-sensitive calcium channel. *Nature* **340**, 230-233.

Minsky, M. (1961): Microskopy apparatus. Filed 7th November 1957 *US patent 3013467*.

Mintz, I.M., Adams, M.E., and Bean, B.P. (1992b): P-type calcium channels in rat central and peripheral neurons. *Neuron* **9**, 85-95.

Mintz, I.M., Venema, V.J., Swiderek, K.M., Lee, T.D., Bean, B.P., and Adams, M.E. (1992a): P-type calcium channels blocked by the spider toxin **w**-Aga-IVA. *Nature* **355**, 827-829.

Monnier, N., Procaccio, V., Stieglitz, P., and Lunardi, J. (1997): Malignant-hyperthermia susceptibility is associated with a mutation of the alpha 1-subunit of the human dihydropyridine-sensitive L-type voltage-dependent

calcium-channel receptor in skeletal muscle. *Am. J. Hum. Genet.* **60**, 1316-1325.

Mori, Y., Friedrich, T., Kim, M.S., Mikami, A., Nakai, J., Ruth, P., Bosse, E., Hofmann, F., Flockerzi, V., and Furuichi, T. (1991b): Primary structure and functional expression from complementary DNA of a brain calcium channel. *Nature* **350**, 398-402.

Mori, Y., Wakamori, M., Oda, S., Fletcher, C.F., Sekiguchi, N., Mori, E., Copeland, N.G., Jenkins, N.A., Matsushita, K., Matsuyama, Z., and Imoto, K. (2000): Reduced voltage sensitivity of activation of P/Q-type Ca2+ channels is associated with the ataxic mouse mutation rolling Nagoya (tg(rol)). *J. Neurosci.* **20**, 5654-5662.

Mukoyama, M. and Mizuno, M. (1976): The cerebellum of the rolling mouse Nagoya. Light- and electromicroscopic observations. *Mod. Med.* **31**, 233-236

Muller, T. and Kettenmann, H. (1995): Physiology of Bergmann glial cells. *Int. Rev. Neurobiol.* **38**, 341-359.

Nagerl, U.V., Novo, D., Mody, I., and Vergara, J.L. (2000a): Binding kinetics of calbindin-D(28k) determined by flash photolysis of caged Ca(2+). *Biophys. J.* **79**, 3009-3018.

Nagerl, U.V., Mody, I., Jeub, M., Lie, A.A., Elger, C.E., and Beck, H. (2000b): Surviving granule cells of the sclerotic human hippocampus have reduced Ca(2+) influx because of a loss of calbindin-D(28k) in temporal lobe epilepsy. *J. Neurosci.* **20**, 1831-1836.

Nakagawa, T., Zhu, H., Morishima, N., Li, E., Xu, J., Yankner, B.A., and Yuan, J. (2000): Caspase-12 mediates endoplasmic-reticulum-specific apoptosis and cytotoxicity by amyloid-beta. *Nature* **403**, 98-103.

Nakai, K. and Horton, P. (1999): PSORT: a program for detecting sorting signals in proteins and predicting their subcellular localization. *Trends in Biochem. Sci.* **24**, 34-35.

Nakayama, N., Kirley, T.L., Vaghy, P.L., McKenna, E., and Schwartz, A. (1987): Purification of putative Ca2+ channel protein from rabbit skeletal muscle. Determination of the amino-terminal sequence. *J. Biol. Chem.* **262**, 6572-6576.

Namura, S., Zhu, J., Fink, K., Endres, M., Srinivasan, A., Tomaselli, K.J., Yuan, J., and Moskowitz, M.A. (1998): Activation and cleavage of caspase-3 in apoptosis induced by experimental cerebral ischemia. *J. Neurosci.* **18**, 3659-3668.

Narahashi, T., Haas, H.G., and Therrien, E.F. (1967): Saxitoxin and tetrodotoxin: comparison of nerve blocking mechanism. *Science* **157**, 1441-1442.

Neher, E. (1998): Vesicle pools and Ca2+ microdomains: new tools for understanding their roles in neurotransmitter release. *Neuron* **20**, 389-399.

Ng, G.Y., Bertrand, S., Sullivan, R., Ethier, N., Wang, J., Yergey, J., Belley, M., Trimble, L., Bateman, K., Alder, L., Smith, A., McKernan, R., Metters, K.,

O'Neill, G.P., Lacaille, J.C., and Hebert, T.E. (2001): Gamma-aminobutyric acid type B receptors with specific heterodimer composition and postsynaptic actions in hippocampal neurons are targets of anticonvulsant gabapentin action. *Mol. Pharmacol.* **59**, 144-152.

Nielsen, H., Engelbrecht, J., Brunak, S., and von Heijne, G. (1997): A neural network method for identification of prokaryotic and eukaryotic signal peptides and prediction of their cleavage sites. *Int. J. Neural. Syst.* **8**, 581-599.

Nijhawan, D., Honarpour, N., and Wang, X. (2000): Apoptosis in neural development and disease. *Annu. Rev. Neurosci.* **23**, 73-87.

Nishimura, K. (1976): Rolling mouse Nagoya. Studies on the pathology of and clinical symptoms associated with cerebellar cortical cells. *Mod. Med.* **31**, 226-236

Noebels, J.L. (1986): Mutational analysis of inherited epilepsies. In: *Basic mechanisms of the epilepsies: molecular and cellular approaches.*, 97-113. Raven Press, New York.

Noebels, J.L. and Sidman, R.L. (1979): Inherited epilepsy: spike-wave and focal motor seizures in the mutant mouse tottering. *Science* **204**, 1334-1336.

Oda, S. (1973): [The observation of rolling mouse Nagoya (rol), a new neurological mutant, and its maintenance (author's transl)]. *Jikken Dobutsu* **22**, 281-288.

Oliet, S.H.R., Piet, R., and Poulain, D.A. (2001): Control of Glutamate Clearance and Synaptic Efficacy by Glial Coverage of Neurons. *Science* **292**, 923-926.

Ophoff, R.A., Terwindt, G.M., Frants, R.R., and Ferrari, M.D. (1998): P/Q-type Ca2+ channel defects in migraine, ataxia and epilepsy. *Trends Pharmacol. Sci.* **19**, 121-127.

Ophoff, R.A., Terwindt, G.M., Vergouwe, M.N., van Eijk, R., Oefner, P.J., Hoffman, S.M., Lamerdin, J.E., Mohrenweiser, H.W., Bulman, D.E., Ferrari, M., Haan, J., Lindhout, D., van Ommen, G.J., Hofker, M.H., Ferrari, M.D., and Frants, R.R. (1996): Familial hemiplegic migraine and episodic ataxia type-2 are caused by mutations in the Ca^{2+} channel gene CACNL1A4. *Cell* **87**, 543-552.

Pan, Z.H. (2001): Voltage-activated Ca2+ channels and ionotropic GABA receptors localized at axon terminals of mammalian retinal bipolar cells. *Vis. Neurosci.* **18**, 279-288.

Parent, L., Schneider, T., Moore, C.P., and Talwar, D. (1997): Subunit regulation of the human brain α_{1E} calcium channel. *J. Membr. Biol.* **160**, 127-140.

Pearson, H.A., Sutton, K.G., Scott, R.H., and Dolphin, A.C. (1995): Characterization of Ca^{2+} channel currents in cultured rat cerebellar granule neurones. *J. Physiol.* **482**, 493-509.

Perez-Reyes, E., Castellano, A., Kim, H.S., Bertrand, P., Baggstrom, E., Lacerda, A.E., Wei, X.Y., and Birnbaumer, L. (1992): Cloning and

expression of a cardiac/brain beta subunit of the L-type calcium channel. *J. Biol. Chem.* **267**, 1792-1797.

Perez-Reyes, E., Cribbs, L.L., Daud, A., Lacerda, A.E., Barclay, J., Williamson, M.P., Fox, M., Rees, M., and Lee, J.-H. (1998): Molecular characterisation of a neuronal low-voltage-activated T type calcium channel. *Nature* **391**, 896-900.

Pinto, A., Gillard, S., Moss, F., Whyte, K., Brust, P., Williams, M., Stauderman, K., Harpold, M., Lang, B., Newsom-Davis, J., Bleakman, D., Lodge, D., and Boot, J. (1998): Human autoantibodies specific for the alpha1A calcium channel subunit reduce both P-type and Q-type calcium currents in cerebellar neurons. *Proc. Natl. Acad. Sci. USA* **95**, 8328-8333.

Plomp, J.J., Vergouwe, M.N., Van den Maagdenberg, A.M., Ferrari, M.D., Frants, R.R., and Molenaar, P.C. (2000): Abnormal transmitter release at neuromuscular junctions of mice carrying the tottering alpha(1A) Ca(2+) channel mutation. *Brain* **123** (Pt 3), 463-471.

Ponting, C.P., Schultz, J., Copley, R.R., Andrade, M.A., and Bork, P. (2000): Evolution of domain families. *Adv. Prot. Chem.* **54**, 185-244.

Pragnell, M., De Waard, M., Mori, Y., Tanabe, T., Snutch, T.P., and Campbell, K.P. (1994): Calcium channel beta-subunit binds to a conserved motif in the I-II cytoplasmic linker of the alpha 1-subunit. *Nature* **368**, 67-70.

Ptacek, L.J., Tawil, R., Griggs, R.C., Engel, A.G., Layzer, R.B., Kwiecinski, H., McManis, P.G., Santiago, L., Moore, M., and Fouad, G. (1994): Dihydropyridine receptor mutations cause hypokalemic periodic paralysis. *Cell* **77**, 863-868.

Qian, J. and Noebels, J.L. (2001): Presynaptic Ca2+ channels and neurotransmitter release at the terminal of a mouse cortical neuron. *J. Neurosci.* **21**, 3721-3728.

Qiao, X., Chen, L., Gao, H., Bao, S., Hefti, F., Thompson, R.F., and Knusel, B. (1998): Cerebellar brain-derived neurotrophic factor-TrkB defect associated with impairment of eyeblink conditioning in Stargazer mutant mice. *J. Neurosci.* **18**, 6990-6999.

Qiao, X., Hefti, F., Knusel, B., and Noebels, J.L. (1996): Selective failure of brain-derived neurotrophic factor mRNA expression in the cerebellum of stargazer, a mutant mouse with ataxia. *J. Neurosci.* **16**, 640-648.

Qin, N., Olcese, R., Stefani, E., and Birnbaumer, L. (1998): Modulation of human neuronal alpha 1E-type calcium channel by alpha 2 delta-subunit. *Am. J. Physiol.* **274**, C1324-C1331

Rakic, P. (1971): Neuron-glia relationship during granule cell migration in developing cerebellar cortex. A Golgi and electronmicroscopic study in Macacus Rhesus. *J. Comp. Neurol.* **141**, 283-312.

Randall, A. and Tsien, R.W. (1995): Pharmacological dissection of multiple types of Ca^{2+} channel currents in rat cerebellar granule neurons. *J. Neurosci.* **15** , 2995-3012.

Randall, A.D. and Tsien, R.W. (1997): Contrasting biophysical and pharmacological properties of T-type and R-type calcium channels. *Neuropharm.* **36**, 879-893.

Restituito, S., Thompson, R.M., Eliet, J., Raike, R.S., Riedl, M., Charnet, P., and Gomez, C.M. (2000): The polyglutamine expansion in spinocerebellar ataxia type 6 causes a beta subunit-specific enhanced activation of P/Q-type calcium channels in Xenopus oocytes. *J. Neurosci.* **20**, 6394-6403.

Rhyu, I.J., Abbott, L.C., Walker, D.B., and Sotelo, C. (1999a): An ultrastructural study of granule cell/Purkinje cell synapses in tottering (tg/tg), leaner (tg(la)/tg(la)) and compound heterozygous tottering/leaner (tg/tg(la)) mice. *Neurosci.* **90**, 717-728.

Rhyu, I.J., Oda, S., Uhm, C.S., Kim, H., Suh, Y.S., and Abbott, L.C. (1999b): Morphologic investigation of rolling mouse Nagoya (tg(rol)/tg(rol)) cerebellar Purkinje cells: an ataxic mutant, revisited. *Neurosci. Lett.* **266**, 49-52.

Ridet, J.L., Malhotra, S.K., Privat, A., and Gage, F.H. (1997): Reactive astrocytes: cellular and molecular cues to biological function. *Trends Neurosci.* **20**, 570-577.

Rios, E., Pizarro, G., and Stefani, E. (1992): Charge movement and the nature of signal transduction in skeletal muscle excitation-contraction coupling. *Annu. Rev. Physiol.* **54**, 109-133.

Rock, D.M., Kelly, K.M., and Macdonald, R.L. (1993): Gabapentin actions on ligand- and voltage-gated responses in cultured rodent neurons. *Epilepsy Res.* **16**, 89-98.

Ruth, P., Rohrkasten, A., Biel, M., Bosse, E., Regulla, S., Meyer, H.E., Flockerzi, V., and Hofmann, F. (1989): Primary structure of the beta subunit of the DHP-sensitive calcium channel from skeletal muscle. *Science* **245**, 1115-1118.

Sadler, M. and Berry, M. (1983): Morphometric study of the development of Purkinje cell dendritic trees in the mouse using vertex analysis. *J. Microsc.* **131** (Pt 3), 341-354.

Sakurai, M. (1990) Calcium is an intracellular mediator of the climbing fiber in induction of cerebellar long-term depression. *Proc. Natl. Acad. Sci. USA* **87**, 3383-3385.

Sastry, P.S. and Rao, K.S. (2000): Apoptosis and the nervous system. *J. Neurochem.* **74**, 1-20.

Schafer, W.R. and Kenyon, C.J. (1995): A calcium-channel homologue required for adaptation to dopamine and serotonin in Caenorhabditis elegans. *Nature* **375**, 73-78.

Schmitz, Y. and Witkovsky, P. (1997): Dependence of photoreceptor glutamate release on a dihydropyridine-sensitive calcium channel. *Neurosci.* **78**, 1209-1216.

Schneider, T., Wei, X., Olcese, R., Costantin, J.L., Neely, A., Palade, P., Perez-Reyes, E., Qin, N., Zhou, J., and Crawford, G.D. (1994): Molecular

analysis and functional expression of the human type E neuronal Ca2+ channel alpha 1 subunit. *Receptors Channels* **2** , 255-270.

Schultz, J., Copley, R.R., Doerks, T., Ponting, C.P., and Bork, P. (2000): SMART: a web-based tool for the study of genetically mobile domains. *Nucleic Acids Res.* **28**, 231-234.

Schumacher, T.B., Beck, H., Steinhauser, C., Schramm, J., and Elger, C.E. (1998): Effects of phenytoin, carbamazepine, and gabapentin on calcium channels in hippocampal granule cells from patients with temporal lobe epilepsy. *Epilepsia* **39**, 355-363.

Scott, V.E., Felix, R., Arikkath, J., and Campbell, K.P. (1998): Evidence for a 95 kDa short form of the alpha1A subunit associated with the omega-conotoxin MVIIC receptor of the P/Q-type Ca2+ channels. *J. Neurosci.* **18**, 641-647.

Seino, S., Chen, L., Seino, M., Blondel, O., Takeda, J., Johnson, J.H., and Bell, G.I. (1992): Cloning of the α_1 subunit of a voltage-dependent calcium channel expressed in pancreatic β cells. *Proc. Natl. Acad. Sci. USA* **89**, 584-588.

Shepherd, G.M. (1988): Neurobiology. *Oxford Univ. Press* Sec. Edit.

Sherman, M.Y. and Goldberg, A.L. (2001): Cellular defenses against unfolded proteins: a cell biologist thinks about neurodegenerative diseases. *Neuron* **29**, 15-32.

Shirokov, R., Ferreira, G., Yi, J.X., and Ríos, E. (1998): Inactivation of gating currents of L-type calcium channels - Specific role of the $\alpha_2\delta$ subunit. *J. Gen. Physiol.* **111**, 807-823.

Shistik, E., Ivanina, T., Puri, T., Hosey, M., and Dascal, N. (1995): Ca^{2+} current enhancement by α2/δ and β subunits in *Xenopus* oocytes: Contribution of changes in channel gating and α1 protein level. *J. Physiol.* **489**, 55-62.

Simmons, M.L., Terman, G.W., Gibbs, S.M., and Chavkin, C. (1995): L-type calcium channels mediate dynorphin neuropeptide release from dendrites but not axons of hippocampal granule cells. *Neuron* **14**, 1265-1272.

Simpson, P.B., Nahorski, S.R., and Challiss, R.A. (1996): Agonist-evoked Ca2+ mobilization from stores expressing inositol 1,4,5-trisphosphate receptors and ryanodine receptors in cerebellar granule neurones. *J. Neurochem.* **67**, 364-373.

Singer, D., Biel, M., Lotan, I., Flockerzi, V., Hofmann, F., and Dascal, N. (1991a): The roles of the subunits in the function of the calcium channel. *Science* **253**, 1553-1557.

Singh, L., Field, M.J., Ferris, P., Hunter, J.C., Oles, R.J., Williams, R.G., and Woodruff, G.N. (1996): The antiepileptic agent gabapentin (Neurontin) possesses anxiolytic-like and antinociceptive actions that are reversed by D-serine. *Psychopharm. (Berl)* **127**, 1-9.

Snead, O.C., III (1992): Evidence for $GABA_B$-mediated mechanisms in experimental generalized absence seizures. *Eur. J. Pharmacol.* **213**, 343-349.

Snell, G.D. (1955): Ducky, a new second chromosome mutation in the mouse. *J. Hered.* **46**, 27-29.

Song, I., Kim, D., Jun, K., Shin, H.-S. (2001): Role of T-type calcium channels in the genesis of absence seizures in mutant mice for α_{1A}, the pore-forming subuinit of the P/Q-type calcium channel. Ann.Meet. Soc. Neurosci. Abstr.

Soong, T.W., Stea, A., Hodson, C.D., Dubel, S.J., Vincent, S.R., and Snutch, T.P. (1993): Structure and functional expression of a member of the low voltage-activated calcium channel family. *Science* **260**, 1133-1136.

Sotelo, C. (1975): Anatomical, physiological and biochemical studies of the cerebellum from mutant mice. II. Morphological study of cerebellar cortical neurons and circuits in the weaver mouse. *Brain Res.* **94**, 19-44.

Sotelo, C. (1990) Axonal abnormalities in cerebellar Purkinje cells of the 'hyperspiny Purkinje cell' mutant mouse. *J. Neurocytol.* **19**, 737-755.

Starr, T.V., Prystay, W., and Snutch, T.P. (1991): Primary structure of a calcium channel that is highly expressed in the rat cerebellum. *Proc. Natl. Acad. Sci. USA* **88**, 5621-5625.

Stea, A., Tomlinson, W.J., Soong, T.W., Bourinet, E., Dubel, S.J., Vincent, S.R., and Snutch, T.P. (1994): Localization and functional properties of a rat brain alpha 1A calcium channel reflect similarities to neuronal Q- and P-type channels. *Proc. Natl. Acad. Sci. USA* **91**, 10576-10580.

Stefani, A., Spadoni, F., and Bernardi, G. (1998): Gabapentin inhibits calcium currents in isolated rat brain neurons. *Neuropharm.* **37**, 83-91.

Stefani, A., Spadoni, F., Giacomini, P., Lavaroni, F., and Bernardi, G. (2001): The effects of gabapentin on different ligand- and voltage-gated currents in isolated cortical neurons. *Epilepsy Res.* **43**, 239-248.

Stephens, G.J., Page, K.M., Burley, J.R., Berrow, N.S., and Dolphin, A.C. (1997): Functional expression of rat brain cloned α1E calcium channels in COS-7 cells. *Pflügers Arch.* **433**, 523-532.

Steriade, M. and Contreras, D. (1998): Spike-wave complexes and fast components of cortically generated seizures. I. Role of neocortex and thalamus. *J. Neurophysiol.* **80**, 1439-1455.

Steriade, M., McCormick, D.A., and Sejnowski, T.J. (1993): Thalamocortical oscillations in the sleeping and aroused brain. *Science* **262**, 679-685.

Steward, O., Kelley, M.S., and Schauwecker, P.E. (1997): Signals that regulate astroglial gene expression: induction of GFAP mRNA following seizures or injury is blocked by protein synthesis inhibitors. *Exp. Neurol.* **148**, 100-109.

Stone, T.W. (2000): Development and therapeutic potential of kynurenic acid and kynurenine derivatives for neuroprotection. *Trends Pharmacol. Sci.* **21**, 149-154.

Strom, T.M., Nyakatura, G., Apfelstedt-Sylla, E., Hellebrand, H., Lorenz, B., Weber, B.H., Wutz, K., Gutwillinger, N., Ruther, K., Drescher, B., Sauer, C., Zrenner, E., Meitinger, T., Rosenthal, A., and Meindl, A. (1998): An L-

type calcium-channel gene mutated in incomplete X-linked congenital stationary night blindness. *Nat. Genet.* **19**, 260-263.

Stuart, G. and Hausser, M. (1994): Initiation and spread of sodium action potentials in cerebellar Purkinje cells. *Neuron* **13**, 703-712.

Stuart, G.J., Dodt, H.U., and Sakmann, B. (1993): Patch-clamp recordings from the soma and dendrites of neurons in brain slices using infrared video microscopy. *Pflugers Arch.* **423**, 511-518.

Sutton, K.G., McRory, J.E., Guthrie, H., Murphy, T.H., and Snutch, T.P. (1999): P/Q-type calcium channels mediate the activity-dependent feedback of syntaxin-1A. *Nature* **401**, 800-804.

Swick, A.G., Janicot, M., Cheneval-Kastelic, T., McLenithan, J.C., and Lane, M.D. (1992): Promoter-cDNA-directed heterologous protein expression in Xenopus laevis oocytes. *Proc. Natl. Acad. Sci. USA* **89**, 1812-1816.

Takahashi, T. and Momiyama, A. (1993): Different types of calcium channels mediate central synaptic transmission. *Nature* **366**, 156-158.

Talley, E.M., Cribbs, L.L., Lee, J.H., Daud, A., Perez-Reyes, E., and Bayliss, D.A. (1999): Differential distribution of three members of a gene family encoding low voltage-activated (T-type) calcium channels. *J. Neurosci.* **19**, 1895-1911.

Tareilus, E., Roux, M., Qin, N., Olcese, R., Zhou, J.M., Stefani, E., and Birnbaumer, L. (1997): A *Xenopus* oocyte β subunit: Evidence for a role in the assembly/expression of voltage-gated calcium channels that is separate from its role as a regulatory subunit. *Proc. Natl. Acad. Sci.USA* **94**, 1703-1708.

Taylor, C.P., Gee, N.S., Su, T.Z., Kocsis, J.D., Welty, D.F., Brown, J.P., Dooley, D.J., Boden, P., and Singh, L. (1998): A summary of mechanistic hypotheses of gabapentin pharmacology. *Epilepsy Res.* **29**, 233-249.

Thompson, C.L., Tehrani, M.H., Barnes, E.M.J., and Stephenson, F.A. (1998): Decreased expression of GABAA receptor alpha6 and beta3 subunits in stargazer mutant mice: a possible role for brain-derived neurotrophic factor in the regulation of cerebellar GABAA receptor expression? *Brain Res. Mol. Brain Res.* **60**, 282-290.

Thornberry, N.A. and Lazebnik, Y. (1998): Caspases: enemies within. *Science* **281**, 1312-1316.

Toru, S., Murakoshi, T., Ishikawa, K., Saegusa, H., Fujigasaki, H., Uchihara, T., Nagayama, S., Osanai, M., Mizusawa, H., and Tanabe, T. (2000): Spinocerebellar ataxia type 6 mutation alters P-type calcium channel function. *J. Biol. Chem.* **275**, 10893-10898.

Touri, F., Hawkes, R., and Riederer, B.M. (1996): Differential distribution of MAP1a and aldolase c in adult mouse cerebellum. *Eur. J. Neurosci.* **8**, 61-68.

Tse, A., Tse, F.W., Almers, W., and Hille, B. (1993): Rhythmic exocytosis stimulated by GnRH-induced calcium oscillations in rat gonadotropes. *Science* **260**, 82-84.

Tsien, R.Y. (1998): The Green Fluorescent Protein. *Annu. Rev. Biochem.* **67**, 509-544.

Ullian, E.M., Sapperstein, S.K., Christopherson, K.S., and Barres, B.A. (2001): Control of Synapse Number by Glia. *Science* **291**, 657-661.

Wakamori, M., Yamazaki, K., Matsunodaira, H., Teramoto, T., Tanaka, I., Niidome, T., Sawada, K., Nishizawa, Y., Sekiguchi, N., Mori, E., Mori, Y., and Imoto, K. (1998): Single tottering mutations responsible for the neuropathic phenotype of the P-type calcium channel. *J. Biol. Chem.* **273**, 34857-34867.

Walker, D., Bichet, D., Campbell, K.P., and De Waard, M. (1998): A beta 4 isoform-specific interaction site in the carboxyl-terminal region of the voltage-dependent Ca2+ channel alpha 1A subunit. *J. Biol. Chem.* **273**, 2361-2367.

Walker, D. and De Waard, M. (1998): Subunit interaction sites in voltage-dependent Ca2+ channels: role in channel function. *Trends in Neurosci.* **21**, 148-154.

Wang, M., Offord, J., Oxender, D.L., and Su, T.Z. (1999): Structural requirement of the calcium-channel subunit alpha2delta for gabapentin binding. *Biochem. J.* **342** (Pt 2), 313-320.

Wang, X., Zelenski, N.G., Yang, J., Sakai, J., Brown, M.S., and Goldstein, J.L. (1996): Cleavage of sterol regulatory element binding proteins (SREBPs) by CPP32 during apoptosis. *EMBO J.* **15**, 1012-1020.

Weiss, G.M. and Pysh, J.J. (1978): Evidence for loss of Purkinje cell dendrites during late development: a morphometric Golgi analysis in the mouse. *Brain Res.* **154**, 219-230.

Welling, A., Bosse, E., Cavalie, A., Bottlender, R., Ludwig, A., Nastainczyk, W., Flockerzi, V., and Hofmann, F. (1993): Stable co-expression of calcium channel α, β and α_2/δ subunits in a somatic cell line. *J. Physiol.* **471**, 749-765.

Westenbroek, R.E., Hell, J.W., Warner, C., Dubel, S.J., Snutch, T.P., and Catterall, W.A. (1992): Biochemical properties and subcellular distribution of an N-type calcium channel alpha 1 subunit. *Neuron* **9**, 1099-1115.

Westenbroek, R.E., Sakurai, T., Elliott, E.M., Hell, J.W., Starr, T.V.B., Snutch, T.P., and Catterall, W.A. (1995): Immunochemical identification and subcellular distribution of the α_{1A} subunits of brain calcium channels. *J. Neurosci.* **15**, 6403-6418.

Wheeler, D.B., Randall, A., and Tsien, R.W. (1996): Changes in action potential duration alter reliance of excitatory synaptic transmission on multiple types of Ca2+ channels in rat hippocampus. *J. Neurosci.* **16**, 2226-2237.

White, W.F., Nadler, J.V., and Cotman, C.W. (1979): The effect of acidic amino acid antagonists on synaptic transmission in the hippocampal formation in vitro. *Brain Res.* **164**, 177-194.

Williams, M.E., Marubio, L.M., Deal, C.R., Hans, M., Brust, P.F., Philipson, L.H., Miller, R.J., Johnson, E.C., Harpold, M.M., and Ellis, S.B. (1994):

Structure and functional characterization of neuronal alpha 1E calcium channel subtypes. *J. Biol. Chem.* **269**, 22347-22357.

Williams, M.E., Washburn, M.S., Hans, M., Urrutia, A., Brust, P.F., Prodanovich, P., Harpold, M.M., and Stauderman, K.A. (1999): Structure and functional characterization of a novel human low-voltage activated calcium channel. *J. Neurochem.* **72**, 791-799.

Witcher, D.R., De Waard, M., Sakamoto, J., Franzini-Armstrong, C., Pragnell, M., Kahl, S.D., and Campbell, K.P. (1993): Subunit identification and reconstitution of the N-type Ca2+ channel complex purified from brain. *Science* **261**, 486-489.

Yamada, K., Fukaya, M., Shibata, T., Kurihara, H., Tanaka, K., Inoue, Y., and Watanabe, M. (2000): Dynamic transformation of Bergmann glial fibers proceeds in correlation with dendritic outgrowth and synapse formation of cerebellar Purkinje cells. *J. Comp. Neurol.* **418**, 106-120.

Yang, Q., Hashizume, Y., Yoshida, M., Wang, Y., Goto, Y., Mitsuma, N., Ishikawa, K., and Mizusawa, H. (2000): Morphological Purkinje cell changes in spinocerebellar ataxia type 6. *Acta Neuropathol. (Berl)* **100**, 371-376.

Yang, S.N., Larsson, O., Branstrom, R., Bertorello, A.M., Leibiger, B., Leibiger, I.B., Moede, T., Kohler, M., Meister, B., and Berggren, P.O. (1999): Syntaxin 1 interacts with the LD subtype of voltage-gated Ca2+ channels in pancreatic beta cells. *Proc. Natl. Acad. Sci. USA* **96**, 10164-10169.

Yano, S., Tokumitsu, H., and Soderling, T.R. (1998): Calcium promotes cell survival through CaM-K kinase activation of the protein-kinase-B pathway. *Nature* **396**, 584-587.

Yuan, J. and Yankner, B.A. (1999): Caspase activity sows the seeds of neuronal death. *Nat. Cell Biol.* **1**, E44-E45

Yue, Q., Jen, J.C., Nelson, S.F., and Baloh, R.W. (1997): Progressive ataxia due to a missense mutation in a calcium- channel gene. *Am. J. Hum. Genet.* **61**, 1078-1087.

Yue, Q., Jen, J.C., Thwe, M.M., Nelson, S.F., and Baloh, R.W. (1998): De novo mutation in CACNA1A caused acetazolamide-responsive episodic ataxia. *Am. J. Med. Genet.* **77**, 298-301.

Zamponi, G.W., Bourinet, E., Nelson, D., Nargeot, J., and Snutch, T.P. (1997): Crosstalk between G proteins and protein kinase C mediated by the calcium channel alpha1 subunit. *Nature* **385**, 442-446.

Zhuchenko, O., Bailey, J., Bonnen, P., Ashizawa, T., Stockton, D.W., Amos, C., Dobyns, W.B., Subramony, S.H., Zoghbi, H.Y., and Lee, C.C. (1997): Autosomal dominant cerebellar ataxia (SCA6) associated with small polyglutamine expansions in the alpha 1A-voltage-dependent calcium channel. *Nature Genet.* **15**, 62-69.

Zwingman, T.A., Neumann, P.E., Noebels, J.L., and Herrup, K. (2001): Rocker is a new variant of the voltage-dependent calcium channel gene Cacna1a. *J. Neurosci.* **21**, 1169-1178.

The ducky mutation in *Cacna2d2* results in altered Purkinje cell morphology and is associated with the expression of a truncated α2δ-2 protein with abnormal function

Jens Brodbeck, Anthony Davies, Jo-Maree Courtney, Alon Meir[°], Nuria Balaguero, Carles Canti, Fraser J. Moss, Karen M. Page, Wendy S. Pratt, Steven P. Hunt[†], Jane Barclay[*%], Michele Rees[*] and Annette C. Dolphin

Departments of Pharmacology and [†]Anatomy and Developmental Biology, University College London, Gower Street, London, WC1E 6BT, UK and [*]Department of Paediatrics and Child Health, Royal Free & University College Medical School, The Rayne Institute, 5 University Street, London, WC1E 6JJ, UK

Current address: [%] Novartis Institute for Medical Sciences, 5 Gower Place, London, WC1E 6BS, UK; [°] Alomone Laboratories, Jerusalem, Israel.

Correspondence: Annette C. Dolphin, Department of Pharmacology, University College London, Gower Street, London, WC1E 6BT, UK

a.dolphin@ucl.ac.uk Tel: +44-20-7679 3054 Fax: +44-20-7813 2808

Running Title: Truncated α2δ-2 in ducky mice

Summary

The mouse mutant ducky, a model for absence epilepsy, is characterized by spike-wave seizures, and cerebellar ataxia. A mutation in *Cacna2d2*, the gene encoding the α2δ-2 voltage-dependent calcium channel accessory subunit has been found to underlie the ducky phenotype. The α2δ-2 mRNA is strongly expressed in cerebellar Purkinje cells. Here we show that *du/du* mice have abnormalities in their Purkinje cell dendritic tree. The mutation in α2δ-2 results in the introduction of a premature stop codon and predicts the expression of a truncated protein encoded by the first three exons of *Cacna2d2*, followed by 8 novel amino acids. We show that both mRNA and protein corresponding to this predicted transcript are expressed in *du/du* cerebellum, and present in Purkinje cells. Whereas the α2δ-2 subunit increased the peak current density of the $Ca_V2.1/\beta4$ channel combination when co-expressed *in vitro*, co-expression with the truncated mutant α2δ-2 protein reduced current density, indicating that it may contribute to the *du* phenotype.

Key words calcium channel, mouse mutant, α2δ subunit, truncation, mutation

Introduction

Voltage-gated Ca^{2+} (Ca_V) channels have been divided functionally into L-, N-, P/Q-, R- and T-types (1). Each Ca_V channel is composed of a pore-forming α1 subunit, associated at least in the case of the Ca_V1 and 2 subfamilies with an intracellular β subunit responsible for trafficking (2), and a membrane-anchored, but predominantly extracellular, α2δ subunit, whose function is less well-defined (2). $Ca_V1.1$ (α1S) is also associated with a γ subunit (γ1), and this may be true for other Ca_V channels (3), although the neuronal γ subunits may also subserve other functions (4). The α1 subunit determines the main biophysical properties of the channel and is modulated by the other subunits (2). Mammalian genes encoding ten α1, four β, eight γ and three α2δ subunits have been identified (1, 5, 6).

A number of spontaneous autosomal recessive mutant mouse strains have now been identified, involving mutations in each of the four different subunits that together compose a voltage-dependent calcium channel. They all have a similar phenotype that includes cerebellar ataxia and spike-wave seizures. Tottering (*Cacna1a*^{tg}) has a point mutation in $Ca_V2.1$ (α1A) (7), and a number of alleles of this mutant have now been identified, as summarized recently (8). Lethargic (*Cacnb4*^{lh}) represents a truncation mutation of the β4 subunit (9). Stargazer (*Cacng2*^{stg}) has a truncation mutation in the γ2 subunit (3), although its role as a calcium channel subunit remains controversial (4), (10, 11). Finally, the two ducky alleles (*Cacna2d2*^{du}, *Cacna2d2*^{du2J}) both predict truncation mutations in the α2δ-2 subunit (12).

Homozygotes for the ducky (*du*) allele are characterized by ataxia and paroxysmal dyskinesia (13). The cerebellum is reduced in size (14), but we have previously found no loss of Purkinje cell (PC) bodies at post-natal day (P) 21 (12). In this study we observed a reduction in calcium channel current in P21 PCs isolated from du/du compared to +/+

cerebella (12). The present study provides evidence that the *du* mutation results in the persistence of PCs with an immature and grossly abnormal morphology, including multiple primary dendrites and a reduction in the size of the PC dendritic tree. This is associated with loss of full-length α2δ-2 protein and expression of a truncated mutant α2δ-2 protein with aberrant function.

Experimental procedures

Construction of du-mut1 α2: The *du* mutant 1 construct (*du*-mut1 α2) was assembled by PCR (Platinum Pfx polymerase; Gibco Life Technologies, Paisley, UK) of *du/du* total brain cDNA using primers corresponding to the cDNA sequence (Genbank AF247140) containing engineered *Sma*I or *Spe*I restriction sites. The primer sequences are F: 5' - TTG(CCCGGG)GAACATGGCGGTGCCCGGCT-3' and R: 5' - TCT(CAGGTC)AGAGTAACCAGAGACCAA-3', with the recognition sites indicated in parentheses. The PCR product was digested with *Sma*I and *Spe*I and ligated into the corresponding sites of a modified pMT2 vector (Genetics Institute, Cambridge, MA). Insert sequence fidelity was determined by automated sequencing (PE Biosystems, Warrington, UK).

Genotyping: Mice were obtained from The Jackson Laboratory (Bar Harbor, ME), and a colony established, as described previously (12). RNA was extracted from samples of mouse brain tissue using RNeasy Mini Kit and QIAshredder (Qiagen Ltd. Crawley, West Sussex, UK). RNA was reverse transcribed using Moloney murine Leukemia virus Reverse Transcriptase (Promega, Southampton, UK) with 0.6 units.ml^{-1} RNasin Ribonuclease Inhibitor (Promega) and 25 ng.µl^{-1} Random Hexamers (Promega). PCR reactions were carried out with primers 49F: 5'-ACGCCCGCTCTTGCTCTTGCT-3' and 11R: 5'-CCTCCAAAAATCCGCATCAC-3' which produce a 156 bp product from both the wild-type and *du* alleles of the *Cacna2d2* transcript. Primers 49F and 50R: 5'-TCAGCCTTGGCATCGTAGTA-3' produce a 387 bp product from the wild-type allele only. Primers 20F: 5'-GCCGCATCTTGAATGGAAAC-3' and 86R: 5'-CAGAGACCAATGAGACTGGA-3' produce a 456bp product from the *du* allele only.

DNA was extracted by incubating 2 mm tail-snip tissue in 75µl of 25 mM NaOH, 0.2 mM Na_2EDTA at 95°C for 30 min followed by cooling to 4°C and addition of 75µl of 40 mM

Tris-HCl. 5µl of the resultant solution was amplified in the PCR reactions. Primers 98F: 5'-ACCTATCAGGCAAAAGGACG-3' and 120R: 5'-AGGGATGGTGATTGGTTGGA-3' produce a fragment of 541bp from a region which is duplicated in the *du* allele. Digestion with *Bsp*HI results in two fragments of 286bp and 273bp from the *du* allele while the wild-type allele remains uncut. Wild-type mice can be identified by the presence of a single band upon agarose gel electrophoresis. Heterozygous and *du/du* mice each show two bands and can by distinguished on the basis of their relative intensities.

Lucifer yellow/neurobiotin injection and quantification: P21 - P26 mice were asphyxiated with CO_2, and the cerebella were sliced parasagittaly at 400 µm in artificial cerebrospinal fluid (in mM: 125 NaCl, 25 $NaHCO_3$, 25 glucose, 2.5 KCl, 1.25 NaH_2PO_4, 2 $CaCl_2$, 1 $MgCl_2$, saturated with 95 % O_2 / 5% CO_2 at 4°C) using a vibratome (Campden Instruments, London, UK). Dendrites and somata of PCs were visualized by infrared differential interference contrast videomicroscopy (15). Glass microelectrodes (outer tip diameter 0.3 µm) were filled with an aqueous solution of 10% lucifer yellow Li salt (Sigma, Poole, UK) and 10% neurobiotin (Vector Laboratories Inc., Burlingame, CA), and backfilled with 1M LiCl. Dye was injected iontophoretically into PC somata, by alternating the current repeatedly from – 40 nA to + 40 nA over 5 min. The tissue slices were then fixed for 1hr in 4% paraformaldehyde, immunostained for neurobiotin with Texas-red-coupled streptavidin (Molecular Probes, Eugene, OR, 25 $\mu g.ml^{-1}$ for 1 h), and viewed by confocal microcopy.Four cells of two genotypes (+/+ and *du/du*) were scanned using identical parameters. Selected fields were optically sectioned using 1 µm steps. The entire z-series was projected as a single composite image by superimposition. The final image was thresholded to form a binary image for analysis by NIH Image J software version1.62. Following skeletonization, the dendritic tree was contained in a minimal rectangle, and the number of dendrites were counted crossing a horizontal and diagonal

line. Branchpoints were determined from the soma to the end of the three longest dendrites for each cell.

Golgi-Cox staining: P24 mice were asphyxiated with CO_2, their brains were removed from the cranium, immediately immersed in 20 ml fixative (34 mM $K_2Cr_2O_7$, 37 mM $HgCl_2$, and 23 mM K_2CrO_4), and left undisturbed for 12 weeks in the dark at 4°C. Vibratome sections (100 µm) were developed for 20 min in a 5% Na_2SO_3 solution, before being mounted on microscope slides and coverslipped with Vectashield (Vector Labs). Slides were viewed on a Leica microscope using 64 x magnification. Image sections were grabbed through an attached CCD camera, using Vision Explorer software (Alliance Vision, Mirmande, France), enabling the deconvolution and projection of different optical planes.

In situ hybridization and immunohistochemistry: Mice (aged P21 - P24) were anesthetized by CO_2 inhalation or pentobarbitone injection (200 $mg.kg^{-1}$, i.p.) and perfused intracardially with 4% paraformaldehyde in phosphate-buffered saline (PBS). The brain was placed in 4% paraformaldehyde at 4°C for 3 h, then transferred into 30% sucrose overnight, before embedding in Cry-M-Bed (Bright Instrument Ltd, Huntingdon, UK) and sectioning. Alternatively, the brain was removed without fixation and frozen in liquid nitrogen. 10 - 25 µm cryostat sections were cut and air-dried onto positively-charged slides (Merck Ltd., Poole, UK).

A cDNA fragment corresponding to *Cacna2d2* 5' (nt 206 - 620, using the numbering system from Genbank AF247139) was subcloned into pBluescript SK+(Stratagene, La Jolla, CA). Sense and anti-sense RNA probes were prepared using T3 or T7 polymerase and Digoxigenin RNA labeling mix, and purified using Quickspin columns (Roche Diagnostics Ltd, Lewes, UK). *In situ* hybridization was carried out as described (16).

Two polyclonal antipeptide antibodies were raised in rabbits to amino acids 16 - 29 and 102 - 117 of α2δ-2. Neither of the peptides used as antigens showed any homology with other protein sequences in the database. They were purified by affinity chromatography using the immobilized synthetic peptide, and stored at 0.5 $mg.ml^{-1}$ in PBS, pH 7.2, at -20°C. For immunohistochemistry of α2δ-2, 25 µm sections were incubated overnight with primary antibody at 4 °C (1.25 $\mu g.ml^{-1}$). This was followed by a biotinylated anti-rabbit IgG secondary antibody (Sigma, 7.2 $\mu g.ml^{-1}$), and a Texas Red-streptavidin conjugate (2 $\mu g.ml^{-1}$). Some tissue sections or cells were also incubated for 1 min with the nuclear dye 4',6-diamidino-2-phenylindole (DAPI, 300 nM, Molecular Probes). They were examined by laser scanning confocal microscopy, using 1 µm optical sections. For peptide controls the appropriately diluted antibody was incubated for 1 hour at 37°C with a 10x higher concentration (w/v) of the immunizing peptide, before applying it to sections. *Transfection of COS-7 cells:* Transfection was performed with Geneporter transfection reagent (Gene Therapy Systems, San Diego, CA). Cells were plated onto coverslips or dishes, 2-3 h prior to transfection. The DNA and Geneporter reagent (6 µg and 30 µl respectively) were each diluted in 500 µl of serum-free medium, mixed, and applied to the cells. After 3.5 h, 1 ml of medium containing 20% serum was added to the cells, which were then incubated at 37°C for 3 - 4 days. For electrophysiological recordings, cells were re-plated 1-6 h prior to use.

Immunocytochemistry on COS-7 cells: The method used is essentially as previously described (17). Cells were fixed with 4% paraformaldehyde in PBS for 15 min at room temperature. For permeabilization, cells were incubated twice for 7 min in a 0.02% solution of Triton X-100 in Tris-buffered saline (TBS), otherwise cells were washed twice with TBS for the same time period. The primary antibodies were used at 1.25 $\mu g.ml^{-1}$. The biotinylated anti-rabbit IgG secondary antibody (7.2 $\mu g.ml^{-1}$) was then incubated for 2 h at

4°C, followed by streptavidin-Texas Red (2 $\mu g.ml^{-1}$). Cells were then incubated for 1 min with DAPI (300 nM) .

Preparation of whole COS-7 cell lysates: COS-7 cells were transfected with either α2δ-2 or *du*-mut1 α2 as described above. On day 4 post-transfection, the cells were resuspended in detergent-free Buffer A. Samples (2 mg total protein) were then solubilized in Buffer A containing 1% CHAPS for immunoaffinity purification of α2δ-2 as described below.

Preparation of cerebellar tissue homogenate: Cerebella, stored at -80°C, were thawed in ice-cold buffer A (10 mM Hepes pH 7.4, 150 mM NaCl, 2 mM EDTA and a protease inhibitors (Complete EDTA free, Roche, 1 tablet / 50 ml buffer)), plus 150 mM sucrose. The tissue was homogenized and the homogenate centrifuged at 5000 x *g* for 10 min at 4°C. The resultant supernatant was diluted x 4 with buffer A, prior to detergent treatment. The protein concentration of samples was determined using either the bicinchoninic acid (BCA) assay (Perbio, Tattenhall, UK) in the presence of 0.5% sodium dodecyl sulfate (SDS), or where the samples were in SDS-polyacrylamide gel electrophoresis (PAGE) buffer, by a modified filter paper dye-binding assay (18).

Immunoaffinity purification of α2δ-2 and du-mut1 α2: Affinity-purified Ab (16-29) or Ab (102-117) (2 mg) were covalently coupled to a 1 ml column of Sepharose-NHS (Pharmacia) according to manufacturers' instructions. The efficiency of coupling was assessed by SDS-PAGE. The columns were pre-washed with 200 mM glycine-HCl, pH 2.4 and neutralized before first use to ensure complete removal of any residual unbound IgG. Control columns contained 2mg of protein A-sepharose-isolated IgG from the corresponding pre-immune rabbit sera. COS-7 cells transfected with either α2δ-2 or *du*-mut1 α2 (2 mg total protein), or cerebellar homogenate (+/+ or *du/du*, 6-20 mg total protein) were solubilized in Buffer A (see above) containing 1% (w/v) CHAPS and placed

on ice for 30 min following sonication for 3 x 10 s. The detergent extracts were cleared by centrifugation (48,000 x *g*, 20 min, 4°C) and then applied to the relevant antibody or control IgG columns which had been pre-equilibrated with Buffer A containing 0.5% CHAPS. The lysates were recirculated through the columns using two opposing syringes for 60 min at 4°C. Unbound material was washed from the columns in Buffer A containing 0.5% CHAPS and then Buffer A + 0.1% CHAPS. Bound proteins were eluted with 200mM glycine-HCl, pH 2.4 and then concentrated for SDS-PAGE and Western blot analysis by precipitation with 10% trichloroacetic acid followed by centrifugation (30,000 x *g*, 30 min, 4°C). Samples of the precipitated proteins were separated on either 10% or 4-20% gradient gels under reducing conditions and then electrophoretically transferred to PVDF membranes for immunodetection. The PVDF membranes were blocked with 3% BSA for 3 hours at 55°C, and incubated overnight with a 1:1000 dilution of either Ab (16-29) or Ab (102-117) followed by a 1:1000 dilution of goat anti-rabbit IgG-horseradish peroxidase conjugate (BioRad Laboratories, Hemel Hempstead, UK) for 1 hour at 20°C and detected using enhanced chemiluminescence (ECL, Amersham Pharmacia Biotech, Little Chalfont, UK). The antibody and control IgG columns were neutralized and washed with 50 mM Tris, pH 7.4, 1M NaCl and 0.02% Na azide and stored in PBS, pH 7.2 with 0.02 % Na azide at 4°C.

Heterologous expression of cDNAs and electrophysiology: Calcium channel expression in COS-7 cells was investigated by whole cell patch clamp recording, essentially as described previously (19), by transfection of rat $Ca_V2.1$ (M64373) E1686R (20), in conjunction with rat β4 (LO2315) and mouse α2δ-2 (AF247139, common brain splice variant, lacking exon 23 and 6 bp of exon 38 (21)) or *du*-mut1 α2 (AF247140) cDNAs cloned into the pMT2 vector. The cDNA for green fluorescent protein (mut3 GFP) (22) was included in the transfection to identify transfected cells from which recordings were made. Transfection was performed as described above, using the ratios for α1, β, α2δ

and GFP of 3 : 1 : 1 : 0.1. In the single channel experiments cDNA for βARK1 Gβγ binding domain was included in the transfections, at the same concentration as the β subunit cDNA (23). For expression in *Xenopus* oocytes, cDNAs encoding rabbit $Ca_V2.1$ (X57689), rat β4 and mouse α2δ-2 or *du*-mut1 α2 cDNAs, were injected intranuclearly as described previously (24), except that 4 nl of the 1:1:1 ratio cDNA mixture was injected at 1 $\mu g.\mu l^{-1}$. In control experiments where α2δ-2 was omitted, the ratio was made up with buffer. Recordings were made using two electrode voltage clamp as described previously (24), using 10 mM Ba^{2+} as charge carrier. Individual I-V relationships were fitted with a modified Boltzmann equation:

$$I = G_{max}(V-V_{rev})/(1+\exp[-(V-V_{50})/k]),$$

where G_{max} is the maximum conductance; V_{rev} is the reversal potential; k is the slope factor and V_{50} is the voltage for 50% current activation.

Single channel recording and analysis: All recordings were taken from cell-attached patches on GFP-positive cells at room temperature (20 - 22°C). Recording pipettes were pulled from borosilicate tubes (World Precision Instruments, Inc., Sarasota, FL, USA), coated with Sylgard (Sylgard 184, Dow Corning, Wiesbaden, Germany), and fire polished to form high resistance pipettes (~10 MΩ with 100 mM $BaCl_2$). The bath solution, designed to zero the resting membrane potential (25) was composed of (in mM): 135 K-aspartate, 1 $MgCl_2$, 5 EGTA and 10 HEPES (titrated with KOH, pH 7.3), and patch pipettes were filled with a solution of the following composition, in mM: 100 $BaCl_2$, 10 tetraethylammonium (TEA) -Cl, 10 HEPES, 200 nM TTX, titrated with TEA-OH to pH 7.4. Both solutions were adjusted to an osmolarity of 320 mOsmol with sucrose. Data were sampled (Axopatch 200B and Digidata 1200 interface, Axon Instruments, Foster City, CA) at 20 kHz and filtered on-line at 1 - 2 kHz. Voltages were not corrected for liquid junction potential (26), measured to be -15 mV in these solutions, in order to be able to compare

the results to other published material. Leak subtraction was performed by averaging segments of traces with no activity from the same voltage protocol in the same experiment, and subtracting this average from each episode using pClamp6 (Axon Instruments). Statistical analysis was performed using paired or unpaired Student's t-test. For the single channel analysis, patches were only used in which 3 or fewer overlapping openings were detected. With an open probability of about 0.5 at +40 mV and at least 20 consecutive stimulations, the number of detectable multiple openings was considered to represent the number of channels active in these patches. Event detection was carried out using the half-amplitude threshold method. Single channel amplitude was determined by a Gaussian fit to the binned amplitude distributions. Mean open and closed times were determined as a single or double exponential fitted to open time distributions. Open time distributions were only collected in episodes or parts of episodes with no overlapping openings. For closed time distributions we used either single channel patches or segments towards the end of episodes in which only one channel remains active and no further overlaps occur. Data are expressed as mean ± SEM. For steady-state inactivation, all the available patches were considered and each normalized to its peak current response during the prepulse to +40 mV. Latency to first opening was measured in 2 ms bins. First latency (FL) histograms from each experiment were divided by the number of episodes collected, the plots were then accumulated and divided by the number of stimulations, to express the data as the FL probability (23, 27). Two- and three-channel patches were also corrected for the apparent number of channels in the patch, according to:

$$FL_1=1-(1-FL_N)^{(1/N)}$$

FL_1 and FL_N are the single channel and multi-channel cumulative first latency functions respectively and N is the apparent number of channels.

Results

Comparison of morphology of *du/du* and +/+ PCs

The *du/du* cerebellum exhibits normal foliation and laminar structure. There are no gaps in the PC layer and their perikarya form a single row. The thickness of each layer is reduced in *du/du* compared to wild-type littermates as previously described (12). Two techniques were used to compare the morphology of cerebellar PCs between the different genotypes in more detail: firstly, classical Golgi impregnation, and secondly microinjection of PC somata with Lucifer yellow and neurobiotin. Both methods revealed a changed PC cytoarchitecture in homozygous *du/du* cerebella at P21-26, which was the latest time period in which morphology could be studied, given that the *du/du* mice die by P35. In the Golgi-impregnated cerebella, PCs were examined in detail in multiple cerebellar sections from 1 +/+ and 6 *du/du* mice. Atypical initial lateral extensions of the primary dendrite were seen in *du/du* but not in +/+ PCs (compare +/+ in Fig. 1A to *du/du* in Fig. 1B, C, F). The primary dendrites may then bend apically in a delayed targeting of the pial surface, which they frequently fail to reach (e.g. Fig. 1 B, C). Thickened tertiary branchlets were found to bend downwards in some *du/du* PCs, giving a 'weeping willow' appearance (Fig.1B, open arrowhead). Additionally, PC somata are frequently multipolar, exhibiting up to three primary dendrites (Fig.1D, E, F, filled arrowhead), which, in the cells shown in Fig.1E and F, extend laterally rather than targeting the pial surface.

Similar results were obtained with the cell-filling technique, for which 4 +/+ and 4 *du/du* PCs were examined in detail. The *du/du* PCs displayed a dendritic arbor that was significantly less complex, reduced in size, and frequently did not reach the border of the molecular layer (compare the typical +/+ PC in Fig. 2A with three *du/du* PCs shown in Fig. 2B). Additionally, the shafts of the main and secondary dendritic branches of *du/du* PCs were often thickened (Fig. 2B). In one *du/du* PC, the dendrites drooped down towards the

granule cell layer giving a 'weeping willow' appearance (Fig. 2B, top right panel), similar to that seen in some of the Golgi-impregnated *du/du* PCs (Fig. 1B). Following skeletonization of the dendritic trees (Fig. 2C), the numbers of dendrites were found to be reduced in *du/du* PCs (Fig. 2D, left panel) and the total length of the dendritic tree was also reduced (Fig. 2D, center panel). However, the number of branch-points on the longest dendrites was unchanged (Fig. 2D, right panel).

The *du* 5' mutant transcript is present and translated in *du/du* cerebellar PCs

We have previously shown, by *in situ* hybridization using a 3' antisense probe, that no full-length transcript for *Cacna2d2* is present in *du/du* cerebellum, whereas a strong signal was obtained in +/+ cerebellar PCs (12). In the present study we performed *in situ* hybridization with a 5' *Cacna2d2* anti-sense RNA probe in order to examine whether a truncated message was present in *du/du* PCs. This confirmed the presence of full-length transcript for *Cacna2d2* in +/+ PCs (Fig. 3A). The data would also not be inconsistent with the additional presence of transcript in small Bergmann glial cell bodies (Fig. 3A, arrowheads, see also Fig. 8), The results also demonstrate a low level of message hybridizing to the 5' probe in *du/du* PCs (Fig. 3B, compared to 3A). This , together with the absence of full length transcript in *du/du* PCs shown in our previous study (12), provide evidence for a low level of transcription of *du* mutant transcript 1 (12) in these cells.

We therefore generated an α2δ-2 antipeptide antibody utilizing an immunizing peptide corresponding to amino acids 102 –117, with the intent of examining whether a mutant protein was expressed in *du/du* cerebellum. This sequence is near the N-terminus of α2δ-2, and also present in the predicted protein product of the *du* mutant transcript 1, termed *du*-mut1 α2 (Fig. 4A). This antibody, called Ab (102–117), was first characterized

against heterologously expressed α2δ-2. On Western blots of gels run under reducing conditions, α2 is separated from the δ moiety to which it is disulfide bonded under native conditions. Ab (102–117) specifically recognized the α2 moiety of α2δ-2 (as a broad band at about 150 kD), and not the α2 moiety of α2δ-1, when both α2δ-1 and α2δ-2 were over-expressed in COS-7 cells (Fig. 4B). It also recognized a ~10 kDa protein product of the *du*-mut1 α2 cDNA expressed in COS-7 cells (Fig. 4B). When Ab (102-117) was used to examine the immunocytochemical localization of α2δ-2 in these cells, the epitope was accessible in non-permeabilized cells, orienting it exofacially (Fig. 4 C, columns 1 and 2, upper panel). Additional intracellular staining was observed when the cells were permeabilized (Fig. 4C, columns 1 and 2, lower panel). When *du*-mut1 α2 was expressed, very little immunostaining was observed in non-permeabilized cells (Fig. 4C, column 3, upper panel), although a large number of cells were present in the field (Fig. 4C, column 4, upper panel), whereas intense intracellular immunostaining, localized to intracellular organelles was observed when the cells were permeabilized (Fig. 4C, columns 3 and 4, lower panel). The lack of staining with the anti-GFP antibody in non-permeabilized GFP-positive cells provides further evidence that the plasma membrane of the cells has not been permeabilized by fixation (Fig. 4D).

The predicted protein MW of the entire *du*-mut1 α2 truncated protein is 16 kDa, which is larger than the ~10 kDa band observed here. We therefore utilized another anti-peptide antibody, generated against the epitope represented by amino acids 16 – 29, which is within the predicted signal sequence of α2δ-2, in order to further examine the processing of the *du*-mut1 α2 protein. When *du*-mut1 α2 was expressed in COS-7 cells, Ab (16 – 29) recognized a 16 kDa band in lysates of these cells (Fig. 5A, lane 1). No smaller MW bands were observed on this gel (but see Fig. 7). This suggested that the signal sequence of *du*-mut1 α2 is at least partly uncleaved when it is expressed in COS-7 cells. Ab (16 – 29) also recognized a well defined 120 kDa protein when full-length α2δ-2

was expressed (Fig. 5A, lane 2), and no bands when α2δ-1 was expressed as a control (Fig. 5A, lane 3). This 120 kDa protein is likely to represent an immature form of α2δ-2 before cleavage of the signal sequence, which normally precedes glycosylation. The protein MW of the α2 moiety including the 6 kDa signal sequence is calculated to be 113 kDa. Unlike Ab (102–117), Ab (16-29) did not recognize a band of 150 kDa, indicating that, as expected, the signal sequence is cleaved from the mature glycosylated form of α2δ-2.

We then examined the immuno-localization of *du*-mut1 α2 in COS-7 cells, using Ab (16-29). Immunostaining for this epitope was not observed at the plasma membrane in non-permeabilized cells expressing α2δ-2, indicating that the signal sequence is cleaved before insertion of α2δ-2 into the plasma membrane. Furthermore this epitope was also generally not observed on the exofacial side of the plasma membrane when *du*-mut1 α2 was expressed (Fig. 5B, non-permeabilized cells). Diffuse intracellular staining was observed when the cells were permeabilized for both α2δ-2 and *du*-mut1 α2-expressing cells (Fig. 5B).

Immunopurification of *du*-mut1 α2 from *du/du* cerebellum

The use of an Ab (102-117) immuno-affinity column allowed the isolation of a low abundance protein of ~10 kDa from *du/du* cerebellum (Fig. 6A, lane 1), which was detected using the same antibody. This protein is very similar in MW to the *du*-mut1 α2 protein isolated in the same way from lysates of COS-7 cells expressing *du*-mut1 α2 (Fig. 6A, lane 2). If a protein product were produced from *du* mutant transcript 2 (accession number AF247141) in *du/du* cerebellum (12), its predicted MW would be ~100 kDa. This would also be recognized by Ab (102-117), but no higher MW immunoreactive bands were observed from 4-20 % gradient gels of proteins isolated from *du/du* cerebellum (data

not shown, n=2). A broad band of protein of ~150 kDa, representing the α2 moiety of α2δ-2, was isolated from +/+ cerebellum using the same immuno-affinity column, and detected using the same antibody (Fig. 6B, lane 1). This protein was the same MW as that isolated by the same antibody from COS-7 cells transfected with α2δ-2, with the broad band probably representing different glycosylation states (Fig. 6B, lane 2).

Using an Ab (16-29) immuno-affinity column, a protein of ~16 kDa was isolated from *du/du* cerebellum, (Fig. 6C, lane 1). This protein is very similar in MW to the *du*-mut1 α2 protein isolated in the same way from COS-7 cells expressing *du*-mut1 α2 (Fig. 6C, lane 2). Furthermore, a protein of about 120 kDa was isolated from +/+ cerebellum using the same immuno-affinity column (Fig. 6D, lane 1). This protein was the same MW as that isolated by the same antibody from COS-7 cells transfected with α2δ-2 (Fig. 6D, lane 2).

The basis for the difference in MW between the *du*-mut1 α2 species recognized by the two antibodies was further examined by PAGE of a larger amount (80 μg protein) of COS-7 cell lysate expressing *du*-mut1 α2, on a high % gradient gel, followed by immunoblotting (Fig. 7A). A 16 kDa band was recognized by both antibodies, but the predominant band recognized by Ab (102-117) was ~10 kDa. This was not recognized by Ab (16-29), which recognized an additional 6 kDa band. The amino acid sequence of *du*-mut1 α2 is shown in Fig. 7B, with the antibody recognition sites (bold) and the predicted site of cleavage of the signal sequence (arrow). The predicted sizes of the peptides obtained before and after cleavage are 16 kDa for full-length *du*-mut1 α2, 10 kDa for *du*-mut1 α2 following cleavage of the signal sequence and 6 kDa for the cleaved signal sequence (Fig. 7C), in agreement with the experimental results.

The immuno-localization of α2δ-2 in the cerebellum was subsequently examined using Ab (102-117). This antibody gave a pattern of immunostaining in the Purkinje cell

layer (PCL) and molecular layer (ML) in sections of +/+ cerebellum, consistent with localization of α2δ-2 in PC bodies and dendrites (Fig. 8A, left panel). The staining was lost when the primary antibody was pre-incubated with the immunizing peptide or when the primary antibody was not used (Fig. 8A). In cerebellar sections from *du/du* mice, Ab (102–117) gave a low level of immunostaining (Fig. 8A, right panel), consistent with the presence of *du*-mut1 α2 in *du/du* PCs. There was also some evidence for staining of Bergmann glia (Fig. 8A, right panel marked with *). We also used Ab (16-29) to determine where the uncleaved form of *du*-mut1 α2 was expressed endogenously in *du/du* cerebellar sections. A low level of immunostaining was observed with this antibody in +/+ PCs , consistent with the presence of the immature 120 kDa form of α2δ-2, with the signal peptide still present, which is likely to be localized to the endoplasmic reticulum (Fig. 8B, left panel). Further evidence was obtained here for staining of Bergmann glia (Fig. 8b, left panel,*). In *du/du* cerebellum, we observed that immunostaining with this antibody was concentrated largely in the cell bodies of PCs (Fig. 8B, right panel). This is likely to represent the 16 kDa uncleaved *du*-mut1 α2 species. The immunostaining was lost when the antibody was pre-incubated with the immunizing peptide (Fig. 8B). No differences were observed between +/+ and *du/du* PCs when Bergmann glia were visualized using an anti-glial fibrillary acidic protein antibody (results not shown).

Modulation of $Ca_V2.1$ Ca^{2+} channel currents by α2δ-2 and *du*-mut1 α2

The possible pathological function of the *du*-mut1 α2 protein encoded by the *Cacna2d2*^{du} gene was investigated using *in vitro* expression and electrophysiology. In order to mimic the PC complement of calcium channel subunits, the cDNAs corresponding to rat $Ca_V2.1$ and β4 were transfected into COS-7 cells, with or without α2δ-2 or *du*-mut1 α2 cDNA, and the resulting Ca_V currents (I_{Ba}) recorded. Co-expression of α2δ-2

increased $Ca_V2.1$ / β4 I_{Ba} currents, inducing a 2.9-fold enhancement of amplitude at 0 mV (Fig. 9A, and I-V relationships in Fig. 9B), with no significant shift in the voltage-dependence of current activation (V_{50} for activation was -8.7 ±0.7 mV (n = 28) for $Ca_V2.1$ / β4 and -10.7 ± 0.8 mV (n = 42) for $Ca_V2.1$ / β4 / α2δ-2). There was no significant effect of α2δ-2 on the activation or inactivation of the $Ca_V2.1$ / β4 combination (Fig. 9A and results not shown).

In contrast, co-expression of *du*-mut1 α2 induced a consistent reduction in $Ca_V2.1$ / β4 I_{Ba} amplitude throughout the voltage range (Fig. 9C and D). This amounted to a 51 % inhibition at 0 mV (Fig. 9E), and also resulted in a +5 mV shift in V_{50} for activation to -3.5 ±1.1 mV (n = 12, $p < 0.01$ compared to $Ca_V2.1$ / β4). The mean current densities at 0 mV under the two different conditions are compared in Fig. 9E. Similar results were obtained when these calcium channel subunits, in this case including rabbit $Ca_V2.1$, were expressed in *Xenopus* oocytes ((12) and data not shown).

Effect of α2δ-2 and *du*-mut1 α2 on single Ca^{2+} channel currents formed by $Ca_V2.1$

We compared single channel parameters between cell-attached patches of COS-7 cells transfected with $Ca_V2.1$ / β4 cDNA, either without α2δ-2 (Fig. 10A), or co-expressed with either full-length α2δ-2 (Fig. 10B) or the *du*-mut1 α2 (Fig. 10C). These experiments were performed in order to differentiate between a mechanism that involves changing the biophysical properties of $Ca_V2.1$ channels and a mechanism that involves changing the trafficking or membrane expression levels of the $Ca_V2.1$ channels, imposed by either α2δ-2 or *du*-mut1 α2.

Once opened, $Ca_V2.1$ channels showed an average single channel conductance of 9.9 ± 0.4 pS (n = 8) for $Ca_V2.1$ / β4, which was not significantly affected by co-expression of α2δ-2 (10.2 ± 0.6 pS, n = 8) or *du*-mut1 α2 (8.8 ± 1.0 pS, n = 6) (Fig. 10D). This

conductance is similar to that of P-type channels recorded from wild-type and *du/du* PCs under the same conditions (12). More detailed analysis demonstrated openings to three distinct amplitude levels, as has also been shown in native Purkinje cells (28), level 2 being the most prominent in our recordings (Fig. 10E, see legend for conductance and amplitude values). Neither the conductance nor the amplitude of the three current levels was significantly affected by expression of α2δ-2 or *du*-mut1 α2 (data not shown).

Neither α2δ-2 nor *du*-mut1 α2 caused any significant change in mean open or closed times, or in the pattern of voltage dependence of $Ca_V2.1$ channels (Fig. 10F). We also examined the activation kinetics by measuring the latency to first opening of the channels in response to a square voltage pulse (Fig. 10G). $Ca_V2.1$ channel activation was not influenced by the subunits examined (Fig. 10G, left), at any voltage (Fig. 10G, right). In addition, the voltage-dependence of inactivation (Fig. 10H) was not influenced by either α2δ-2 or *du*-mut1 α2.

Although the presence of α2δ-2 caused an approximately 3-fold increase in whole cell current amplitude, all the single channel parameters were indistinguishable between the three conditions. This implies that the basic active unit in the whole cell current (an individual channel) remains unchanged, and the modulation by α2δ-2 must involve an alteration in the number of active channels in the membrane.

Discussion

PCs from *du/du* mice have a reduced dendritic arbor

PC somata form a monolayer by 10 days postnatally in the mouse, and their dendrites reach the pial surface at day 20, coinciding with the completion of granule cell migration and concomitant parallel fiber production (29). The PC soma typically exhibits one primary dendrite, which emerges apically, and one axonal process projecting in the opposite direction. The PC dendritic trees develop most dramatically between postnatal day 9 and 20, reaching 80% of their adult dimension in this period (30). PCs from *du/du* mice appear immature, reduced both in size and complexity, with multiple primary dendrites and small arbors that often terminate well below the pial surface. Thickened secondary and tertiary dendritic trunks are also present. The multipolar appearance of some of the *du/du* PCs may be a remnant of their immature stage (in which the normal resorption of all somatic filopodia fails to occur), with some of these processes continuing to develop into dendrites as found in weaver and staggerer mouse mutants (31).

Thus, although we have shown that PCs are not lost in *du/du* cerebella at P21 (12), we now find that the PC dendritic tree is reduced in size, and shows other abnormalities, such as 'weeping willow' dendrites, and dendritic thickening. Similar abnormalities have been found in a number of the spontaneously occurring $Ca_V2.1$ mouse mutants (8), and some of these (in particular tg^{la}) also show PC loss in older mice (32). The mechanism of the altered PC morphology in *du/du* mice may result either from the reduced PC calcium channel currents, which we observed in P5 - P9 PCs, before the extensive growth of the dendritic arbor (12), or more directly from the loss of α2δ-2, with the possible additional consequences of expression of a truncated mutant α2 protein. A number of the human genetic diseases involving $Ca_V2.1$, for example familial hemiplegic migraine (33), cerebellar ataxia and PC degeneration are associated with mutations that have been

shown to produce a reduction in $Ca_V2.1$ calcium currents *in vitro* (34). However, the mechanism whereby such molecular changes are translated into morphological and functional abnormalities remains to be determined.

A truncated mutant protein derived from the 5'mutant transcript of *Cacna2d2* is expressed in *du* mice

The *in situ* hybridization study demonstrates that although wild-type *Cacna2d2* transcript is absent from the brain of *du/du* mice, because of the genomic rearrangement that disrupts *Cacna2d2* (12), a 5' mutant transcript (*du* mutant transcript 1) is present in *du/du* PCs. This transcript is predicted to encode a protein (*du*-mut1 α2) that lacks most of the α2 subunit and the whole of the δ subunit, including its transmembrane domain. It is frequently the case that mRNA encoding mutant transcripts, where a frame-shift or point mutation introduces one or more premature stop or nonsense codons, is unstable and subject to nonsense-mediated mRNA decay (35). Indeed, although a second mutant transcript 2, predicted to be formed from exons 2-39, was identified by RT-PCR and northern blot in *du/du* mouse brain, it was not observed by *in situ* hybridization in *du/du* PCs (12). Furthermore, the 5' *du* mutant transcript 1 appeared to be present at a low level in *du/du* brain (12). In order to determine whether this mutant transcript was translated, we used two α2δ-2 anti-peptide antibodies, which were raised against peptides within the *du*-mut1 α2 sequence, Ab (16-29) and Ab (102–117).

It has been established, from studies with site-directed antipeptide antibodies, that the topology of the α2δ-1 subunit is such that the α2 subunit, which has an N terminal leader signal sequence, is entirely extracellular (36-38). The α2 subunit is disulfide-bonded to a transmembrane δ subunit, and both subunits have been found to be involved in the interaction with the α1C subunit (38, 39). Now that two other α2δ subunit genes have been cloned, it is assumed that they have the same topology, and indeed, high

homology is present between the N termini of α2δ-1 and α2δ-3, with the clear prediction of a cleaved signal peptide in both sequences. In contrast, although a putative signal peptide is found in α2δ-2, it is much longer. Using prediction analysis, it is found to have a potential cleavage site after position 64 (40) (Fig 7B), whereas only 2% of eukaryotic signal peptides are longer than 35 residues (40). In particular, it has a longer sequence N-terminal to the putative hydrophobic signal sequence (approximately 42 amino acids) than α2δ-1 or α2δ-3 (which are approximately 3 and 11 amino acids, respectively). Such "n regions" are found to be less than 25 amino acids in 80% of secreted or transmembrane proteins where they occur (41). Therefore it remains unclear whether this signal sequence is cleaved efficiently, as cleavage is often delayed when the signal sequence is long (42). This results in extended transit times through the endoplasmic reticulum-Golgi apparatus, which may be required for highly glycosylated proteins (42). Such an explanation is likely to be the reason for our observation using Ab (16 –29), of a 120 kDa immuno-labeled protein when α2δ-2 was expressed in COS-7 cells. This is likely to represent the α2 moiety of full-length α2δ-2 (predicted protein MW 113 kD), which is immature in that it has an uncleaved signal peptide and, judging by the MW, no added carbohydrate.

It appears that in the case of *du*-mut1 α2 expressed in COS-7 cells, the truncated protein is processed such that the signal sequence remains at least in part uncleaved, since both Ab (16-29) and Ab (102-117) recognized a band of ~16 kDa, the predicted size for the uncleaved *du*-mut1 α2, and Ab (16-29) also recognized a fainter band of about 6 kDa, which would represent the cleaved signal peptide. However the predominant band recognized by Ab (102–117) but not Ab (16-29) was a ~10 kDa protein, which is therefore likely to represent *du*-mut1 α2 with its signal peptide cleaved. This result corresponded exactly with the MW of the native *du*-mut1 α2 immunocaptured from *du/du* cerebellum by the same antibody, indicating that it is a stable *in vivo* species in these mice. This study

also confirmed the previous indication (12), that *du* mutant transcript 2, which would be recognized by Ab (102-117) is not translated. A 16 kDa protein was immunocaptured by Ab (16-29) from *du/du* cerebellum, indicating that the signal sequence remains, in part, uncleaved from *du*-mut1 α2. The reason that this species was not also immunocaptured by Ab (102-117) may indicate that Ab (102-117) is of lower affinity, as also suggested by the data in Fig. 8.

Immuno-localization of α2δ-2 and *du*-mut1 α2 in cerebellum

In cerebellar sections, we found, using Ab (102-117) that α2δ-2 is expressed in wild-type PC somata and also in the ML of the cerebellum, suggesting localization in PCs. It is also possible that some of the immunostaining arises from cerebellar afferents, or from Bergmann glia, and this will be investigated in the future. In *du/du* cerebellum, a low level of immunostaining was observed with the same antibody. These results support the finding that *du*-mut1 α2 is expressed in *du/du* cerebellum. Immunoreactivity in *du/du* cerebellar sections was also observed using Ab (16-29), where staining, presumably representing the uncleaved *du*-mut1 α2 was concentrated in PC somata. In agreement with the expression study in COS-7 cells and the immunopurification data from cerebellum, this suggests that *du*-mut1 α2 retains, in part, the putative signal sequence at its N terminus, and does not appear to be secreted. When *du*-mut1 α2 was expressed in COS-7 cells both Ab (16-29) and Ab (102–117) recognized an epitope that was only expressed intracellularly, indicating that *du*-mut1 α2 is unlikely to be secreted or inserted into the plasma membrane as a transmembrane protein.

The functional interaction of the $Ca_V2.1$/β4 combination with α2δ-2

The similarity of the ducky phenotype to that observed in mice with mutations in genes encoding the $Ca_V2.1$ (7) and β4 (9) subunits and their predominant PC expression pattern suggests that α2δ-2 contributes to the P-type current. This is reinforced by our finding that the currents formed by both rat and rabbit $Ca_V2.1$ co-expressed with β4, which is the main PC β subunit, were strongly enhanced by α2δ-2, in two expression systems (COS-7 cells and *Xenopus* oocytes).

Previous *in vitro* studies have shown that α2δ-1, α2δ-2 and α2δ-3 subunits act to increase the maximum conductance of a number of expressed calcium channel α1/β subunit combinations at the whole cell level (2, 43-46). However, this may be dependent to some extent on the specific combination of α1 and β subunits expressed. Furthermore, the effects of α2δ subunits on kinetics and voltage-dependence of activation are more minor (2, 44). We have also investigated this for the calcium channel subunit combinations used in the present study, and show that α2δ-2 had no influence on voltage-dependent properties and had no effect on single channel conductance or other biophysical parameters of the $Ca_V2.1$ / β4 channels themselves. This implies that α2δ-2 probably has its main effect on the lifetime of the channel complex in the plasma membrane, either by enhancing trafficking or reducing turnover. In agreement with this proposed mechanism, it has previously been found that α2δ-1 increased the amount of $Ca_V1.2$ protein expressed in Xenopus oocytes (47).

In contrast, the protein product of *du* mutant transcript 1, *du*–mut1 α2, produced a consistent reduction in $Ca_V2.1$ / β4 currents in COS-7 cells. Thus, while loss of full-length α2δ-2 is likely to be the most important contributing factor, the expression of the truncated *du*-mut1 α2 may also contribute to the *du/du* phenotype, via an additional suppressive effect, possibly by interfering with the correct trafficking of α1 subunits.

Acknowledgements

We thank the Medical Research Council (UK), The Wellcome Trust and Epilepsy Research Foundation for support. We also thank Professor R. M. Gardiner for his support and encouragement, Dr. Kevin Bittman, Dr. David Becker and Dr. Marina Mione for generously sharing their expertise and Mick Keegan for excellent technical assistance.

Abbreviations

Ab: antibody; ATP: adenosine triphosphate; FL: first latency; GCL: granule cell layer; HEPES: N-[2-hydroxyethyl] piperazine-N'-[2-ethanesulfonic acid]; kDa: kilodaltons; ML: molecular layer; MW: molecular weight; PBS: phosphate-buffered saline; PC: Purkinje cell; PCL: Purkinje cell layer; TBS: Tris-buffered saline; TEA: tetraethylammonium; TTX: tetrodotoxin.

References

1. Catterall, W.A. (2000) *Annu.Rev.Cell Dev.Biol.* **16**, 521-555

2. Walker, D. and De Waard, M. (1998) *TiNS* **21**, 148-154

3. Letts, V.A., Felix, R., Biddlecome, G.H., Arikkath, J., Mahaffey, C.L., Valenzuela, A., Bartlett, F.S., Mori, Y., Campbell, K.P., and Frankel, W.N. (1998) *Nature Genet.* **19**, 340-347

4. Chen, L., Chetkovich, D.M., Petralia, R.S., Sweeney, N.T., Kawasaki, Y., Wenthold, R.J., Bredt, D.S., and Nicoll, R.A. (2000) *Nature* **408**, 936-943

5. Ertel, E.A., Campbell, K.P., Harpold, M.M., Hofmann, F., Mori, Y., Perez-Reyes, E., Schwartz, A., Snutch, T.P., Tanabe, T., Birnbaumer, L., Tsien, R.W., and Catterall, W.A. (2000) *Neuron* **25**, 533-535

6. Burgess, D.L., Gefrides, L.A., Foreman, P.J., and Noebels, J.L. (2001) *Genomics* **71**, 339-350

7. Fletcher, C.F., Lutz, C.M., O'Sullivan, T.N., Shaughnessy, J.D., Jr., Hawkes, R., Frankel, W.N., Copeland, N.G., and Jenkins, N.A. (1996) *Cell* **87**, 607-617

8. Zwingman, T.A., Neumann, P.E., Noebels, J.L., and Herrup, K. (2001) *J.Neurosci.* **21**, 1169-1178

9. Burgess, D.L., Jones, J.M., Meisler, M.H., and Noebels, J.L. (1997) *Cell* **88**, 385-392

10. Kang, M.G., Chen, C.C., Felix, R., Letts, V.A., Frankel, W.N., Mori, Y., and Campbell, K.P. (2001) *J.Biol.Chem.* **276**, 32917-32924

11. Sharp, A.H., Black, J.L., III, Dubel, S.J., Sundarraj, S., Shen, J.P., Yunker, A.M.R., Copeland, T.D., and McEnery, M.W. (2001) *Neuroscience* **105**, 599-617

12. Barclay, J., Balaguero, N., Mione, M., Ackerman, S.L., Letts, V.A., Brodbeck, J., Canti, C., Meir, A., Page, K.M., Kusumi, K., PerezReyes, E., Lander, E.S., Frankel, W.N., Gardiner, R.M., Dolphin, A.C., and Rees, M. (2001) *J.Neurosci.* **21**, 6095-6104

13. Snell, G.D. (1955) *J.Hered.* **46**, 27-29

14. Meier, H. (1968) *Acta Neuropathol.Berl.* **11**, 15-28

15. Stuart, G.J., Dodt, H.U., and Sakmann, B. (1993) *Pflugers Archiv-European Journal Of Physiology* **423**, 511-518

16. Eisenstat, D.D., Liu, J.K., Mione, M., Zhong, W.M., Yu, G.Y., Anderson, S.A., Ghattas, I., Puelles, L., and Rubenstein, J.L.R. (1999) *J.Comp.Neurol.* **414**, 217-237

17. Brice, N.L., Berrow, N.S., Campbell, V., Page, K.M., Brickley, K., Tedder, I., and Dolphin, A.C. (1997) *Eur.J.Neurosci.* **9**, 749-759

18. Macart, M. and Gerbaut, L. (1982) *Clin.Chim.Acta* **122**, 93-101

19. Berrow, N.S., Brice, N.L., Tedder, I., Page, K., and Dolphin, A.C. (1997) *Eur.J.Neurosci.* **9**, 739-748

20. Hans, M., Urrutia, A., Deal, C., Brust, P.F., Stauderman, K., Ellis, S.B., Harpold, M.M., Johnson, E.C., and Williams, M.E. (1999) *Biophys.J.* **76**, 1384-1400

21. Barclay, J. and Rees, M. (2000) *Mamm.Genome* **11**, 1142-1144

22. Cormack, B.P., Valdivia, R.H., and Falkow, S. (1996) *Gene* **173**, 33-38

23. Meir, A., Bell, D.C., Stephens, G.J., Page, K.M., and Dolphin, A.C. (2000) *Biophys.J.* **79**, 731-746

24. Canti, C., Page, K.M., Stephens, G.J., and Dolphin, A.C. (1999) *J.Neurosci.* **19**, 6855-6864

25. Meir, A. and Dolphin, A.C. (1998) *Neuron* **20**, 341-351

26. Neher, E. (1995) in *Single-Channel Recording* (Sakmann, B. and Neher, E., eds) pp. 147-153, Plenum Press, New York

27. Imredy, J.P. and Yue, D.T. (1994) *Neuron* **12**, 1301-1318

28. Usowicz, M.M., Sugimori, M., Cherksey, B., and Llinás, R. (1992) *Neuron* **9**, 1185-1199

29. Fujita, S. (1967) *J.Cell Biol.* **32**, 272-288

30. Sadler, M. and Berry, M. (1984) *Proceedings Of The Royal Society Of London Series B-Biological Sciences* **221**, 349-367

31. Sotelo, C. (1975) *Advances in Neurology* **12**, 335-351

32. Heckroth, J.A. and Abbott, L.C. (1994) *Brain Res.* **658**, 93-104

33. Ophoff, R.A., Terwindt, G.M., Vergouwe, M.N., van Eijk, R., Oefner, P.J., Hoffman, S.M., Lamerdin, J.E., Mohrenweiser, H.W., Bulman, D.E., Ferrari, M., Haan, J., Lindhout, D., van Ommen, G.J., Hofker, M.H., Ferrari, M.D., and Frants, R.R. (1996) *Cell* **87**, 543-552

34. Hans, M., Luvisetto, S., Williams, M.E., Spagnolo, M., Urrutia, A., Tottene, A., Brust, P.F., Johnson, E.C., Harpold, M.M., Stauderman, K.A., and Pietrobon, D. (1999) *J.Neurosci.* **19**, 1610-1619

35. Culbertson, M.R. (1999) *Trends In Genetics* **15**, 74-80

36. Brickley, K., Campbell, V., Berrow, N., Leach, R., Norman, R.I., Wray, D., Dolphin, A.C., and Baldwin, S. (1995) *FEBS Lett.* **364**, 129-133

37. Gurnett, C.A., De Waard, M., and Campbell, K.P. (1996) *Neuron* **16**, 431-440

38. Gurnett, C.A., Felix, R., and Campbell, K.P. (1997) *J.Biol.Chem.* **272**, 18508-18512

39. Felix, R., Gurnett, C.A., De Waard, M., and Campbell, K.P. (1997) *J.Neurosci.* **17**, 6884-6891

40. Nielsen, H., Engelbrecht, J., Brunak, S., and vonHeijne, G. (1997) *Protein Eng.* **10**, 1-6

41. Martoglio, B. and Dobberstein, B. (1998) *Trends Cell Biol.* **8**, 410-415

42. Li, Y., Luo, L.Z., Thomas, D.Y., and Kang, C.Y. (1994) *Virology* **204**, 266-278

43. Mori, Y., Friedrich, T., Kim, M.-S., Mikami, A., Nakai, J., Ruth, P., Bosse, E., Hofmann, F., Flockerzi, V., Furuichi, T., Mikoshiba, K., Imoto, K., Tanabe, T., and Numa, S. (1991) *Nature* **350**, 398-402

44. Klugbauer, N., Lacinova, L., Marais, E., Hobom, M., and Hofmann, F. (1999) *J.Neurosci.* **19**, 684-691

45. Dolphin, A.C., Wyatt, C.N., Richards, J., Beattie, R.E., Craig, P., Lee, J.-H., Cribbs, L.L., Volsen, S.G., and Perez-Reyes, E. (1999) *J.Physiol.* **519**, 35-45

46. Hobom, M., Dai, S., Marais, E., Lacinova, L., Hofmann, F., and Klugbauer, N. (2000) *Eur.J.Neurosci.* **12**, 1217-1226

47. Shistik, E., Ivanina, T., Puri, T., Hosey, M., and Dascal, N. (1995) *Journal of Physiology (Lond.)* **489**, 55-62

Figure legends

Figure 1 Comparison of +/+ and *du/du* PC morphology by Golgi impregnation

Light micrographs showing individual Golgi impregnated PCs, of +/+ (A) and *du/du* (B-F) cerebellum. Parasagittal sections for both genotypes were taken from an identical region of the vermis (see diagram top left). (A) typical +/+ PC with dendritic processes reaching the pial surface. (B-F) *du/du* PCs were characterized by the absence of an apically-oriented main dendrite. The cell in (B) also exhibits a 'weeping willow'-like dendrite bending back towards the granule cell layer (arrowhead). The cells in D, E, F show multiple primary dendrites emerging from the perikaryon (open arrowheads).

Figure 2 Comparison of +/+ and *du/du* PC morphology by cell filling

Lucifer yellow/neurobiotin injection of cerebellar PCs of (A) +/+ (neurobiotin staining for one representative cell shown, as morphology of all +/+ PCs was similar) and (B) *du/du* (3 cells shown, to illustrate variation in morphologies observed, the first imaged with neurobiotin staining, and the other two with lucifer yellow). (C) skeletonized dendritic tree of the cells shown in A and B, for evaluation of arborization complexity, independent of dendritic width. This is quantified in (D). Left panel: the number of dendrites per cell crossing a horizontal (H) and diagonal (D) line. Center panel: number of black pixels as indication of the whole area covered by skeletonized dendrites. Right panel: number of branch points. For all panels of (D), n = 4 for both +/+ and *du/du* PCs. Asterisks indicate a statistically significant difference: * $p<0.05$, ** $p<0.01$, Student's t test.

Figure 3 Analysis of *Cacna2d2* mutant transcript 1 expression in P21 +/+ and *du/du* cerebellum

In situ hybridization of +/+ and *du/du* sections with 5' *Cacna2d2* anti-sense (A/S) RNA probes designed to detect *du* mutant transcript 1 in *du/du* mice. This probe will also

detect wild-type transcript. Analyses were carried out on +/+ (A) and *du/du* sections (B). The arrowheads in A indicate the presence of a signal from smaller cell bodies, possibly Bergmann glial cells. No signal was detected on hybridization of control sense RNA to +/+ sections (C and D). ML = molecular layer, PCL = Purkinje cell layer, GCL = granule cell layer. Scale bar = 100 μm.

Figure 4 Specificity of Ab (102-117) and localization of α2δ-2 and *du*-mut1 α2 in COS-7 cells

(A) Schematic representation of α2δ-2 protein to show location of the Ab (102–117) binding site in relation to the end of exon 3.

(B) Immunoblots to show the specificity of the anti-α2δ-2 Ab (102 – 117), using lysates (20 μg protein) from COS-7 cells over-expressing α2δ-2 (lane 1, 150 kD) or α2δ-1 as a control (lane 2) on 4-12 % gradient SDS PAGE gels, and *du*-mut1 α2 (lane 3, ~10 kD) on a 4 – 20 % gel. The positions of the MW markers are shown next to the blots.

(C) COS-7 cells transfected with cDNAs for GFP and α2δ-2 (columns 1 and 2) or *du*-mut1 α2, (columns 3 and 4). Cells were either not permeabilized (upper row) or permeabilized with Triton X-100 (lower row). Immunostaining with Ab (102–117) is shown in columns 1 and 3, and DAPI fluorescence to identify cell nuclei is shown in columns 2 and 4. The scale bars are all 40 μm. For clarity, the GFP fluorescence is not shown.

(D) COS-7 cells transfected with cDNA for GFP alone. Cells were either not permeabilized (upper row) or permeabilized with Triton X-100 (lower row). GFP transfection was used as a control to show lack of immunostaining with anti-GFP Ab (left column) of this intracellular antigen in non-permeabilized cells. GFP fluorescence is shown in the right column. Scale bar (40 μm) applies to all sections.

Figure 5 Specificity of Ab (16-29)

(A) Immunoblots to show the specificity of Ab (16-29), using lysates (20 µg protein) from COS-7 cells over-expressing *du*-mut1 α2 (lane 1, 16 kD) on a 15 % SDS PAGE gel, or α2δ-2 (lane 2, 120 kD), or α2δ-1 as a control (lane 3) on 4-12 % gradient gels. The positions of the molecular weight markers are shown next to the blots.

(B) Immunostaining using Ab (16-29) in COS-7 cells transfected cDNA for full-length α2δ-2 (left panel) or *du*-mut1 α2 (right panel). Cells were either not permeabilized (upper row) or permeabilized with Triton X-100 (lower row), as described in Methods. Scale bars 10 µm.

Figure 6 Immuno-purification of *du*-mut1 α2 from *du/du* cerebellum and the α2 moiety of full-length α2δ-2 from +/+ cerebellum

Immunoblot analysis of α2δ-2 proteins immunocaptured from detergent-solubilized *du/du* or +/+ cerebellar membranes using column-immobilized peptide antibodies. Samples were separated on either 4 – 20 % gradient gels (panels A and B), a 20% gel (panel C), or on a 7.5% gel (panel D). Arrows indicate the major protein bands detected. Panels A and C: proteins from *du/du* cerebella (lane 1) or from COS-7 cells expressing *du*-mut1 α2 (lane 2) isolated using Abs (102-117) and (16-29), respectively. The respective apparent MWs are ~10 and 16 kDa. Panels B and D: proteins from +/+ cerebella (lane 1) or from COS-7 cells expressing full-length α2δ-2 (lane 2) isolated with Abs (102-117) and (16-29), respectively. The respective apparent MWs are 150 and 120 kDa.

Figure 7 Processing of *du*-mut1 α2

(A) Immunoblot analysis of *du*-mut1 α2 and fragments derived from cleavage of the signal peptide. Lysate (80 µg protein) of COS-7 cells expressing *du*-mut1 α2 was separated on a 10-20% gradient gel and probed with Ab (16-29) (lane 1) or Ab (102-117) (lane 2). A 16 kDa band is detected with both antibodies. Ab (16-29) also recognizes a band of 6 kDa, and Ab (102-117) recognizes a major band of ~10 kDa.

(B) Amino acid sequence of *du*-mut1 α2. The respective binding sites for Ab (16-29) and Ab (102-117) are shown in bold. The entire signal leader sequence is underlined with its predicted cleavage site marked by an arrow (40).

(C) shows the calculated MW values for *du*-mut1 α2 (16 kD), and the two proteolytic fragments: *du*-mut1 α2 following cleavage of the signal sequence (solid line, ~10 kD) and the cleaved signal sequence (dotted line, ~6 kD).

Figure 8 Immunohistochemistry in +/+ and *du/du* cerebellum

(A) Ab (102-117) detected the presence of α2δ-2 and *du*-mut1 α2 protein in +/+ and *du/du* sections, respectively. The affinity of the antibody for α2δ-2 and *du*-mut1 α2 may be different, therefore relative intensities cannot be compared directly. Results are representative of four experiments. (B) Ab (16-29) detected the presence of immature α2δ-2 in a +/+ cerebellar section (left) and *du*-mut1 α2 protein in a *du/du* cerebellar section (right). Representative of 3 experiments.

In both (A) and (B) the calibration bar is 30 µm. ML = molecular layer, PCL = Purkinje cell layer, GCL = granule cell layer. The label + peptide indicates that the primary antibody was preincubated with the immunizing peptide before application to the section. The * indicates examples of the presence of immunoreactivity in a smaller cell body and process, possibly a Bergmann glial cell.

Figure 9 Selectivity of enhancement of $Ca_V2.1/\beta4$ currents by $\alpha2\delta$-2 and inhibition by *du*-mut1 $\alpha2$

(A) Examples of I_{Ba} recorded from COS-7 cells transfected with $Ca_V2.1/\beta4/\alpha2\delta$-2 or $Ca_V2.1/\beta4$. The holding potential was –80 mV, and steps were to between –40 and +65 mV in 5 mV steps, delivered every 15 s. The charge carrier was 5 mM Ba^{2+}. The scale bars represent 10 $pA.pF^{-1}$ and 10 ms.

(B) I-V relationships for $Ca_V2.1/\beta4$ (O, n = 28) and $Ca_V2.1/\beta4/\alpha2\delta$-2 (■, n = 42) peak I_{Ba} density in COS 7 cells.

(C) Examples of the maximum I_{Ba} recorded at 0 mV from COS-7 cells transfected with $Ca_V2.1/\beta4$, $Ca_V2.1/\beta4/\alpha2\delta$-2, or $\alpha1A/\beta4/$*du*-mut1 $\alpha2$, as in (A). Co-expression of $\alpha2\delta$-2 induced a large enhancement of $Ca_V2.1/\beta4$ I_{Ba}, whereas *du*-mut1 $\alpha2$ induced a reduction of $Ca_V2.1/\beta4$ I_{Ba}.

(D) Mean I-V relationships for $Ca_V2.1/\beta4$ (O) and $Ca_V2.1/\beta4/$*du*-mut1 $\alpha2$ (▲) peak I_{Ba} density in COS 7 cells, fitted with a combined Boltzmann and linear function, as described in Methods.

(E) Histogram of mean data, for the transfection conditions shown beneath the bars, from COS-7 cells. $Ca_V2.1/\beta4$ (open bar, n = 13, controls for $Ca_V2.1/\beta4/\alpha2\delta$-2 transfections); $Ca_V2.1/\beta4/\alpha2\delta$-2 (black bar, n = 42); $Ca_V2.1/\beta4$ (open hatched bar, n = 15, performed in parallel with $\alpha1A/\beta4/$*du*-mut1 $\alpha2$ transfections) or $\alpha1A/\beta4/$*du*-mut1 $\alpha2$ (black hatched bar, n = 12). Statistical significance of differences indicated given by asterisks: ** $p < 0.001$; * $p < 0.05$ (Student's independent two tailed t test).

Figure 10 Comparison between the effect of $\alpha2\delta$-2 or *du*-mut1 $\alpha2$ on single channel parameters of $Ca_V2.1$.

(A) Single channel activity (maximum of two simultaneous overlapping openings) of $Ca_V2.1$ / β4 without the α2δ-2 auxiliary subunit. Top, the voltage protocol: holding potential –100mV. A 2 s. long pulse, here to +30 mV, delivered every 10 s. Bottom, 5 representative traces of single channel activity. Openings are downward deflections and a continuous line marks both the closed and open states, in traces with overlapping openings an additional dashed line marks the second level.

(B) Single channel activity (maximum of two simultaneous overlapping openings) arising from $Ca_V2.1$ / β4 co-expressed with the α2δ-2 auxiliary subunit. Format as in (A).

(C) Single channel activity (maximum of two simultaneous overlapping openings) arising from $Ca_V2.1$ / β4 co-expressed with the *du*-mut1 α2. Format as in (A).

(D) Average single channel conductance for the 3 conditions depicted in panels (A - C) (O, n=8; □, n=8; Δ, n=6) respectively. Conductance was determined by linear fits to the data shown. See text for mean fit values.

(E) Left: examples of single channel activity at +30 mV for $Ca_V2.1$ / β4 where more than one amplitude level was observed. Continuous lines mark the three amplitude levels, depicted by ■, level 1; ●, level2; ▲, level 3. Right: Single channel I-V plot to show the distinct conductances for data such as that shown. The single channel conductances for the three levels are 8.2 ± 1.2 pS, 12.1 ± 1.05 pS and 16.2 ± 0.46 pS (n = 6) and the corresponding amplitudes at +30 mV are -0.43 ± 0.027 pA, -0.63 ± 0.038 pA and -0.69 ± 0.033 pA.

(F) Mean open (left) and closed (right) times were similar at all voltages examined, for the 3 conditions respectively (O, n=8; □, n=8; Δ, n=6).

(G) FL probability histogram, for the 3 conditions respectively (O, n=8; □, n=8; Δ, n=5). Left: mean (± S.E.M, shown every 10 ms for clarity) cumulative FL probability distributions at +30 mV, and right: FL probability at 20 ms for all voltages examined.

(H) Steady-state inactivation of $Ca_V2.1$ ensemble currents from single and multi-channel patches. Left: An example of inactivation experiment. Top: the voltage protocol, holding potential, -100mV, followed by a 2 s. prepulse(pp) to a potential (V_{pp}) between –80 and +40 mV, followed by a test pulse to+40 mV for 100ms. Bottom: average ensemble currents (from the data as shown in (B) with a V_{pp} of +40 mV (left) and test pulse responses to V_{pp} of –80, +10 and +40 mV are superimposed. Right: all currents were normalized to the peak prepulse current at +40 mV and the ratio plotted as a function of V_{pp}. Data of the type shown in (A -C) respectively (O, n=11; □, n=11; Δ, n=4).

Figure 1

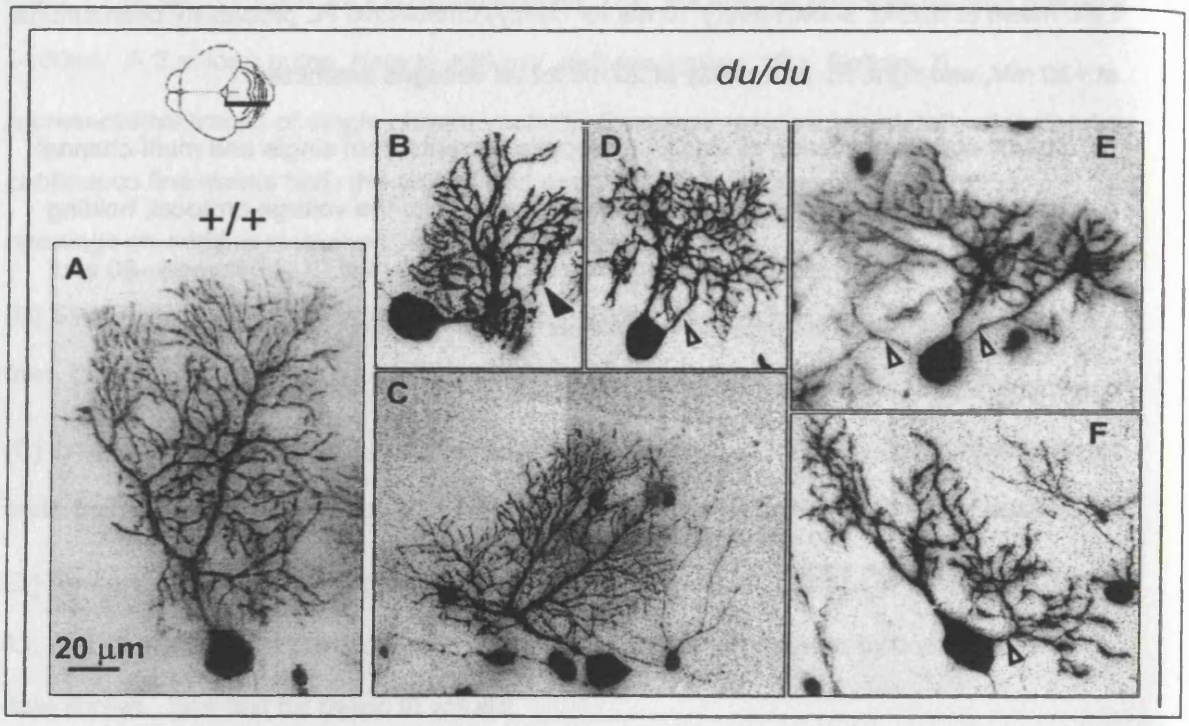

Figure 2

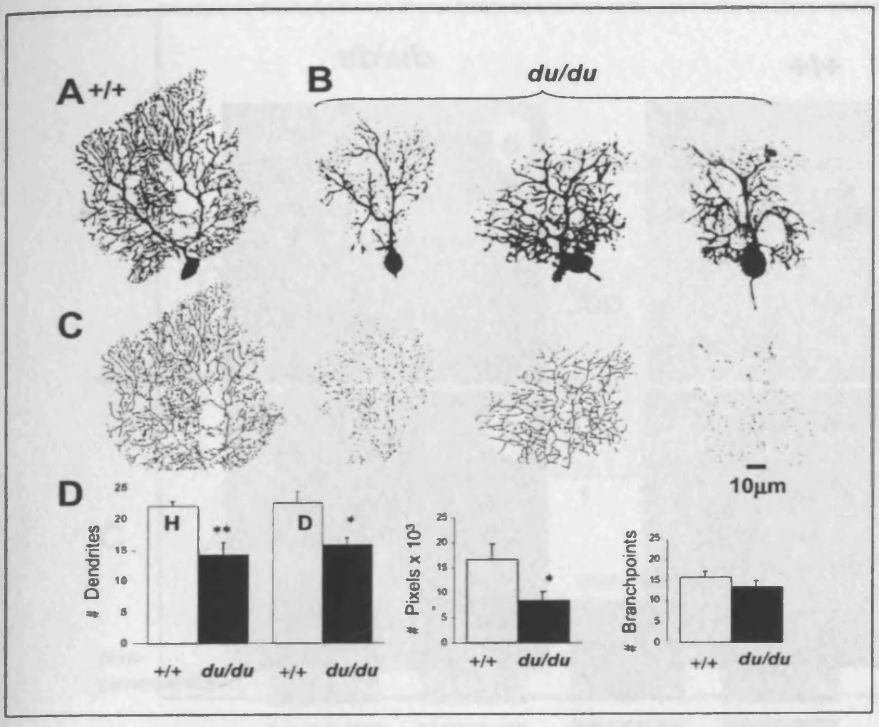
A +/+
B
du/du
C
10µm
D
Dendrites
H
D
**
*
+/+
du/du
+/+
du/du
Pixels x 10³
*
+/+
du/du
Branchpoints
+/+
du/du

Figure 3

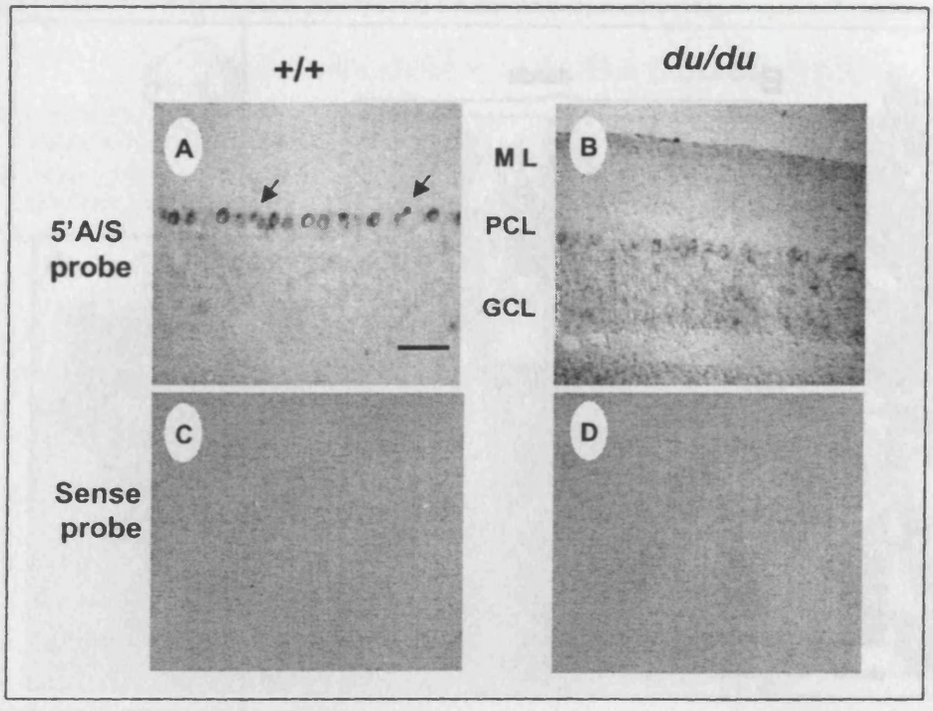

Figure 4

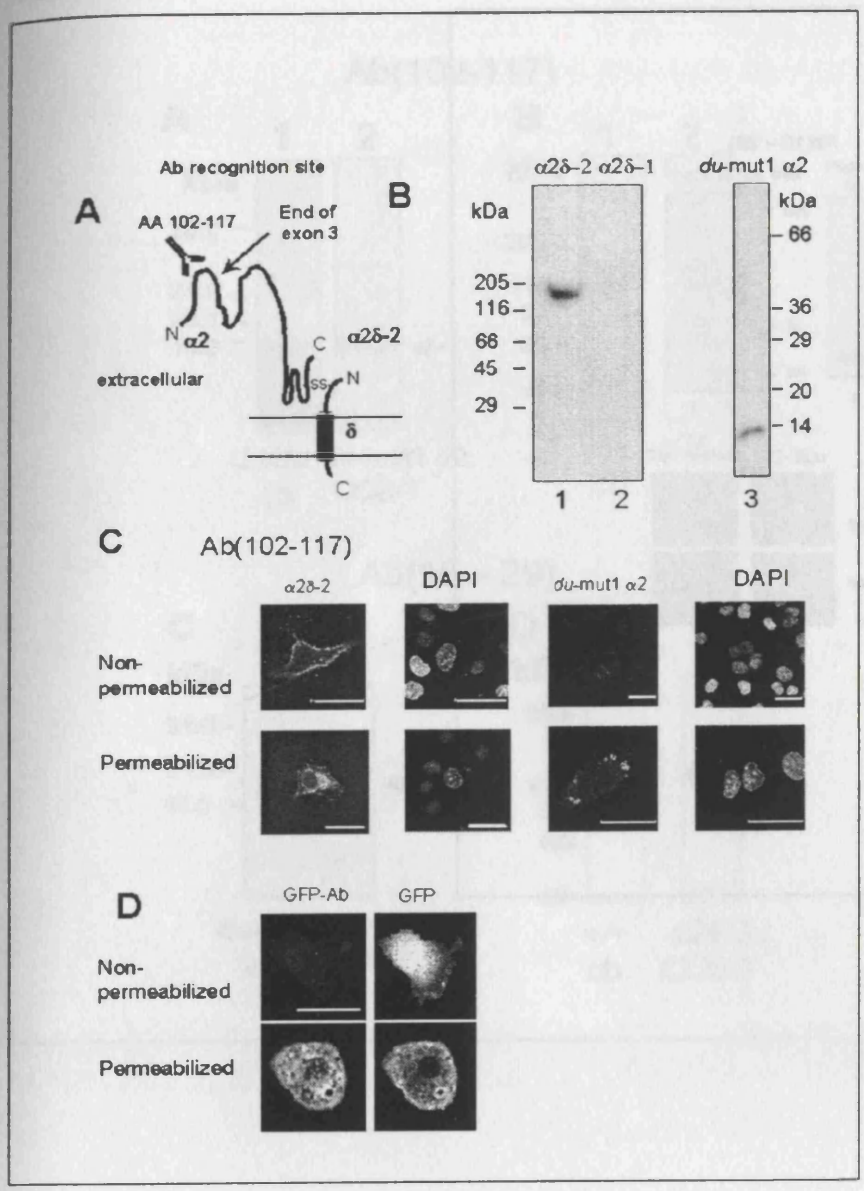
A
Ab recognition site
AA 102-117
End of exon 3
N
α2
C
α2δ-2
extracellular
ss
N
δ
C
B
α2δ-2 α2δ-1
du-mut1 α2
kDa
205
116
66
45
29
1
2
kDa
66
36
29
20
14
3
C
Ab(102-117)
α2δ-2
DAPI
du-mut1 α2
DAPI
Non-permeabilized
Permeabilized
D
GFP-Ab
GFP
Non-permeabilized
Permeabilized

Figure 5

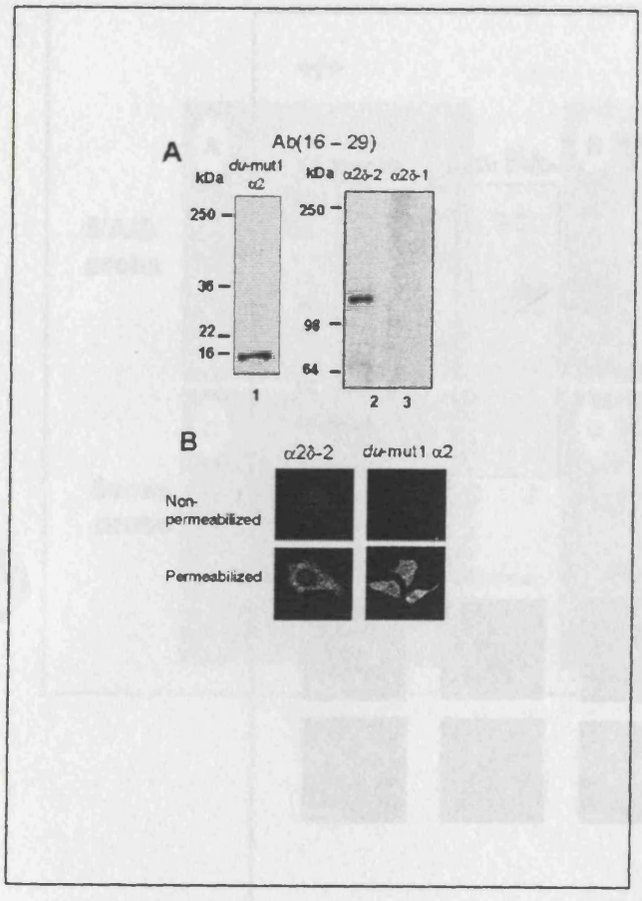
A
Ab(16 – 29)
kDa
du-mut1 α2
250
36
22
16
1
kDa
α2δ-2
α2δ-1
250
98
64
2
3
B
α2δ-2
du-mut1 α2
Non-permeabilized
Permeabilized

Figure 6

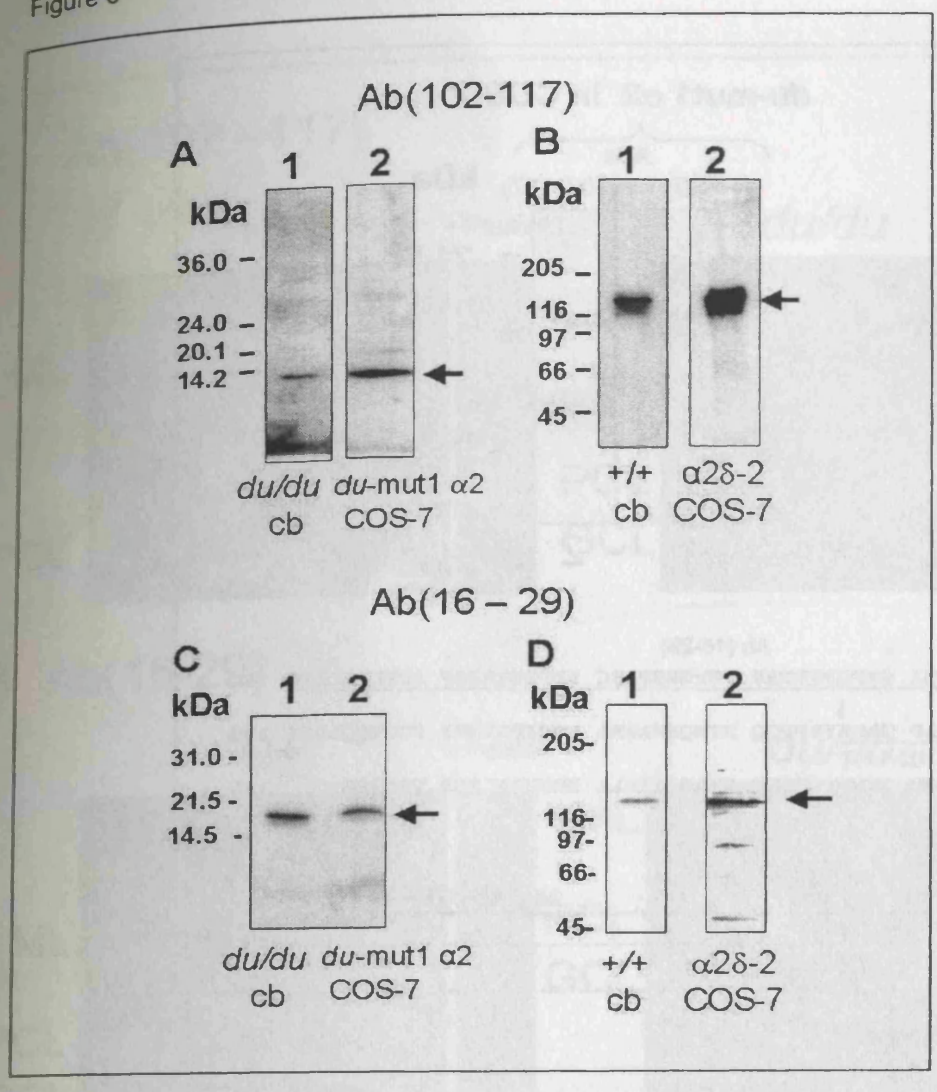
Ab(102-117)
A
1
2
kDa
36.0
24.0
20.1
14.2
du/du cb
du-mut1 α2 COS-7
B
1
2
kDa
205
116
97
66
45
+/+ cb
α2δ-2 COS-7
Ab(16 – 29)
C
1
2
kDa
31.0
21.5
14.5
du/du cb
du-mut1 α2 COS-7
D
1
2
kDa
205
116
97
66
45
+/+ cb
α2δ-2 COS-7

Figure 7

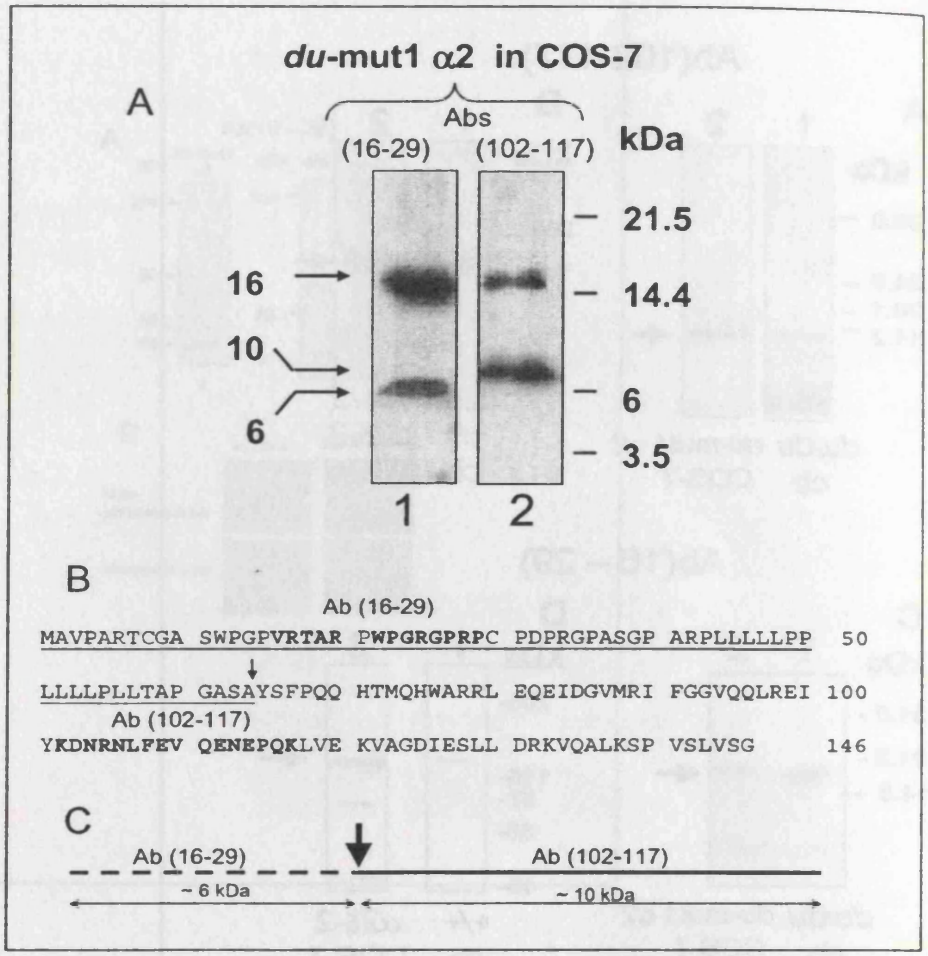
du-mut1 α2 in COS-7
A
Abs
(16-29)
(102-117)
kDa
21.5
14.4
6
3.5
16
10
6
1
2
B
Ab (16-29)
MAVPARTCGA SWPGPVRTAR PWPGRGPRPC PDPRGPASGP ARPLLLLLPP 50
LLLLPLLTAP GASAYSFPQQ HTMQHWARRL EQEIDGVMRI FGGVQQLREI 100
Ab (102-117)
YKDNRNLFEV QENEPQKLVE KVAGDIESLL DRKVQALKSP VSLVSG 146
C
Ab (16-29)
Ab (102-117)
~ 6 kDa
~ 10 kDa

Figure 8

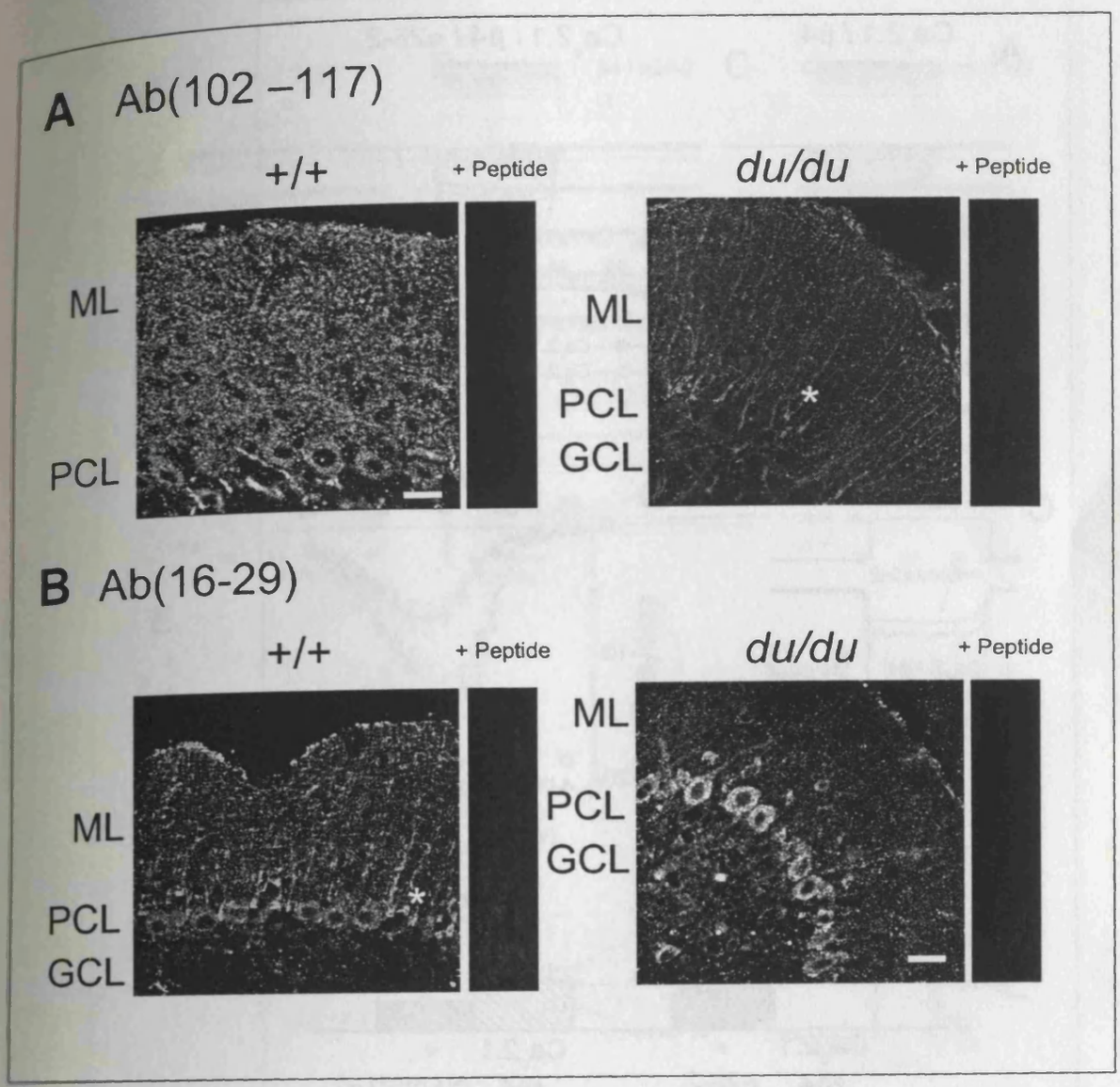
A Ab(102 –117)
+/+
+ Peptide
du/du
+ Peptide
ML
PCL
ML
PCL
GCL
B Ab(16-29)
+/+
+ Peptide
du/du
+ Peptide
ML
PCL
GCL
ML
PCL
GCL

Figure 9

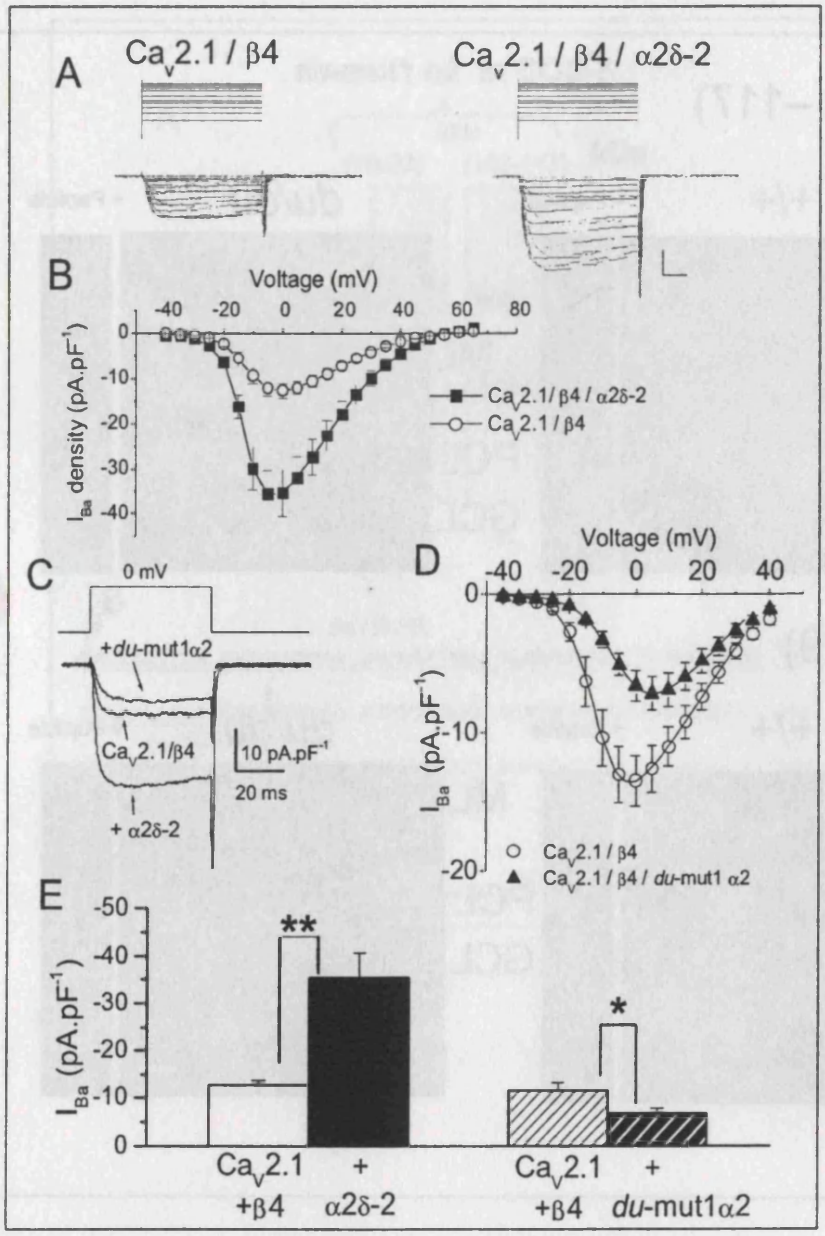
A
Ca$_V$2.1 / β4
Ca$_V$2.1 / β4 / α2δ-2
B
Voltage (mV)
-40 -20 0 20 40 60 80
0 -10 -20 -30 -40
I_{Ba} density (pA.pF^{-1})
Ca$_V$2.1 / β4 / α2δ-2
Ca$_V$2.1 / β4
C
0 mV
+du-mut1α2
Ca$_V$2.1/β4
10 pA.pF^{-1}
20 ms
+ α2δ-2
D
Voltage (mV)
-40 -20 0 20 40
0 -10 -20
I_{Ba} (pA.pF^{-1})
Ca$_V$2.1 / β4
Ca$_V$2.1 / β4 / du-mut1 α2
E
-50 -40 -30 -20 -10 0
I_{Ba} (pA.pF^{-1})
**
*
Ca$_V$2.1 +β4 + α2δ-2
Ca$_V$2.1 +β4 + du-mut1α2

Figure 10

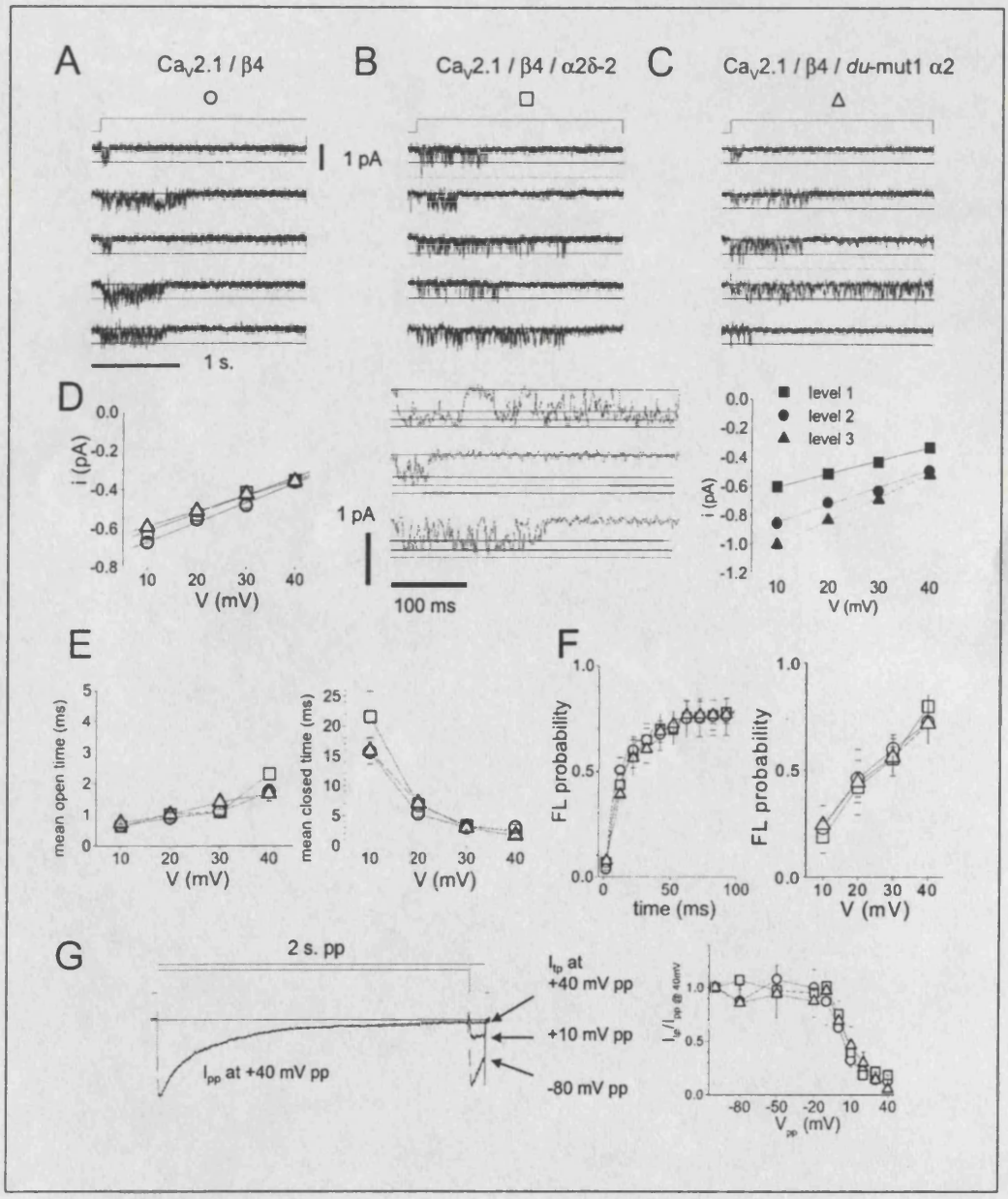
A
Ca$_V$2.1 / β4
B
Ca$_V$2.1 / β4 / α2δ-2
C
Ca$_V$2.1 / β4 / du-mut1 α2
1 pA
1 s.
D
i (pA)
V (mV)
1 pA
100 ms
level 1
level 2
level 3
E
mean open time (ms)
mean closed time (ms)
V (mV)
F
FL probability
time (ms)
V (mV)
G
2 s. pp
I$_{pp}$ at +40 mV pp
I$_{tp}$ at +40 mV pp
+10 mV pp
-80 mV pp
V$_{pp}$ (mV)

The Journal of Neuroscience, August 15, 2001, 21(16):6095–6104

Ducky Mouse Phenotype of Epilepsy and Ataxia Is Associated with Mutations in the *Cacna2d2* Gene and Decreased Calcium Channel Current in Cerebellar Purkinje Cells

Jane Barclay,[1] Nuria Balaguero,[2] Marina Mione,[3] Susan L. Ackerman,[4] Verity A. Letts,[4] Jens Brodbeck,[2] Carles Canti,[2] Alon Meir,[2] Karen M. Page,[2] Kenro Kusumi,[5] Edward Perez-Reyes,[6] Eric S. Lander,[5] Wayne N. Frankel,[4] R. Mark Gardiner,[1] Annette C. Dolphin,[2] and Michele Rees[1]

[1]Department of Paediatrics and Child Health, Royal Free and University College Medical School, The Rayne Institute, London, WC1E 6JJ, United Kingdom, Departments of [2]Pharmacology and [3]Anatomy and Developmental Biology, University College London, London, WC1E 6BT, United Kingdom, [4]The Jackson Laboratory, Bar Harbor, Maine 04609, [5]Whitehead Institute for Biomedical Research, Cambridge, Massachusetts 02142, and [6]Department of Pharmacology, University of Virginia Health System, Charlottesville, Virginia 22908-0735

The mouse mutant ducky, a model for absence epilepsy, is characterized by spike-wave seizures and ataxia. The ducky gene was mapped previously to distal mouse chromosome 9. High-resolution genetic and physical mapping has resulted in the identification of the *Cacna2d2* gene encoding the $\alpha 2\delta 2$ voltage-dependent calcium channel subunit. Mutations in *Cacna2d2* were found to underlie the ducky phenotype in the original ducky (*du*) strain and in a newly identified strain (du^{2J}). Both mutations are predicted to result in loss of the full-length $\alpha 2\delta 2$ protein. Functional analysis shows that the $\alpha 2\delta 2$ subunit increases the maximum conductance of the $\alpha 1A/\beta 4$ channel combination when coexpressed *in vitro* in *Xenopus* oocytes. The Ca^{2+} channel current in acutely dissociated *du/du* cerebellar Purkinje cells was reduced, with no change in single-channel conductance. In contrast, no effect on Ca^{2+} channel current was seen in cerebellar granule cells, results consistent with the high level of expression of the *Cacna2d2* gene in Purkinje, but not granule, neurons. Our observations document the first mammalian $\alpha 2\delta$ mutation and complete the association of each of the major classes of voltage-dependent Ca^{2+} channel subunits with a phenotype of ataxia and epilepsy in the mouse.

Key words: epilepsy; ataxia; calcium channel; subunit; Purkinje cell; cerebellum; mouse mutant

Five spontaneous autosomal recessive mouse mutations impart a phenotype that includes epileptic seizures with features similar to those occurring in human idiopathic generalized epilepsy (IGE) (Puranam and McNamara, 1999). Tottering ($Cacna1a^{tg}$, $Cacna1a^{tg\text{-}la}$), slow-wave epilepsy ($Slc9a1^{swe}$), lethargic ($Cacnb4^{lh}$), stargazer ($Cacng2^{stg}$, $Cacng2^{stg\text{-}wag}$), and ducky (*du*) exhibit bilaterally synchronous spike-wave discharges (SWDs) on cortical electroencephalogram (EEG) recordings. These are accompanied by behavioral arrest and respond to the human anti-absence drug ethosuximide (Noebels et al., 1997). The electrophysiological hallmark of human absence epilepsy is 3 Hz SWDs. In mice, the frequency is usually 5–7 Hz (Noebels, 1991), except for those in $Slc9a1^{swe}$ (1–3 Hz) (Cox et al., 1997). Mutations in genes encoding voltage-dependent calcium channel (VDCC) subunits underlie three of these phenotypes: the genes encoding the $\alpha 1A$ (*Cacna1a*), $\beta 4$ (*Cacnb4*), and $\gamma 2$ (*Cacng2*) subunits are mutated in tottering (Fletcher et al., 1996), lethargic (Burgess et al., 1997), and stargazer (Letts et al., 1998) mice, respectively.

Voltage-dependent Ca^{2+} currents have been measured in all excitable cells and are implicated in many cellular processes (Berridge et al., 1998). They have been divided on the basis of kinetics and pharmacology into L-, N-, P/Q-, R-, and T-types (Catterall, 1998). Each VDCC is composed of a pore-forming $\alpha 1$ subunit that may be associated with an intracellular β, a membrane-spanning γ, and a membrane-anchored, but predominantly extracellular, $\alpha 2\delta$ subunit. The $\alpha 1$ subunit determines the main biophysical properties of the channel and is modulated by the other subunits (Walker and De Waard, 1998). Mammalian genes encoding 10 $\alpha 1$, four β, eight γ, and three $\alpha 2\delta$ subunits have been identified (for a comprehensive list, see Ertel et al., 2000; Burgess et al. 2001).

Homozygotes for the ducky (*du*) allele are characterized by an ataxic, wide-based gait and paroxysmal dyskinesia (Snell, 1955). They display reduced size and a failure to breed or survive beyond 35 d. Neuropathological studies revealed dysgenesis of selective regions of the CNS, including the cerebellum, medulla, and spinal cord (Meier, 1968). Axonal dystrophy and demyelination were also reported. Heterozygotes show no obvious phenotype. The *du* locus was localized to mouse chromosome 9 by linkage to the phenotypic markers dilute and short ear (Snell, 1955).

To identify and characterize the *du* locus, a positional cloning strategy was adopted. High-resolution genetic mapping identified

Received March 2, 2001; revised May 10, 2001; accepted June 1, 2001.

This work was supported by the Medical Research Council (UK), The Wellcome Trust, the Epilepsy Research Foundation, and National Institutes of Health Grants NS32801 (to V.A.L.) and NS31348 (to W.N.F.). We thank Dr. David Hosford and Randy Byers for generously sharing their expertise; Mick Keegan, Chantal Longo, Jo-Maree Courtney, and Eileen Sun for excellent technical assistance; the Human Genome Mapping Project Resource Centre for access to resources; and Hannah Mitchison and Anna-Elina Lehesjoki for useful comments.

N.B. and M.M. contributed equally to this work.

Correspondence should be addressed to Michele Rees, Department of Paediatrics and Child Health, Royal Free and University College Medical School, The Rayne Institute, 5 University Street, London, WC1E 6JJ, UK. E-mail: m.rees@ucl.ac.uk.

J. Barclay's present address: Novartis Institute for Medical Sciences, 5 Gower Place, London WC1E 6BS, UK.

the gene encoding the VDCC α2δ2 subunit as a positional and functional candidate. Mutations in this gene were identified in the original *du* strain and in a new allele, du^{2J}. This paper presents evidence that the gene underlying the ducky phenotype encodes the α2δ2 subunit and explores the effect of a mutation on Ca^{2+} channel function in *du/du* brain.

MATERIALS AND METHODS

Genetic and physical mapping

Mice were obtained from The Jackson Laboratory (Bar Harbor, ME). DNA was prepared from tail biopsies or liver samples by standard methods. Microsatellite markers were amplified as described previously (Dietrich et al., 1996). Recombinants were identified by agarose gel electrophoresis or PAGE or single-strand conformation polymorphism (*MDB1432*) analysis. Yeast artificial chromosome (YAC) clones were identified by PCR-based library screens (Haldi et al., 1996) or from a web-based database of clones (Nusbaum et al., 1999). Genomic clones were obtained from the Human Genome Mapping Project Resource Centre (Cambridge, UK).

Candidate gene analysis

Total RNA was prepared from frozen tissue using RNAzol B (Biogenesis, Sandown, NH) and used to prepare mRNA or cDNA using mRNA purification or First Strand cDNA synthesis kits (Amersham Pharmacia Biotech, Little Chalfont, UK). Northern blot analysis of 10 μg of cerebellar mRNA using Duralon UV nylon membrane and full-length *Cacna2d2* or human β actin as probes (Stratagene, La Jolla, CA) was performed using the suggested conditions of the manufacturer to optimize the identification of the wild-type 5.5 kb *Cacna2d2* transcript. This may have resulted in underestimation of the quantity of smaller transcripts (<2 kb). The full-length *Cacna2d2* cDNA was assembled using degenerate primers, reverse transcription (RT)-PCR, rapid amplification of cDNA ends (RACE), and sequencing. All primer sequences are available on request. RACE was performed using the 5′/3′ RACE kit (Roche Diagnostics, Hertfordshire, UK). Sequencing was performed on an ABI 373XL sequencer using TaqFS chemistry (PE Applied Biosystems, Foster City, CA). Genomic DNA was embedded in agarose and subjected to pulsed field gel electrophoresis (PFGE) on a Bio-Rad (Hercules, CA) clamped homogeneous electrical field electrophoresis system.

Electrode implantation and EEG measurements

Homozygous du^{2J} and control unaffected mice (8–12 weeks of age) were tested for spontaneous seizure activity. Mice were anesthetized with tribromoethanol (400 mg/kg, i.p.) and placed in a stereotaxic holder fitted with a mouse incisor bar. Burr holes were drilled (1 mm posterior to bregma, 1 mm lateral to midline) on both sides of the skull. Two Teflon-coated bipolar electrodes were implanted at 0.4–0.8 mm below the dura. Three screws were placed at the periphery of the skull to anchor the dental cap. Mice were allowed to recover for 2 d before EEG recordings were measured. The parameters for determining spike-wave discharges were described previously (Hosford et al., 1995).

In situ *hybridization and immunohistochemical analyses*

Mice [aged postnatal day 21 (P21) to P24] were terminally anesthetized by CO_2 inhalation and perfused with 4% paraformaldehyde. The brain was dissected into cold paraformaldehyde and then transferred through a sucrose gradient before embedding in OCT (Agar) and sectioning. Alternatively, the brain was removed without fixing and frozen in liquid nitrogen. Cryostat sections (10–15 μm) were cut and air dried onto positively charged slides (BDH Laboratory Supplies, Poole, UK).

cDNA fragments corresponding to α2δ2 [nucleotide (nt) 3705–4909], α2δ1 (nt 3521–3895), and α2δ3 (nt 2581–3602) were subcloned into pBluescript SK+. Sense and antisense RNA probes were prepared using T3 or T7 polymerase and digoxigenin (DIG) RNA labeling mix and purified using Quick spin columns (Roche Diagnostics). *In situ* hybridization was performed as described previously (Eisenstat et al., 1999).

Immunohistochemistry was performed on perfused tissue and isolated cells with a polyclonal calbindin D28K antibody (Chemicon, Harrow, UK) and on perfused tissue alone with a polyclonal calretinin antibody (Chemicon).

Heterologous expression of cDNAs

cDNAs encoding rabbit α1A (X57689), rat β4 (LO2315), and mouse α2δ2 (predominant brain splice variant that lacks exon 23 and 6 bp of exon 38, as described by Barclay and Rees, 2000) cDNAs, cloned into the pMT2 vector, were injected intranuclearly into *Xenopus* oocytes as described previously (Canti et al., 1999), except that 4 nl of cDNA mixture was injected at 1 μg/μl. Recordings were made using two-electrode voltage clamp as described previously (Canti et al., 1999).

Purkinje cell and granule cell preparation and I_{Ba} measurement

Purkinje neurons. Cells were dissociated from P4–P8 mice (Mintz et al., 1992) and plated onto concanavalin-A (2 μg/ml)-coated coverslips. Whole-cell I_{Ba} was recorded 1–4 hr later with 5 mM Ba^{2+} as described previously (Mintz et al., 1992). Purkinje cell (PC) identity was confirmed by positive calbindin immunostaining ($n > 70$).

Cerebellar granule cells. Granule cells (GCs) were isolated and cultured from P6–P8 mice, and whole-cell I_{Ba} was recorded as described previously using 10 mM Ba^{2+} (Pearson et al., 1995), except that the internal pipette solution contained (in mM): 100 HEPES, 30 EGTA, 0.57 $CaCl_2$, 2.25 $MgCl_2$, 3.68 ATP, and 0.1 GTP (Tris salt), pH 7.2 (320 mOsm).

Cells were used for analysis when the holding current at the holding potential was <20 pA for GCs and <50 pA for PCs. The holding current did not differ between genotypes. Leak current was subtracted using P/8 protocol. Individual *I–V* relationships were fitted with the modified Boltzmann equation $I = G_{max} * (V - V_{rev})/(1 + \exp[-(V - V_{50})/k])$, where G_{max} is the maximum conductance, V_{rev} is the reversal potential, k is the slope factor, and V_{50} is the voltage for 50% current activation.

Single-channel recording

All recordings were performed as described by Meir et al. (2000). Experiments were performed on cell-attached patches from PCs at room temperature (20–22°C). Recording pipettes were pulled from borosilicate tubes (World Precision Instruments, Sarasota, FL), coated with Sylgard (Sylgard 184; Dow Corning, Wiesbaden, Germany), and fire polished to form high-resistance pipettes (~10 MΩ with 100 mM $BaCl_2$). The bath solution was composed of (in mM): 135 K-aspartate, 1 $MgCl_2$, 5 EGTA, and 10 HEPES (titrated with KOH, pH 7.3). The patch pipettes were filled with a solution of the following composition (in mM): 100 $BaCl_2$, 10 tetraethylammonium (TEA)-Cl, 10 HEPES, and 200 nM TTX, titrated with TEA-OH to pH 7.4. Both solutions were adjusted to an osmolarity of 320 mOsm with sucrose. Data were sampled (Axopatch 200B and Digidata 1200 interface; Axon Instruments, Foster City, CA), at 5 kHz and filtered on-line at 1 kHz. Voltages were not corrected for liquid junction potential (Neher, 1995) measured to be −15 mV in these solutions.

Leak subtraction was performed by averaging segments of traces with no activity from the same voltage protocol in the same experiment and subtracting this average from each episode using pClamp6 (Axon Instruments). Event detection was performed using the half-amplitude threshold method. Single-channel amplitude was determined by either a Gaussian fit to the binned amplitude distributions or the mean amplitude in two experiments at +10 mV when there was a small number of events.

All results are presented as mean ± SEM, and statistical differences were determined by the Student's *t* test.

GenBank accession numbers

DNA and protein sequences described here have been deposited in GenBank under the following accession numbers: wild-type *Cacna2d2*, AF247139; *du* mutant transcript 1, AF247140; *du* mutant transcript 2, AF247141; and du^{2J} mutant transcript, AF247142.

RESULTS

Genetic and physical mapping of the *du* locus

Two genetic crosses were used to refine the location of *du* (Fig. 1*a*). Progeny representing 1460 meioses (564 backcross progeny and 448 intercross progeny) were typed with microsatellite markers 53.6–63.4 centimorgans (cM) from the centromere on mouse chromosome 9 (Dietrich et al., 1996). This region was assembled in overlapping yeast artificial chromosome (YAC) clones (Fig. 1*b*). Sequence tagged sites (STSs) to *Dag1* and *Lamb2* (Skynner

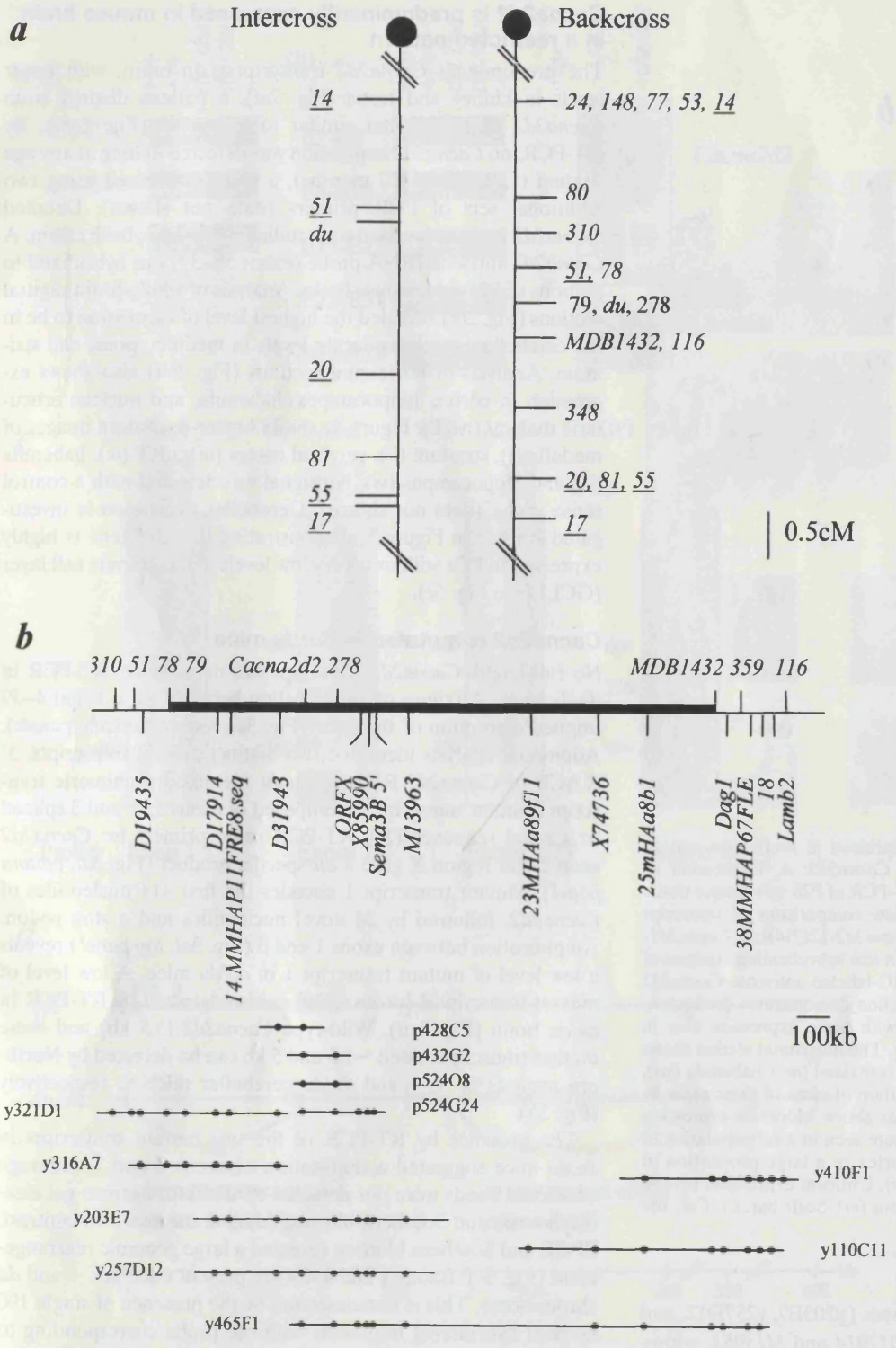

Figure 1. Genetic and physical maps define the *du* critical region. *a*, Genetic map around the *du* locus. The relation of the *du* gene to markers is shown to scale on partial chromosome linkage maps. Eight hundred ninety-six meioses of the (TKDU-+/*du* × STOCK $Dll3^{pu}$ + $Tyr^{c\text{-}ch}$/+ *p* $Tyr^{c\text{-}ch}$) F1 intercross place *du* between *D9Mit51* and *D9Mit20* (2.9 ± 0.1 cM). Five hundred sixty-four meioses from an intersubspecific backcross [(TKDU-+/*du* × CAST/Ei) × TKDU-+/*du*] show that *D9Mit78* and *MDB1432* flank *du*, placing it in a 0.8 ± 0.3 cM interval. *D9Mit* prefixes have been removed from the markers for clarity. *Underlined* markers were typed in both crosses. *b*, Physical map of the *du* region. Markers ordered genetically are shown above the *horizontal line*, and those ordered on the physical map only are placed below. The region around *du* is indicated by a *filled bar*. A contig of YACs was assembled as illustrated. Library identification is prefixed with *y*. Four PAC clones are indicated and prefixed with *p*. Marker content in genomic clones is indicated by *filled circles* aligned with markers on the physical map. Gene symbols are as follows: *Sema3B*, *semaphorin3B*; *Dag1*, *dystroglycan1*; *Lamb2*, *laminin*β*2*.

et al., 1995) localized both genes distal to the *du* critical region (Fig. 1*b*). The human orthologs of these genes map to chromosome 3p21 (Skynner et al., 1995). The STS sequences *D31943*, *M13963*, and *X85990* demonstrated significant similarities with *CISH* (Uchida et al., 1997), *GNAT1* (Blatt et al., 1988), and *SEMA3B* (Sekido et al., 1996), respectively. These genes map to human 3p21.3, indicating that the *du* gene is in a region of conserved linkage with this region.

Cacna2d2 is a candidate gene for the *du* locus

Cacna2d2 was identified as a candidate gene for *du* as a direct result of the conservation of linkage of human chromosome 3p21.3 with this region of mouse chromosome 9. Human chromosome 3p21.3 is frequently deleted in small cell lung carcinoma and has been the target of positional cloning efforts. One transcript (human gene *CACNA2D2*; GenBank accession number AF042792) isolated from this region showed 55.6% homology with the α2δ1 VDCC subunit gene (Klugbauer et al., 1999; Gao et al., 2000). Two mouse expressed sequence tags (GenBank accession numbers AA000341 and AA008996) with 91 and 82% nucleotide identity to *CACNA2D2* were identified by Basic Local Alignment Search Tool analysis. This mouse sequence (gene *Cacna2d2*) was used to design a genomic PCR assay to test YACs

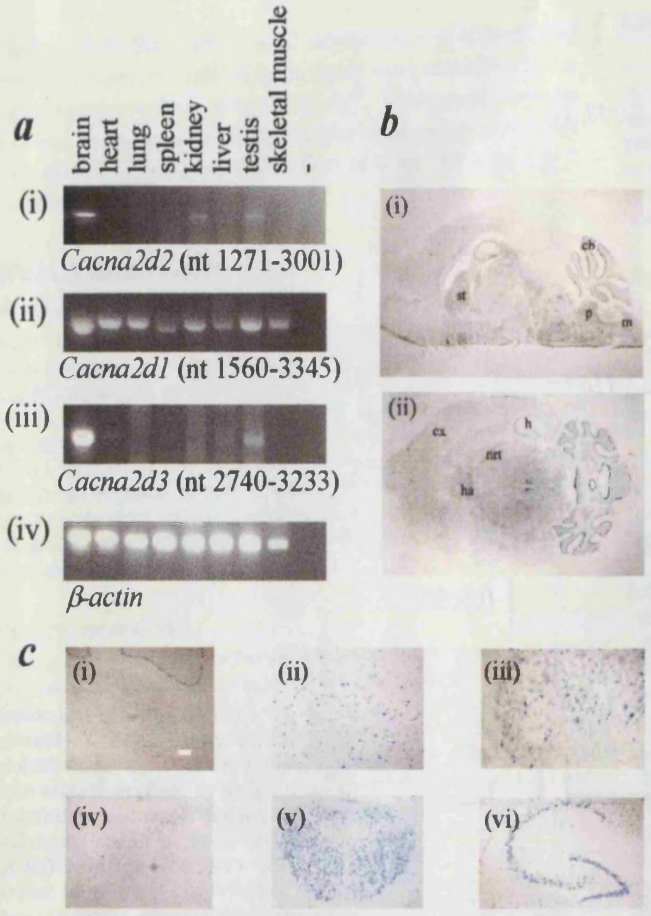

Figure 2. *Cacna2d2* is predominantly expressed in brain in a pattern distinct from *Cacna2d1* but similar to *Cacna2d3*. *a*, Expression of *Cacna2d2*, *Cacna2d1*, and *Cacna2d3* by RT-PCR of P28 +/+ mouse tissue RNA. β-Actin primers were used to allow comparisons of transcript levels. Negative control was no RNA. *i*, *Cacna2d2*-12F/14R; *ii*, *Cacna2d1*-1F/1R; *iii*, *Cacna2d3*-1F/1R; *iv*, β-actin. *b*, *In situ* hybridization analyses of whole-brain sections (P21 +/+) with a DIG-labeled antisense *Cacna2d2* RNA probe (nt 3705–4909). *i*, Sagittal section demonstrates the highest level of expression in cerebellum (*cb*), with some expression also in medulla (*m*), pons (*p*), and striatum (*st*). *ii*, The horizontal section shows expression in cortex (*cx*), nucleus reticularis thalami (*nrt*), habenula (*ha*), and hippocampus (*h*). *c*, Detailed examination of some of these areas by *in situ* hybridization with the same probe as above. Moderate expression is seen in medulla (*i*), and higher levels were seen in a subpopulation of cells of the striatum (*ii*) and cerebral cortex in a large proportion of cortical neurons throughout all layers (*iii*). Uniform expression is seen in nRT (*iv*), habenula (*v*), and hippocampus (*vi*). Scale bar: *Ci–Ciii*, 100 μ m; *Civ*, *Cv*, 50 μm.

from the *du* contig. Three positive clones (y203E7, y257D12, and y465F1) placed *Cacna2d2* between *D17914* and *M13963*, within the candidate interval (Fig. 1*b*). STS content mapping of four overlapping *Cacna2d2*-positive P1-artificial chromosomes (PACs) orientated the gene as 5′ to 3′ in a proximal to distal direction (Fig. 1*b*). An intragenic (CA)n repeat (α2δ2–43.21) was nonrecombinant with *du* in the backcross. Therefore, *Cacna2d2* was a good positional and functional candidate for *du*.

The 5.5 kb *Cacna2d2* cDNA (GenBank accession number AF247139) shared 91% nucleotide identity with *CACNA2D2*. The genomic structure of the *Cacna2d2* gene has been determined (see Fig. 3*d*) (Barclay and Rees, 2000). Overall, mouse α2δ2 shares 95% identity and 96.5% similarity with the human protein.

Cacna2d2 is predominantly expressed in mouse brain in a restricted pattern

The predominant *Cacna2d2* transcript is in brain, with lower levels in kidney and testis (Fig. 2*ai*), a pattern distinct from *Cacna2d1* (Fig. 2*aii*) but similar to *Cacna2d3* (Fig. 2*aiii*). By RT-PCR, no *Cacna2d2* expression was detected in lung at any age studied (1, 2, 6, and 20 months), a result confirmed using two additional sets of PCR primers (data not shown). Detailed *Cacna2d2* brain expression was studied by *in situ* hybridization. A *Cacna2d2* antisense RNA probe (exons 38–39) was hybridized to sections of P21 +/+ mouse brain. Analysis of whole-brain sagittal sections (Fig. 2*bi*) revealed the highest level of expression to be in the cerebellum, with moderate levels in medulla, pons, and striatum. Analysis of horizontal sections (Fig. 2*bii*) also shows expression in cortex, hippocampus, habenula, and nucleus reticularis thalami (nRT). Figure 2*c* shows higher-resolution images of medulla (*i*), striatum (*ii*), cerebral cortex (*iii*), nRT (*iv*), habenula (*v*), and hippocampus (*vi*). No signal was detected with a control sense probe (data not shown). Cerebellar expression is investigated further in Figure 5, demonstrating that the gene is highly expressed in PCs with only very low levels in the granule cell layer (GCL) (see Fig. 5*e*).

Cacna2d2 is mutated in *du/du* mice

No full-length *Cacna2d2* transcript was detected by RT-PCR in *du/du* mice. A failure of amplification between exon 1 and 4–39 implied disruption of the gene (Fig. 3*ai*, *top* and *middle panels*). Additional analysis identified two distinct mutant transcripts. 3′ RACE of *Cacna2d2* RNA in *du/du* identified a chimeric transcript (mutant transcript 1) composed of exons 1, 2, and 3 spliced to a novel sequence (X). RT-PCR using primers for *Cacna2d2* exon 1 and region X gave a *du*-specific product (Fig. 3*ai*, *bottom panel*). Mutant transcript 1 encodes the first 414 nucleotides of *Cacna2d2*, followed by 24 novel nucleotides and a stop codon. Amplification between exons 1 and 3 (Fig. 3*ai*, *top panel*) reveals a low level of mutant transcript 1 in *du/du* mice. A low level of mutant transcript 2 (exons 2–39) is also detected by RT-PCR in *du/du* brain (Fig. 3*aii*). Wild-type *Cacna2d2* (5.5 kb) and these mutant transcripts sized ~1.5 and 5 kb can be detected by Northern analysis of +/+ and *du/du* cerebellar mRNA, respectively (Fig. 3*b*).

The presence by RT-PCR of the two mutant transcripts in *du/du* mice suggested a duplication of exons 2 and 3, although additional bands were not detected by standard agarose gel electrophoresis and Southern blotting (data not shown). In contrast, PFGE and Southern blotting revealed a large genomic rearrangement (Fig. 3*c*). Exons 1 and 4–39 are present once per + and *du* chromosome. This is demonstrated by the presence of single 190 kb *Not*I hybridizing fragments with the probe corresponding to these exons (Fig. 3*ci*,*ciii*) in both genotypes. Exons 2–3 and region X are present once per + chromosome and twice per *du* chromosome, as indicated by the single (190 kb) and double (190 and 600 kb) *Not*I fragments (Fig. 3*cii*), respectively. This supports a genomic duplication of exons 2–3 and region X. The large size (>150 kb) of this duplication precludes its identification by conventional PCR and sequencing or Southern blotting because internal primer sites and restriction sites have been duplicated without disruption, preventing any distinction between original and duplicated exons. The wild-type position of region X as 3′ to the *Cacna2d2* gene was confirmed by PCR amplification of the PAC clones (Fig. 1*b*). In genomic DNA, the copy of region X common to +/+ and *du/du* contains two B2 repeat elements, and

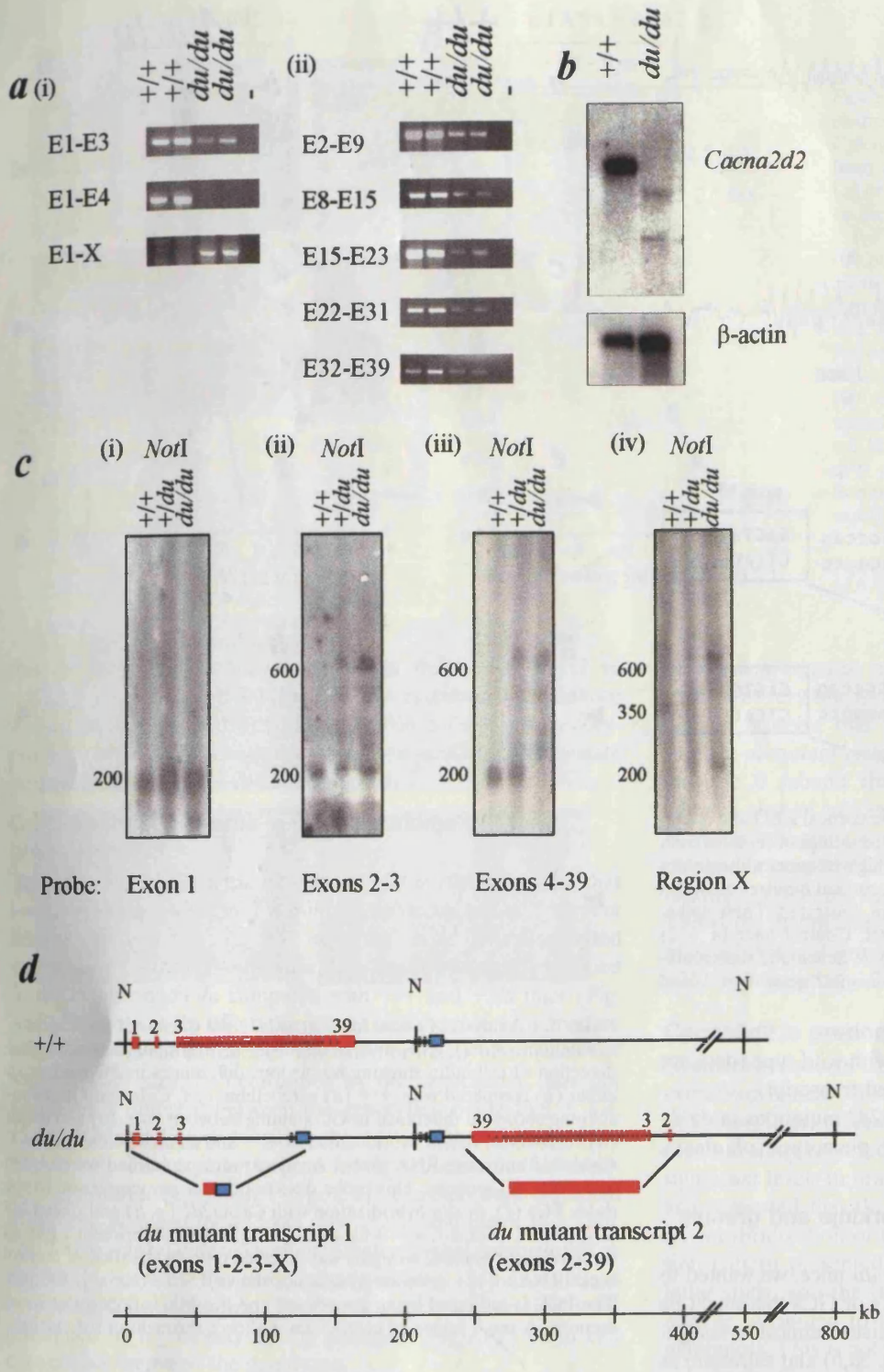

Figure 3. The *du* mutation is a genomic rearrangement involving the *Cacna2d2* gene. *a*, Two mutant transcripts can be identified by RT-PCR of total brain RNA from *du*/*du* mice. Two +/+, two *du*/*du* samples, and a negative control (no RNA) are shown per gel. *i*, *Top*, Normal size amplification product of exons 1–3 is shown in +/+ and *du*/*du* RNA, with reduced levels in the latter. *Middle*, Amplification between exons 1 and 4 does not produce a product in *du*/*du* RNA, suggesting disruption of the *Cacna2d2* gene in this region. *Bottom*, Amplification of the *du*-specific chimeric transcript of *Cacna2d2* exons 1, 2, and 3 and a novel sequence X. *ii*, Overlapping PCR fragments spanning exons 2–39 of *Cacna2d2* can be detected in +/+ and *du*/*du* RNA, with lower levels observed in *du*/*du* samples. *b*, Wild-type *Cacna2d2* transcript (5.5 kb) is absent from *du*/*du* brain by Northern analysis using cerebellar mRNA and full-length *Cacna2d2* as a probe. Low levels of two *du*-specific bands (~1.5 and 5 kb) are detected. The filter was rehybridized with β-actin as a control for RNA loading. *c*, PFGE shows duplication of *Cacna2d2* exons 2 and 3 and region X in *du*/*du* genomic DNA. Southern analysis of *Not*I-digested genomic DNA separated by PFGE from +/+, +/*du*, and *du*/*du* mice is shown. Blots were hybridized with *Cacna2d2* probes: *i*, exon 1; *ii*, exons 2–3; *iii*, exons 4–39; *iv*, region X. Sizes are in kilobases. *d*, A scale representation of the genomic region containing *Cacna2d2* (*red*) and region X (*blue*) in +/+ and *du*/*du* mice. *N*, *Not*I sites. The presence of one or two B2 repeats 5′ to region X is marked by a *vertical line*. The mutant transcripts 1 and 2 produced from each region in *du*/*du* are represented by *colored boxes*. The *Cacna2d2* gene is arranged 5′ to 3′ in +/+. In *du*/*du*, exons encoding mutant transcript 1 are shown in a 5′ to 3′ direction, and those encoding mutant transcript 2 are inverted and shown 3′ to 5′. The distance between exon 3 and region X is unknown but is >12 kb. The scale bar is in kilobases.

the *du*-specific copy contains a single B2 repeat (Fig. 3*d*). A plausible mutation mechanism, possibly mediated by the B2 repeats, is a head to tail duplication of *Cacna2d2* exons 2–39 and region X, followed by a deletion including exons 4–39 of the original *Cacna2d2*.

A second, distinct mutation of *Cacna2d2* in du^{2J}/du^{2J} mice

Recently, a spontaneous, autosomal recessive mouse mutant, with ataxia and paroxysmal dyskinesia, arose at The Jackson Laboratory. Breeding experiments established it as a novel ducky allele: du^{2J}. Cortical EEG recordings from du^{2J}/du^{2J} revealed infrequent bilateral SWDs of high amplitude (500 μV) and 5–7 Hz (Fig. 4*a*). These spontaneous discharges were accompanied by behavioral arrest. To determine whether these discharges were seizure related, an intraperitoneal injection of ethosuximide (100 mg/kg) was given, and the discharges were abolished.

Mutational analysis of *Cacna2d2* in du^{2J}/du^{2J} mice by RT-PCR and genomic sequencing revealed a 2 bp deletion (TG) within exon 9 (Fig. 4*b*) predicted to cause premature truncation of the protein (GenBank accession number AF247142). Sequence analysis of 45 subclones of the du^{2J}/du^{2J} RT-PCR product failed to detect any wild-type transcript (data not shown). Northern analysis of mRNA from du^{2J}/du^{2J} brain showed no difference in

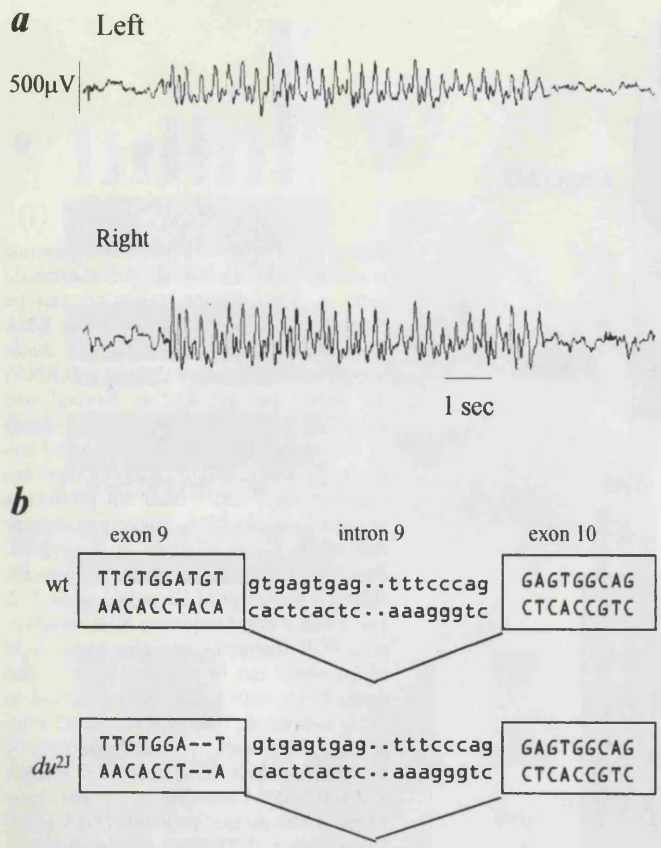

Figure 4. du^{2J}/du^{2J} mice show 5–7 Hz SWD on cortical EEG and a 2 bp deletion in *Cacna2d2*. *a*, Representative EEG recordings of seizures from homozygous du^{2J}/du^{2J} mice ($n = 8$). Low- and high-frequency filters were set at 0.3 and 35 Hz, respectively. Traces from cortical bipolar electrodes implanted in the left and right hemispheres are illustrated. These spike-wave discharges accompanied behavioral arrest. Control mice ($n = 2$) showed no abnormal activity (data not shown). *b*, Schematic representation of exons 9 and 10 and intron 9 of the *Cacna2d2* gene in +/+ and du^{2J}/du^{2J} genomic DNA.

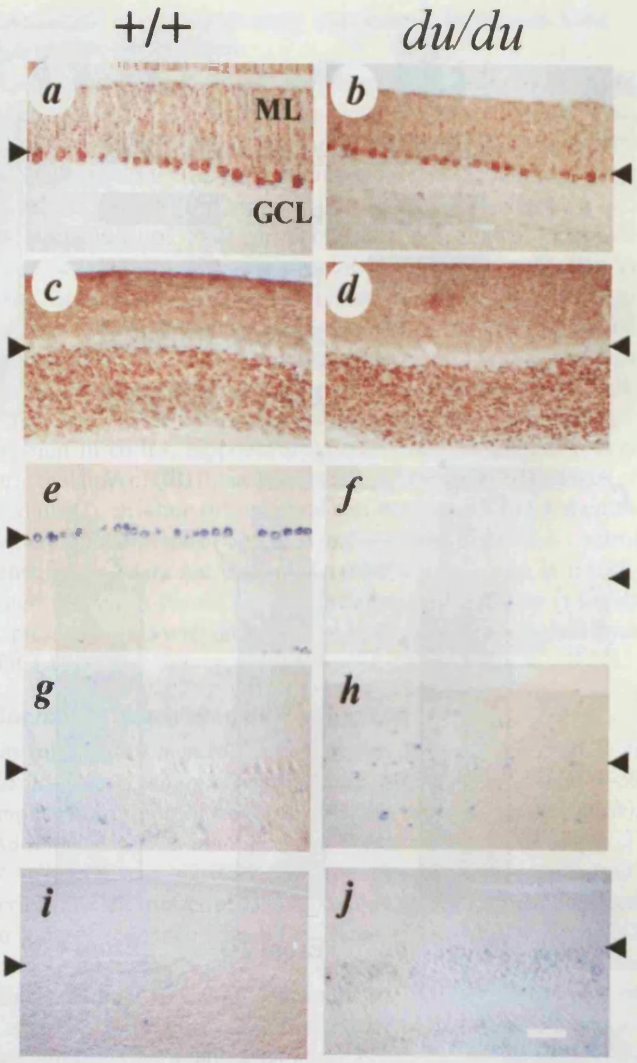

Figure 5. Analysis of *Cacna2d2*, *Cacna2d1*, and *Cacna2d3* expression in cerebellum of P21 +/+ and *du/du* mice. *a*, *b*, Immunohistochemical detection of calbindin showing no obvious differences in PC number in *du/du* (*b*) compared with +/+ (*a*) cerebellum. *c*, *d*, Calretinin immunostaining shows no difference in GC staining between +/+ (*c*) and *du/du* (*d*) cerebellum. *In situ* hybridization of +/+ and *du/du* sections with a 3′ *Cacna2d2* antisense RNA probe. Analyses were performed on +/+ (*e*) and *du/du* (*f*) sections. This probe does not detect any expression in the *du/du* PCs (*f*). *In situ* hybridization with *Cacna2d1* (*g*, *h*) and *Cacna2d3* (*i*, *j*) probes. (For *a–j*, $n = 3$ for each genotype and experiment.) For all three riboprobes used, no signal was detected on hybridization of control sense RNA to +/+ sections (results not shown). Scale bar: *a–j*, 100 μm. The PCL is indicated by an *arrowhead*, and the ML is *uppermost* in all sections. A small region of cerebellum is shown throughout for clarity.

Cacna2d2 transcription levels compared with wild type (data not shown), suggesting stability of the mutated transcript.

These observations suggest that *Cacna2d2* mutations in *du/du* and du^{2J}/du^{2J} mice underlie the ducky phenotype of ataxia, SWDs, and paroxysmal dyskinesia.

Immunohistochemistry of *du/du* Purkinje and granule cells reveals no cell loss

In view of the cerebellar pathology in *du/du* mice, we wanted to identify whether there was any loss of PCs or GCs that might be responsible for this. However, immunohistochemical investigations using calbindin as a PC marker (Fig. 5*a*,*b*) and calretinin as a GC marker (Fig. 5*c*,*d*) did not identify loss of cell bodies in *du/du* cerebella at P21 (Fig. 5*b*,*d*). Similar observations were made for du^{2J}/du^{2J} (data not shown).

Absence of full-length α2δ2 in *du/du* cerebellar Purkinje cells

In situ hybridization with a 3′ *Cacna2d2* anti-sense RNA probe (Fig. 5*e*,*f*) was used to demonstrate the presence of full-length *Cacna2d2* message in +/+ PCs (Fig. 5*e*) and its absence in *du/du* PCs (Fig. 5*f*).

The possibility of compensatory upregulation of *Cacna2d1* (Fig. 5*g*,*h*) and *Cacna2d3* (Fig. 5*i*,*j*) transcript levels in *du/du* cerebella was investigated by *in situ* hybridization with antisense RNA probes. No major differences were observed in their distribution in *du/du* compared with +/+ cerebellum, and in particular there was no compensatory expression of α2δ1 or α2δ3 mRNA in *du/du* PCs.

Modulation of Ca^{2+} channel currents by α2δ2

The physiological function of the α2δ2 subunit encoded by the *Cacna2d2* gene was investigated using *in vitro* expression and electrophysiology. To mimic the composition of the predominant calcium channels in cerebellar Purkinje cells, we examined the effect of α2δ2 when coexpressed with α1A and β4 in *Xenopus* oocytes. Coexpression of α2δ2 induced a large enhancement of α1A current amplitude (Fig. 6*a*,*b*). For example, at 0 mV, the increase was from -0.55 ± 0.15 ($n = 14$) to -1.8 ± 0.27 μA ($n = 13$), and there was a small hyperpolarization of current activation,

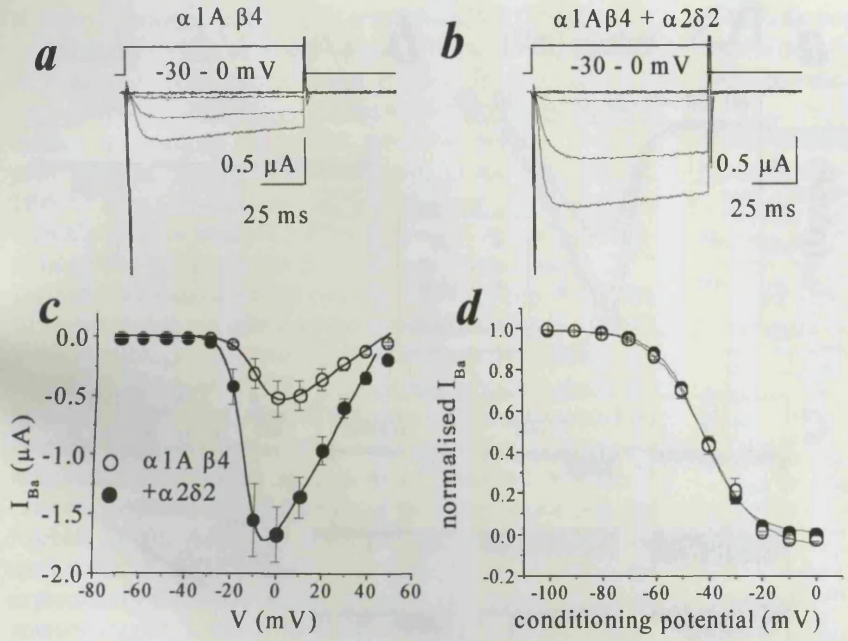

Figure 6. The effect of α2δ2 on α1A/β4 calcium channel currents expressed in *Xenopus* oocytes. *a*, *b*, Calcium channel currents recorded in 5 mM Ba^{2+} from *Xenopus* oocytes injected with either α1A/β4 (*a*) or α1A/α2δ2/β4 (*b*). For clarity, only the currents on the rising phase of the *I–V* relationship are shown. *c*, *I–V* relationship of α1A/β4 (○) and α1A/α2δ2/β4 (●) peak currents (n = 14 and 13, respectively). The mean *I–V* relationships were fitted with a combined Boltzmann and linear fit, as described in Materials and Methods. No significant differences were observed in the V_{rev} or k (results not shown). *d*, Steady-state inactivation of α1A/β4 (○) and α1A/α2δ2/β4 (●) currents (n = 14 and 13, respectively) were obtained by stepping to the conditioning potential for 25 sec, before measuring the current at the test potential of 0 mV. Individual data were fitted with a single Boltzmann equation of the form $I/I_{max} = 1/(1 + \exp[(V - V_{50})/k])$, where k is the slope factor and V_{50} is the voltage for 50% steady-state inactivation of the current. The $V_{50(inactivation)}$ was −41.73 ± 1.0 mV for α1A/β4 and −41.68 ± 1.1 mV for α1A/α2δ2/β4.

the voltage for 50% activation shifting from −6.4 ± 0.7 to −12.0 ± 1.4 mV ($p < 0.01$) (Fig. 6*c*). The maximum conductance was increased from 0.013 ± 0.003 to 0.036 ± 0.005 μS by coexpression of α2δ2. There was no effect of α2δ2 on steady-state inactivation of α1A/β4 currents (Fig. 6*d*).

Ca^{2+} channel currents in *du/du* Purkinje cells and granule cells

The effects of α2δ2 on the α1A/β4 current *in vitro* suggested that loss of wild-type α2δ2 may result in a reduction in Ca^{2+} current density. To test this, I_{Ba} was examined in acutely dissociated cerebellar PCs from P4–P8 mice. I_{Ba} density was clearly reduced in the PCs from *du/du* compared with +/+ and +/*du* mice (Fig. 7*a*,*b*). There was no effect on voltage dependence of activation (Fig. 7*a*) or on the kinetics of activation or inactivation (data not shown). Cell size, as determined by the capacitance, was not significantly different between the genotypes, being 14.9 ± 1.4, 15.1 ± 0.9, and 17.6 ± 1.7 pF in the +/+, +/*du*, and *du/du* PCs, respectively. To examine the basis for the reduction in the whole-cell I_{Ba} in *du/du* PCs, single P-type Ca^{2+} channels were examined in the cell-attached mode from +/+, +/*du*, and *du/du* PCs (Fig. 7*c*). There was no difference in the single-channel conductance or amplitude between the three genotypes (Fig. 7*d*). In cultured cerebellar GCs, taken from P6–P8 mice, there was no significant difference in I_{Ba} density at any potential (Fig. 7*e*,*f*) or in cell capacitance between the genotypes.

DISCUSSION

Our data provide strong evidence that the ducky phenotype is associated with mutations in the *Cacna2d2* gene. This is discussed together with a consideration of the normal expression pattern and function of the VDCC α2δ2 accessory subunit it encodes and how disruption of this function leads to the phenotypic features of ataxia and spike-wave seizures.

Cacna2d2 is disrupted in *du* and du^{2J} mice

These studies demonstrate that wild-type *Cacna2d2* transcript is absent from the brain of *du/du* and du^{2J}/du^{2J} mice. In *du/du* mice, a genomic rearrangement disrupts *Cacna2d2* and duplicates a nonfunctional open reading frame, region X, although the exact mechanism remains unclear. Mutant transcripts 1 and 2 are present at very low levels in *du/du* mice and, if translated, would encode proteins that are unlikely to function normally. The product of mutant transcript 1 would lack most of the α2 subunit and the δ subunit that includes the transmembrane domain, whereas that of mutant transcript 2 is unlikely to be trafficked correctly without a signal sequence. In du^{2J}/du^{2J} mice, a 2 bp deletion in exon 9 of *Cacna2d2* would result in a truncated protein lacking >800 amino acids, including the transmembrane domain. This is the first mammalian phenotype associated with disruption of an α2δ subunit gene and should allow the physiological roles of α2δ2 and the other α2δ subunits to be characterized further.

Cacna2d2 is predominantly expressed in mouse brain

Northern analysis of *CACNA2D2* in human tissue showed highest expression in heart, pancreas, and skeletal muscle and lower levels in kidney, liver, placenta, and brain (Klugbauer et al., 1999). A separate study reported highest expression in lung and testis and significant levels in brain, heart, and pancreas (Gao et al., 2000) and suggested that the pattern in the former study may reflect cross-hybridization of the probe with *CACNA2D1*. The expression pattern presented here corresponds more closely with the latter study, and the differences observed (particularly in lung) may be attributed to species differences and/or developmental differences. This is not unprecedented (Fougerousse et al., 2000).

In brain, *Cacna2d2* expression was highest in cerebellar PCs but was also detected in cerebral cortex, hippocampus, cerebellar GCs, nRT, habenula, pons, and medulla. The genes encoding the α2δ1, α2δ2, and α2δ3 subunits show generally distinct patterns of expression within the cerebellum. *Cacna2d1* is predominantly expressed in the GCL, *Cacna2d2* is predominant in the Purkinje cell layer (PCL), and *Cacna2d3* expression is detected in the molecular layer (ML) (Klugbauer et al., 1999; Hobom et al., 2000; present study). Most of the α1, β, and γ subunit genes share at least one region of expression with *Cacna2d2*, making it difficult to predict *in vivo* interactions based on expression profiles. However, the similarity of the ducky phenotype to that observed in mice with mutations in genes encoding the α1A and β4 subunits (Fletcher et al., 1996; Burgess et al., 1997) and their predominant

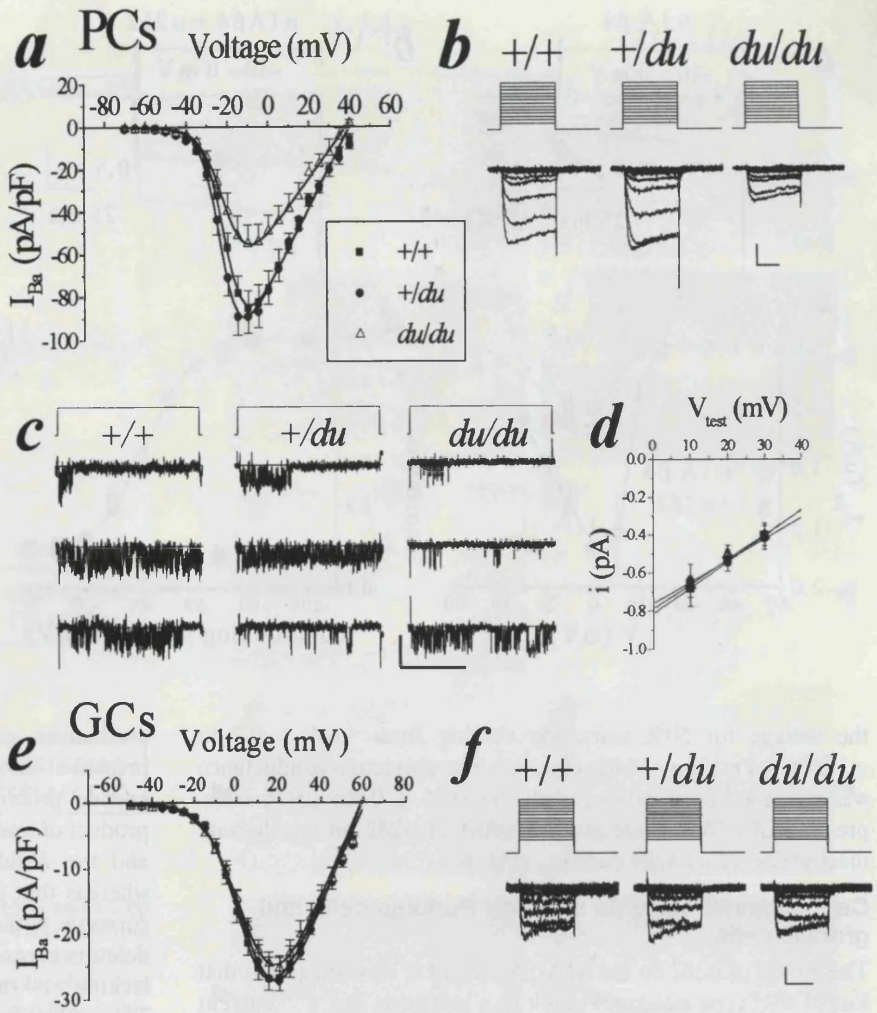

Figure 7. Calcium channel currents in cerebellar Purkinje cells and granule cells. *a*, *I–V* relationships in PCs from +/+ (n = 19), +/*du* (n = 32), and *du*/*du* (n = 14) mice. Genotypes as indicated in the figure. Cells were held at −80 mV. At −10 mV, the I_{Ba} density was −84.9 ± 8.2, −90.5 ± 7.8, and −54.2 ± 8.9 pA/pF in the +/+, +/*du*, and *du*/*du* PCs, respectively ($p < 0.05$ for *du*/*du* vs +/+; $p < 0.01$ for *du*/*du* vs +/*du*). There was no significant difference between the genotypes in the kinetics of activation or in the inactivation over 50 msec. The 10–90% rise times at −10 mV were 3.5 ± 0.2, 3.4 ± 0.2, and 3.9 ± 0.2 msec in +/+, +/*du*, and *du*/*du* PCs, respectively, and the respective percentage of inactivation in 50 msec was 13.6 ± 1.3, 16.4 ± 0.9, and 17.1 ± 2.0%. Calibration: 30 pA/pF, 20 msec. *b*, Example current traces from +/+, +/*du*, and *du*/*du* PCs. The currents were elicited by 50 msec voltage steps from −70 to −10 mV. I_{Ba} density is reduced in PCs from *du*/*du* mice compared with +/+ mice. *c*, Ca^{2+} channel activity in cell-attached patches from PCs of +/+ (*left*; two overlapping openings are evident, indicative of at least two channels active in the patch of membrane recorded), +/*du* (*middle*; two channels in patch), and *du*/*du* (*right*; single channel) mice. *Top*, The voltage protocol; holding potential, −70 mV; test potential, +20 mV, for 500 msec, delivered every 5 sec. Three representative current traces are shown for each cell; openings are *downward deflections*, and the *horizontal lines* that run through the *traces* represent the closed state. Calibration: 1 pA, 250 msec. *d*, Similar single-channel conductance for VDCCs in PCs of +/+, +/*du*, and *du*/*du* mice using the same symbols as in *a*. Single-channel amplitudes were measured at three different voltages and averaged for each population. n = 3–4, 4–5, and 2–6 patches for +/+, +/*du*, and *du*/*du*, respectively. The single-channel conductance was determined by fitting a linear function to the mean data and was 13.8, 11.4, and 13 pS, respectively. *e*, *I–V* relationships for GCs from +/+ (n = 35), +/*du* (n = 18), and *du*/*du* (n = 23) mice. Cells were held at −70 mV. The mean *I–V* relationships were fitted with a combined Boltzmann and linear fit. *f*, Example current traces from +/+, +/*du*, and *du*/*du* GCs. The currents shown were elicited by 100 msec depolarizing voltage steps from −50 to +15 mV. Calibration: 10 pA/pF, 50 msec.

PC expression pattern suggests that α2δ2 contributes to the P-type current.

α2δ2 interacts *in vitro* with the α1A/β4 combination

In vitro studies have shown that α2δ1 and α2δ3 subunits increase peak current amplitude and alter the kinetics of inactivation for a number of different α1 subunits (Walker and De Waard, 1998; Dolphin et al., 1999; Klugbauer et al., 1999). *In vitro* studies with human α2δ2 also demonstrate increased peak current amplitude for several α1 subunits (Gao et al., 2000). Our results show that mouse α2δ2 causes a 2.8-fold increase in maximum conductance for the α1A/β4 subunit combination when coexpressed in *Xenopus* oocytes.

Mechanism of the altered Ca^{2+} channel current in *du*/*du* PCs

The *in vitro* expression data suggested that disruption of α2δ2 expression in ducky mice may result in a decrease of the Ca^{2+} channel current in cells that express *Cacna2d2*. Electrophysiological recordings from isolated *du*/*du* PCs confirmed this hypothesis, with a 35% decrease in the peak P-type Ca^{2+} current density in *du*/*du* compared with +/+ PCs. This result has been confirmed recently by Ca^{2+} imaging experiments (J. Brodbeck and A. C. Dolphin, unpublished results). Furthermore, the comparable single P-type Ca^{2+} channel conductance in the two genotypes indicates that the reduction in I_{Ba} density reflects either a change in the number of functional channels or their open probability. The ducky mouse represents the first example of an accessory VDCC subunit mutant with a measurable effect in PCs. Recordings from α1A mutant mice PCs also revealed changes in the P-type Ca^{2+} current compared with that in wild-type PCs (Dove et al., 1998; Lorenzon et al., 1998; Wakamori et al., 1998; Jun et al., 1999). Similar studies performed on lethargic mice, however, showed no differences from wild type, potentially as a result of compensation by other β subunits (Burgess et al., 1999). The low levels of *Cacna2d1* and *Cacna2d3* transcripts in the PCs may preclude such compensation in PCs of *du*/*du* mice, and indeed no upregulation of these mRNAs was seen in *du*/*du* PCs. *In vitro* recordings from cultured *du*/*du* and +/+ GCs demonstrated no significant difference in the Ca^{2+} channel current, consistent with the lower expression levels of *Cacna2d2* in the GCL.

Calcium channel dysfunction and the ducky phenotype

It is likely that several features of the ducky phenotype, including the SWDs, ataxia, and paroxysmal dyskinesia, are attributable to loss of full-length functional α2δ2 in neurons of ducky mice. The occurrence of these traits in other mice with mutations in genes encoding VDCC subunits supports this hypothesis.

Homozygous *Cacna1a*^{tg}, *Cacnb4*^{lh} *Cacng2*^{stg}, *du*, and *du*^{2J} mice

all exhibit generalized bilaterally symmetrical SWDs with a frequency of 5–7Hz (Noebels and Sidman, 1979; Noebels et al., 1990; Hosford et al., 1992; present study). Evidence from animal models suggests that SWDs are generated by aberrant thalamocortical oscillations involving neocortical pyramidal neurons, thalamic relay neurons, and GABAergic neurons of the nRT (Snead, 1995). T-type Ca^{2+} currents underlie thalamic oscillations, and VDCCs have an essential role in presynaptic release of neurotransmitters, providing two potential mechanisms linking Ca^{2+} currents and thalamocortical circuits (Coulter, 1997). Reduction of excitatory but not inhibitory synaptic transmission in the thalamus of lethargic and tottering mice has been documented previously (Caddick et al., 1999), and it was proposed that a net enhanced GABAergic input in thalamocortical neurons may synchronize them into a burst firing mode. In contrast, hippocampal neurotransmitter release appears to be stabilized by a Ca^{2+} current compensatory mechanism in the same mice (Qian and Noebels, 2000). Additional work is required to elucidate the mechanism of SWD generation in ducky mice. However, the expression of *Cacna2d2* within the nRT and cortical pyramidal neurons suggests a similar mechanism may be involved.

An ataxic gait is first detectable between P10 and P21 in tottering, lethargic, stargazer, and ducky homozygotes (Snell, 1955; Green and Sidman, 1962; Dickie, 1964; Noebels et al., 1990). The high levels of expression of all the corresponding VDCC subunit genes in cerebellar neurons, particularly PCs, provides an obvious anatomical correlate with the presumed cerebellar dysfunction underlying the ataxia. PC loss has been documented in some, but not all, of these mutant strains; for example, it is observed in tg^{la} (Heckroth and Abbott, 1994). In *du/du* mice, no loss of PC somata was seen, but preliminary findings indicate major PC dendritic abnormalities (Brodbeck and Dolphin, unpublished results). The *du/du* PCs in which a reduced Ca^{2+} channel current was documented were obtained, for technical reasons, from ducky mice too young and developmentally immature to manifest an ataxic gait. However, it is reasonable to assume that the functional deficit is also present in older mice, and its presence before the overt phenotype is seen demonstrates that it is not merely a secondary effect. It is noteworthy that mutations in the human ortholog of the tottering gene *CACNA1A* are associated with ataxia and are also associated *in vitro* with a reduced whole-cell Ca^{2+} channel current (Hans et al., 1999).

There is one noticeable phenotypic difference between the *du/du* and du^{2J}/du^{2J} mice. Homozygous du^{2J} mice lack the characteristic "ducky" gait, potentially reflecting differences in the relative effects or stabilities of the mutant gene products. Additionally, the two mutations are maintained on different genetic backgrounds (*du* on TKDU and du^{2J} on C57BLKS/J), and this has an effect in other channelopathy phenotypes (Sprunger et al., 1999). Alternatively, these differences could result from involvement of other genes that are either disrupted or duplicated by the *du* rearrangement but unaltered in du^{2J}/du^{2J} mice. Several other genes lie within the *du* interval, including a semaphorin (Sekido et al., 1996).

These observations complete the association of mutations in all four main categories of VDCC subunits with a phenotype in mouse that includes SWDs and ataxia. A central role for disturbed neuronal calcium channel function can therefore be invoked. In the case of α2δ2, this is reinforced by the finding that a high-affinity binding site of the anti-epileptic drug gabapentin in brain has been identified as α2δ (Gee et al., 1996). In conclusion, these observations extend the occurrence of epileptogenic mutations to the last major category of genes encoding VDCC subunits and further strengthen the argument that such genes represent an important class of candidates for human IGEs.

REFERENCES

Barclay J, Rees M (2000) Genomic organisation of the mouse and human α2δ2 voltage dependent calcium channel subunit genes. Mamm Genome 11:1142–1144.

Berridge MJ, Bootman MD, Lipp P (1998) Calcium: a life and death signal. Nature 395:645–648.

Blatt C, Eversole-Cire P, Cohn VH, Zollman S, Fournier RE, Mohandas LT, Nesbitt M, Lugo T, Jones DT, Reed RR, Weiner LP, Sparkes RS, Simon MI (1988) Chromosomal localization of genes encoding guanine nucleotide-binding protein subunits in mouse and human. Proc Natl Acad Sci USA 85:7642–7646.

Burgess DL, Jones JM, Meisler MH, Noebels JL (1997) Mutation of the Ca^{2+} channel β subunit gene *Cchb4* is associated with ataxia and seizures in the lethargic (*lh*) mouse. Cell 88:385–392.

Burgess DL, Biddlecombe GH, McDonough SI, Diaz ME, Zilinski CA, Bean BP, Campbell KP, Noebels JL (1999) Beta subunit reshuffling modifies N- and P/Q-type Ca^{2+} channel subunit compositions in lethargic mouse brain. Mol Cell Neurosci 13:293–311.

Burgess DL, Gefrides LA, Foreman PJ, Noebels JL (2001) A cluster of three novel Ca^{2+} channel γ subunit genes on chromosome 19q13.4: evolution and expression profile of the γ subunit gene family. Genomics 71:339–350.

Caddick SJ, Wang C, Fletcher CF, Jenkins NA, Copeland NG, Hosford DA (1999) Excitatory but not inhibitory synaptic transmission if reduced in lethargic (*Cacnb4*^{lh}) and tottering (*Cacna1a*^{tg}) mouse thalami. J Neurophysiol 81:2066–2074.

Canti C, Page KM, Stephens GJ, Dolphin AC (1999) Identification of residues in the N terminus of α1B critical for inhibition of the voltage-dependent calcium channel by Gβγ. J Neurosci 19:6855–6864.

Catterall WA (1998) Structure and function of neuronal Ca^{2+} channels and their role in neurotransmitter release. Cell Calcium 24:307–323.

Coulter DA (1997) Thalamocortical anatomy and physiology. In: Epilepsy: a comprehensive textbook (Pedley JE, Pedley TA, eds), pp 341–351. Philadelphia: Lippincott-Raven.

Cox GA, Lutz CM, Yang C-L, Biemesderfer D, Bronson RT, Fu A, Aronson PS, Noebels JL, Frankel WN (1997) Sodium/hydrogen exchanger gene defect in slow-wave epilepsy mutant mice. Cell 91:139–148.

Dickie MM (1964) Lethargic (*lh*) mouse. Mouse News Lett 30:31.

Dietrich WF, Miller J, Steen R, Merchant MA, Damron-Boles D, Husain Z, Dredge R, Daly MJ, Ingalls KA, O'Connor TJ, Evans CA, DeAngelis MM, Levinson DM, Kruglyak L, Goodman N, Copeland NG, Jenkins NA, Hawkins TL, Stein L, Page DC, Lander ES (1996) A comprehensive genetic map of the mouse genome. Nature 380:149–152.

Dolphin AC, Wyatt CN, Richards J, Beattie RE, Craig P, Lee J-H, Cribbs LL, Volsen SG, Perez-Reyes E (1999) The effect of α2-δ and other accessory subunits on expression and properties of the calcium channel α1G. J Physiol (Lond) 519:35–45.

Dove LS, Abbott LC, Griffith WH (1998) Whole-cell and single-channel analysis of P-type calcium currents in cerebellar Purkinje cells of leaner mutant mice. J Neurosci 18:7687–7699.

Eisenstat DD, Liu JK, Mione M, Zhong W, Yu G, Anderson SA, Ghattas I, Puelles L, Rubenstein JL (1999) DLX-1, DLX-2, and DLX-5 expression define distinct stages of basal forebrain differentiation. J Comp Neurol 414:217–237.

Ertel EA, Campbell KP, Harpold MM, Hofmann F, Mori Y, Perez-Reyes E, Schwartz A, Snutch TP, Tanabe T, Birnbaumer L, Tsien RW, Catterall WA (2000) Nomenclature of voltage-gated calcium channels. Neuron 25:533–535.

Fletcher CF, Lutz CM, O'Sullivan TNJ, Hawkes R, Frankel WN, Copeland NG, Jenkins NA (1996) Absence epilepsy in tottering mutant mice is associated with calcium channel defects. Cell 87:606–617.

Fougerousse F, Bullen P, Herasse M, Lindsay S, Richard I, Wilson D, Suel L, Durand M, Robson S, Abitbol M, Beckmann JS, Strachan T (2000) Human–mouse differences in the embryonic expression patterns of developmental control genes and disease genes. Hum Mol Genet 9:165–173.

Gao B, Sekido Y, Maximov A, Saad M, Forgacs E, Latif F, Wei MH, Lerman M, Lee J-H, Perez-Reyes E, Besprozvanny I, Minna JD (2000) Functional properties of a new voltage-dependent calcium channel α2δ-2 auxiliary subunit gene (*CACNA2D2*). J Biol Chem 275:12237–12242.

Gee NS, Brown JP, Dissanayake VU, Offord J, Thurlow R, Woodruff GN (1996) The novel anticonvulsant drug, gabapentin (neurontin), binds to the α2δ subunit of a calcium channel. J Biol Chem 271:5768–5776.

Green MC, Sidman RL (1962) Tottering: a neuromuscular mutation in the mouse. J Hered 53:233–237.

Haldi M, Stickland C, Linm P, VanBerkel V, Chen X, Noya D, Korenberg J, Husain Z, Miller J, Lander E (1996) A comprehensive large-insert

yeast artificial chromosome library for physical mapping of the mouse genome. Mamm Genome 10:767–769.
Hans M, Luvisetto S, Williams ME, Spagnolo M, Urrtia A, Tottene A, Brust PF, Johnson EC, Harpold MM, Stauderman KA, Pietrobon D (1999) Functional consequences of mutations in the human α1A calcium channel subunit linked to familial hemiplegic migraine. J Neurosci 19:1610–1619.
Heckroth JA, Abbott LC (1994) Purkinje cell loss from alternating sagittal zones in the cerebellum of leaner mutant mice Brain Res 658:93–104.
Hobom M, Dai S, Marais E, Lacinova L, Hofmann F, Klugbauer N (2000) Neuronal distribution and functional characterization of the calcium channel α2δ2 subunit. Eur J Neurosci 12:1217–1226.
Hosford DA, Clark S, Cao Z, Wilson WA; Lin F-H, Morrisett RA, Huin A (1992) The role of $GABA_B$ receptor activation in absence seizures of lethargic (*lh/lh*) mice. Science 257:398–401.
Hosford DA, Lin F-H, Kraemer DL, Cao Z, Wang Y, Wilson JT (1995) Neural network of structures in which $GABA_B$ receptors regulate absence seizures in the lethargic (*lh/lh*) mouse model. J Neurosci 15:7367–7376.
Jun K, Piedras-Renteria ES, Smith SM, Wheeler DB, Lee SB, Lee TG, Chin H, Adams ME, Scheller RH, Tsien RW, Shin HS (1999) Ablation of P/Q-type Ca^{2+} channel currents, altered synaptic transmission, and progressive ataxia in mice lacking the alpha1A-subunit. Proc Natl Acad Sci USA 96:15245–15250.
Klugbauer N, Lacinova L, Marais E, Hobom M, Hofmann F (1999) Molecular diversity of the calcium channel α2δ subunit. J Neurosci 19:684–691.
Letts VA, Felix R, Biddlecombe GH, Arikkath J, Mahaffey CL, A V, Bartlett FS, Mori Y, Campbell KP, Frankel WN (1998) The mouse stargazer gene encodes a neuronal Ca^{2+}-channel γ subunit. Nat Genet 19:340–347.
Lorenzon NM, Lutz CM, Frankel WN, Beam KG (1998) Altered calcium channel currents in Purkinje cells of the neurological mutant mouse leaner. J Neurosci 18:4482–4489.
Meier H (1968) The neuropathology of ducky, a neurological mutation of the mouse. A pathological and preliminary histochemical study. Acta Neuropathol (Berl) 11:15–28.
Meir A, Bell DC, Stephens GJ, Page KM, Dolphin AC (2000) Calcium channel β subunit promotes voltage-dependent modulation of α1B by Gbγ. Biophys J 79:731–746.
Mintz IM, Adams ME, Bean BP (1992) P-type calcium channels in rat central and peripheral neurons. Neuron 9:85–95.
Neher E (1995) Voltage offsets in patch-clamp experiments. In: Single-channel recording (Sakmann B, Neher E, eds), pp 147–153. New York: Plenum.
Noebels JL (1991) Mutational analysis of spike-wave epilepsy phenotypes. In: Genetic strategies in epilepsy research (Anderson VE, Hauser WA, Leppik IE, Noebels JL, Rich SS, eds), pp 201–212. Amsterdam: Elsevier.
Noebels JL, Sidman RL (1979) Inherited epilepsy: spike-wave and focal motor seizures in the mutant mouse tottering. Science 204:1334–1336.
Noebels JL, Qiao X, Bronson RT, Spencer C, Davisson MT (1990) Stargazer: a new neurological mutant on chromosome 15 in the mouse with prolonged cortical seizures. Epilepsy Res 7:129–135.
Noebels JL, Fariello RG, Jobe PC, Lasley SM, Marescaux C (1997) Genetic models of generalized epilepsy. In: Epilepsy: a comprehensive textbook. (Pedley JE, Pedley TA, eds), pp 457–465. Philadelphia: Lippincott-Raven.
Nusbaum C, Slonim DK, Harris KL, Birren BW, Steen R, Stein LD, Miller J, Dietrich WF, Nahf R, Wang V, et al. (1999) A YAC-based physical map of the mouse genome. Nat Genet 22:388–393.
Pearson HA, Sutton KG, Scott RH, Dolphin AC (1995) Characterization of Ca^{2+} channel currents in cultured rat cerebellar granule neurones. J Physiol (Lond) 482:493–509.
Puranam HA, McNamara JO (1999) Seizure disorders in mutant mice: relevance to human epilepsies. Curr Opin Neurobiol 9:281–287.
Qian J, Noebels JL (2000) Presynaptic Ca^{2+} influx at a mouse central synapse with Ca^{2+} channel subunit mutations. J Neurosci 20:163–170.
Sekido Y, S B, Latif F, Chen JY, Duh FM, Wei MH, Albanesi JP, Lee CC, Lerman MI, Minna JD (1996) Human semaphorins A(V) and IV reside in the 3p21.3 small cell lung cancer deletion region and demonstrate distinct expression patterns. Proc Natl Acad Sci USA 93:4120–4125.
Skynner M, Gangadharan U, Coulton GR, Mason RM, Nikitopolou A, Brown SD, Blanco G (1995) Genetic mapping of the mouse neuromuscular mutation kyphoscoliosis. Genomics 25:207–213.
Snead OC (1995) Basic mechanisms of generalized absence seizures. Ann Neurol 37:146–157.
Snell GD (1955) Ducky, a new second chromosome mutation in the mouse. J Hered 46:27–29.
Sprunger LK, Escayg A, Tallaksen-Greene S, Albin RL, Meisler MH (1999) Dystonia associated with mutation of the neuronal sodium channel *Scn8a* and identification of the modifier locus *Scnm1* on mouse chromosome 3. Hum Mol Genet 8:471–479.
Uchida K, Yoshimura A, Inazawa J, Yanagisawa K, Osada H, Masuda A, Saito T, Takahashi T, Miyajima A (1997) Molecular cloning of *CISH*, chromosome assignment to 3p21.3, and analysis of expression in fetal and adult tissues. Cytogenet Cell Genet 78:209–212.
Wakamori M, Yamazaki K, Martsunodaira H, Teramoto T, Tanaka I, Niidomes T, Sawada K, Nishizawa Y, Sekiguchi N, Mori E, Mori Y, Imoto K (1998) Single tottering mutations responsible for the neuropathic phenotype of the P-type calcium channel. J Biol Chem 273:34857–34867.
Walker D, De Waard M (1998) Subunit interaction sites in voltage-dependent Ca^{2+} channels: role in channel function. Trends Neurosci 21:148–154.